# Analysis of ABCG2 pharmacology and oligomerisation by solution based fluorescence correlation spectroscopy

Aaron J. Horsey

Thesis submitted to the University of Nottingham for the degree of Doctor of Philosophy

September 2018

# Abstract

ABCG2 is a human ATP-binding cassette (ABC) transporter. It has a broad substrate range that includes a number of small molecule drugs as well as endogenous metabolites. With its expression in barrier tissues (e.g. kidney epithelium) ABCG2 has a strong influence on pharmacokinetics in addition to other physiological roles (e.g. urate excretion). ABCG2 is also expressed in several tumours and confers resistance to various chemotherapy agents. The detailed interactions and mechanisms that support such polyspecificity are not well-established and progress in understanding ABCG2 pharmacology has been limited.

The aim of this project was to develop novel, solution-based analysis methods to investigate ABCG2 pharmacology. Styrene-maleic acid copolymer lipid particles (SMALPs) were used to isolate ABCG2 in nanodiscs from a mammalian expression system (HEK293T). SMALP-ABCG2 particles were then characterised by fluorescence correlation spectroscopy (FCS) to investigate the stoichiometry of ABCG2 complexes and the pharmacology of their substrate binding.

ABCG2 tagged with GFP or SNAP-tag was expressed in HEK293T cells. The appropriate plasma membrane localisation was demonstrated by confocal microscopy and the activity of the fusion proteins were validated using mitoxantrone efflux assays. ABCG2 fusion proteins were extracted from HEK293T cell membrane preparations using SMALPs. This process yielded solubilised

ABCG2 that was analysed by dynamic light scattering and FCS. These analysis confirmed ABCG2 was extracted into single SMALP particles of 10-20nm diameter with <5% aggregation. Photon counting histogram analysis was performed on FCS data gathered from SMALP-ABCG2 as well as monomeric (CD86) and dimeric (CD28) control proteins also extracted in SMALPs. The brightness of ABCG2 (51000cpms$^{-1}$) was compared to that of the monomeric control (27000cpms$^{-1}$) and the dimeric control (60000cpms$^{-1}$). This revealed that ABCG2 was extracted as a dimer; the minimum functional unit. Subsequent extraction of ABCG2 from larger scale HEK293T membrane preparations facilitated purification of SMALP-ABCG2 by immobilised metal ion affinity chromatography at concentrations of up to 2µM.

Binding of a fluorescent drug substrate of ABCG2 (BODIPY-FL-prazosin) to SMALP-ABCG2 was also analysed using FCS. In the presence of SMALP-ABCG2 (initially 20-30nM) both fast-moving free drug (700µm$^2$s$^{-1}$) and a much slower protein-bound drug (37µm$^2$s$^{-1}$) species could be quantified. This was extended into assessing substrate and inhibitor interactions where FCS was used in competition binding assays. Inhibition of BODIPY-FL-prazosin binding by unlabelled prazosin was observed, but not by the known transport inhibitor Ko143.

Overall, the techniques developed in this project represent an improved workflow for the purification and assessment of protein complex stoichiometry. This extends to a novel platform for investigating substrate and inhibitor binding and recognition mechanisms.

# Acknowledgements

Firstly, I would like to express my utmost gratitude to my supervisors Dr Ian Kerr, Dr Nick Holliday and Dr Steve Briddon. Throughout the entirety of this project their advice and guidance have been invaluable. Despite busy schedules I have been privileged to enjoy the enthusiasm (and comedy) of Monday afternoon meetings almost without fail for the past three and a half years. Most recently these thanks are redoubled for the support and constructive feedback I have received whilst writing this thesis.

Secondly, I would like to thank all those in the lab, the school and the wider university that have supported my research efforts. I am particularly grateful to Deb Briggs for her training, cloning skills and patience that have been essential to the progression of my project. I have been honoured to have shared much of my PhD journey with Parth Kapoor who has always been keen to help me whenever needed. This also extends to Meg. Our near continuous discussions (and coffee breaks) have helped interpretate many of the ideas explored in this project and her support has been truly immeasurable. In the wider school and university I would like to thank Tim Self and Graham Rance who have contributed significant training, time and advice during this project. I would also like to thank Sue and Carol for their support work which has kept my tissue culture work in particular up and running.

My gratefulness is also extended to the University of Nottingham and the Nottingham-Rothamsted DTP who have delivered this excellent opportunity. The BBSRC-funded DTP programme provided financial support and training throughout the project and the unrivalled facilities provided by the university made this work possible. During this project I also had the opportunity to work for the Royal Microscopy Society and I would like to thank them for such a positive experience. In particular, I would like to thank Professor Susan Anderson and Kate Wooding for their time and support as well as the hundreds of teachers who responded to my requests for information.

Finally, and most importantly, I would like to thank my fiancé, friends and family. Their support and understanding through this entire project has been fundamental to my enjoyment of it. Bernadette has always been there to help and encourage. She has, through no fault of her own, shared every aspect of this project with me and done so with saint-like patience and understanding. My friends, especially those also on their own PhD journey, have also been invaluable and I wish each of them the successes all their hard work deserves. My whole family have always been keen to help and my parents in particular have provided continuous support that has kept me going and this thesis is dedicated to them.

# Declaration

This thesis, “Analysis of ABCG2 pharmacology and oligomerisation by solution based fluorescence correlation spectroscopy”, is the result of my own work undertaken during my period of registration at the University of Nottingham under the supervision of Dr Ian Kerr, Dr Nicholas Holliday and Dr Stephen Briddon.

Aaron Horsey

Student ID: 4234968

September 2018

# Abbreviations

| | |
|---|---|
| **ABC** | ATP binding cassette |
| **ACF** | autocorrelation function |
| **ADP** | adenosine diphosphate |
| **ANOVA** | analysis of variance |
| **AOTF** | acousto optic tunable filter |
| **AP1** | activator protein 1 |
| **AP2** | activator protein 2 |
| **ATCC** | American type culture collection |
| **ATP** | adenosine triphosphate |
| **AUC** | area under the curve |
| **BCRP** | breast cancer resistance protein |
| **BD-P** | BODIPY-FL-prazosin |
| **BLAST** | Basic Local Alignment Search Tool |
| **BSA** | bovine serum albumin |
| **BV** | bed volume |
| **CCD** | charge-coupled device |
| **CFP** | cyan fluorescent protein |
| **CFTR** | cystic fibrosis transmembrane conductance regulator |
| **CIP** | calf intestinal phosphatase |
| **$C_{max}$** | maximum serum concentration |
| **CMFDA** | chloromethylfluorescein diacetate |
| **CMV** | cytomegalovirus |
| **CPM** | counts per molecule |
| **cpms-1** | counts per molecule per second |
| **Ctrl** | control |
| **DAPI** | 4',6-diamidino-2-phenylindole |
| **DDI** | drug-drug interaction |
| **DIBMA** | diisobutylene maleic acid |
| **DLS** | dynamic light scattering |
| **DMEM** | Dulbecco's Modified Eagle Medium |
| **DMSO** | Dimethyl sulfoxide |
| **dNTPs** | deoxyribonucleotide triphosphates |
| **EDTA** | Ethylenediaminetetraacetic acid |
| **EM** | electron microscopy |
| **ER** | endoplasmic reticulum |
| **FBS** | foetal bovine serum |
| **FCS** | fluorescence correlation spectroscopy |
| **FITC** | Fluorescein isothiocyanate |
| **FRAP** | fluorescence recovery after photobleaching |
| **GFP** | green fluorescence protein |

| | |
|---|---|
| **GI tract** | gastrointestinal tract |
| **GPCR** | G protein–coupled receptor |
| **GST** | glutathione S-transferase |
| **GWAS** | genome wide association study |
| **HDL** | high density lipoprotein |
| **HEK** | human embryonic kidney |
| **HeNe** | helium neon |
| **HRP** | horseradish peroxidase |
| **IgGκ** | immunoglobulin Gκ |
| **IMAC** | immobilised metal ion affinity chromatography |
| **LB** | Luria broth |
| **MATE** | Multi-antimicrobial extrusion protein |
| **MDR** | multidrug resistance |
| **MDR1** | multidrug resistance protein 1 |
| **MHC** | major histocompatibility complex |
| **MIB** | membrane isolation buffer |
| **miRNA** | microRNA |
| **mRNA** | messenger RNA |
| **MRP1** | multidrug resistance-associated protein 1 |
| **MSB** | maltose binding protein |
| **MSP** | membrane scaffold protein |
| **MST** | microscale thermophoresis |
| **MX** | mitoxantrone |
| **MWCO** | Molecular weight cut-off |
| **NBD** | nucleotide binding domain |
| **NCBI** | National Center for Biotechnology Information |
| **NFKb** | nuclear factor kappa-light-chain-enhancer of activated B cells |
| **NSB** | non-specific binding |
| **NSCLC** | non-small cell lung cancer |
| **OAT** | organic anion transporter |
| **OATP** | organic anion transporter polypeptide |
| **OCT** | organic cation transporter |
| **PBS** | phosphate buffered saline |
| **pcDNA** | protamine complementary DNA |
| **PCH** | photon counting histogram |
| **PCR** | polymerase chain reaction |
| **PDB** | protein database |
| **PEI** | Polyethylenimine |
| **PFA** | paraformaldehyde |
| **PhiP** | (4,5-b)pyridine |
| **R6G** | rhodamine 6G |
| **S9** | Syto 9 |
| **SAR** | structure activity relationship |
| **SBP** | substrate binding protein |

| | |
|---|---|
| **SDS** | sodium dodecyl sulfate |
| **SDS-PAGE** | SDS-polyacrylamide gel electrophoresis |
| **SMA** | styrene maleic acid |
| **SNP** | single nucleotide polymorphism |
| **Sp1** | specificity protein 1 |
| **SUR** | Sulfonylurea receptor |
| **SV40** | simian virus 40 |
| **TAP** | Transporter associated with antigen processing |
| **TEV** | Tobacco etch virus |
| **TMD** | transmembrane domain |
| **TRITC** | Tetramethylrhodamine |
| **VLCFA** | very long chain fatty acid |
| **YFP** | yellow fluorescent protein |

**1 Introduction ..... 1**

1.1 Crossing the Cell Membrane ..... 1
1.2 The ABC Transporter Family ..... 10
1.3 ABCG2 and its Role in Health and Disease ..... 24
1.4 Pharmacological Importance of ABCG2 ..... 39
1.5 Methods to Study Transporter Pharmacology ..... 48
1.6 Aims of the Study ..... 59

**2 Methods ..... 61**

2.1 Cloning and Molecular Biology ..... 61
2.2 Cell Culture and Handling ..... 68
2.3 Preparation of Membrane Fractions ..... 72
2.4 SMALP Preparation and Use ..... 74
2.5 Sizing of SMALP solubilised proteins by dynamic light scattering (DLS) ..... 75
2.6 Purification and Concentration of ABCG2 ..... 76
2.7 Protein Analysis by SDS-PAGE and western blot ..... 77
2.8 Whole cell functional assays ..... 80
2.9 Standard and Confocal Imaging ..... 82
2.10 FCS and PCH Analysis ..... 83
2.11 Binding analysis by FCS ..... 87
2.12 Statistical analysis ..... 88

**3 Plasmid Construct Generation ..... 89**

3.1 Design and engineering of fluorescent and His- tagged ABCG2 protein constructs for metal ion affinity purification ..... 89
3.2 Generation of pcDNA3.1(+)zeo-ABCG2 constructs ..... 94
3.3 Generation of pcDNA4/TO-ABCG2 constructs ..... 97
3.4 Generation of oligomeric control constructs ..... 100
3.5 Summary of construct generation and utilisation ..... 101

**4 Expression, characterisation and solubilisation of ABCG2 ..... 103**

4.1 Chapter Overview ..... 103
4.2 Generation of stable cell lines ..... 103
4.3 Demonstration of protein and tag expression by western blot analysis ..... 107
4.4 Demonstration of protein localisation by confocal microscopy ..... 109
4.5 Determination of transport activity in tagged ABCG2 constructs ..... 111
4.6 Optimisation of expression ..... 112
4.7 Membrane preparation ..... 120
4.8 Labelling strategy ..... 121
4.9 Detergent-free extraction of ABCG2 ..... 123
4.10 Summary ..... 127

**5 Determination of SMALP-encapsulated ABCG2 stoichiometry by FCS and PCH ..... 128**

5.1 Chapter overview ..... 128
5.2 Sizing of SMALP solubilised protein samples by DLS ..... 129
5.3 Diffusion of SMALP-ABCG2 measured in solution by FCS ..... 134
5.4 PCH analysis in the determination of SMALP-ABCG2 oligomeric state ..... 143

5.5 Summary ..... 147

**6 Investigation of ABCG2 interaction with a transport substrate and inhibitor by FCS ..... 150**

6.1 Overview ..... 150
6.2 Purification of SMALP-ABCG2 ..... 152
6.3 Development of an FCS-based binding assay ..... 157
6.4 Investigation of transport substrate and inhibitor interaction with ABCG2 173
6.5 Summary ..... 178

**7 Discussion ..... 181**

7.1 Key Findings and Limitations ..... 181
7.2 Future Perspectives ..... 186

**8 References ..... 192**

**9 Appendix ..... 221**

9.1 Sequencing Data ..... 221
9.2 FCS Data Processing ..... 222
9.3 List of Publications ..... 223
9.4 DTP Notice to Examiners ..... 224
9.5 Placement Report and Reflection ..... 225

# List of Figures

Figure 1.1 – Schematic of the cell membrane. ..... 1
Figure 1.2 – Schematic of the Membrane Crossing Mechanisms. ..... 5
Figure 1.3 – Example Cell Types and Transport Networks. ..... 9
Figure 1.4 – Core domain organisations of ABC transporters. ..... 11
Figure 1.5 – Type I and Type II TMD folds. ..... 12
Figure 1.6 – Structure of a nucleotide binding domain dimer. ..... 15
Figure 1.7 – Structure of human ABCB1. ..... 21
Figure 1.8 – Structure of bovine ABCC1. ..... 24
Figure 1.9 – General topology of the ABCG2 Monomer. ..... 27
Figure 1.10 – Comparison of ABC transporter folds. ..... 29
Figure 1.11 – Structure of human ABCG2. ..... 31
Figure 1.12 – Schematic of the ATP-switch model. ..... 34
Figure 1.13 – Schematic representation of membrane solubilisation by SMA. ..... 51
Figure 1.14 – A Jablonski diagram. ..... 54
Figure 1.15 – Schematic representation of a confocal microscope setup. ..... 56
Figure 1.16 - Schematic demonstrating the typical FCS instrumentation and outputs. ..... 58
Figure 3.1 – Schematic representation of the interactions associated to IMAC. ..... 90
Figure 3.2 – Schematic outline of the main ABCG2 encoding DNA vectors used in this study. ..... 93
Figure 3.3 – Outline of N-terminal short His-tag oligo insert cloning. ..... 95
Figure 3.4 – Successful introduction of polyhistidine tags was confirmed by DNA sequencing. ..... 96
Figure 3.5 – Summary of pcDNA4T/O construct generation. ..... 99
Figure 3.6 – Schematic outline of the CD86 and CD28 control vectors. ..... 100
Figure 4.1 – Outline of the generation of a stable cell line by Zeocin® mediated selection. ..... 105
Figure 4.2 – Demonstration of tagged ABCG2 expression by fluorescence microscopy. ..... 106
Figure 4.3 – Demonstration of tagged ABCG2 expression by Western blot analysis. ..... 108
Figure 4.4 – Expression of ABCG2 at the plasma membrane of stably expressing HEK293T cells. ..... 110
Figure 4.5 – Function of N-terminally tagged ABCG2 expressed at different levels in HEK293T cells. ..... 112
Figure 4.6 – Selection of high and low ABCG2 expressing clones. ..... 114
Figure 4.7– Increased expression of ABCG2 upon the addition of sodium butyrate. ..... 115
Figure 4.8– Investigating increased expression by the use of a tetracycline inducible cell line. ..... 117
Figure 4.9 – Adaptation to suspension culture. ..... 119
Figure 4.10 – Isolation of ABCG2 containing membrane fractions. ..... 121
Figure 4.11 – Labelling of SNAP-tag ABCG2. ..... 123

Figure 4.12 – Solubilisation of membrane proteins by styrene maleic acid. 125
Figure 4.13 – Western blots showing the solubilisation efficiency of DIBMA. 126
Figure 5.1 - Principles of DLS in the calculation of particle size. 130
Figure 5.2 - Example DLS traces and particle sizing summary. 132
Figure 5.3 - Effect of laser power and read time in optimisation of FCS data acquisition. 137
Figure 5.4- Curve fitting in ACF interpretation. 139
Figure 5.5 - Example autocorrelation curves and deviations from the curve fitting. 140
Figure 5.6 - Summary of diffusion coefficients and component fractions for CD86, CD28 and ABCG2. 142
Figure 5.7- Effect of bin time on PCH analysis. 144
Figure 5.8 - Summary of PCH molecular brightness analysis. 146
Figure 6.1 – Comparison of nickel and cobalt ions in IMAC for SMALP-ABCG2. 153
Figure 6.2 – Optimisation of SMALP-ABCG2 purification by cobalt ion affinity chromatography. 155
Figure 6.3 – Concentration and quantification of purified ABCG2. 157
Figure 6.4 – Principles of an FCS based SMALP-ABCG2 binding assay. 159
Figure 6.5– Selection of drug substrates for FCS analysis. 161
Figure 6.6 – Assessment of compound recovery by FCS. 163
Figure 6.7 – Summary of initial BD-P binding analysis to SMALP-ABCG2. 165
Figure 6.8 – Analysis of approaches to fit the FCS Binding data. 167
Figure 6.9 – Simulated transporter binding data. 169
Figure 6.10 – Binding analysis of BD-P to varying concentrations of SMALP-ABCG2. 170
Figure 6.11 – Effect of incubation time on non-specific binding to plate surfaces and the measured BD-P concentration by FCS. 173
Figure 6.12 – Analysis of BD-P binding using the FCS assay and optimised conditions. 174
Figure 6.13 – Inhibition of BD-P binding to SMALP-ABCG2 by addition of prazosin. 176
Figure 6.14 – Analysis of BD-P binding inhibition by prazosin and Ko143. 177
Figure 7.1 – Example fluorophores for *de novo* drug synthesis.. 187
Figure 7.2 – Workflow for improved drug design supported by an FCS screening assay. 190

# List of Tables

Table 1.1 – Example non-chemotherapeutic ABCG2 substrates. ..... 44
Table 1.2 – Example perpetrator drugs involved in ABCG2-mediated drug-drug interactions with rosuvastatin. ..... 46
Table 2.1 - Components of restriction digest reactions. ..... 62
Table 2.2 - Components of ligation reactions ..... 62
Table 2.3 - Summary of mutagenesis primers. ..... 65
Table 2.4 - Components of a typical PCR reaction. ..... 66
Table 2.5 - Thermocycling protocol for site-directed mutagenesis reactions. ..... 67
Table 2.6 - Sequencing primers used in this study. ..... 67
Table 2.7 – Antibodies used for western blotting in this project. ..... 80
Table 3.1 - Summary of the main fluorescent protein constructs used in this study. ... 102

# 1 Introduction

## 1.1 Crossing the Cell Membrane

### 1.1.1 Basics of the Cell Membrane

Biological membranes are absolutely essential for life as we know it; separating what is a cell, and its compartments, from the environment (Watson, 2015). Controlling which substances can pass through this membrane by selective permeability facilitates basic life functions in the individual cell (e.g. the movement of mRNA from nucleus to cytoplasm for translation during protein synthesis) to the whole organism (e.g. propagation of electrical signal through the nervous system when you stub your toe) (Gall, 1954; Dubin and Patapoutian, 2010; Watson, 2015). The membrane is a fundamental cellular feature and has become better understood as time has gone by but continues to fascinate and raise more questions about how it functions. Discussed below are the basics of the cell membrane structure, function and how it can be overcome.

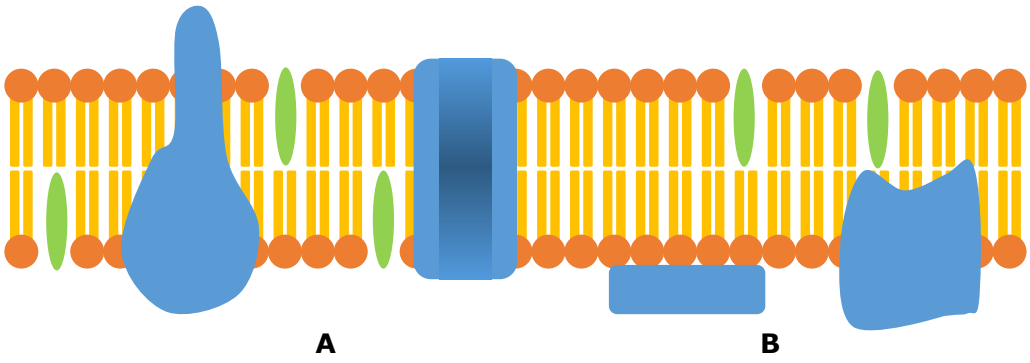


**Figure 1.1 – Schematic of the cell membrane.** The lipids (orange/yellow) are arranged in a lamellar fashion with inward facing hydrophilic tails. This bilayer is peppered with cholesterol (green) and proteins (blue). These proteins are either integrated into the membrane (**A**) or interact only with the surface or periphery (**B**).

Historically, there have been a number of iterations of overall membrane structure models. Current theory builds upon the Fluid Membrane Mosaic Model first proposed in 1972 (Singer and Nicolson, 1972). This describes a mobile, dynamic membrane that forms the perimeter of a cell (Nicolson, 2014). It is important to recognise that the nature of a particular cell membrane is highly variable between cell type/function, species or cellular activation state (Goñi, 2014). However, the overall structure remains relatively conserved (see Figure 1.1). The most prevalent component is the phospholipid bilayer with inner and outer leaflet of lipid molecules arranged in a lamellar fashion (Singer and Nicolson, 1972). This is known to consist of several lipid types segregated into regions or rafts with many intracellular, extracellular and transmembrane interactions (Nicolson, 2014). The lipids in the bilayer are all arranged with hydrophobic tails in the centre with hydrophilic head groups facing either the intracellular or extracellular space. Importantly, there is an asymmetry of lipid distribution. In mammalian cells for example phosphatidylcholine and sphingomyelin are found predominantly in the outer leaflet with phosphatidylserine and phosphatidylethanolamine found more in the inner leaflet (Watson, 2015). This asymmetry has structural (e.g. curvature of the membrane) and functional (e.g. phosphatidylserine exposure on the outer leaflet as an apoptotic signal) importance. It also helps ensure the correct orientation of membrane associated proteins (Goñi, 2014). These membrane proteins can be surface or peripheral, with limited interaction with the lipid bilayer. They can also, as is the case for

ABCG2, be integral membrane proteins reliant on being embedded in the bilayer for correct structure and function (Lee, 2004). The positions and movements of the proteins and lipid regions can be guided by interactions with each other but also by interactions with cytoskeletal components (Szymanski *et al.*, 2015). Facilitated or impeded movement or natural diffusion of lipid and protein components make the membrane a very dynamic environment key to a number of cellular processes. However, it is impossible to escape the principal role of the membrane as a selective barrier.

### 1.1.2 Function as a Barrier

Surprisingly, the exact extent to which the lipid bilayer forms a barrier is still under debate. Though universally accepted is that the cell membrane restricts the movement of molecules in to and out of cells, some argue that this barrier is near absolute (Dobson and Kell, 2008). This argument suggests that there is a negligible level of truly 'passive' diffusion across the membrane particularly referring to hydrophobic drugs (Kell, Dobson and Oliver, 2011). Instead, this model points to the multiplicity of, as yet unidentified, carriers that will allow the substances to cross membranes. Proponents of this model suggest that experimental systems employing artificial membranes or cultured cell monolayers introduce systematic errors that result in any observed 'background' diffusion (Kell, 2015). Others argue that this is in fact not the case and that some passive diffusion will occur (Scott *et al.*, 2017). In particular, lipophilic molecules are considered to be able to cross through the membrane, and molecules with relatively increased hydrophilicity

find this increasingly energetically unfavourable (Watson, 2015). Considering the near impossible task of generating a demonstrably realistic protein-free artificial membrane, this may be a difficult argument to settle and certainly fell beyond the scope of this project. In whichever case, it will be true that the membrane significantly restricts the movement of compounds between the intracellular and extracellular environments. Despite the barrier function being the underlying feature of the membrane this does pose a number of challenges. How do cells get the nutrients they needs to survive? Or get rid of toxic metabolites or other damaging substances? Mechanisms to pass molecules across the membrane when necessary have subsequently evolved. These are considered here with a bias towards the pharmacological relevance which is a main concern of this project.

### 1.1.3 Crossing the Barrier

The cell membrane, even as a particularly good barrier separating the cell from the environment, is overcome to facilitate any number of biological processes. This occurs via several mechanisms. Bearing in mind the above arguments, gaseous molecules (e.g. $CO_2$ and $O_2$) readily pass through the membrane by simple diffusion, though the vast majority of transport is protein mediated (Yang and Hinner, 2015). The mechanisms by which proteins facilitate the movement of substances across membranes are incredibly diverse (Hediger *et al.*, 2004).

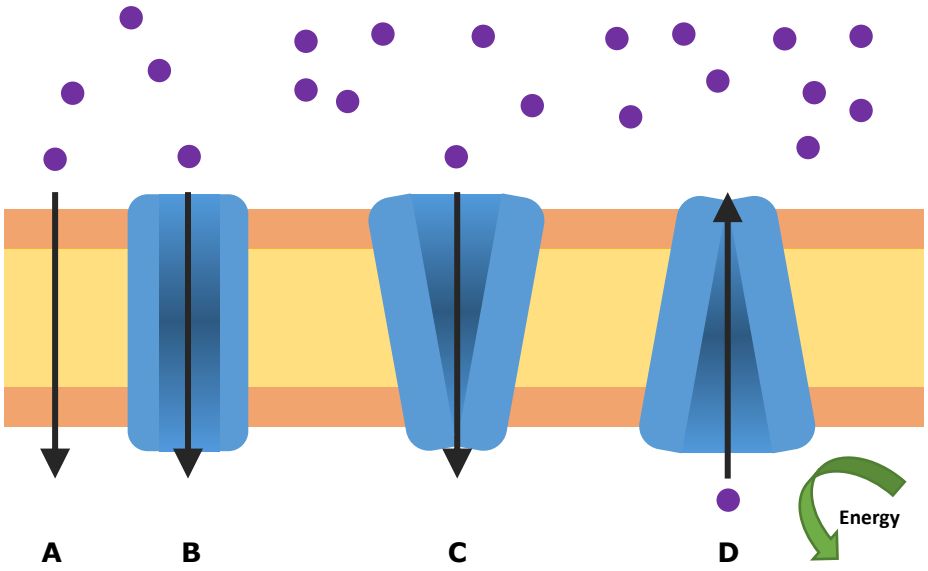


**Figure 1.2 – Schematic of the Membrane Crossing Mechanisms.** Molecules (purple) can move across the membrane (orange/yellow) by free (**A**), channel-mediated (**B**) or carrier-mediated (**C**) diffusion or by active transport (**D**).

At the basic level, they are characterised as “downhill” or “uphill” referring to the concentration gradient across the membrane of a particular substance. When a substance is moved down its concentration gradient, this mechanism is passive, requiring no additional energy expenditure by the cell (Brooker *et al.*, 2010; Ware, Zhang and Huang, 2012). This movement is facilitated by channels. Channels form hydrophilic pathways that allow certain ions to pass through whilst preventing the free travel of others (Yang and Hinner, 2015). Key examples include those involved in the propagation of action potentials such as voltage-gated sodium channels. These heteromeric proteins consist of pore-forming α–subunits complexed with auxiliary β-subunits (Catterall, Goldin and Waxman, 2005). The selectivity of these channels is generally governed by the hydration shell of the permeant molecule

and facilitated by the overall size of the hydrophilic pore and the charge of any inward facing residues (Thompson *et al.*, 2009; Watson, 2015). It is important to note that, though these systems do not require energy to accommodate transmembrane movement of molecules which are free to move through the hydrophilic pore, they can be gated (opened and closed) *inter alia* by voltage, ligand, pH or mechanical force and therefore activated/de-activated depending on the requirements of the cell (Brooker *et al.*, 2010; Ware, Zhang and Huang, 2012). Carrier proteins are another major family of proteins involved in the passive movement of substances across the membrane. These generally have a much slower rate of membrane transport than channels (Brooker *et al.*, 2010). Rather than forming a continuous aqueous pore, the binding of the transported molecule occurs at a high affinity site located on the side of the membrane with the highest concentration of the transported molecule. This results in conformational changes that expose the transported molecule to the opposite side of the membrane and simultaneously transfer it to a low affinity site from which it dissociates and the carrier resets (Jardetzky, 1966; Watson, 2015). As mentioned, the energy associated to the movement of substances by channels or carriers is provided by the potential energy associated to the concentration gradient maintained across the membrane. As such, movement of molecules by channels is always from high concentration to low concentration environments. The potential energy of a gradient for one molecule can also power the transport of another against its concentration gradient by secondary active transport or by pumps in primary

active transport. The line between channels and pumps is blurred as shown by CFTR. This is a channel for chloride ions masquerading in the primary sequence of an ABC transporter. It is gated by the hydrolysis of ATP and therefore has similar features to ABC transporters but with a transport mechanism that is very different (Anderson *et al.*, 1991; Bear *et al.*, 1992; Nagel *et al.*, 1992).

As the name suggests, pumps (or active transporters) require a separate source of energy (Brooker *et al.*, 2010). The energy source used for a particular active transport mechanism characterises it as either primary or secondary active transport. Though light can be used as source of energy (e.g. bacterial rhodopsin (Oesterhelt and Tittor, 1989)) these energy sources are either ATP (primary active transport) or the potential energy from the concentration gradient of a second molecule (secondary active transport) (Brooker *et al.*, 2010). Key primary transporter families are P-type ATPases and ATP-binding cassette (ABC) transporters with the latter described below in Section 1.2. P-type ATPases consist of α-helical bundles and are mainly involved in cation uptake or efflux (Palmgren and Nissen, 2011). For example, the $Na^+/K^+$-ATPase which is important in maintaining the gradient of each ion in neurons (Clausen, Hilbers and Poulsen, 2017). Secondary active transporters are another incredibly diverse family in terms of function. The overall transport mechanism utilised is referred to as coupled (or co-transport) (Watson, 2015). The energy to move one substance against its concentration gradient is provided by the movement of another with its gradient. For example, the sodium-calcium exchanger exports a single calcium

ion using the energy stored in the electrochemical gradient of sodium ions by importing three of these (Yu and Choi, 1997). Secondary active transport is either unidirectional (symport) or bidirectional (antiport) (with the example sodium-calcium exchanger being an antiporter) (Brooker *et al.*, 2010).

Although the focus of this work is on the human multidrug transporter ABCG2 it is important to maintain an awareness of the overall system defining drug entry and exit to and from the cell. There are all manner of transporters expressed in humans each with important physiological roles. They form an intricate system governing the uptake, distribution and excretion of nutrients, toxins and many other substances (Konig, Muller and Fromm, 2013). Examples of small molecule importers and exporters in ABCG2 expressing cells are shown Figure 1.3 where several transporter families are represented. The OATP (organic anion transporter polypeptide) family have many different identified substrates including bile acids and hormones (Mikkaichi *et al.*, 2004). The OAT (organic anion transporter) family is a subset of solute carrier subfamily 22 that are responsible for transporting a number of common drug types (including antivirals, antibiotics and diuretics) (Nigam *et al.*, 2015). The OCT (organic cation transporter) family also has a broad range of transport substrates that includes a number of drugs including metformin (antidiabetic) and oxaliplatin (chemotherapy agent) (Nies *et al.*, 2011; Roth, Obaidat and Hagenbuch, 2012). There is also the MATE (multidrug and toxic compound extrusion) family which is associated to antibiotic resistance in bacteria but is also found in humans where, for example, MATE1 is found in the liver and

kidney and transports toxic cations into the bile or urine (Otsuka *et al.*, 2005; Kuroda and Tsuchiya, 2009). Even in just these example cell types, the complexity of the network defining drug uptake and efflux is apparent.

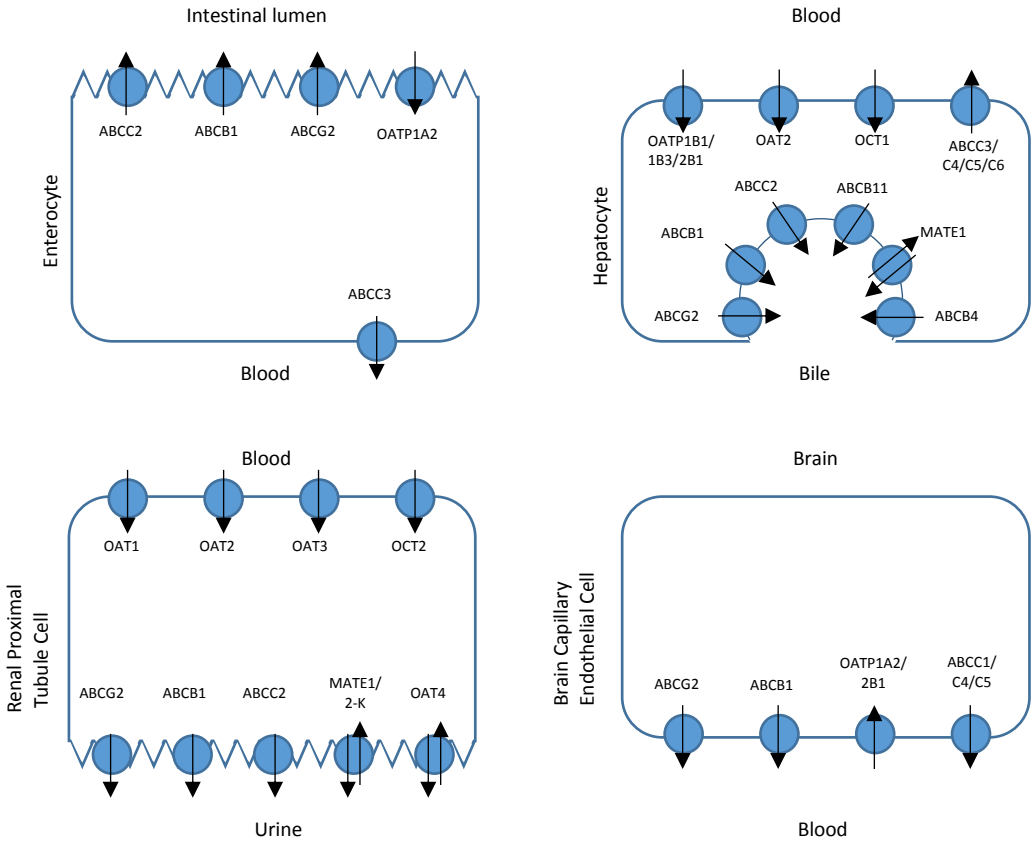


**Figure 1.3 – Example Cell Types and Transport Networks.** Barrier cell types expressing ABCG2 also express other transporters and channels that act in a complex network to mediate uptake and excretion of substances. ATP binding cassette (ABC), organic anion transporter polypeptide (OATP), organic anion transporter (OAT), organic cation transporter (OCT) and multidrug and toxic compound extrusion (MATE) families are all represented (adapted from König et al 2013).

## 1.2 The ABC Transporter Family

### 1.2.1 Family Introduction

The ABC transporter family is represented in all organisms, both prokaryotic and eukaryotic and has been increasingly well understood since the first discoveries (Higgins *et al.*, 1986; Dassa, 2011). The subject of this project, ABCG2, is a human multidrug efflux pump but, even just in humans, ABC transporters have a wide range of physiological roles (Vasiliou, Vasiliou and Nebert, 2009). Depending on their tissue distribution, they are associated to the transport of endogenous compounds for storage in intracellular compartments, reducing adsorption from or facilitating excretion to the lumen and protection from toxic compounds at the cellular level (Dean, Hamon and Chimini, 2001). These roles extend to pharmaceutical agents and, as later discussed, to limiting efficacy of these (Giacomini *et al.*, 2010). Despite the variety there are, as in any family, a number of common traits.

### 1.2.2 General Architecture

A functional ABC transporter consists of at least four domains; two nucleotide binding domains (NBDs) and two transmembrane domains (TMDs). The organisation of these domains for several transporters is summarised in Figure 1.4. In humans and other eukaryotes, they are expressed as either full transporters or 'half-transporters'. These are formed by either a single polypeptide or a homo- or hetero-oligomers respectively (Hyde *et al.*, 1990; Jones

and George, 2004). Other domain organisations also occur but, in humans, the majority of ABC transporters are formed of a single polypeptide (Wilkens, 2015).

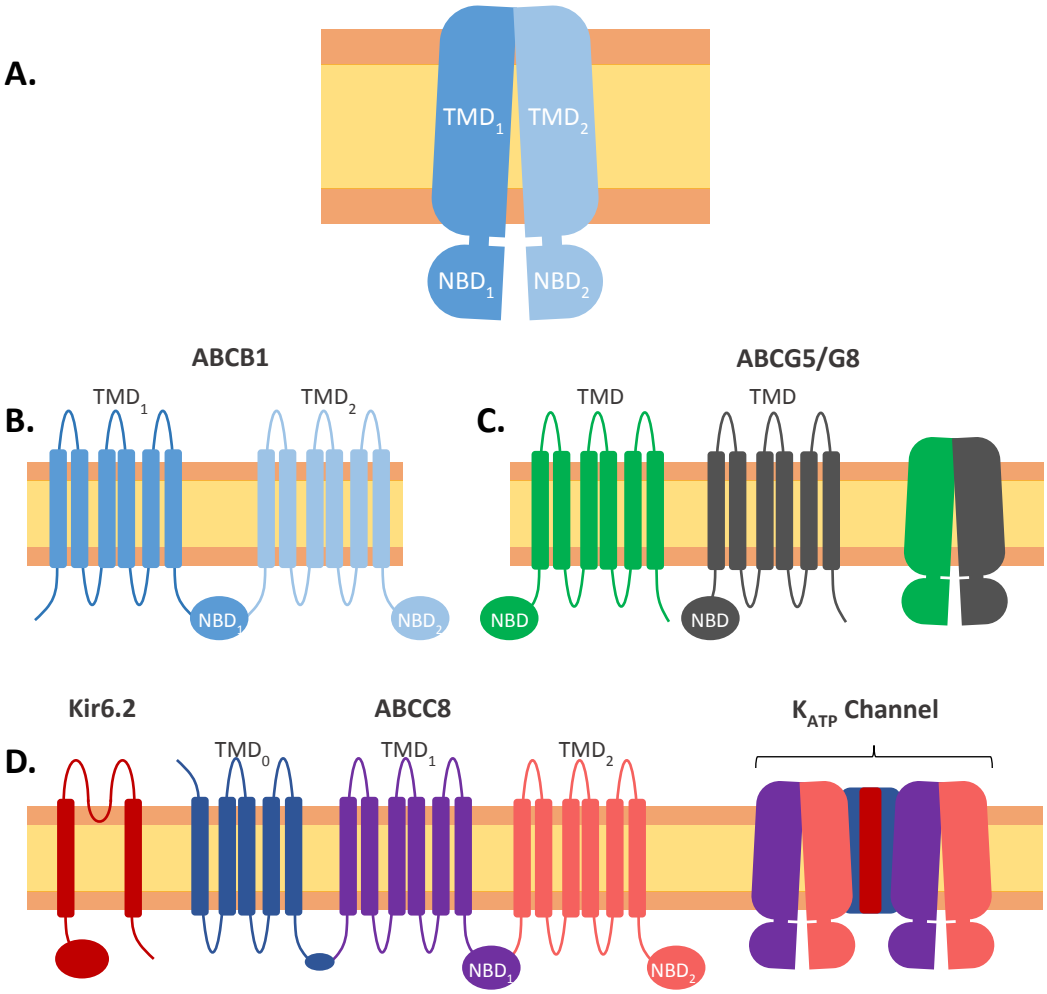


**Figure 1.4 – Core domain organisations of ABC transporters.** A typical ABC transporter consists of two intracellular nucleotide binding domains (NBDs) and two membrane spanning domains (TMDs) (**A**). In humans, the majority of these proteins are encoded by a single polypeptide as is the case for ABCB1 (**B**) (Aller *et al.*, 2009). They can also be 'half-transporters' that form dimers to function, for example the ABCG5/G8 heterodimer (**C**) (J.-Y. Lee *et al.*, 2016). More complex arrangements are also seen such as in ABCC8 which form tetramers (8 NBDs total) surrounding a central pore of tetrameric Kir6.2 via interactions with the $TMD_0$ of ABCC8 which all together form a $K_{ATP}$ channel (**D**) (Li *et al.*, 2017).

The TMDs consist of 6-11 membrane spanning α–helices joined by intracellular and extracellular loops (Dean, Hamon and Chimini, 2001). These TMDs form the sites for the determination of transport substrate selectivity. As such, to support the wide ranging functions of ABC transporters there is significant variation in the composition, in terms of the residues forming each helix, and three-dimensional structure of these domains between or even within transporter subfamilies (Hafkemeyer *et al.*, 1998; Wilkens, 2015). The number and position of helices can be different and there can be large differences in the overall folding of ABC transporters. One of the principal distinctions is between Type I and Type II folds. This stems from classification of prokaryotic ABC transporters where Type I transporters have transmembrane helices that 'cross-over' in contrast to Type II transporters that do not (ter Beek, Guskov and Slotboom, 2014). Examples of these bacterial proteins are MalFGK and BtuCD respectively (see Figure 1.5) (Hvorup *et al.*, 2007; Oldham *et al.*, 2007).

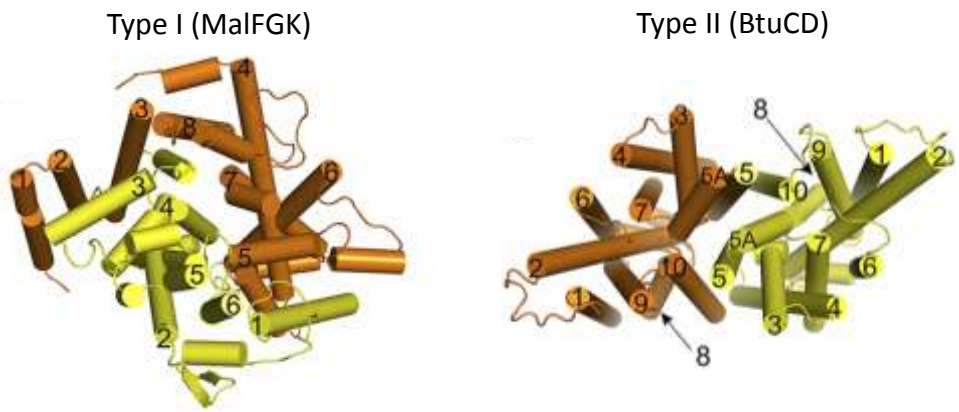


**Figure 1.5 – Type I and Type II TMD folds.** A top-down view of the transmembrane domains of MalFGK (left) and BtuCD (right) shows the cross-over of helix bundles in Type I bacterial ABC importers (MalFGK) compared to the distinct bundles of Type II importers (BtuCD) (adapted from: ter Beek et al. 2014).

In terms of functional differences between these classifications, Type I importers tend to be capable of higher capacity, lower affinity transport than Type II importers. This is associated to a greater number of substrate binding proteins (SBPs) which are a fundamental part of bacterial ABC importer function (ter Beek, Guskov and Slotboom, 2014). Though similar folds are observed, human ABC transporters (see Section 1.3.2) do not have SBPs and the functional importance of these different classes is not yet clear.

The NBDs of an ABC transporter are located in the cytoplasm. Most importantly they contain sequences that allow them to bind, then hydrolyse ATP to ADP (Hyde *et al.*, 1990; Linton and Higgins, 2007). The energy released provides power for all manner of energy dependent biological reactions. In the case of ABC transporters, the energy is used in a 'power stroke' through which a protein undergoes conformational changes that result in the translocation of the respective transport substrate and/or the resetting of the transporter to a conformation ready for another transport cycle (Chen *et al.*, 2003). In contrast to the variation observed in the TMDs between different ABC transporters, there are a number of conserved elements in the NBDs (Hyde *et al.*, 1990; Linton and Higgins, 2007; Wilkens, 2015). Two well-established ATP binding sequences seen in other ABC proteins, the Walker-A and Walker-B motifs, can be identified (Walker *et al.*, 1982). The glycine rich Walker-A motif (GXXGXGK(S/T), where X = any residue) has an important role in nucleotide binding through the formation of interactions between the glycine residues and phosphates of ATP. The serine/threonine residues coordinate $Mg^{2+}$

binding and the conserved lysine residue of the Walker-A motif appears critical for ATP hydrolysis activity (Azzaria, Schurr and Gros, 1989; Muller *et al.*, 1996; Smith *et al.*, 2002; Henriksen, Gether and Litman, 2005; Ambudkar, Kim and Sauna, 2006). The aspartate in the Walker-B motif (hhhhDE, where h = hydrophobic residue) also appears to be involved in $Mg^{2+}$ coordination and interactions with water molecules during the hydrolysis cycle (Walker *et al.*, 1982; Hanson and Whiteheart, 2005). The conserved glutamate residue within the Walker-B motif has also been shown to be important in NBD function where substitution for the neutral glutamine results in non-functional mutant isoforms of ABC proteins (e.g. E171Q mutation of MJ0796 expressed in *E. coli* – see Figure 1.6) (Smith *et al.*, 2002). In these isoforms there is tightly bound nucleotide and it is suggested that the glutamate residue therefore plays an important role by cleaving the phosphoanhydrous bonds in the ATP (Smith *et al.*, 2002; Tombline *et al.*, 2005; Hou *et al.*, 2009). Other NBD sequences are also found specifically in ABC transporters (Higgins *et al.*, 1986; Higgins, 1992). There is an aromatic residue, ABC signature motif (LSGGQ) along with the Q-, D- and H- loops that contain glutamine, aspartate and histidine residues respectively (Ambudkar *et al.*, 2006). The conserved aromatic residue, located N-terminal to the Walker-A motif is believed to participate in the binding of ATP as indicated by structural data (Smith *et al.*, 2002; Dawson and Locher, 2006). These data explain the reduced activity patterns seen in mutational studies of this residue (Ambudkar *et al.*, 2006; Carrier *et al.*, 2007).

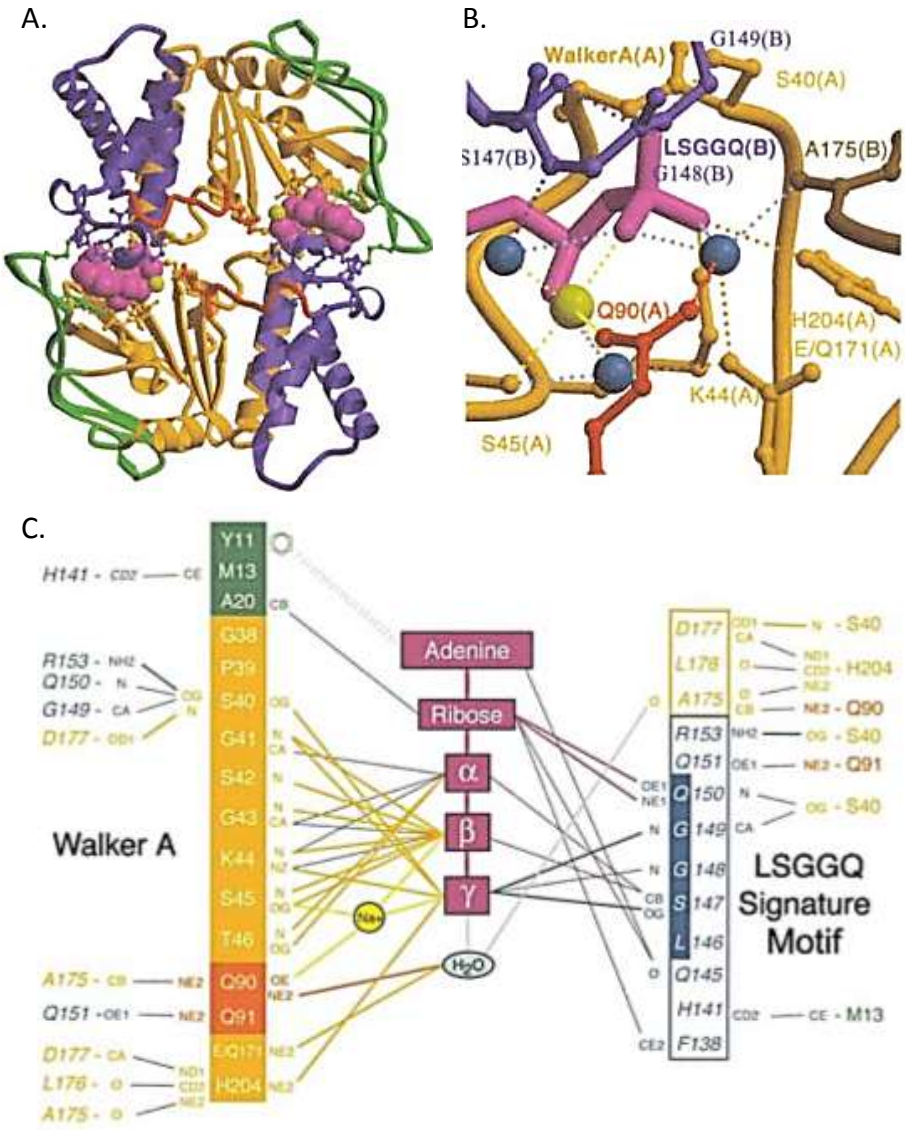


**Figure 1.6 – Structure of a nucleotide binding domain dimer.** The overall structure of the NBD dimer from MJ0796 (E171Q), a Type I expressed in *E. coli* (**A**) shows nucleotides (magenta, space-filling representation) and the associated Na+ cofactor 'sandwiched' between the Walker-A motif (purple) of one subunit "A" and the ABC signature motif (yellow) of the other subunit "B". Inspection of the active site (**B**) shows several hydrogen bonds between nucleotide (magenta, stick representation) and protein side chains (dashed line colour indicates donor residue). A summary of the side-chain:nucleotide interaction is also shown (**C**) (adapted from: Smith et al. 2002).

The ABC signature motif is also shown by mutagenesis studies as playing an important role in transporter function (Hyde *et al.*, 1990); mutations of the leucine and second glycine residues reduce ATPase activity in the case of ABCB1 and mutations of the serine residue in both NBDs of ABCB1 showed a reduced activity compared to a single mutation (Bakos *et al.*, 1997; Tombline *et al.*, 2004). This could indicate a synergistic effect which is supported by structural data from NBD-NBD dimers that indicate "head-to-tail" arrangement with the ABC signature motif forms an ATP binding interface with the Walker-A motif of the opposite NBD. This results in a nucleotide being occluded at two composite sites formed from both NBDs (see Figure 1.6 (A)) (Smith *et al.*, 2002; Tombline *et al.*, 2004; Procko *et al.*, 2006). The Q-, D- and H- loops mentioned earlier have been shown to perform important steps in enabling ATP hydrolysis and the communication of downstream energy and signals (Ambudkar *et al.*, 2006). Mutations in the Q-loop have been shown to reduce transport activity but not ATP binding (Urbatsch *et al.*, 2000). This implies that the flexibility enabled by the glutamine residue may be important for the Q-loop in the communication between TMD and NBD (Jones and George, 2002; Lawson, O'Mara and Kerr, 2008). The D-loop is found near the binding interface of the NBD dimer. It may facilitate communication between the NBD active sites and also contribute to the formation of the NBD occluded state (Jones and George, 2012; Hopfner, 2016). H-loop mutations can reduce ATPase activity and structural data indicate interactions with ATP possibly as a catalyst during hydrolysis (Zhou, Ojeda-May and Pu, 2013).

The above NBD features are common across the ABC transporter superfamily despite the substantial variation in function. This conservation has historically allowed the identification of new family members based on homology (Higgins, 1992). In terms of further classification, the ABC families found in humans are distinguished based on amino acid similarity and domain organisation (Dean, Hamon and Chimini, 2001).

### 1.2.3 Overview of Human ABC Protein Functions

The ABC family is one of the largest membrane protein families and there are 48 ABC proteins found in humans. Most of the known functions in humans involves the transport of hydrophobic compounds out of the cell for secretion or transport to other organs though also within the cell in some metabolic pathways (Dean, Hamon and Chimini, 2001). Though the sequence homology is conserved in the NBDs, differences exist that allow the distinction into seven subfamilies. These are labelled A-G with each subfamily having a number of members.

**ABCA proteins**

There are 12 full transporters with ABCA1 and ABCA4 being the best studied. ABCA1 is involved in cholesterol and HDL transport and is associated to some disorders in these pathways (Albrecht and Viturro, 2007). ABCA4 is associated to vision, transporting vitamin A derivatives in photoreceptor cells. Mutations in ABCA4 are associated to macular degeneration in Stargardt disease (Khan *et al.*, 2018).

**ABCB proteins**

This subfamily contains both full and half transporters. The best studied family member is ABCB1 which was the first human ABC transporter to be cloned and has since been the best studied (Ling and Thompson, 1974; Juliano and Ling, 1976). It is described in more detail below. Other important family members in ABCB2 and ABCB3 which are better known as TAP-1 and TAP-2 (transporter associated with antigen processing). These form a heterodimer capable of transporting small peptides into the ER that are subsequently presented as antigens by the MHC Class I system (Nöll *et al.*, 2017).

**ABCC proteins**

This family consists of 12 transporters with a large range of functions (Dean, Hamon and Chimini, 2001). One key example is ABCC1 which is a multidrug transporter described in detail later. Other examples include ABCC4 which is involved in nucleoside transport and ABCC5 which is another multidrug transporter associated to resistance to purine derivatives (Sauna, Nandigama and Ambudkar, 2004). As well as multidrug transport roles, another key member of this family is ABCC8 (or SUR1) which acts as a regulatory subunit of ATP-sensitive potassium channels (de Wet *et al.*, 2008).

**ABCD proteins**

This family is found expressed in peroxisomes and is associated to peroxisomal uptake of very long chain fatty acids (VLCFA). Dysfunctional ABCD1 can cause the

X-linked adrenoleukodystrophy disorder that results in the accumulation of VLCFA due to reduced peroxisomal oxidation (Hlaváč and Souček, 2015).

**ABCF proteins (and ABCE1)**

The ABCF family has three members and the ABCE family in human consists of just one protein; an oligo-adenylate binding protein (Dean, Hamon and Chimini, 2001). Interestingly, these families are defined by members that have no TMDs. They are not therefore associated to any membrane transport functions (Vasiliou, Vasiliou and Nebert, 2009).

**ABCG proteins**

This subfamily is atypical in that it consists of 'reverse half-transporters' that have N-terminal NBDs in contrast to other ABC transporter families (Dean, Hamon and Chimini, 2001; Vasiliou, Vasiliou and Nebert, 2009). ABCG2 is described in detail later but other important family members include ABCG5 and ABCG8 which form a heterodimer associated to transport of sterols in the liver and large intestine (J.-Y. Lee *et al.*, 2016).

Whilst this offers only an overview of the ABC families found in humans, one key message is that this superfamily is incredibly diverse in terms of the functional roles performed by each protein. In this project, multidrug transport was the primary concern.

### 1.2.4 The Multidrug Transporters

One of the major challenges in therapeutic drug treatment or even drug development is inefficacy due to resistance. Most infamously this can occur in

cancer treatment leading to much poorer prognoses (Fletcher *et al.*, 2016). Solid primary tumours can often be surgically removed, systemic or metastatic cancers require chemotherapy. In either case, the development of resistance to chemotherapy agents is known to reduce long-term survival rates. There are a plethora of mechanisms for this to occur including glutathione S-transferase mediated detoxification, reduced angiogenesis or alterations to drug targets (Krishna and Mayer, 2000). Another mechanism is by the expression of multidrug transporters that facilitate efflux of cytotoxic drugs (Konig, Muller and Fromm, 2013).

The triumvirate of ABCB1, ABCC1 and ABCG2 are the main ABC transporter efflux pumps implicated in this multidrug resistance (Szakács *et al.*, 2006). ABCG2, as the main subject of this study, is discussed in Section 1.3 with descriptions of these other important ABC transporters given below.

**ABCB1**

ABCB1 (or P-glycoprotein), was the first identified human ABC transporter and is expressed as a full transporter (Ling and Thompson, 1974; Juliano and Ling, 1976). The structure was recently resolved (3.4Å) by Kim & Chen (2018) in the presence of ATP (see Figure 1.7).

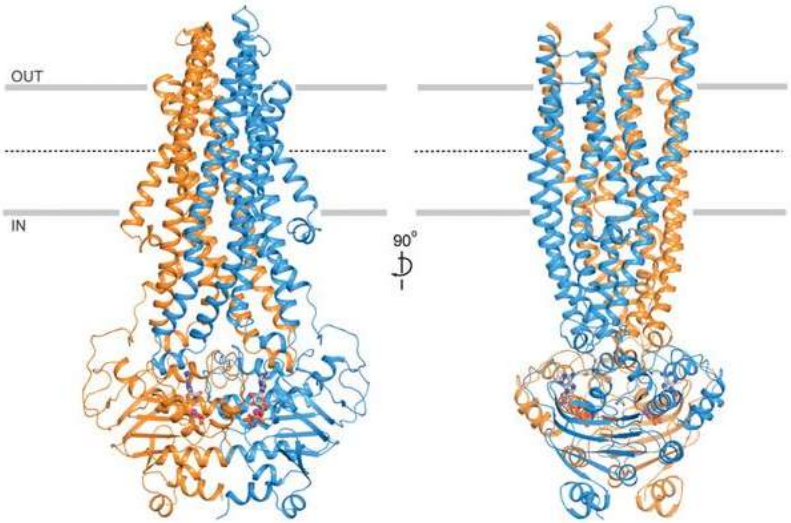


**Figure 1.7 – Structure of human ABCB1.** The different subunits of E556Q/E1201Q double mutant ABCB1 are displayed in orange and blue. ATP is found between the NBDs and the TMDs appear in an outward-facing conformation (adapted from: Kim & Chen 2018).

In the presence of ATP, ABCB1 appears to adopt an outward-facing orientation in terms of the drug binding region which supports ATP binding promoting drug release as opposed to ATP hydrolysis (Martin *et al.*, 1999; Kim and Chen, 2018).

ABCB1 has been associated to poor treatment outcomes in acute leukaemia, and overexpression is also associated to poorer outcomes in breast cancer (Marie, Zittoun and Sikic, 1991; Trock, Leonessa and Clarke, 1997). When expressed in cancer cells, it can confer resistance to various chemotherapy agents including doxorubicin and vinblastine (Sharom, 2011). In addition to these agents, other therapeutically important compounds have been identified as ABCB1 substrates. These include members from a number of families such as antibiotics, synthetic and natural opioids and calcium channel blockers (Cascorbi, 2011). A number of single nucleotide polymorphisms (SNPs) occur in the *MDR1* gene that encodes ABCB1 which have been associated to altered bioavailability patterns for some

drugs and differing resistance to therapeutics (Hodges *et al.*, 2011). Most common SNPs are 1236C>T (G412G), 2677G>T (A893S) and 3435C>T (I1145I) with 435C>T in particular being associated to disease predisposition and response to drug treatment though the mechanism by which this occurs is unknown (Fung and Gottesman, 2009).

There are a number of potential physiological substrates for ABCB1 including a number of peptides, lipids and cytokines such as interleukins 2 and 4 (Rao, Fine and Scarborough, 1994; Drach *et al.*, 1996). However, it appears that it does not play an essential physiological role except under chemical challenge based on normal phenotypes being observed in mouse studies even in double knockout experiments (Schinkel *et al.*, 1994). These mice did however have much different responses when chemically challenged with a 100-fold increased sensitivity to the neurotoxin ivermectin for example with much higher drug concentrations found in the brain tissue of knockout mice (Schinkel *et al.*, 1997). The impact ABCB1 has on the transported drug substrates is amplified due to the broad tissue distribution across several important barrier sites. For example, it is expressed at the apical surface of renal tubular cells, bile canaliculi, and intestinal epithelium as well as at the luminal surface of capillary endothelial cells in the blood-testes and blood-brain barriers (Cascorbi, 2011).

**ABCC1**

ABCC1 (or multidrug resistance associated protein 1 (MRP1)) was identified in and cloned from a multidrug resistant small cell lung cancer cell line (Cole *et al.*, 1992).

As well as the subunits of a typical full transporter, ABCC1 also has an additional $TMD_0$ with an unclear function (Yang *et al.*, 2007; Jiye and Jianting, 2011; Johnson and Chen, 2017). As has been shown in several studies, the most well-known endogenous transport substrate for ABCC1 is cysteinyl leukotriene C4 (see Figure 1.8) (Johnson and Chen, 2017). ABCC1 also transports glucuronides and sulphate conjugates of steroid hormones and bile salts (Leier *et al.*, 1994; Deeley, Westlake and Cole, 2006). In terms of multidrug resistance, ABCC1 can transport a number of therapeutic drugs including doxorubicin, vincristine and etoposide (Deeley, Westlake and Cole, 2006; Slot, Molinski and Cole, 2011). ABCC1 is expressed in the basolateral membrane of epithelial cells in most tissues. Levels are higher in the lung, testes, kidney and other barrier sites. This is conducive to the suggestion that its primary role is in the prevention of toxin accumulation induced tissue damage (Cole, 2014). As well as playing a protective role in normal tissues, ABCC1 is associated to poorer clinical outcomes in a number of cancers (including prostate cancer and breast cancer) (Deeley, Westlake and Cole, 2006; Slot, Molinski and Cole, 2011).

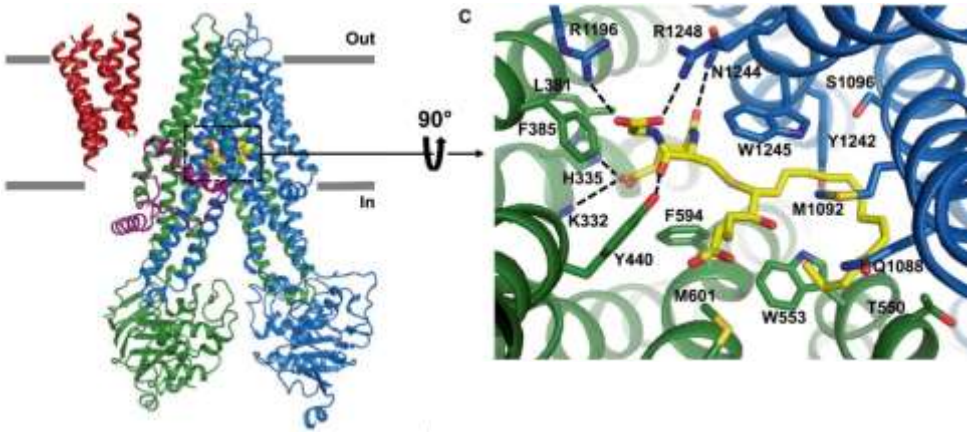


**Figure 1.8 – Structure of bovine ABCC1.** The left hand panel shows TMD0 (red) attached via the Lasso region (purple) to subunit 1 (green). Leukotriene C4 (yellow) is found in the drug binding region between TMD1 (green) and TMD2 (blue). This binding region is highlighted (right) with key residues indicated (adapted from: Johnson & Chen 2017).

Interestingly, the recent structural data (Figure 1.8) indicate that substrate binding, which requires composite binding sites in *both* TMDs, may promote ATP binding by bringing the NBDs into closer proximity (Johnson and Chen, 2017).

## 1.3 ABCG2 and its Role in Health and Disease

### 1.3.1 Genetics and Regulation of Expression

The human *ABCG2* gene stretches over 66kb including 16 exons ranging from 60 to over 500bp and 15 introns. The gene is located on chromosome 4, 4q21-4q22 (Bailey-Dell *et al.*, 2001). The translational start site is in the second exon with the ABC signature sequence found in exon 6. Similarly to those described for other ABC transporters, the promoter for the *ABCG2* gene is TATA-less and has multiple Sp1, AP1 and AP2 sites. It is located more than 300bp away from the transcriptional start site (Bailey-Dell *et al.*, 2001). There are a number of regulatory elements in the *ABCG2* promoter; oestrogen response element,

progesterone response element, hypoxia response element, NFkB response element and an aryl hydrocarbon response element (Ee *et al.*, 2004; Krishnamurthy *et al.*, 2004; Yasuda *et al.*, 2006; To *et al.*, 2011; Zhang *et al.*, 2018). As a result there are a number of transcriptional mechanisms by which the expression of ABCG2 can be regulated.

Expression can also be regulated by epigenetic factors including promoter histone hyperacetylation or hypomethylation of the CpG island. These mechanisms have been reported in some drug resistant cancer cell lines (To, Zhan and Bates, 2006; Turner *et al.*, 2006).

Regulation by post-translational mechanisms have also been reported, for example the reduced maturation induced by treatment of some cancer cell lines with oestradiol (Imai *et al.*, 2005). Several miRNAs have also been shown to regulate ABCG2 expression (Robey *et al.*, 2009). For example, miR-212, miR-328, miR-519 and miR-520 each directly inhibit ABCG2 expression (Li *et al.*, 2011; Turrini *et al.*, 2012; Haenisch, Werk and Cascorbi, 2014).

Though there can be varied stimuli for altered expression of ABCG2, none have yet been successfully exploited for therapeutic purposes.

### 1.3.2 Current Structural Understanding

Knowledge of protein structure is a keystone to the understanding of function. This dogmatic view appears no less true in the study of ABCG2 where, at the start of this study, knowledge in both regards has been limited. Since it was first discovered, even during the course of this project, remarkable strides have been

made in the structural understanding of ABCG2 structure (Doyle *et al.*, 1998; McDevitt *et al.*, 2006; Mark F. Rosenberg *et al.*, 2015; Taylor *et al.*, 2017; Jackson *et al.*, 2018). These data have helped rationalise efforts to improve the understanding of the biochemistry underlying transporter function (Haider *et al.*, 2015; Cox *et al.*, 2018). Continued improvements to our understanding of ABCG2 may one day open the door to targeted inhibitors and genuine progress in drug design efforts to overcome transporter mediated pharmacological problems.

As briefly described above, as a member of the 'G' subfamily of ABC transporters, ABCG2 is a 'reverse half transporter' (Mao and Unadkat, 2015). This means that it is in the reverse orientation compared to the typical ABC transporter with an N-terminal NBD (Kerr, Haider and Gelissen, 2011). As a 'half transporter' it is expressed as a monomeric unit with only one NBD and TMD and forms at least homodimers in order to function (Robey *et al.*, 2009). The monomeric unit peptide is 665 amino acids in length with a molecular weight of 72kDa. The TMD consists of 6 transmembrane segments with short α-helical extensions to TM helices 5 and 6 adopting a fold unique to the ABCG family (Wang *et al.*, 2008; László, Sarkadi and Hegedüs, 2016). Some other notable features of the transmembrane region are located in the extracellular loop between helices 5 and 6 (Mo, Qi and Zhang, 2012). There are cysteine residues at positions 592 and 608 that form an intramolecular disulphide bond and also the single N-linked glycosylation site N596 (Henriksen *et al.*, 2005; Wakabayashi *et al.*, 2007; Nakagawa *et al.*, 2009). These are both implicated in trafficking and stability. There is also another

cysteine residue at position 603 that is involved in the formation of an intermolecular bond with a previously suggested role in ABCG2 oligomerisation. However, neither oligomerisation nor transporter activity are affected by mutation of this residue (Kage, Fujita and Sugimoto, 2005; Haider *et al.*, 2011; Mo, Qi and Zhang, 2012).

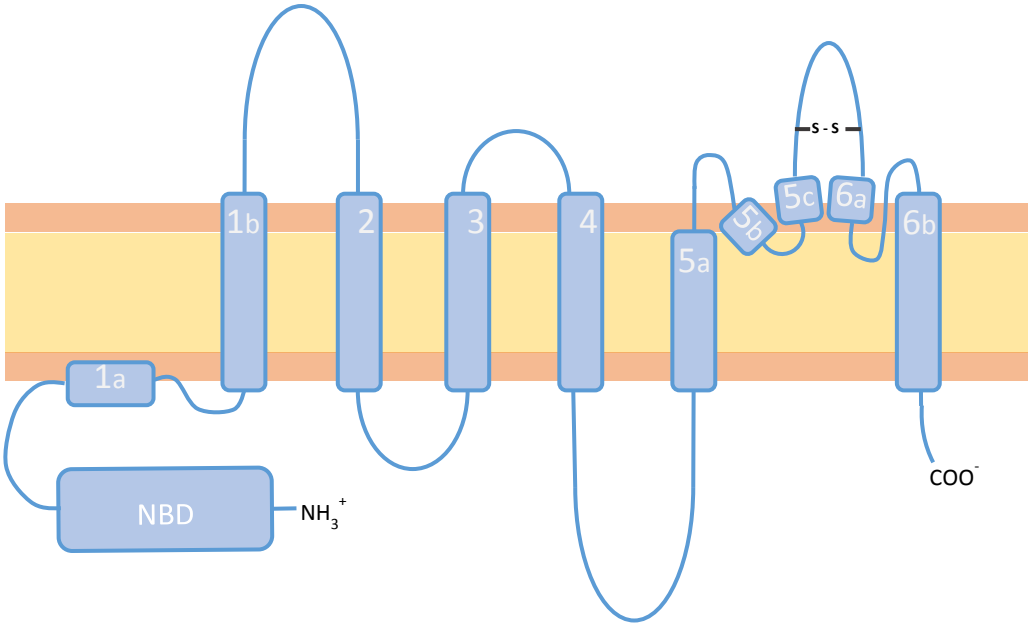


**Figure 1.9 – General topology of the ABCG2 Monomer.** The monomeric unit of ABCG2 consists of 655 amino acid residues arranged in 'reverse' compared to the typical ABC transporter format with an N-terminal nucleotide binding domain (NBD). There are 6 transmembrane helices (TMDs) (approximate position of the membrane shown in orange/yellow). The single intramolecular disulphide bond between helices 5 and 6 is also shown (adapted from: Horsey et al. 2016; Jackson et al. 2018).

Based on the common pattern in other ABC transporters, the probability was that ABCG2 also functioned as a dimer. However, there was also considerable evidence for higher order oligomers. Tetrameric ABCG2 has been indicated by native gel

electrophoresis and EM (electron microscopy) studies with some EM data also indicating the presence of stable homo-octameric units (Xu *et al.*, 2004; McDevitt *et al.*, 2009; Dezi *et al.*, 2010). However, the presence of these structures in EM grids may be indicative of protein packing rather than direct evidence of physiological relevance. In whole cells, fluorescence correlation spectroscopy analysis not too dissimilar to that employed in this project and stepwise photobleaching analysis were used that indicated a predominantly tetrameric organisation (Wong *et al.*, 2016). In the face of this however, the most recent structural data have resolved only dimeric ABCG2 isoforms (Taylor *et al.*, 2017; Jackson *et al.*, 2018).

For several decades the structures of membrane proteins in general have significantly lagged behind in terms of number and resolution compared to soluble proteins. This lack of high resolution structural data was reflected in our limited understanding of ABCG2 and a crystal structure at atomic resolution is still absent at the time of writing this thesis though much progress is promised with the advent of cryo-EM 'resolution revolution' (Bai et al. 2014; Kapoor et al. *in press*). However, the x-ray crystal structure of the heterodimeric sterol transporter ABCG5/G8 has been recently resolved and subsequently proven to be an incredibly useful tool in understanding 'G' family ABC transporters (J.-Y. Lee *et al.*, 2016). In particular this data described a compact structure with no crossing-over of helices, dissimilar to all other ABC exporter proteins, for example ABCB1 (J.-Y. Lee *et al.*, 2016) (see Figure 1.10).

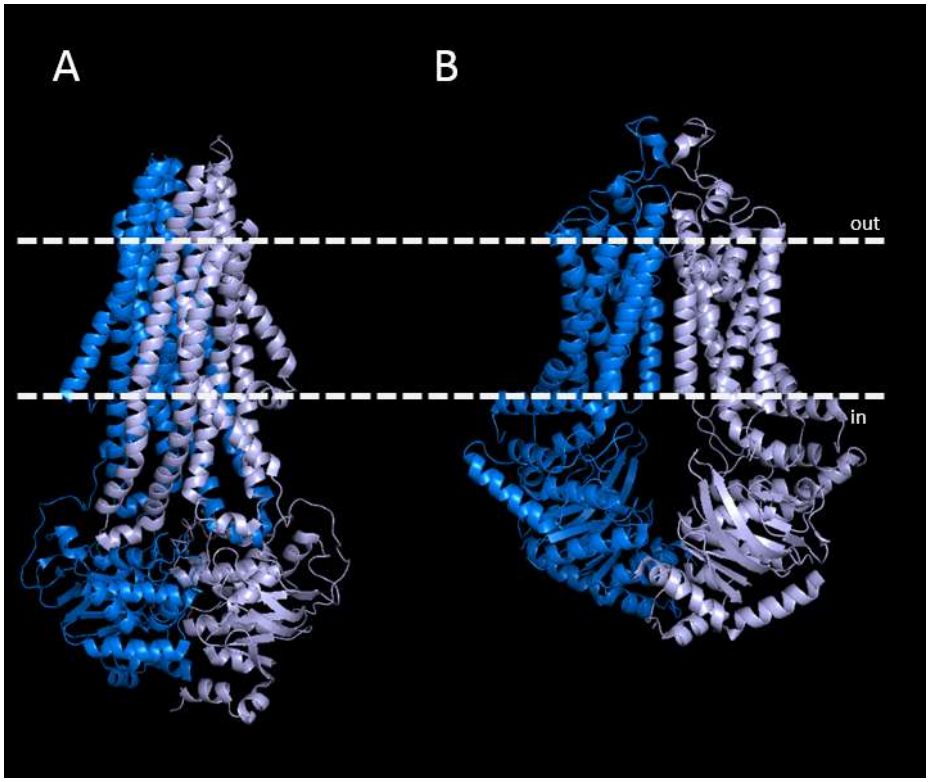


**Figure 1.10 – Comparison of ABC transporter folds.** ABCB1 (A) resolved by x-ray crystallography (PDB: 6C0V) follows a Type I fold with crossing-over of helices and an extended appearance compared to ABCG2 (B) with NBDs protruding into the cytoplasm. The cryo-EM structure of ABCG2 (PDB: 6FFC) resolved in the presence of MZ29 shows a more compact structural fold similar to Type II (Jackson *et al.*, 2018; Kim and Chen, 2018).

The compact arrangement which resembles a bacterial Type II importer is supported by the presence of a "G-family fold". Predictably, this structure was followed by homology models for ABCG2 that included the fold indicated by the ABCG5/G8 structure (László, Sarkadi and Hegedüs, 2016; Khunweeraphong, Stockner and Kuchler, 2017). In ABCG2, the fold appears to form a transmission interface composed of elbow helix, intracellular loop 1 and the upper surface of the NBD dimer (Figure 1.11). Mutations in this region severely impact protein function. For example, E451D mutations had reduced transport activity but

hyperactive ATPase indicated this mutation uncoupled drug recognition and hydrolysis (Khunweeraphong, Stockner and Kuchler, 2017). The homology models were accompanied by cryo-EM data (see Figure 1.11) for ABCG2 dimers that again supported the "G-family fold" (Taylor *et al.*, 2017; Jackson *et al.*, 2018). Overall the structural data were similar and, as the cryo-EM data were gathered using protein stabilised by an inhibitory Ko143 derivative (MZ29), it is possible that any differences represent the protein being resolved in an inhibited state. Downstream from the generation of structures, using the homology model based on the ABCG5/G8 structure, a possible binding site was identified by molecular docking analysis that supported novel mutational analysis (Cox *et al.*, 2018). This site was not present in the central cavity, a canonical site for drug binding, but instead in an intracellular, lipid facing site on the TMDs (Figure 1.11).

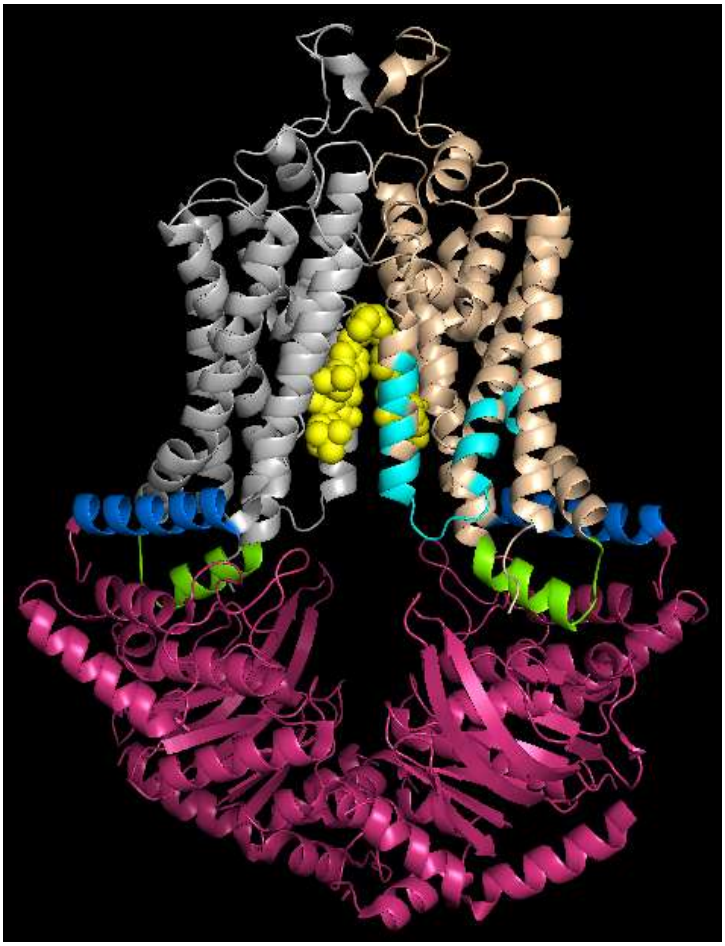

**Figure 1.11 – Structure of human ABCG2.** ABCG2 has a compact structure with NBDs (pink) that are kept close to the cell membrane by the "G-Family Fold". This fold consists of the elbow helix (dark blue), the intracellular loop 1 (green) and the surface of the NBDs. The central cavity of the cryo-EM structure shown here (PDB:6FFC) is occupied by an inhibitory Ko143 derivative, MZ29 (yellow) but other regions have been shown to have drug binding capacity (light blue) (Khunweeraphong, Stockner and Kuchler, 2017; Cox *et al.*, 2018; Jackson *et al.*, 2018)

### 1.3.3 The Transport Mechanism

With the advent of improved structural data some advances were also achieved in the understanding of ABCG2 molecular mechanisms. A full molecular model of ABCG2 transport mechanism would involve the description of the protein in a number of transient conformations as the transported substrate was moved through the membrane. This mechanism might not necessarily be the same for different structural classes of substrate (Cox *et al.*, 2018). Resolving the labyrinth of possible conformational changes representing the transport cycle would not necessarily involve the generation of high resolution structural data in each step. However, the research field remains someway off this level of molecular understanding. Significant knowledge of ABCG2 transport mechanism does exist. At the most basic level, the transport cycle must consist of both the recognition of and then transport of substrate.

For some time the general consensus has been that there are multiple drug binding sites on ABCG2 (Clark, Kerr and Callaghan, 2006). This means that rather than there being a single binding site capable of recognising the multitude of different transport substrates there are a series of spatially separate sites (Shukla *et al.*, 2006; Giri *et al.*, 2009). Though it is often assumed that several sites could exist within the central cavity of ABCG2 (Mao and Unadkat, 2015), this is not necessarily the case. Recent ABCG2 structural data reaffirmed the importance of the central cavity and identified sites that may be common to the transport of many different substrates. However, these data were resolved with the cavity

occupied by bound inhibitor (*de novo* synthesised Ko143 derivative) as opposed to transport substrate (Jackson *et al.*, 2018). The cavity of ABCG2 appeared to be lined with some residues that have been shown to affect transport. However, several other residues affecting transporter lie outside of this region (Robey *et al.*, 2003; Ejendal *et al.*, 2006; Haider *et al.*, 2015; Cox *et al.*, 2018). Further examination of possible transport pathways will come in the main discussion following data collected during this thesis that impacts on this interpretation.

In terms of the transport cycle itself, the most commonly used model is the ATP switch model (Higgins and Linton, 2004; Linton and Higgins, 2007). Substrate binding induces conformational change that increases the affinity for ATP at the NBDs. Binding of ATP induces conformational changes that pass the substrate from the initial site to an outward facing low affinity site and substrate is released (McDevitt *et al.*, 2008; Johnson and Chen, 2018). ATP hydrolysis occurs in the fully closed NBDs and the protein is reset via the release of ADP and inorganic phosphate (Higgins and Linton, 2004; Linton and Higgins, 2007). This process (shown in Figure 1.12) will likely become better defined as better structural data become available and is likely to be variable based on the differing nature of ABCG2 substrates.

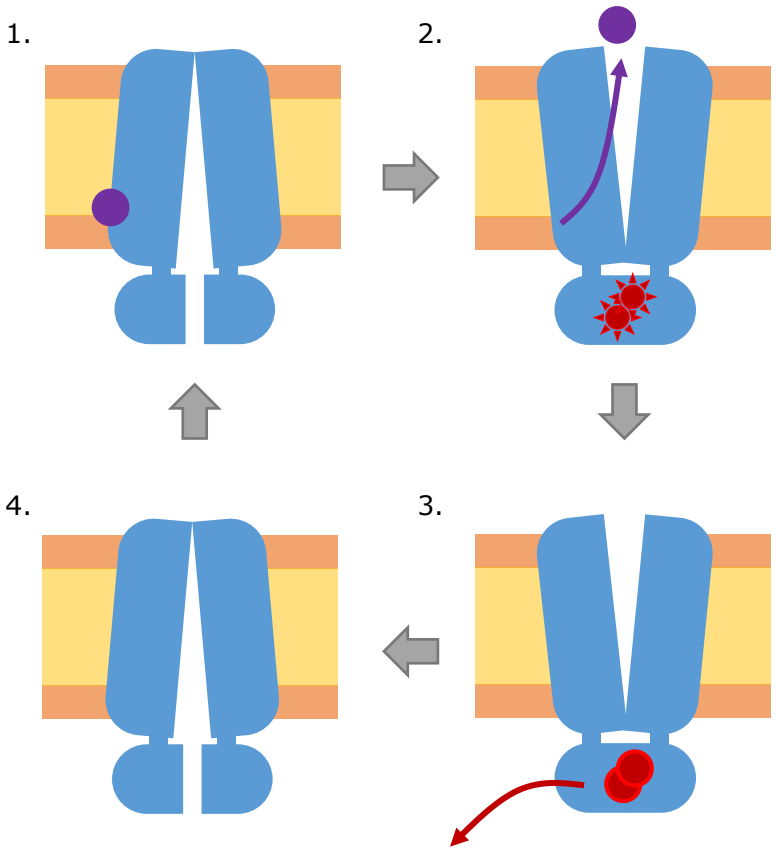


**Figure 1.12 – Schematic of the ATP-switch model.** Substrate binding initiates conformational changes that promote the binding of ATP (1). The binding of ATP induces further conformational changes that result in the transporter moving to an outward-facing state allowing for substrate to be released (2). The closed dimer facilitates the hydrolysis of ATP to ADP which is then released (3) with the energy produced used to reset the transporter (4).

### 1.3.4 Role in Healthy Tissues

ABCG2 is widely recognised as a multidrug transporter and, even in healthy tissues this has been where the main focus of work has been (Robey *et al.*, 2009). This function and the wide reaching impact on pharmacology are considered in Section 1.4. There is much overlap considering the exogenous toxin extrusion (or adsorption restriction) function of ABCG2 but there are also a number of important functions in endogenous transport processes.

**Blood-brain barrier**

Other ABC transporters, including ABCB1 for example, have been shown to be active in the function of the blood-brain barrier (Mahringer and Fricker, 2016). ABCG2 is expressed on the luminal side of brain endothelial capillaries (Hori *et al.*, 2004). Based on mRNA analysis, there is several hundred fold less expression in the cortex tissue consistent with a barrier tissue expression pattern (Cisternino *et al.*, 2004). ABCG2 has been shown to have higher mRNA expression levels than either ABCB1 or ABCC1 at the blood-brain barrier (Eisenblätter, Hüwel and Galla, 2003; Zhang *et al.*, 2003). Evidence continues to build that ABCG2 has an important role in restricting the penetration of a number of compounds (e.g. the anticancer drug temozolomide) into brain tissue (Mao and Unadkat, 2015; de Gooijer *et al.*, 2018). As well as therapeutic drugs, this has been shown to include amyloid-beta, the principal component of amyloid plaques associated to Alzheimer's disease. ABCG2 appears to restrict the permeability to amyloid-beta of brain endothelial tissue (Do *et al.*, 2012).

**Kidney**

In the kidney, ABCG2 has been identified in proximal tubule and cortical tubule cells (Fetsch *et al.*, 2006; Huls *et al.*, 2008). These data implicated ABCG2 in the renal excretion of drugs as well as endogenous metabolites (Robey *et al.*, 2009). Urate for example, which is the end product of purine metabolism in humans, was identified as a transport substrate of ABCG2 following genome wide association study (GWAS) analysis that showed elevated serum urate levels associated to SNPs in ABCG2 (Woodward *et al.*, 2009; Woodward, 2015).

**Gastrointestinal tract**

The highest expression of ABCG2 in the GI tract is in the duodenum and expression then decreases along the digestive tract (Gutmann *et al.*, 2005). Expression in this system indicated that the transporter may have a role in limiting the absorption of some drugs (Robey *et al.*, 2009). Work has indicated a role in limiting the uptake of dietary carcinogens (e.g. 2-amino-1-methyl-6-phenylimidazo (4,5-b)pyridine (PhIP) - found in cooked meats) (van Herwaarden *et al.*, 2003). As discussed below, expression in this system plays a key role in drug distribution.

**Liver**

Expression of ABCG2 has been observed in hepatocytes, canalicular membrane tissue, bile ducts and the blood vessel endothelium in humans (Maliepaard *et al.*, 2001; Vander Borght *et al.*, 2006). Though there is no evidence for a liver specific endogenous metabolite for ABCG2, it transports its substrates into bile for biliary excretion (Mao and Unadkat, 2015).

**Placenta**

ABCG2 is expressed in the syncytiotrophoblasts of embryonic villus. Here it plays a role in protecting the developing foetus by transporting toxins from the foetal to the maternal space (Jonker *et al.*, 2000). For example, PhIP was shown to be transported in experiments with perfused human placental tissue (Myllynen *et al.*, 2008).

**Breast Tissue**

Interestingly, where the proposed role in the placenta is in the protection of the foetus, ABCG2 appears to possibly concentrate toxins in breast milk (van Herwaarden *et al.*, 2006). This may stem from a physiological role of secreting riboflavin (B vitamin required for the metabolism of fats) which has been shown to be a physiological role of ABCG2 (van Herwaarden *et al.*, 2007).

**Testes**

ABCG2 is found in the luminal capillary endothelial wall of the testes. Here it is believed to play a role in protecting germinal stem cells from exposure to toxins (Fetsch *et al.*, 2006; Robey *et al.*, 2009).

**Haematopoietic Stem Cells**

The expression of ABCG2 in a subpopulation of bone marrow cells appears to protect some haematopoietic stem cells from toxin exposure and hypoxia-induced stress response (Goodell *et al.*, 1996; Zhou *et al.*, 2002). However, ABCG2 is not necessary for normal haematopoiesis (Jonker *et al.*, 2002). In fact the absence of

any ABCG2 antigens defines the Jr(a-) blood group which confers no known physiological consequence (Castilho and Reid, 2013).

### 1.3.5 Role in Disease

The most recognised role of ABCG2 in disease is based on its drug efflux capacity. As a result of this the protein is involved in the restriction of available therapeutic concentrations by preventing absorption or promoting excretion (Giacomini *et al.*, 2010). This includes a role in multidrug resistance in cancer treatment but ABCG2 is also associated to other diseases.

ABCG2 expression is upregulated in Alzheimer's disease patient brain tissue, and the protein is involved in the transport of amyloid-beta protein across the membrane. Aberrant trafficking of amyloid-beta could contribute to the accumulation observed in Alzheimer's disease (Xiong *et al.*, 2009; Do *et al.*, 2012). Based on the role of ABCG2 in the excretion of urate, reduced functionality has been associated to hyperuricemia and gout. The Q141K (421C>A) polymorphism in particular is associated to predisposition to this condition via its impact on NBD stability and decreased protein expression (Woodward *et al.*, 2009, 2013; Woodward, 2015). This SNP has a frequency of approximately 30% in Asian populations, 10% in Caucasian populations and <5% in African and African-American populations (Lepper *et al.*, 2005). This SNP has also been shown to affect the pharmacokinetics of diflomotecan during a phase I study where heterozygous 421C/A individuals had significantly higher plasma concentrations compared to homozygous wild-type individuals (Sparreboom *et al.*, 2004).

Based on better characterisation of physiological transport substrates of ABCG2, the role of this protein in other diseases will probably become more apparent. However, ABCG2 is already much better known for its impact on disease and therapy via drug transport. Through genetic variation in the transporter, expression in cancer tissue or even just endogenous expression in healthy tissue, ABCG2 has a significant role in drug distribution and pharmacology.

## 1.4 Pharmacological Importance of ABCG2

ABCG2 plays a major role in the limiting the efficacy of therapeutic drugs by extruding them from cells (Natarajan *et al.*, 2012). This can limit the bioavailability in both normal, healthy tissues and, most infamously, in cancer tissues.

**ABCG2 in Cancer**

Expression of ABCG2 in a number of cancer tissues is associated to multidrug resistance (Ross and Nakanishi, 2010). It was first cloned from placental tissue and breast cancer tumour cell lines (Allikmets *et al.*, 1998; Doyle *et al.*, 1998). As a result of its identification in multidrug resistant breast cancer derived cells, it has historically been referred to as breast cancer resistance protein (BCRP). A common theme is the difficulty in associating ABCG2 expression in cancer tissues to resistance mediated by its transport function. It is possible that expression is, in some cases, simply as a marker for other mechanisms stemming from cancer associated signalling pathways (e.g. for cell proliferation and metastasis) (Xiang *et al.*, 2011; Natarajan *et al.*, 2012).

There is significant evidence implicating ABCG2 in the most common haematological malignancies other than multiple myeloma (Raaijmakers *et al.*, 2005; Robey *et al.*, 2009). In acute myeloid leukaemia ABCG2 appears to have a strong prognostic value despite few of the frontline treatments being known to be transport substrates (Natarajan *et al.*, 2012). For example high ABCG2 expression has been associated to failure to achieve complete remission following treatment including a non-substrate anthracycline, cytosine arabinoside (Steinbach *et al.*, 2002). Nonetheless other studies have also concluded on the association of higher ABCG2 and lower overall survival rates but not always lower frequencies of complete remission (Benderra *et al.*, 2005; Uggla *et al.*, 2005). In acute lymphoid leukaemia, though some common therapies include known ABCG2 substrates (e.g. methotrexate) there is less convincing evidence for linking ABCG2 expression and clinical outcome (Suvannasankha *et al.*, 2004). Several studies found no correlation between the mRNA expression of ABCG2 and paediatric patient outcome (Sauerbrey *et al.*, 2002; Kourti *et al.*, 2007). One study even found that higher ABCG2 mRNA levels were associated to better 5-year survival frequencies (Cortez *et al.*, 2009). In chronic myeloid leukaemia, a number of newer drug treatments have been shown to be substrates of ABCG2 but these drugs, nilotinib, imatinib and dasatinib, also act as ABCG2 inhibitors (Burger *et al.*, 2004; Houghton *et al.*, 2004; Brendel *et al.*, 2007; Hiwase *et al.*, 2008; Tiwari *et al.*, 2009; Dohse *et al.*, 2010). The overall impact of ABCG2 expression on their efficacy is difficult to quantify. It is possible that co-administration of these with other

chemotherapeutics increases the sensitivity of cells to those other agents (Oostendorp *et al.*, 2009).

There is a particularly mixed picture in solid tumours based on an overall lack of studies having been performed. The relationship between ABCG2 expression and overall clinical outcome has been mainly assessed in non-small cell lung cancer (NSCLC) and breast cancer (Natarajan *et al.*, 2012). One breast cancer study reported correlation between ABCG2 mRNA expression and anthracycline-based agents (5-fluorouracil, adriamycin/epirubicin, and cyclophosphamide) but not with cyclophosphamide, methotrexate, and 5-fluorouracil-treated patients (Burger *et al.*, 2003). This is despite anthracyclines not being recognised as ABCG2 substrates meaning the role of this protein is difficult to elucidate. In NSCLC, a study found high ABCG2 expression to be a predictor for short survival in patients with advanced disease treated with platinum-based chemotherapy (Ota *et al.*, 2009). Another study showed the response to platinum-based chemotherapy again correlated with the expression of ABCG2 but not with other transporters (Yoh *et al.*, 2004). Platinum conjugated therapies have not otherwise been shown to by ABCG2 substrates however.

Some recent studies have focussed on the role of a side population of cells with "stem cell-like" properties including quiescence and drug resistance that are found in many tumours (Natarajan *et al.*, 2012). ABCG2 is a major contributor to this side-population phenotype and is often co-expressed with stem cell markers including CD133, Nrf2, Notch1 and Oct-4 (Li, Zeng and Ying, 2011; Pauklin *et al.*,

2011; Yang, Ma and Liu, 2015). For example, colon cancer cells grown from clinical resection samples showed a number of stem cell properties including ABCG2 expression and were resistant to irinotecan (an ABCG2 substrate) (Fang *et al.*, 2010). This was also observed *in vitro* where SW480 colon cancer cells were should to be resistant to ininotecan and Fluorocil which are both ABCG2 substrates (Theile *et al.*, 2009).

Though some associations between ABCG2 and cancer have been highlighted above, the details of its role in pathogenesis and subsequent treatment remain elusive. ABCG2-mediated multidrug resistance in cancer is nonetheless the focus of ongoing research with no current clinical data yielding an effective method to overcome this phenomenon. This is alongside studies of the much wider pharmacological impact based on the range of other affect drug families.

**ABCG2 in Drug Distribution: Trouble, Tool or Target?**

The list of known ABCG2 substrates and inhibitors has been ever increasing. Above, some details were given where ABCG2 expression can influence clinical outcome of treatment with chemotherapy agents. There is also a broad substrate range outside of chemotherapy with some examples summarised in Table 1.1. Healthy tissues in which ABCG2 is most highly expressed tend to be at key barrier sites. This expression pattern lends itself to limiting the adsorption and

| Antibiotics | |
|---|---|
| Erythromycin (Janvilisri *et al.*, 2005) | 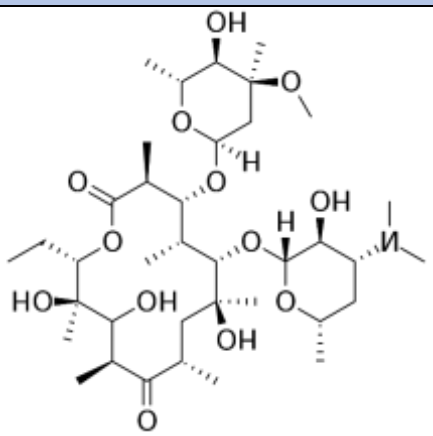 |
| Moxidectin (Perez *et al.*, 2009) | 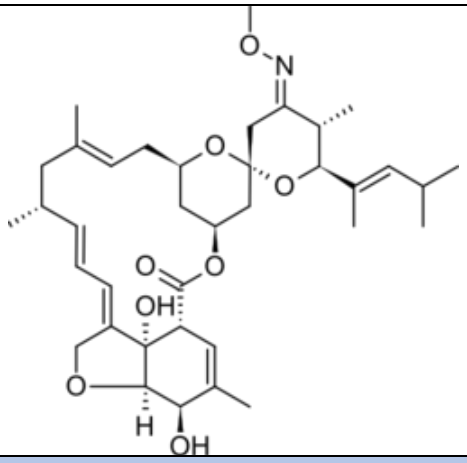 |
| **Antivirals** | |
| Ganciclovir (Hu and Liu, 2010) | 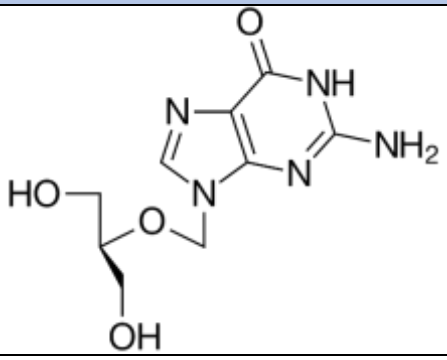 |
| Abacavir (Pan, Giri and Elmquist, 2007) | 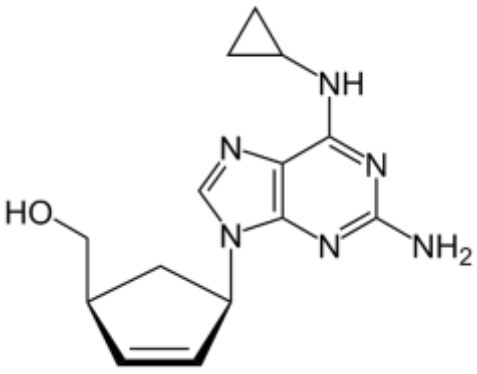 |

| Anti-inflammatories | |
|---|---|
| (van der Heijden *et al.*, 2004) | 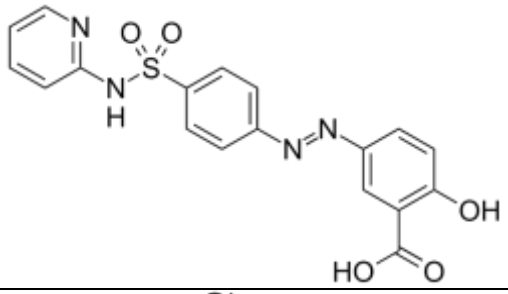 |
| Diclofenac (Lagas *et al.*, 2009) | 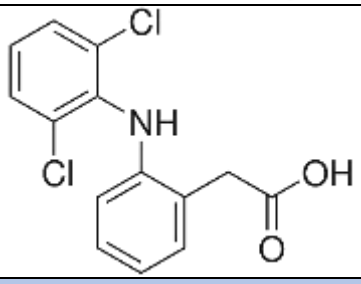 |
| **Others** | |
| Rosuvastatin (HMG-CoA reductase inhibitor) (Huang, Wang and Grimm, 2006) | 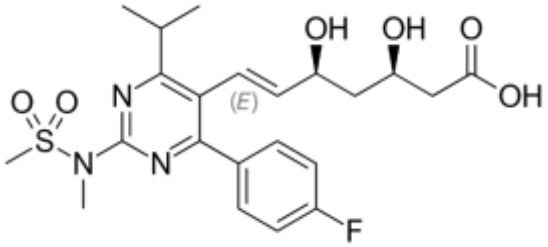 |
| Prazosin (alpha-1-adrenergic receptor antagonist) (Litman *et al.*, 2000) | 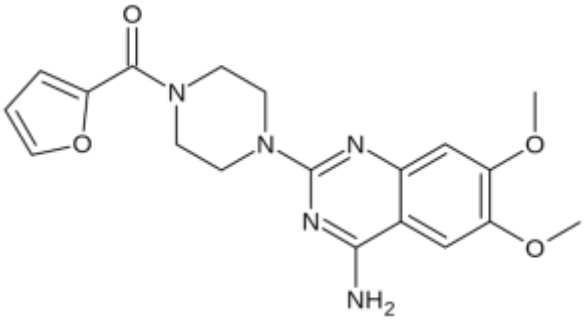 |
| Kaempferol (flavonoid) (An, Gallegos and Morris, 2011) | 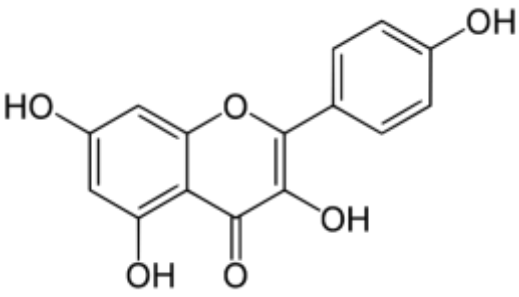 |

**Table 1.1 – Example non-chemotherapeutic ABCG2 substrates.** In addition to chemotherapy agent transport capacity, ABCG2 also transports a variety of other drugs with some examples given here.

subsequent bioavailability of drug substrates (Mao and Unadkat, 2015; Horsey *et al.*, 2016).Current understanding is aided by a number of studies in based on mouse models. For example, in the kidney and liver, ABCG2 is involved in the excretion of drugs. In Abcg2$^{-/-}$ mice or those co-administered with the inhibitor pantoprazole the systematic clearance of intravenously administered methotrexate was much reduced compare to wild type mice (Breedveld *et al.*, 2004).

Another challenge is in variable pharmacogenetics of ABCG2. The best studied SNP is Q141K which has been associated to predisposition to gout. In example studies, due to reduced transporter activity in patients with the Q141K polymorphism, the AUC (area under the curve) and $C_{max}$ (maximum concentration) in plasma pharmacokinetic studies was increased for orally administered statins including rosuvastatin, atorvastatin and simvastatin (J E Keskitalo *et al.*, 2009; Jenni E Keskitalo *et al.*, 2009; Birmingham *et al.*, 2015). Therefore the expression of ABCG2 in healthy tissues can limit the bioavailability of drugs and population variation can mean the response in different individuals may be different (Giacomini *et al.*, 2013). For example patients with the above ABCG2 polymorphism have an increased susceptibility to gefitinib-induced diarrhoea whilst undergoing treatment with this drug (Cusatis *et al.*, 2006).

Another common clinical consideration is drug-drug interactions (DDIs). ABCG2 has been implicated in a number of DDIs (Giacomini *et al.*, 2010). As an example, rosuvastatin is affected by a number of different drugs that are summarised in

Table 1.2. This occurrence was also observed in an early study that showed co-administration of topotecan with the inhibitor elacridar increased the bioavailability of topotecan from 40% to 97% by oral administration in cancer patients (Kruijtzer *et al.*, 2002). So, as well as being a pharmacological challenge, it is possible that ABCG2-mediated DDIs could also provide a tool for enhancing therapies.

Considering its importance in the absorption and distribution of drugs, regulatory guidelines have been released that incorporate suggestions for assessing the impact of ABCG2 and other transporters (Giacomini *et al.*, 2010; EMA, 2012; Prueksaritanont *et al.*, 2013). There are particular considerations that need to be taken into account. In reference to the ABCG2-mediated variation in potential response to drugs based on polymorphisms, drug trials where the impact of

| Perpetrator Drug | ΔAUC (%) | $\Delta C_{max\ (\%)}$ | Reference |
|---|---|---|---|
| Tipranavir/Ritonavir | 37 | 123 | (Pham *et al.*, 2009) |
| Atazanavir/Ritonavir | 213 | 600 | (Busti *et al.*, 2008) |
| Lopinavir/Ritonavir | 110 | 370 | (Kiser *et al.*, 2008) |
| Cyclosporine | 610 | 960 | (Simonson *et al.*, 2004) |
| Eltrombopag | 55 | 103 | (Allred *et al.*, 2011) |
| GSK1292263 | 39 | - | (Polli *et al.*, 2013) |

**Table 1.2 – Example perpetrator drugs involved in ABCG2-mediated drug-drug interactions with rosuvastatin.** The drugs (or drug combinations) along with the associated changes in AUC and $C_{max}$ are given.

ABCG2 is suspected should take this into account. A typical trial cohort may not contain enough patients carrying the Q141K variant. As a result, it would not be possible to perform appropriate analysis to assess the impact of this on drug pharmacokinetics (Lee *et al.*, 2015). To resolve this, an alternative investigation might have to include genotyping subjects prior to enrolment to ensure adequate numbers of wild-type and Q141K isotypes are accounted for (Lee *et al.*, 2015). In the case of DDIs, investigations are recommended to assess whether investigational drugs inhibit any clinically relevant transporters. This includes ABCG2 and data should be available prior to progressing to phase III studies (EMA, 2012). Ideally, there would be a widely accepted, model compound to use as an ABCG2 substrate to use in in vitro examination of the interaction of new drugs with ABCG2. No such "probe substrate" is yet used universally which does leave the guidelines open to interpretation. It is possible that a single probe substrate would not be suitable for ABCG2 due to the multiple binding sites and translocation pathways. Knowledge in this area will certainly continue to develop. Regardless of its problematic influence over *in vivo* pharmacology, some efforts have been made in therapeutically targeting ABCG2 itself. In line with the idea of using co-administration to facilitate beneficial DDIs, efforts have principally aimed for specific inhibition of ABCG2 (Kruijtzer *et al.*, 2002; Kuppens *et al.*, 2007; Furman *et al.*, 2009). This has not been achieved as yet. There have historically been some promising inhibitor compounds including Ko143 and elacridar (Allen *et al.*, 2002; Kruijtzer *et al.*, 2002; Kuppens *et al.*, 2007; Furman *et al.*, 2009). Though

a number of potential therapeutic inhibitors were explored, any clinical safety data remains lacking (Robey *et al.*, 2011) For example trials of elacridar were stopped due to inefficacy associated to poor bioavailability (in part due to very low solubility) (Sane, Agarwal and Elmquist, 2012; Tournier *et al.*, 2017). One recent study took an approach using a series of approved compounds and exploring the effect on ABCG2 activity and identified febuxostat as a possible candidate (Miyata *et al.*, 2016).

Overall, a better understanding of ABCG2 pharmacology is required. This will be facilitated by the development of better methods to probe ABCG2:substrate interactions in wild type and mutant protein variants. Some current approaches are described in the following section alongside the principal techniques developed and employed in this project.

## 1.5 Methods to Study Transporter Pharmacology

Evidence from *in vivo* studies using mouse models and also from clinical observations in human patients have provided important data identifying ABCG2 as an MDR drug pump with a diverse range of chemical substrates (Mao and Unadkat, 2015). Due principally to the overlap of function with other transporters and the complex nature of the interaction between different substrates and inhibitors, a full understanding of ABCG2 will only be achieved using a variety of *in vitro* techniques. These allow for transporters to be analysed in isolation and there are a number of examples (DeGroot, 2009).

Whole cell assays of transport function were utilised in this project for demonstrating retained activity in the presence of the fluorescence and purification tags. The results of this are discussed in Section 4.5. Other biochemical techniques are often used. Vesicular transport assays use inside-out vesicles derived from the plasma membranes of transporter expressing cells. Subsequently, the accumulation of drug inside the vesicles can be measured as a determinant of transporter activity (Ozvegy, Varadi and Sarkadi, 2002). Alternatively, other whole cell transport assays (e.g. flow cytometry) can also be used to measure overall transport but none of these techniques can distinguish anything about particular steps in the transport cycles.

Another popular assay type are those measuring ATPase activity. Drug-induced changes in ATPase activity can indicate drug transporter interaction but the transport of drug is not actually measured so the nature of the interaction can not necessarily be resolved (Ambudkar, 1998; DeGroot, 2009).

Drug binding assays can be used to quantify interaction with transport substrates but current methods are limited. For example, tryptophan quenching (see below) is indirect and radioligand binding is restricted in scope due to the limited availability of radiolabelled substrates.

This project sought to enhance the toolset available for ABCG2 research and develop novel methods for measuring transporter:drug interactions. As discussed below, development of a detergent free isolation strategy and analysis methods based on ‘single-particle’ microscopy were explored.

### 1.5.1 SMALPs as a 'detergent-free' method for isolating ABCG2

Traditionally, detergents would be used to extract membrane proteins from cells into micelles (Seddon, Curnow and Booth, 2004). In this process the native lipids surrounding the target protein are displaced with detergent molecules at concentrations above the critical micelle concentration (Rothnie, 2016). Though incredibly useful, it can be a laborious (and expensive due to materials cost) process to optimise and often produces protein that is unstable or unsuitable for downstream analysis due to the removal of functionally relevant lipids (Seddon, Curnow and Booth, 2004; Gulati *et al.*, 2014). In the early 2000s, an alternative strategy was described that used polymers of styrene-maleic acid (SMA) to form nanodiscs containing membrane proteins and the associated annular lipid component (Knowles *et al.*, 2009; Dafforn, Overduin and Knowles, 2010). This offered a platform for extracting membrane proteins in the absence of traditional detergents (Jamshad *et al.*, 2011; Gulati *et al.*, 2014; Rothnie, 2016).

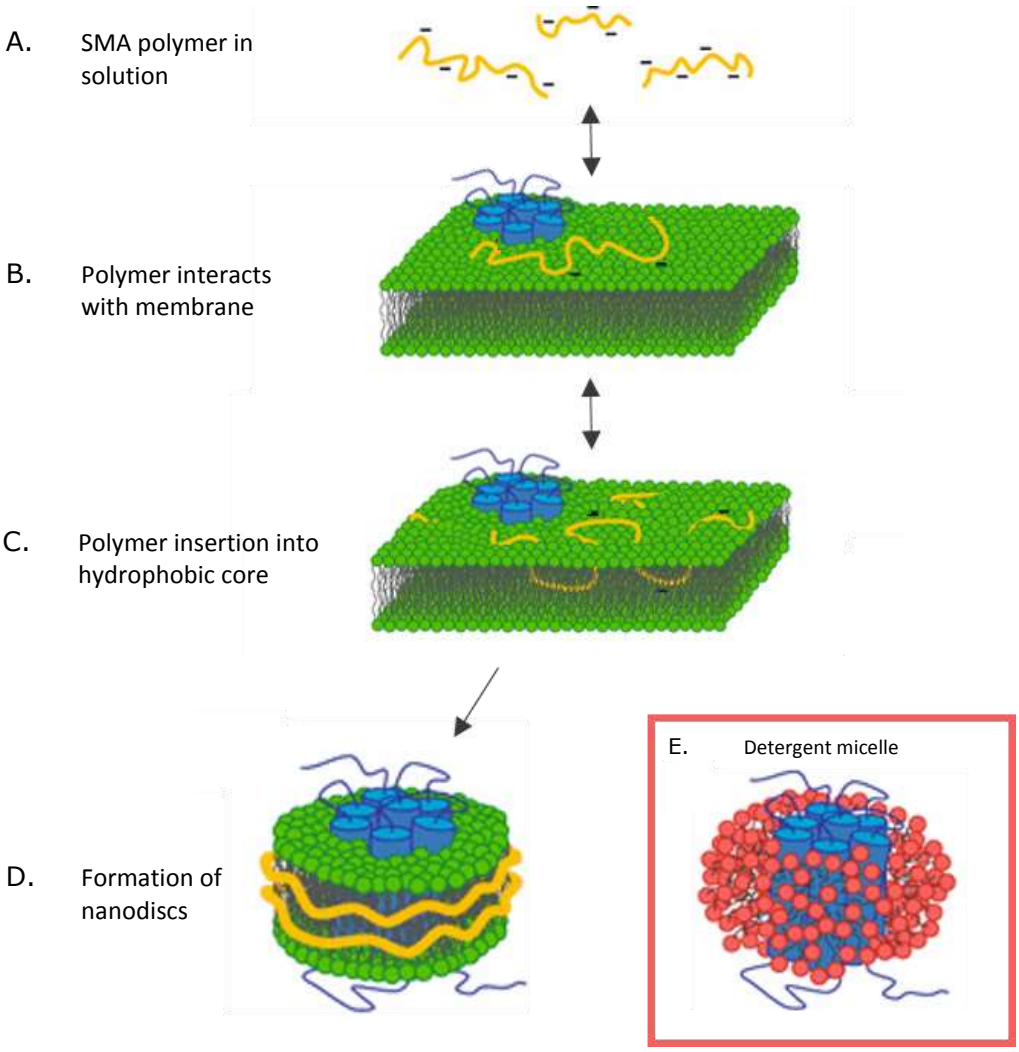


**Figure 1.13 – Schematic representation of membrane solubilisation by SMA.** Negatively charged SMA polymers (yellow) in solution (A) interact with the surface of the membrane (green) due to the hydrophobic effect (B). As more polymers interact, the membrane is disturbed as polymers start to insert into the hydrophobic core of the membrane (C). Eventually, nanodiscs of lipid containing membrane proteins (blue) are encapsulated by polymer rings to form SMALP nanodiscs (D). This is in contrast to detergent molecules (red) that interact directly with hydrophobic protein regions (blue cylinders) and replace annular lipids in the formation of detergent micelles (E) (adapted from Dörr et al 2016).

A copolymer of styrene-maleic acid is readily available and prepared as described in Section 2.4. This polymer can insert into membranes and isolate small discs (or 'patches') of lipid bilayer. The polymer forms a ring that encircles the bilayer in an SMA lipid particle (SMALP) as shown in Figure 1.13 (Gulati *et al.*, 2014). Recent data have offered a potential description for the molecular mechanism of SMALP formation (Scheidelaar *et al.*, 2015; Xue *et al.*, 2018). The hydrophobic effect elicits the interaction between SMA polymers and the membranes (Scheidelaar *et al.*, 2015). On the binding of several copolymer particles, membrane defects appear, which develop into aqueous pores which grow, resulting in membrane disruption (Xue *et al.*, 2018). The data result from molecular dynamics simulations for which the timescale is too short to show complete solubilisation. However, additional simulations show small nanodiscs are a thermodynamically preferred end stage which is reflective of *in vitro* observations of particles of approximately 10nm in diameter (S. C. Lee *et al.*, 2016; Xue *et al.*, 2018).

Since this platform was first described it has been employed in a large and ever growing number of studies. The studied proteins and expression systems include popular bacterial, insect and mammalian systems (Rothnie, 2016). Interestingly, SMALPs have already proven successful in isolating ABC transporters with a number of different assays being explored (Gulati *et al.*, 2014). In particular, the multidrug transporters described above (ABCB1 and ABCC1) as well as ABCG2 have been isolated in SMALPs from insect High Five and mammalian MCF7-FLV and HEK cell lines in previous studies. For example, SMALP encapsulated ABCG2

binding substrates has been shown by intrinsic tryptophan quenching and increased pheophorbide A (an ABCG2 substrate) fluorescence (Gulati *et al.*, 2014). Prior to this study however, there was little evidence of ABC transporter oligomeric state in SMALPs despite the importance of this factor. Existing studies nonetheless support the use of SMALP encapsulated ABC transporters and this project sought to expand on this by the development of solution-based fluorescence microscopy analysis.

### 1.5.2 Fluorescence Correlation Spectroscopy

For many years now, fluorescence has been an incredibly useful tool in allowing the observation of biochemical processes. The details of the fluorescence techniques used in this study, particularly in reference to the data processing, are given in the appropriate results sections. Below is an overview of the basics of fluorescence microscopy and spectroscopy.

**Principles of fluorescence**

The phenomenon of fluorescence results in the emission of photons from a fluorophore. High energy incident light excites a valence electron in a given fluorophore moving it to a higher energy state. A photon is released during the transition of an excited electron back to its ground state and usually occurs over the course of nanoseconds. The emitted electron has a longer wavelength and lower energy than the incident photon because some energy is lost as the excited valence electron moves in the different excited states. This process is repeated under constant illumination with excitation light and is summarised in the

Jablonski diagram in Figure 1.14 (Jameson, 2014). The difference in the excitation and emission energy is known as the Stokes shift and defines the excitation and emission spectra of a given fluorophore. This difference allows for the specific excitation of the fluorophore of interest by using a defined laser wavelength or filter set and similarly allows for the collection of emitted light only from the target fluorophore. This is an underlying principle of fluorescence microscopy.

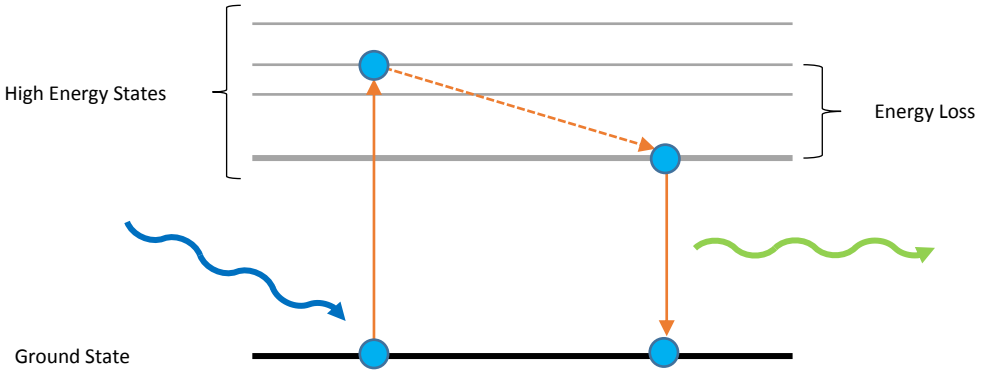


**Figure 1.14 – A Jablonski diagram.** When a fluorophore is excited a valence electron (blue circle) is moved from its ground state to a high energy state by absorbing an incident photon (blue wave). Some energy is lost by movement between high energy states then the electron moves back to its ground state emitting a photon (green wave) in the process.

**Confocal microscopy**

Where fluorescence microscopy allows for the collection of signal from objects of interest, confocal microscopy represents an advance by excluding signal from fluorophores outside the focal plane. As a result, the images produced can be of very high quality and resolve much better spatial information (Inoué, 2006). The basic concept has remained much the same as that first described in a patent in 1957 (Minsky, 1957, 1988). Essentially, using pinhole at the light source left only a single point of excitation through which the observed sample was moved meaning any light from outside the focal area was not collected. A modern confocal setup (see Figure 1.15) is certainly much improved, typically using a laser as the excitation light source. This is reflected through the sample by a dichroic mirror. A scanning mirror within the microscope allows the laser to scan across the sample while the sample remains still. Emitted light from the sample then passes back through the dichroic mirror which only allows the emission light to pass through (so the excitation light is excluded). The pinhole is positioned to only allow light emitted from the focal plane to reach the detector. The detector (typically a photomultiplier tube for imaging) converts the collected light to an electrical signal. This is processed by a computer to form a high resolution image in a pixel by pixel manner.

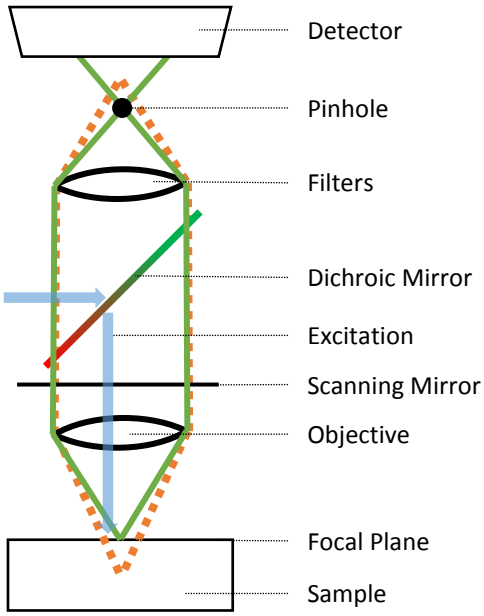


**Figure 1.15 – Schematic representation of a confocal microscope setup.** An excitation laser beam (blue arrow) is reflected onto the sample by a dichroic mirror. Due to the pinhole, only light from a single focal point (green outline) reaches the detector. Out-of-focus light (orange dotted line) is excluded.

### Fluorescence correlation spectroscopy (FCS)

Where the standard concept of a fluorescence microscope is that you can construct images from the gathered data, it is also possible to perform other measurements. FCS is used to measure fluorescent particles as they move through a small fixed confocal volume, as generated through the optical processes described in the previous section. It is an established biophysical technique and has been extensively reviewed (Elson, 2011). In this project it was used in the novel application of measuring the diffusion of SMALP-encapsulated ABCG2 in solution. In particular, FCS is able to determine concentration, brightness and mobility (in the form of a diffusion coefficient) of fluorescent particles. The technique itself was first introduced during the 1970s where, by distinguishing

bound and unbound fluorescent species based on differing mobility, it was used to investigate the kinetics of ethidium bromide binding to DNA (Magde, Elson and Webb, 1972). FCS was able to resolve the change in mobility to identify bound (slow moving) ethidium bromide from free (fast moving) molecules. In these historical experiments, a laser beam of uniform diameter was passed through a flat cell containing the sample which provided a practically two dimensional system. This was soon followed by the use of a confocal microscope that facilitated the observation of a defined three dimensional Gaussian detection volume by the exclusion of unfocused light by the use of a pinhole as described above. Throughout the 1990s further improvements were made to the typical FCS setup (Rigler and Widengren, 1990; Qian and Elson, 1991; Rigler *et al.*, 1993). These improvements resulted in a significant increase in signal-to-noise ratio and a decrease in the required acquisition time was achieved, broadening the biological application of FCS. Figure 1.16 shows the setup used for FCS in this study (based on Kilpatrick & Hill 2016). As in a scanning confocal microscope setup, a pinhole is used to exclude out-of-focus light. In FCS this pinhole is therefore responsible for the creation of a small defined confocal volume of 0.25-0.5fL. As fluorescent particles move through this volume they become excited. Fluctuations in emitted light intensity as particles diffuse in and out of the confocal volume are measured by an amplified photodetector – an avalanche photodiode in the case of this study (Figure 1.16 (A)) – and recorded. This method is discussed further, in particular reference to data processing, in the appropriate results chapters below.

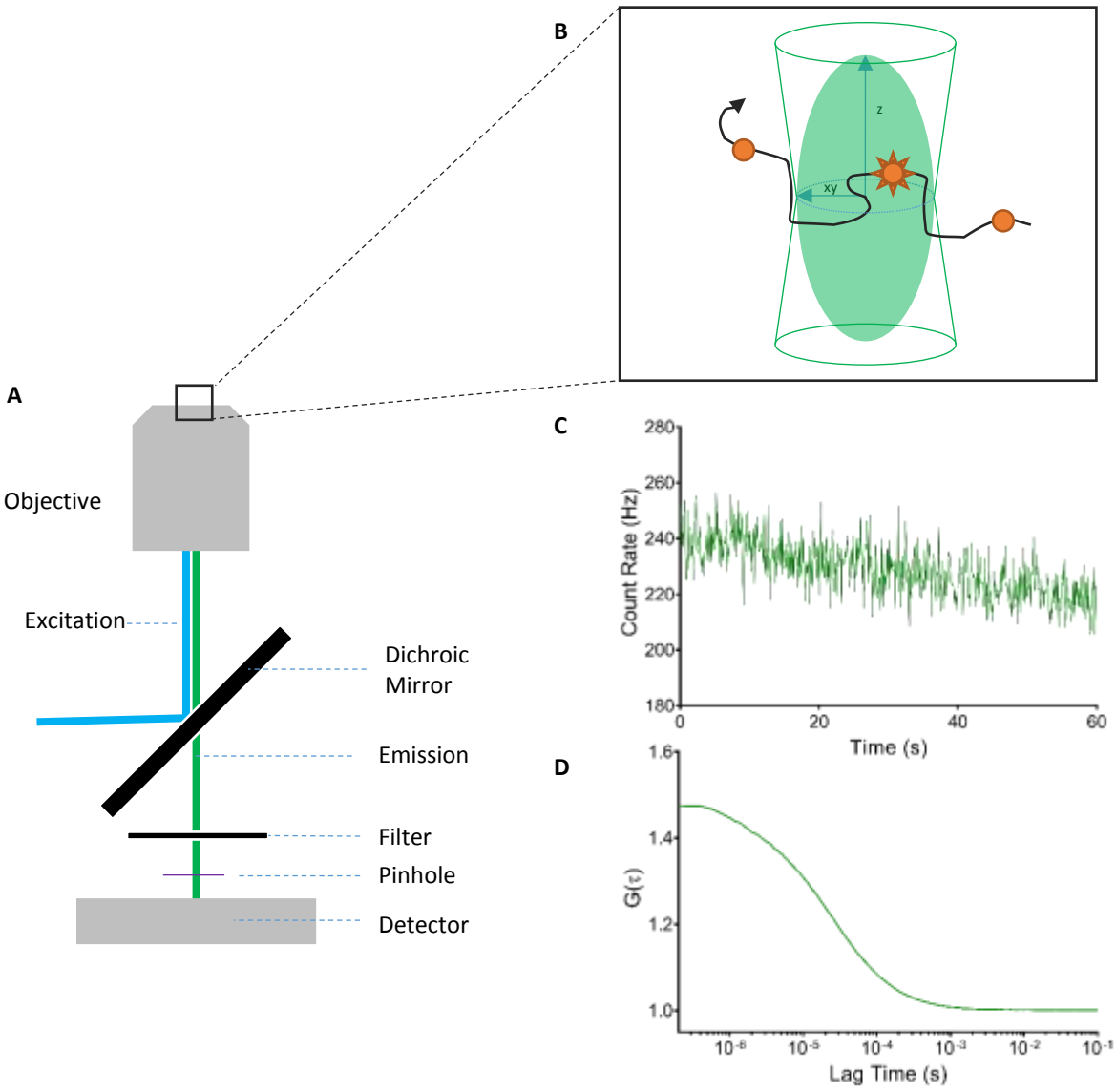


**Figure 1.16 - Schematic demonstrating the typical FCS instrumentation and outputs.** The instrument (**A**) typically consists of a confocal microscope with a high numerical aperture lens and a sensitive detector (e.g. an avalanche photo diode). The pinhole creates a Gaussian-shaped detection volume (**B**) of approximately 0.3-0.5fL in size with dimensions z and xy defined by measurements using a calibration fluorophore with known diffusion coefficient. As excited fluorescent particles (orange) pass through the detection volume, the fluctuations in fluorescence intensity are recorded over time (**C**). The autocorrelation function ($G_{(T)}$) is calculated by comparing the difference in intensity from the average intensity at a given time point to that at a range of subsequent time point (lag times). This can then be plotted (**D**) and fitted to mathematical models to determine parameters for the measured particles including dwell time and the number of particles.

## 1.6 Aims of the Study

Our understanding of ABCG2 continues to expand but is certainly far from complete. In particular, further knowledge on the mechanisms of transport substrate recognition and translocation is needed. Better understanding in these areas could lead to improved drug design processes that can overcome the issues associated to multidrug transport phenomena. There has been significant structural and biochemical progress that will contribute to this but to assist the future advances of this field of research more tools are required. In pursuit of this the overall aim of this project was to generate *in vitro* methods to analyse ABCG2 and its interactions with substrates and inhibitors in isolation.

Initially, this required the generation of ABCG2 constructs with a suitable fluorescent tag and affinity tag for purification and to express these constructs in mammalian cells. As part of this process another aim was to optimise the expression level and subsequent yield to support downstream purification efforts and validate protein function and localisation.

The second aim was to utilise recently described 'detergent-free' methods for solubilising ABCG2. This would then support the aim of purifying ABCG2 in order to study it in isolation.

The final aim of the project was to develop a fluorescence microscopy based method for studying the oligomerisation of ABCG2 and subsequently the interactions with substrates and inhibitors. The development of this overall platform would facilitate future studies of the mechanisms of ABCG2 substrate recognition and provide an improved toolset for assessing substrate/inhibitor interactions perhaps in the context of screening and drug design processes.

The following chapter describes the methods used in this project. The subsequent chapters discuss the results of these experiments alongside the background theory to the techniques and data processing of fluorescence correlation spectroscopy. A final discussion with comment on the future perspectives of this work is given at the end of this thesis.

# 2 Methods

## 2.1 Cloning and Molecular Biology

### 2.1.1 Materials and Reagents

Starting vectors encoding GFP_ABCG2, SNAP-tag_ABCG2, CD86_GFP or CD28_GFP in the pcDNA3.1(+)zeo backbone were provided by Dr Ian Kerr (University of Nottingham). The pcDNA4/TO starting vector was provided by Dr Nicholas Holliday (University of Nottingham). Enzymes and associated buffers were acquired from New England Biolabs (Hitchin, UK) with other reagents obtained from Sigma-Aldrich (Poole, UK) unless stated otherwise.

### 2.1.2 Restriction digest -

Restriction digest reactions were set up according to Table 2.1 below. The optimal buffer conditions were chosen based on supplier guidelines. Restriction digest reactions were typically performed for 1 hour at 37°C. DNA loading dye was added to the digested DNA and the mixtures were loaded, alongside molecular weight marker, onto 0.7% (w/v) agarose gels containing 0.5µg $mL^{-1}$ethidium bromide. Electrophoresis was then performed in TBE buffer (90mM Tris, 90mM boric acid, 2nM EDTA pH 8.0). Digested DNA bands were visualised using an ultraviolet transilluminator. The visualised bands were compared to the molecular weight marker.

| Reagent | Quantity |
|---|---|
| DNA Vector | 200-500ng |
| Enzyme(s) | 5-10 units (0.25-0.5µL) |
| 10x Enzyme Buffer | 1.5µL |
| Water | Made up to 15µL |

**Table 2.1 - Components of restriction digest reactions.**

### 2.1.3 Ligation -

Where DNA digest was performed to isolate specific DNA fragments for transfer into a different vector, these fragments were ligated into the new vector. The desired bands were excised from the agarose gel. The DNA was extracted using a NucleoSpin Gel and PCR Clean-up kit (Macherey-Nagel) following the manufacturer's instructions. The purified DNA was dephosphorylated by treatment with CIP (Calf Intestinal Phosphatase) at 37°C for 30 minutes followed by a deactivation of the enzyme by incubation at 65°C for 30 minutes. Ligation reactions were then set up according to Table 2.2 below and performed either overnight at 16°C or for 2 hours at room temperature depending on requirements.

| Reagent | Quantity |
|---|---|
| DNA Vector:Insert | 1:3 molar ratio |
| 10x T4 Ligase Buffer | 2µL |
| Water | Make up to 20µL |
| T4 DNA Ligase | 400 units (1µL) |

**Table 2.2 - Components of ligation reactions**

### 2.1.4 Short oligo linker cloning

For the insertion of polyhistidine tags as described in Section 3, short *de novo* DNA sequences were cloned into the appropriate vector. Oligonucleotide pairs were designed that encoded a hexahistidine sequence flanked with overhangs that formed the appropriate restriction digest sites to enable insertion into the target vector. These were supplied 5' phosphorylated. The oligonucleotide pairs were annealed by mixing in equal amounts and heating to 85°C before rapid cooling to 50°C. The heating and cooling process was repeated five times. The annealed primer pairs were ligated into the appropriate vector as described above in Section.

### 2.1.5 Transformation of competent cells

100µL of competent DH5α E. coli (provided by Deborah Briggs, University of Nottingham) was thawed on ice. 5µL of ligation reaction or 100ng of plasmid DNA was added. The cells were then left on ice for 30 minutes, heat shocked at 42°C for 90 seconds, left on ice for 2 minutes then 900µL LB was added and the cells were then incubated while shaking at 37°C for 1 hour. Transformed cells were then plated onto ampicillin supplemented (100µg $mL^{-1}$) supplemented LB agar plates. 1/10 and 9/10 volume of the transformed cells were transferred onto two separate plates and these were incubated overnight at 37°C.

### 2.1.6 Plasmid preparation

Single colonies of transformed DH5α grown overnight on selective LB agar plates were picked and inoculated into 5mL of LB medium containing 100μg $mL^{-1}$ ampicillin. These cultures were grown overnight at 37°C with shaking. Glycerol stocks were made for long-term storage by mixing 500μL of overnight culture with 500μL 30% (v/v) glycerol and storing this at -80°C. Where required for further DNA preparation, glycerol stocks were first streaked on selective LB agar plates and plasmid DNA was then prepared as described in this section. Following glycerol stock preparation, the remaining bacterial culture (~4.5mL) was pelleted by centrifugation at 2000g for 5 minutes. DNA was extracted from the resulting pellet by use of a NucleoSpin Plasmid kit (Macherey-Nagel) following the manufacturer's protocol. In summary, bacterial pellets were lysed by exposure to alkaline conditions and chromosomal DNA was precipitated (along with other insoluble material) by neutralising the solution and adjustment to high salt concentration. The lysate was then cleared by centrifugation and the plasmid DNA containing supernatant was applied to silica columns. The adsorbed DNA was washed with a solution containing ethanol and then eluted in a low-salt buffer. Concentration and purity of the eluted DNA was determined using sample absorbance measured using a Nanodrop 2000 (Thermo Fisher). Absorbance at 260nm ($A_{260}$) was used to calculate DNA concentration automatically within the associated software and purity was assessed using the $A_{260}/A_{280}$ ratio (where $A_{280}$ measures the protein

concentration in the solution). Only DNA with an $A_{260}/A_{280}$ ratio of >1.7 were used for transfection.

### 2.1.7 Mutagenic primer design

Mutagenic primers were designed to alter cloning sites or introduce other desired mutations into template DNA. The sequence of DNA to be altered was identified and assessed by BLAST (NCBI) to ensure the targeted sequences in the template vector were unique. The required base changes were manually planned and the required primer pairs were designed as appropriate. These primers were extended by at least 8 base pairs both 3' and 5' to the intended mutation, GC content was kept at 40-60% whilst GC clamping was ensured on both 3' and 5' ends of the primers. The properties of the resulting primers were predicted using Primer3 (Koressaar and Remm, 2007; Untergasser *et al.*, 2012). They are summarised in Table 2.3 with their uses described in Chapter 3.

| Primer Name | Sequence | Length (bp) | Tm (°C) | GC (%) |
|---|---|---|---|---|
| GFP_ATG-CTG_FOR | CACGCTAGCCTGGAGGTGAGC | 21 | 60.2 | 67 |
| SNAP_ATG-CTG_FOR | CTTGCCACCCTGGACAAAGAC | 21 | 56.3 | 57 |
| KpnI_Intro_For | CTATAGGGGTACCCAAGCTGG | 21 | 56.3 | 57 |

**Table 2.3 - Summary of mutagenesis primers.** Forward sequences shown for primers designed to remove the start codons from the GFP or SNAP-tag® ABCG2 constructs and introduce a KpnI site for cloning as described in Chapter 3.

### 2.1.8 PCR

Polymerase chain reaction (PCR) was used for amplifying DNA mutagenesis products. Cycling was performed in a SensoQuest Thermocycler (SensoQuest, Göttingen, Germany) with reactions prepared in thin-walled PCR tubes. The constituents of a typical PCR reaction are summarise in Table 2.4.

| Component | Quantity |
|---|---|
| dNTPs | 20µM each |
| 5x polymerase buffer | 10µL |
| Forward/Reverse Primers | 2µM |
| Template DNA | 1µL |
| Water | Made up to 50µL |
| Polymerasen (typically *Pfu*) | 2 units |

**Table 2.4 - Components of a typical PCR reaction.**

For site-directed mutagenesis reactions, the cycling protocol was based on the QuikChange Site-Directed Mutagensis method (Agilent) as summarised in Table 2.5 below. The resulting PCR products were digested with DpnI which removed parental DNA (methylated) leaving only the PCR product (non-methylated) for transformation into DH5α as described above.

| Step | Temperature (°C) | Cycles | Time |
|---|---|---|---|
| 1 | 98 | 1 | 30s |
| 2 | 98 | 15 | 10s |
| 3 | 52-58 | 15 | 30s |
| 4 | 72 | 15 | 4 minutes |
| 5 | 20 | 1 | ∞ |

**Table 2.5 - Thermocycling protocol for site-directed mutagenesis reactions.**

### 2.1.9 DNA sequencing

Where possible, diagnostic digests were employed to reveal successful cloning or mutagenesis reactions. Once these had been confirmed all constructs were sent to Source Bioscience (Nottingham, UK) for DNA sequencing. The sequencing primers used are summarised below in Table 2.6. Chromatograms provided were analysed using Chromas Lite (Technelysium Pty Ltd) or SnapGene (GSL BioTech) and the sequences were aligned against predicted sequences by BLAST (NCBI).

| Primer Name | Sequence | pcDNA3.1(+)zeo-His-GFP-ABCG2 (909-3656) | pcDNA3.1(+)zeo-His-SNAP-ABCG2 (928-3477) |
|---|---|---|---|
| p31zeo_up | CAGTACATCAATGGGCGTGG | 690-1590 | 690-1590 |
| SeqR1 | TCGTGGTGCTCCATTTAT | 1140-1980 | 820-1810 |
| SeqF0 | GAGTGGCTTTCTACCTTGTC | 1900-2740 | 1720-2600 |
| SeqF2 | GCAGGGACGAACATTC | 2450-3270 | 2270-3160 |
| Seq482 | AACTCTTTGTGGTAGA | 3070-3840 | 2900-3690 |

**Table 2.6 - Sequencing primers used in this study.** A series of sequencing primers were used for each construct to ensure coverage of the whole protein encoding region. The start/stop positions of the constructs are shown in brackets.

## 2.2 Cell Culture and Handling

### 2.2.1 Cell lines and storage

HEK293T cells (ATCC® CRL-3216) and TREx™-293 (Thermo Fisher, R71007) cells were used for protein expression. These were transfected with plasmid DNA prepared as described in the above sections. When stable cell lines had been generated as described below, aliquots were frozen for long-term storage. Cell pellets were suspended in ice-cold freezing medium (90% FBS (foetal bovine serum), 10% DMSO). For adherent cell lines 6mL was used. For suspension cell lines the cell density was adjusted to $2x10^6$ cells $mL^{-1}$. 1mL aliquots of cells resuspended in freezing medium were frozen in cryotubes at -80°C using an insulated container to ensure a gradual rate of cooling. After 3-5 days, cell aliquots were moved to liquid nitrogen for long-term storage purposes.

### 2.2.2 Passage/maintenance of adherent cell cultures

Cells were grown in DMEM (Dulbecco's Modified Eagle Medium, $4.5gL^{-1}$ glucose, $0.11gL^{-1}$ sodium pyruvate, $0.58gL^{-1}$ L-glutamine) supplemented with 10% v/v FBS and 1% (w/v) each penicillin and streptomycin unless otherwise stated. When cells were approximately 80% confluent based on visual inspection these cultures were passaged (typically twice weekly). Media was removed, cells were washed once with pre-warmed PBS then incubated with 0.4-1.2mL 1x trypsin/EDTA in PBS (phosphate buffered saline) at 37°C for up to 5 minutes. Cells were then detached and removed from the flasks in 5mL medium and centrifuged at 500g for 5 minutes. Pellets were resuspended in fresh media and a fraction was seeded into

a new flask (typically 1/10 or 1/20). Cell stocks were normally maintained in 25cm$^2$ or 75cm$^2$ flasks at 37°C with 5% $CO_2$. For large scale protein expression in adherent cultures, these stocks were used to seed several 78.5cm$^2$ or 500cm$^2$ dishes as required.

### 2.2.3 Maintenance of suspension cultures

To facilitate greater cell densities and ultimate yields for protein expression, HEK293T cells were adapted to grow in suspension as described in Section 4.6.4. Cells were grown in DMEM supplemented with 10% v/v FBS and 1% (w/v) each penicillin and streptomycin. Typically stocks of 80mL were grown in 250mL flat bottomed round flasks sealed loosely with a foil cap. They were seeded at 2.5-4x10$^5$ cells mL$^{-1}$ depending on requirements. These stocks were kept at 37°C with 5% $CO_2$ on a shaker platform set to 180RPM. When required, the cell stocks were used to seed larger 250mL cultures at 4x10$^5$ cells mL$^{-1}$ in 1L flat bottomed round flasks.

### 2.2.4 Measurement of cell viability by Trypan blue exclusion

To determine cell viability, equal volume of 0.4% trypan blue solution in PBS and cells were mixed (typically 100-200µL of each). This cell solution was applied to a haemocytometer and examined immediately with % viability calculated by:

*Equation 2.1*

$$\%\, Viability = \left(1 - \frac{Count_{blue}}{Count_{total}}\right) \times 100$$

Where $Count_{blue}$ is the number of cells that have taken up trypan blue dye and appear blue and $Count_{total}$ is the total number of observed cells.

### 2.2.5 Poly-L-lysine treatment of coverglass

To ensure HEK293T cell attachment to untreated surfaces poly-L-lysine was used which facilitates ionic interactions between the positively charged attachment surface and the cell membrane. This was used prior to imaging and for activity assays. A stock of 5mg $mL^{-1}$ poly-L-lysine was stored at -20°C. A working solution of 0.1mg $mL^{-1}$ was obtained by dilution in sterile water. After further 0.2 µm filter sterilisation the solution was applied to the growing surface (e.g. 96-well plate) and left for at least 20 minutes. Excess poly-L-lysine was removed by two washes with PBS prior to cell seeding.

### 2.2.6 Fixation

When required, cells were fixed with 4% (w/v) paraformaldehyde (PFA) in PBS. Media was removed from adherent cell cultures and they were washed once with PBS. 4% PFA was then applied and left for 10 minutes then removed. The fixed cells were then washed twice with PBS.

### 2.2.7 Transfection and selection of stable cell lines

For the expression of recombinant proteins, HEK293T or TREx™-293 cells were transfected with plasmid DNA generated as described in Chapter 3. Using the appropriate selection agents, cell lines stably expressing the required proteins were selectively grown.

### 2.2.8 Transfection

Cells were seeded in 6-well plates at $2.5x10^5$ cells $mL^{-1}$. 24 hours after seeding, medium was replaced with DMEM supplemented with 5% (v/v) FBS for 2 hours prior to transfection. PEI (Polyethylenimine) was slowly added to 2µg DNA at an approximate nitrogen:phosphate ratio of 15:1. After 5 minutes to allow the formation of DNA/PEI complexes, this transfection mixture was added to the cells. After 24 hours, the medium was changed to that supplemented with 10% (v/v) FBS.

### 2.2.9 Stable cell line selection

As discussed in Section 4.2 and shown in Figure 4.1, stable cell lines were generated expressing various constructs. Cells transfected as above were harvested by repeated pipetting with PBS then transferred to $25cm^2$ flasks and incubated at 37°C 5% $CO_2$. These cells settled overnight and medium was then replaced with selection medium (DMEM supplemented with 200µg $mL^{-1}$ zeocin™). Media was replaced every 2-3 days with fresh selection medium. Following death of the majority of cells, small colonies of selected cells grew to confluence. When healthy colonies were observed after selection, cells were maintained as in Section 2.2.2 with DMEM supplemented with 40µg $mL^{-1}$ zeocin™. Aliquots were also prepared for long-term storage as described in Section 2.2.1.

### 2.2.10 Generation of clonal cell lines

Cell suspensions of the stable cell lines were prepared at 5 cells $mL^{-1}$ in DMEM. 200µL were then seeded into poly-L-lysine coated 96-well plates (see Section

2.2.4) and incubated at 37°C 5% $CO_2$. After several days, wells were observed by microscopy and those containing more than a single colony were discontinued. Wells containing only one colony were grown up to approximately 50% confluency before transfer to a 24-well plate and a replica 96-well plate in DMEM containing 40µg $mL^{-1}$ zeocin™. The cells were then screened based on fluorescence intensity by confocal microscopy of the 96-well plate and clones with higher or lower relative expression levels were then expanded. In the case of SNAP-tag® lines, these were first labelled with 0.3µM SNAP-Cell® TMR-Star for 1 hour at 37°C with 5% CO2. This was followed by three washes in medium (DMEM supplemented with 10% FBS) with the final wash being left for 30 minutes. All clones were then fixed with PFA as in Section 2.2.6. Cells were then stained with Hoechst 33342 (2µg $mL^{-1}$) for 15 minutes followed by a wash with PBS. Clones were then imaged using an ImageXpress Micro XLS High-Content Analysis System using DAPI (Hoechst 33342) and TRITC (TMR-Star) excitation / emission filter sets, and a Zeiss 20x long working distance air objective. Image z-offset and exposure time for acquisition were automatically optimised for focus and intensity, and these settings were preserved across clones. The obtained images were visually inspected and manually assessed for relative brightness as an indicator of protein expression level.

## 2.3 Preparation of Membrane Fractions

Cell pellets were collected from either adherent (by resuspension in PBS) or suspension cell cultures by centrifugation at 1000g for 5-15 minutes at 4°C. If not

used immediately, cell pellets were stored at -80°C. Where larger quantities of protein were required, multiple pellets were combined. Pellets were washed three times with ice-cold PBS then resuspended in at least 5x pellet volume of ice-cold membrane isolation buffer 1 (MIBI, 0.01M Tris pH7.4, 0.25M sucrose, 0.2mM $CaCl_2$) supplemented with protease inhibitor cocktail set III (Calbiochem) diluted 1:100. Lysis by sonication was appropriate for smaller volumes (see Section 2.7.1), but for the larger volumes used for membrane preparations nitrogen cavitation was used. A nitrogen cavitation vessel (Parr Instrument Company) was pre-cooled on ice and attached to a nitrogen cylinder. The cell suspension was applied to the vessel which was then sealed and the system was allowed to equilibrate at a pressure of 1000psi on ice for 5 minutes. The cavitation vessel outlet was then opened to release the sample which was rapidly returned to atmospheric pressure leading to cell lysis. The sample was reapplied to the vessel and the process was repeated. The resulting cell lysate was collected in a 50mL tube and was then centrifuged at 1500g for 15 minutes at 4°C. The supernatant was then collected and centrifuged at 100000g for 45 minutes at 4°C. The supernatant was removed and the remaining pellet consisted of the cell membrane material. This was resuspended in membrane isolation buffer 4 (MIBIV, 0.01M Tris pH7.4, 0.25M sucrose) by repeated shearing through a 25G needle. Cell membranes were used immediately or stored at -80°C.

## 2.4 SMALP Preparation and Use

SMA2000 (Cray Valley) was the principal SMA (Styrene Maleic Acid) polymer used in this project. It was provided as a styrene-maleic anhydride co-polymer that needed to be hydrolysed in order to become active for membrane solubilisation. Once activated, the polymer was used to solubilise cell membrane material prepared as in the above Section (2.3) into SMALPs (Styrene Maleic Acid Lipid Particles). These steps were performed following a method similar to that described by Rothnie et al. (2016).

### 2.4.1 Preparation of activated SMA polymer

25g SMA2000 powder was dissolved in 250mL 1M NaOH overnight. The solution was then brought to a boil using a heating mantle and refluxed for 2-3 hours. The refluxed solution was allowed to cool then transferred to polycarbonate centrifuge tubes. The polymer was precipitated by the gradual addition of concentrated HCl (approximately 40mL HCl in total across the 250mL polymer solution) and 100mL distilled water was also added. This suspension was centrifuged at 10000g at room temperature for 10 minutes before the supernatant was removed and replaced with 150mL distilled water. These wash steps were repeated a further three times. After the final wash step, the polymer precipitate was dissolved in 240mL 0.6M NaOH with stirring for several hours or overnight. The alkalinity was adjusted (from approximately pH 13) to pH 8 by the addition of concentrated HCl. The polymer solution was then transferred to two

1L borosilicate flat bottomed round flasks and frozen by immersing the flask in liquid nitrogen whilst rotating resulting in the frozen polymer solution being spread over the internal surface of the flask. This was then stored at -20°C before being freeze-dried. The resulting powder was stored at room temperature.

### 2.4.2 Solubilisation of membrane proteins into SMALPs

Unless otherwise stated, SMALP solubilisation was performed using isolated cell membrane material resuspended in SMA buffer (150mM NaCl, 50mM Tris pH8) at 100mg $mL^{-1}$ with 2.5% (w/v) SMA co-polymer powder. This solution was incubated at room temperature for 1 hour whilst rotating, then centrifuged at 100000g for 20 minutes at 4°C to pellet insoluble material. The supernatant containing the solubilised membrane proteins was collected and was used immediately for analysis or purification as required.

## 2.5 Sizing of SMALP solubilised proteins by dynamic light scattering (DLS)

The hydrodynamic radii of SMALP encapsulated proteins were measured by DLS. Solubilised membranes prepared as described above were diluted 10-fold in SMA buffer. 50uL of sample was then applied to a dark walled low volume cuvette (Hellma, HL105-201-15-40) and analysed using a Zetasizer Nano instrument (Malvern Instruments). Acquisition settings were automatically optimised in the associated software. The system was equilibrated at 25°C and 10 seconds of data was collected per read with 5-10 reads constituting a single measurement. Three

replicate measurements were performed per sample. The mean particle sizes and proportions of the three replicates were used to calculate average measurements for each experiment.

## 2.6 Purification and Concentration of ABCG2

Following the optimisation detailed in Section 6.2, solubilised ABCG2 was purified for downstream analysis.

### 2.6.1 His-tag Purification

Solubilised His-tagged protein was mixed with cobalt resin (pre-washed three times in SMA buffer) at a ratio of 100µL resin per 1mL of solubilised protein solution (the volume of resin is described as the bed volume or BV). This was mixed slowly by end-over-end rotation overnight at 4°C. The solution was poured into a gravity flow column fitted with a fresh frit and the flow-through was collected. The resin was washed three times with 5xBV SMA buffer. Protein was then eluted by the application of 2xBV SMA buffer supplemented with 50mM imidazole three times. Further elution was also performed with 200mM and 2M imidazole each at 2xBV and repeated three times.

### 2.6.2 Concentration

Protein elution fractions containing ABCG2 were identified by SDS-PAGE analysis. These were pooled and passed through a 0.22µm filter to remove any large

particulate contaminants. The pooled elution fractions (typically 3-6mL total) were applied to 10000mwco concentrators (Sartorius, VS0601). These were centrifuged at 500-1000g to reduce the solution volume to approximately 500µL. The solution was then topped up to 5mL with SMA buffer and this process was repeated until the original concentration of imidazole in solution had been reduced at least 100-fold to <0.5mM. The concentration of ABCG2 was determined by SDS-PAGE as described in Section 2.7.3 below followed by densitometric analysis in comparison to a standard curve of BSA (see Section 6.2). Samples were then used immediately or stored at 4°C until use.

## 2.7 Protein Analysis by SDS-PAGE and western blot

### 2.7.1 Cell harvest

For the analysis of protein expression, cells were harvested in ice-cold PBS. The resulting cell suspensions were pelleted by centrifugation at 500g for 5 minutes. If not used immediately, cell pellets were stored at -20°C. Pellets were then washed twice with PBS before resuspension in 250µL-1mL PBS supplemented with 1% (v/v) glycerol and protease inhibitor cocktail set III diluted 1:100. Cells were then lysed by sonication using three 10 second bursts interspersed with 30 seconds pauses on ice. Complete lysis was ensured by visual inspection of the lysed material by microscopy.

### 2.7.2 Protein assay

Where necessary to ensure equal protein loading in SDS-PAGE and western blot analysis, protein concentrations were determined by using a modified Lowry assay. This was performed using Bio-Rad DC protein assay kit reagents and protocol. Concentrations were calculated by comparison against a standard curve of 0.2 – 2 mg/mL of BSA.

### 2.7.3 Sample preparation and SDS-PAGE

SDS-PAGE (sodium dodecyl sulphate polyacrylamide gel electrophoresis) was performed based on adaptions of the Laemmli method (Laemmli, 1970). Protein samples were made up in protein loading buffer (62.5mM Tris base, 2% (w/v) SDS, 10% (v/v) glycerol, 0.01% (w/v) bromophenol blue, 0.5%(w/v) dithiothreitrol (DTT)) and were heated to 99°C for 5 minutes. Unless otherwise stated 8% (w/v) acrylamide resolving gels prepared in resolving buffer (375mM Tris pH8.8, 0.1% (w/v) SDS) and 4% (w/v) acrylamide stacking gels prepared in stacking buffer 125mM Tris pH 6.8, 0.1% (w/v) SDS) were used. The gels were placed in gel electrophoresis tanks filled with protein running buffer (25mM Tris base pH8.4, 190mM glycine, 0.1 % (w/v) SDS). Prepared samples were loaded into the gels alongside molecular weight markers (typically SeeBlue® Plus2 Pre-stained Protein Standard (Bio-Rad Laboratories). A constant current of 20-45mA per gel was applied for 45-60 minutes to separate proteins by electrophoresis. Gels were removed from the tanks, rinsed with distilled water then stained (typically with

InstantBlue™ for 1 hour at room temperature, rocking). Stained gels were washed with distilled water and imaged using an Odyssey scanner (LI-COR Biosciences).

### 2.7.4 Western blot analysis

For the detection of specific proteins, western blot analysis was performed. Protein samples were prepared and run on polyacrylamide gels as described above in Section 2.7.3. Instead of staining the protein, it was transferred onto nitrocellulose membranes. This was carried out in a transfer tank filled with transfer buffer (25mM Tris, 190mM glycine, 20% (v/v) methanol) at a constant current of 200mA for 1.5-2 hours at 4°C. On completion of transfer, membranes were removed from the transfer tank. Non-specific binding of primary antibody was prevented by blocking the membranes with 5% marvel in PBS/T (0.1%) (PBS supplemented with 0.1% v/v Tween-20) for 1 hour at room temperature, rotating. Blots were subsequently incubated overnight at 4°C with primary antibody raised against the protein of interest (see Table 2.7). Blots were washed three times with PBS/T (0.1%) to remove unbound primary antibody and were then incubated for 1 hour at room temperature with secondary antibody (see Table 2.7). The membranes were then washed three times with PBS/T (0.1%) before the application of SuperSignal West Pico Chemiluminescent HRP substrate for the detection of secondary antibody binding. A working solution formed of equal amounts of peroxide and enhancer solutions was prepared and the blots were incubated in this for 1 minute. They were then drained, covered in cling film and

imaged using a LAS-2000 instrument (Fujifilm) with exposure times of 10 seconds – 30 minutes (typically 2 minutes). An image of the molecular weight standards was obtained simultaneously and overlaid which allowed identification of protein molecular weight.

| Antibody | Source | Target | Dilution | Secondary | Source |
|---|---|---|---|---|---|
| BXP-21 | Merck Biosciences | ABCG2 | 1:500 | HRP conjugated polyclonal rabbit anti-mouse IgGκ | DAKO |
| Anti-GFP | Sigma-Aldrich | GFP | 1:500 | | |
| His Tag HRP-conjugated Antibody | R&D Systems | His-tag | 1:1000 | - | - |

**Table 2.7 – Antibodies used for western blotting in this project.**

### 2.7.5 Densitometric analysis of band intensity

Gel or blot images were opened in ImageJ, protein lanes were identified and band intensities automatically measured. The intensity of each band of interest was exported to Excel where protein concentrations of proteins were calculated based on comparison to a standard curve of BSA (bovine serum albumin 66.5kDa).

## 2.8 Whole cell functional assays

### 2.8.1 Plate-based accumulation assay

HEK293T cells stably expressing His-SNAP-ABCG2 or His-GFP-ABCG2 were seeded at cells per well onto poly-L-lysine coated (see Section 2.2.4) 96-well clear-

bottomed blackout plates (Greiner Bio-One 655090). When confluent (typically left to grow overnight), cells were incubated for 2 hours at 37°C 5% $CO_2$ with DMEM supplemented with 8µM mitoxantrone in either the presence of absence of 0.5µM Ko143 or 0.1% DMSO (solvent control). Cells were washed twice with ice-cold PBS and fixed with PFA (see Section 2.2.6). The accumulation of intracellular mitoxantrone resulted in an increased fluorescence intensity. This was measured using a Flexstation (Molecular Devices) with an excitation wavelength of 608nm and emission wavelength of 686nm. To calculate the percentage of Ko143 inhibitable mitoxantrone accumulation, the corrected fluorescence intensity was first determined for each cell line and condition by subtracting the fluorescence of the solvent control. The percentage Ko143 inhibitable mitoxantrone accumulation ($A_{Ko143}$) was then calculated using Equation 2.2 below.

*Equation 2.2*

$$A_{Ko143} = \frac{I_{MX+Ko143} - I_{MX}}{I_{MX}} \times 100\%$$

Where $I_{MX+Ko143}$ is the corrected fluorescence intensity of cells treated with both mitoxantrone (MX) and Ko143 and $I_{MX}$ is the corrected fluorescence intensity of cells incubated with only mitoxantrone.

## 2.9 Standard and Confocal Imaging

### 2.9.1 Basic imaging techniques

Cells were regularly observed as part of a maintenance routine by standard microscopy using an inverted microscope. Cell lines were also checked for expression of fluorescently tagged protein by visual inspection. Live cells were imaged in standard tissue culture plasticware and medium unless otherwise stated using a Zeiss Axiovert 100S inverted microscope equipped with a 10× objective and an Axiocam CCD camera (Carl Zeiss). Images were captured using both the phase contrast and FITC or TRITC filtersets as required.

### 2.9.2 Confocal imaging to demonstrate plasma membrane ABCG2 localisation

For the demonstration of membrane localisation, an LSM710 confocal microscope (Carl Zeiss) equipped with a plan-apochromat 63x/1.40 Oil Ph3 M27 objective and 488 nm argon laser was used. In analysing GFP fusion proteins, 2% laser power was used for excitation and emission was collected at 493-598nm (based on an automatically excitation/emission channel separation in the associated software). Gain and offset settings were adjusted to maintain signal within the linear range of the detector and maintained within each experiment. High resolution images (1024x1024 pixels with an 8-bit image depth) were captured in the fluorescence channel alongside phase contrast images.

## 2.10 FCS and PCH Analysis

For the study of ABCG2 isolated in SMALPs at “single-molecule” sensitivity, fluorescence correlation spectroscopy (FCS) and photon counting histogram (PCH) analysis were used. By measuring fluctuations in fluorescence, based on the movement of fluorescent particles in and out of the defined confocal volume, FCS analysis reveals information on the concentration and diffusion coefficient of the particles in the volume. PCH analysis can be performed on the same data to determine the molecular brightness of the measured particles. This can be used to describe the oligomeric state of the measured proteins.

### 2.10.1 Instrument set up and data acquisition

FCS measurements were performed on a Zeiss LSM510NLO Confocor 3 confocal microscope (Carl Zeiss, Jena, Germany) equipped with a 40x Apochromat NA 1.2 M27 water immersion objective and argon (488nm excitation) and helium-neon (HeNe) (633nm excitation) lasers. For each experiment, the appropriate laser was switched on 2 hours prior to use to allow the system to equilibrate. The instrument was calibrated as described below before data acquisition. Following calibration, solutions containing fluorescently tagged protein were added to the wells of a Nunc™ Lab-Tek™ 8-well chambered #1.5 cover glass (subsequently referred to as “8-well plate”) (Thermo Fisher, 155411). The samples were prepared depending on the requirement for the experiment with a final volume of 150-300µL applied to the well. GFP tagged, SNAP-Surface® Alexa Fluor® 488 or SNAP-Cell® Oregon Green® labelled samples were excited with 488nm laser and emission was

collected with a 505-550nm bandpass filter. SNAP-Cell® TMR-Star or SNAP-Surface® Alexa Fluor® 647 labelled samples were excited with 633nm laser and emission was collected with a 655nm longpass filter. Data were collected by measuring fluorescence intensity fluctuations (e.g. 3x 10-100 second traces) at a fixed laser power as determined in the optimisation of a particular set of experiments. Data were then analysed using Zen 2010 (Carl Zeiss) software.

### 2.10.2 Calibration and FCS analysis

At the start of each FCS experiment the system was calibrated. In the case of the 488nm excitation rhodamine 6G was used and for the 633nm excitation Cy5 was used based on the excitation/emission spectra of these fluorophores. 1µM and 20nM solutions of rhodamine 6G were used and 500nM and 10nM solutions of Cy5 were used. The microscope system including the appropriate lasers were switched on 2 hours prior to use to allow the system to equilibrate to room temperature. 200µL of each solution was applied to wells in an 8-well plate. The chambered cover glass was mounted onto the microscope objective and the confocal volume was positioned in solution 200µm above the upper coverslip surface in the higher concentration calibration solution. The x, y position of the pinhole (set to 1 Airy unit) and the collar were adjusted to achieve the maximum signal. A 60 second fluorescence fluctuation trace was then recorded for the lower concentration solution of the appropriate calibrant. The dwell time, $\tau_{D,}$ and structural parameter, S, were determined by fitting the generated autocorrelation

curves to a 1-component 3D free diffusion model, including correction for fluorophore triplet state/blinking (*A*) as defined by:

*Equation 2.3*

$$G_{(\tau)} = 1 + A\frac{1}{N} \cdot \sum_{i=1}^{m} \cdot \Phi_i \cdot (1 + \frac{\tau}{\tau_{Di}})^{-1}(1 + \frac{\tau}{S^2\tau_{Di}})^{-0.5}$$

Where:

$$A = 1 + (T_\tau \cdot e^{\frac{\tau}{\tau_\tau}}) \cdot (1 - T_\tau)^{-1}$$

And N = particle number, $\Phi_i$= fraction of species (i) from the total number of species (m), $\tau_D$= diffusion (or dwell) time, $T_\tau$ = triplet fraction, $\tau_\tau$ = triplet relaxation time (given in µs) and S = structural parameter.

Then, using the known diffusion coefficient of rhodamine 6G (2.8 x $10^{-10}$ $m^2s^{-1}$) or Cy5 (3.16 × $10^{-10}$·$m^2s^{-1}$) the radius at the waist ($W_{xy}$) of the confocal volume was calculated using:

*Equation 2.4*

$$W_{xy} = (4 \cdot D^{Cal} \cdot {\tau_D}^{Cal})^{0.5}$$

This waist radius allowed the determination of diffusion coefficients of the proteins based on their measured $\tau_D$ based on:

*Equation 2.5*

$$D = {W_{xy}}^2/4\tau_D$$

The concentration ($C$) of species (i) was obtained using:

*Equation 2.6*

$$C_i = \frac{N \cdot \Phi_i}{N_A} \cdot \frac{1}{\pi^{3/2} \cdot {W_{xy}}^2 \cdot W_z}$$

Where:

$$W_z = S \cdot W_{xy}$$

When obtaining the fluorescence traces for the protein samples, S was fixed to that obtained in the calibration sample for a particular experiment while the $\tau_D$ and N were allowed to vary freely unless otherwise stated. Diffusion coefficients were calculated for each independent experiment then averaged for reporting. Diffusion coefficients and component concentrations are presented as a mean ±SD or ±SEM of at least 3 independent experiments and assessed for significant differences by one-way ANOVA followed by post-hoc tests as specified.

### 2.10.3 PCH analysis

The same raw data used for FCS analysis was also subjected to PCH analysis for the determination of molecular brightness. In Zen 2010 software, 1-component or 2-component 3D PCH models were used (Huang, Perroud and Zare, 2004). These models were fitted against frequency distributions of the amplitudes in the fluorescence fluctuation trace when sampled using specified bin times (described in the respective results sections). The average molecular brightness (cpms) and number of particles (N) in the confocal volume was also determined. A first order correction factor was applied to account for single photon excitation and the variation from a true Gaussian detection volume (Huang, Perroud and Zare, 2004). This was calculated using a 1-component 3D PCH model in Zen 2010 fitted to the data from the calibration read performed as in Section 2.10.2. When fitting the data from experimental samples, while the first order correction factor was fixed to that obtained for the calibration sample, the molecular brightness and number of particles were allowed to vary freely unless otherwise stated. Molecular

brightness data were reported as mean ± SD for at least 3 independent experiments.

## 2.11 Binding analysis by FCS

ABCG2 was purified and the concentration determined as in Section 2.6. After samples were prepared, analysis of compound binding was performed by FCS.

### 2.11.1 Drug binding assays

FCS was used to measure the binding of BODIPY-FL-prazosin to SMALP encapsulated ABCG2. 150uL of 50nM BODIPY-FL-prazosin was applied to the wells of an 8-well plate at left at room temperature for 30 minutes. Varying concentrations of SMALP-ABCG2 were made up in SMA buffer to a volume of 150µL in a 0.5mL Eppendorf tube. The protein samples were applied to the pre-incubated 8-well plate and left again for 30 minutes at room temperature before being analysed by FCS. Three 10 second fluctuation traces were recorded for each sample with the replicate data combined to form a single measurement. At least three measurements were performed over n=3 independent experiments with data reported as either component fraction or measured concentration.

### 2.11.2 Competition binding assays

Solutions of SMALP-ABCG2 were made up in SMA buffer and incubated with the appropriate inhibitor for 30 minutes in a volume of 100µL. These were then mixed with 100µL of BODIPY-FL-prazosin with or without the associated inhibitor to give a final volume of 200µL containing 100nM ABCG2, 50nM BODIPY-FL-prazosin and

the inhibitors as appropriate. These solutions were left to equilibrate at room temperature for 30 minutes before being applied to an 8-well plate and incubated again for 30 minutes before being analysed by FCS. Three 10 second fluctuation traces were recorded for each sample with the replicate data combined to form a single measurement. At least three measurements were performed over n=3 independent experiments with data reported as % Bound by:

*Equation 2.7*

$$\%\, Bound = \frac{C_{\tau_{D2}}{}^{Competitor}}{C_{\tau_{D2}}} \times 100\%$$

Where $C_{\tau_{D2}}$ is the concentration of the bound component and $C_{\tau_{D2}}{}^{Competitor}$ is the concentration of the bound component in the presence of a binding competitor.

## 2.12 Statistical analysis

Statistical analysis was performed in GraphPad Prism 7. In experiments with at least three independent replicates were assessed for differences between conditions by one-way ANOVA. This was followed by post-hoc analysis as described for the reporting of significance values and differences were assumed to be significant where $p<0.05$.

# 3 Plasmid Construct Generation

## 3.1 Design and engineering of fluorescent and His-tagged ABCG2 protein constructs for metal ion affinity purification

An important element of this study was the focus on ABCG2 expression and function in cells of human origin and its subsequent extraction within a near-native membrane environment. HEK293T was the main cell line used with pcDNA3.1(+)zeo as the vector backbone for DNA construct engineering. In order to support efforts to purify ABCG2 and analyse the generated protein constructs by fluorescence microscopy, both an appropriate purification tag and fluorescence tag were required.

### 3.1.1 Purification tags

It is possible to purify native proteins by serial chromatography steps involving separation based on size, charge or isoelectric point for example (Janson, 2011). This is labour intensive and optimised parameters are specific to an individual protein, meaning the whole process may need to be repeated if investigating another protein or even a mutant isoform of the same protein. In addition the use of SMALPs minimises selectivity of chromatography techniques by reducing the differences in size and charge of encapsulated protein. Also, an eventual aim would be to apply the tools developed in this project to other transporters or receptors so a reproducible protocol would be preferred. The use of affinity tags

is far more widespread (Waugh, 2005; Arnau *et al.*, 2006). The overall scheme involves the expression of a recombinant protein fused to an affinity tag, enabling its purification via the use of an appropriate affinity matrix. There are many available options including glutathione S-transferase (GST) tags (Smith and Johnson, 1988), Maltose Binding Protein (MSB) tags (di Guan *et al.*, 1988), Streptavidin tags (Schmidt and Skerra, 1993) but by far the most popular is the His-tag (Young, Britton and Robinson, 2012).

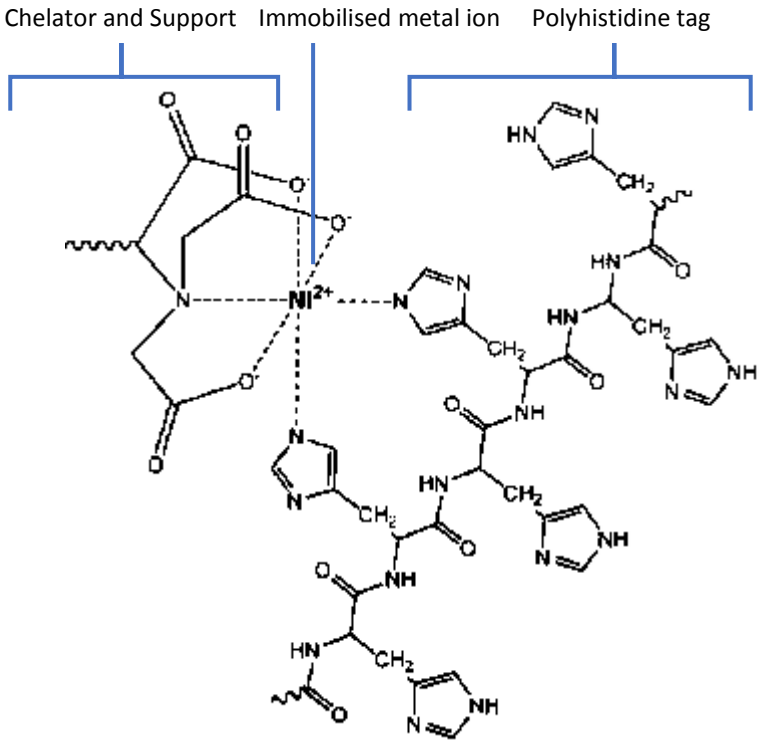


**Figure 3.1 – Schematic representation of the interactions associated to IMAC.** The polyhistidine region of the protein of interest forms ionic bonds with the metal ion immobilised by dative bonds with the chelator complex anchored covalently to a supporting resin.

The His-tag consists of six or more consecutive histidine residues. Purification of polyhistidine –tagged fusion proteins is based on the affinity for resin immobilised metal ions ($Ni^{2+}$, $Co^{2+}$ or $Cu^{2+}$). This binding interaction can then be overcome by the use of excess imidazole as shown in Figure 3.1. Compared to other tags, a hexahistidine tag has a small size and does not usually affect protein folding at physiological pH. In addition, it is relatively simple to introduce and was employed for this study for these reasons.

### 3.1.2 Fluorescence tags

As discussed above, fluorescence has proved to be an incredibly useful tool in the study of protein characteristics and functionality. There are several ways to label proteins for fluorescence based studies; the expression of fusion proteins with fluorescent protein tags (e.g. GFP, CFP or YFP (Day and Davidson, 2009)), with tags for chemical labelling (SNAP-tag, CLIP-tag or Halo tag (Crivat and Taraska, 2012)) or by monitoring the binding of a fluorescent ligand to the protein of interest. In effect, each of these were employed in this study for different reasons based on the particular advantages of each. A GFP-tag was used in the study of oligomeric state of ABCG2 in SMALPs because it was used similarly in a previous study done in live cells (Wong *et al.*, 2016). It overcomes the potential issues with labelling efficiency associated to the use of chemical labels. The GFP tag itself has some limitations, for example incomplete maturation leading to difficulties of interpreting brightness measurements (Chen *et al.*, 2010). These difficulties were

accounted for by the use of appropriate controls and confirmation of tagged ABCG2 transport activity (Section 4.5) as previously reported (Haider *et al.*, 2011, 2015). SNAP-tag fusion proteins were also employed. SNAP-tagged proteins were used instead of GFP to provide greater versatility in terms of range of available fluorophores excitation and emission spectra. The system is described later in Section 4.8. This meant, without having several cell lines expressing different fluorescent proteins, is was possible to simply select an appropriate SNAP ligand to avoid interference with fluorescent ABCG2 transport substrates. Finally, fluorescent substrates for ABCG2 were also used though in the context of specific binding experiments (see Chapter 6) rather than monitoring protein.

### 3.1.3 Design Summary

As illustrated in Figure 3.2 the generated constructs contained a polyhistidine ($His_6$) and a fluorescence tag fused N-terminally to ABCG2. Tags located C-terminally to ABCG2 have been previously reported as being detrimental to proper ABCG2 function (Haider *et al.*, 2011). The use of a polyhistidine tag is standard for protein purification by immobilised metal ion affinity chromatography (IMAC), and GFP and SNAP-tag fluorescence tags were employed in this study. All the generated constructs used are summarised in Table 3.1 and the detail of construct generation is given in this chapter.

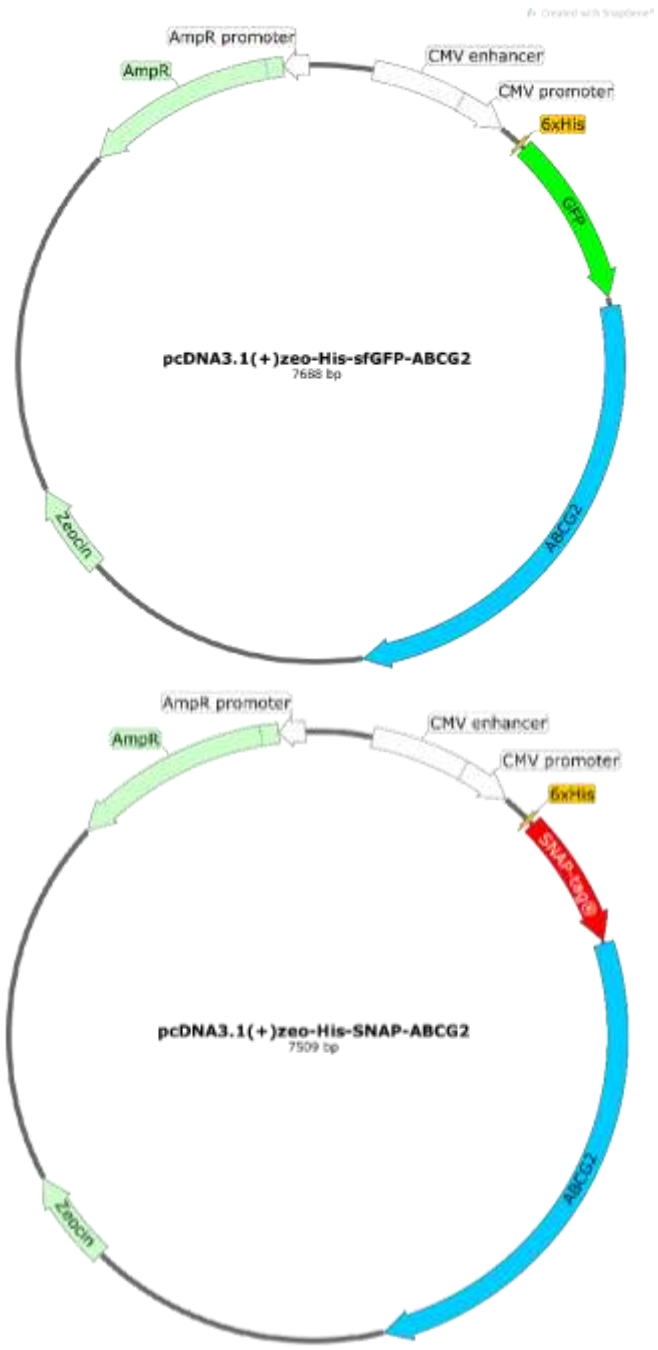


**Figure 3.2 – Schematic outline of the main ABCG2 encoding DNA vectors used in this study.** The vectors in the pcDNA3.1(+)zeo backbone encode ABCG2 fused N-terminally by a polyhistidine tag (His) and either GFP or SNAP-tag®. The vector also contains the CMV promoter system for enhanced expression, the bacterial ampicillin resistance gene (AmpR) for genetic engineering in addition to Zeocin resistance for stable selection of mammalian cell lines.

## 3.2 Generation of pcDNA3.1(+)zeo-ABCG2 constructs

Fluorescence-tagged ABCG2 suitable for purification by IMAC was expressed in a stable HEK293T cell line. HEK293T are a widely used and versatile cell line, well established within many institutions. Starting vectors pcDNA3.1(+)zeo-GFP-ABCG2 (Wong *et al.*, 2016) and pcDNA3.1(+)zeo-SNAP-ABCG2 were provided by Dr Ian Kerr (University of Nottingham). These encoded ABCG2 N-terminally tagged with GFP or SNAP-tag in the pcDNA3.1(+)zeo vector. The vector conveys resistance to Zeocin™ for the purpose of stable mammalian cell line generation and encodes the bacterial ampicillin resistance gene allowing for selection of bacterial strains in genetic engineering processes. The vector contains multiple restriction sites used for cloning and diagnostic digests. There is a strong cytomegalovirus (CMV) promoter region to increase protein expression in mammalian cells. The initial vectors did not encode purification tagged proteins so cloning efforts sought to address this; short oligonucleotide pairs were annealed to form a double stranded DNA insert that encoded a hexahistidine tag flanked by a 5' start codon, 5' or 3' overhangs for ligation into the target vector and extra bases where necessary to maintain the reading frame. The inserts were engineered to contain additional restriction sites compared to the template DNA. The presence of the inserts could be screened for by restriction digest with NcoI in the case of pcDNA3.1(+)zeo-His-GFP-GFP and MscI in the case of pcDNA3.1(+)zeo-His-SNAP-ABCG2. The overall process of "short oligo insert cloning" is outlined in Figure 3.3 and in Methods 2.1.4. The starting vectors were digested with NheI for the GFP construct or HindIII for the SNAP-tag construct. Inserts were ligated in and the resulting construct transformed into competent bacterial cells as described in Methods 2.1.5.

Colonies resistant to ampicillin were collected and grown up overnight following which plasmid DNA was extracted. Insertion of the tag was confirmed by restriction digest for 1 hour at 37°C with the above enzymes as shown in Figure 3.3 (C).

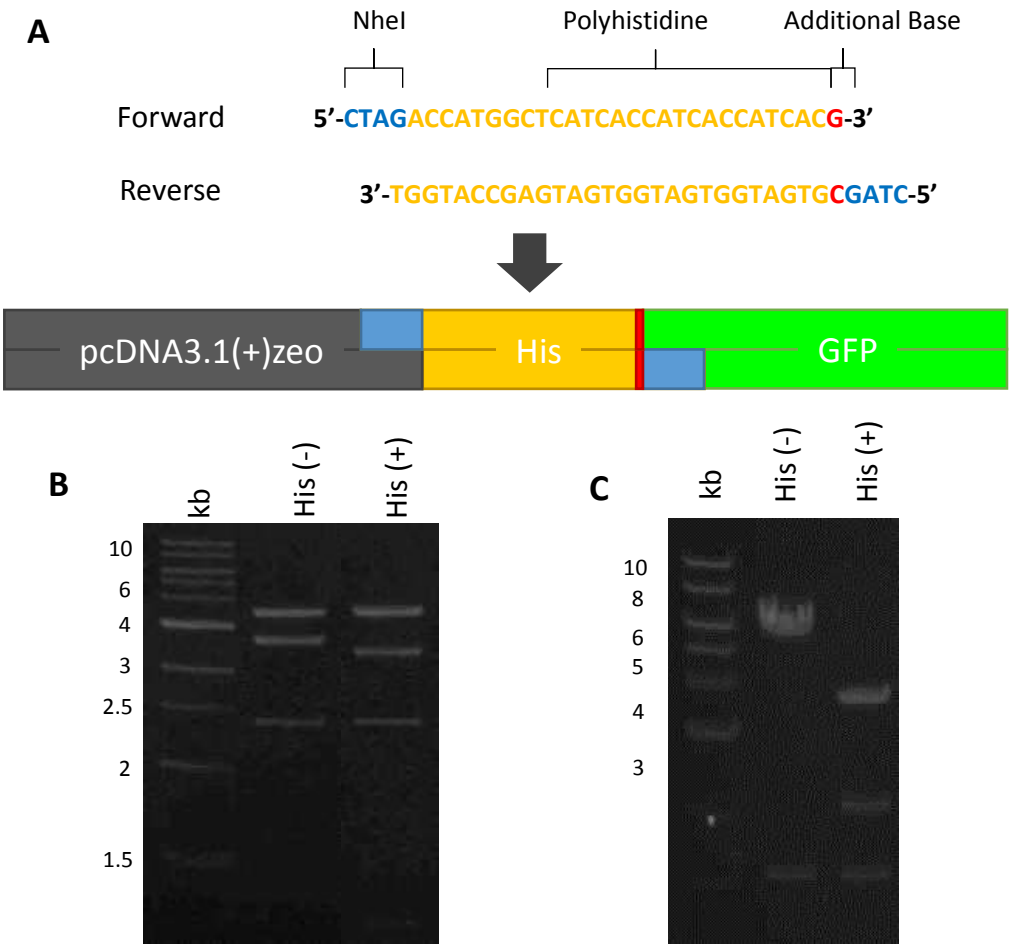


**Figure 3.3 – Outline of N-terminal short His-tag oligo insert cloning.** Schematic representation (**A**) of the process by which short single stranded oligonucleotide pairs were annealed to form a double stranded sequence. Single stranded oligo pairs were annealed to form a short double stranded DNA sequence encoding a hexahistidine tag that could be ligated into NheI digested pcDNA3.1(+)zeo-GFP-ABCG2. Successful introduction of the tag could be screened for by diagnostic DNA digest with NcoI and analysis by agarose gel electrophoresis – the 3.7kb band being reduced in size by about 400bp (**B**). The same strategy was used for the SNAP-tag construct where a diagnostic digest with MscI indicated the successful introduction of the polyhistidine tag (**C**).

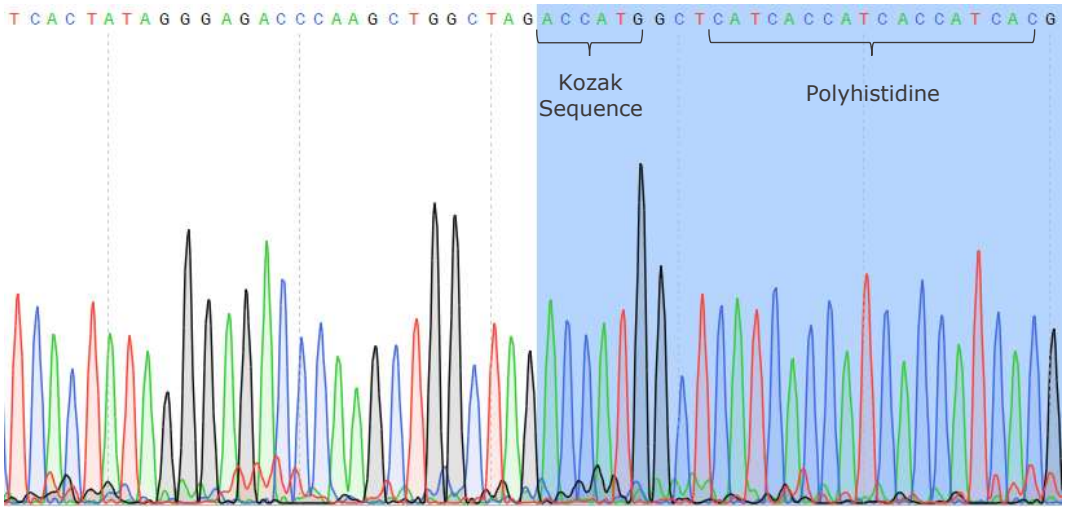


**Figure 3.4 – Successful introduction of polyhistidine tags was confirmed by DNA sequencing.** The correct orientation and position of the polyhistidine inserts as well as maintenance of the reading frame and lack of inadvertent mutations across the entire sequence of both constructs was confirmed by DNA sequencing. Chromatograms like that obtained above which shows start region of the His_GFP_ABCG2 construct (highlighted blue) using primer p3.1zeo-up were visually assessed for quality (e.g. defined peaks, contamination). The obtained sequences were then compared to predicted construct sequences by BLAST (NCBI) alignment, together with checking that the coding regions were in frame at the point of tag fusion.

The new constructs retained an internal start codon (between His tag and GFP or SNAP tag) which was removed by site-directed mutagenesis using primers GFP_ATG→CTG_For/Rev and SNAP_ATG→CTG_For/Rev (see Table 2.3). This precluded translation of fluorescence tagged ABCG2 without the polyhistidine tag. The final DNA sequences were confirmed by Sanger sequencing of the entire ABCG2 coding region before use in further processes. The chromatograms obtained were assessed for quality by direct observation of the sequence traces. BLAST (NCBI) assessment according to the predicted sequences revealed the correct orientation and position of the inserts as well as maintenance of the reading frame and lack of inadvertent mutations across the entire sequence of both constructs.

The final constructs are outlined in Figure 3.2, an example chromatogram is given in Figure 3.4 and example BLAST (NCBI) analysis is included in Supplementary Figure 9.1.

## 3.3 Generation of pcDNA4/TO-ABCG2 constructs

It was not initially clear whether optimal protein expression levels would be obtained in a constitutive expression system. Another option was to explore the use of inducible cell lines such as the tetracycline induction system. These systems are often used to regulate expression of a protein of interest with a degree of control that is not afforded by constitutively expressing lines such as the clonal HEK293T lines described in Chapter 4. To generate the inducible system, the tagged ABCG2 constructs described earlier were cloned into pcDNA4/TO. The starting vector was provided by Dr Nicholas Holliday (University of Nottingham). Much like the pcDNA3.1(+)zeo backbone, the pcDNA4/TO vector conveys resistance to Zeocin™, encodes the bacterial ampicillin resistance gene and there is a strong CMV promoter regulatory region. In addition to these features, the pcDNA4/TO vector also encodes two tetracycline operators. This vector is used in conjunction with the pcDNA6/TR plasmid which encodes the tetracycline repressor protein, and is stable transfected in the TREx™-293 cell line. In the absence of tetracycline, the tetracycline repressor protein prevents transcriptional activation via the CMV promoter by binding the tetracycline operators. In the presence of tetracycline, the tetracycline repressor protein releases the tetracycline operator sites which subsequently allows transcription forward of the CMV promoter. The ABCG2 constructs from Section 3.2 were

cloned into pcDNA4/TO forward of the CMV promoter in a two-step process as outlined in Figure 3.5. There was no 5' restriction site suitable for sub-cloning either the His_SNAP_ABCG2 or His_GFP_ABCG2 constructs in pcDNA3.1(+)zeo. A unique KpnI site was introduced via site-directed mutagenesis with the KpnI_Intro_For/Rev primers indicated in Table 2.3. The novel restriction site was then utilised alongside a pre-existing 3' restriction site for XbaI to excise the His_FP_ABCG2 encoding regions which were then ligated into pcDNA4/TO. These products were transformed into competent bacterial cells and individual colonies were picked and grown up in liquid broth. Plasmid DNA was isolated from these liquid cultures and screened for construct insertion by digest with PvuII. Following this, DNA sequences were confirmed by Sanger sequencing and BLAST analysis (see Supplementary Figure 9.1) of the entire ABCG2 coding region before use in further processes.

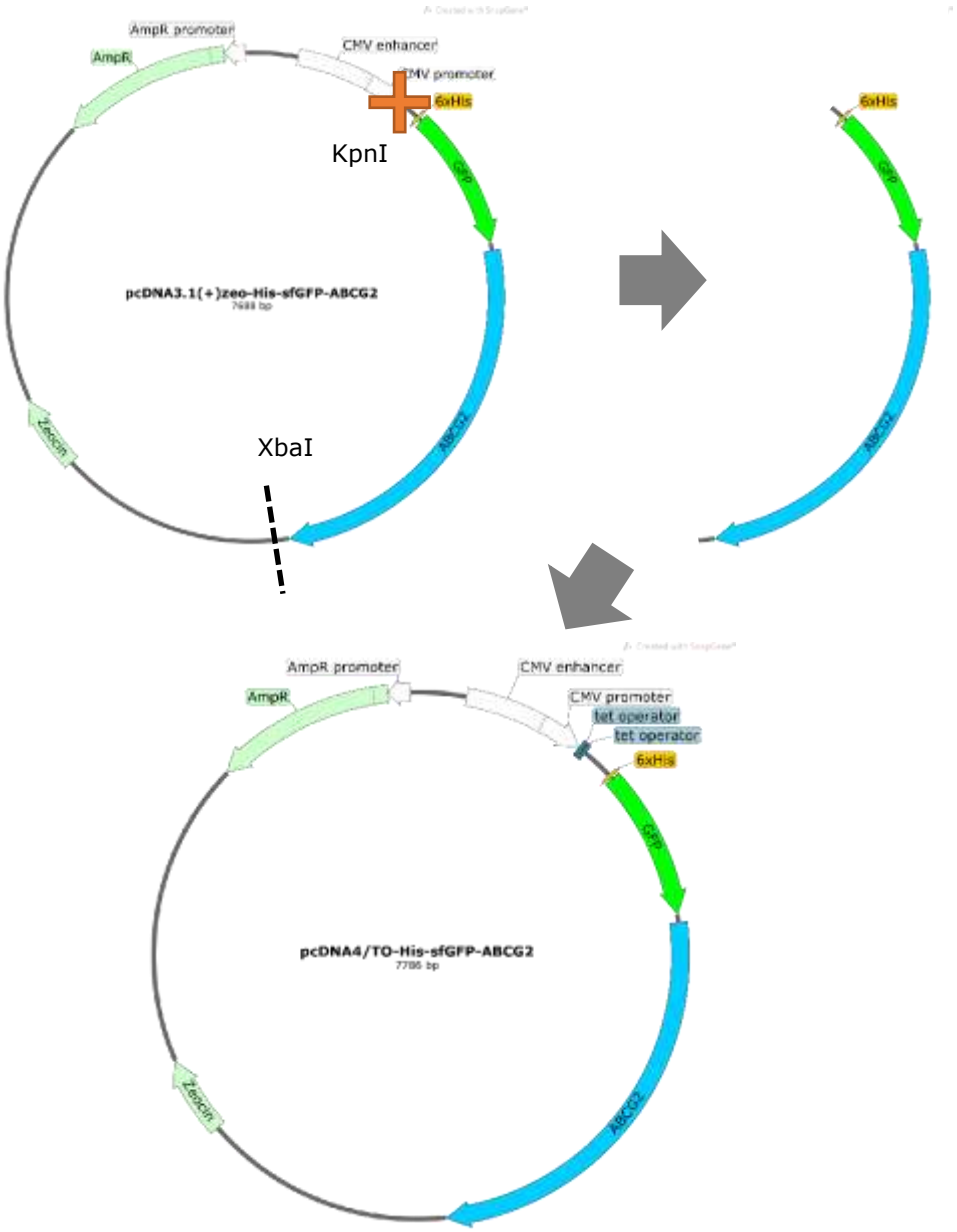


**Figure 3.5 – Summary of pcDNA4T/O construct generation.** Site directed mutagenesis was used to introduce a novel (KpnI) restriction site (red cross) 5' to the His_FP_ABCG2 construct. This site was then used alongside a pre-existing 3' XbaI site (dotted lines) to excise the desired construct. This product was then ligated into the pcDNA4/TO backbone.

## 3.4 Generation of oligomeric control constructs

In this study knowledge of ABCG2 oligomeric state would be important for the interpretation of subsequent experiments. Therefore control proteins of characterised oligomeric state were required. CD86 and CD28 act as known monomeric and dimeric membrane proteins respectively and have been successfully used in previous studies for the same purpose (Wong *et al.*, 2016). Starting vectors encoding each CD86_GFP or CD28_GFP in the pcDNA3.1(+)zeo backbone were provided by Dr Ian Kerr (University of Nottingham). These were C-terminally tagged with polyhistidine to support attempts purification by IMAC by oligo overlap cloning in a process similar to that described in Figure 3.3. Following the addition of the polyhistidine tag, the original stop codon (i.e that proceeding the fluorescent protein tag) was removed by site directed mutagenesis using the primers CD86_TAA→CTT_For/Rev (see Table 2.3) to ensure translation of the full oligomeric control fusion proteins. The constructs are summarised in Figure 3.6.

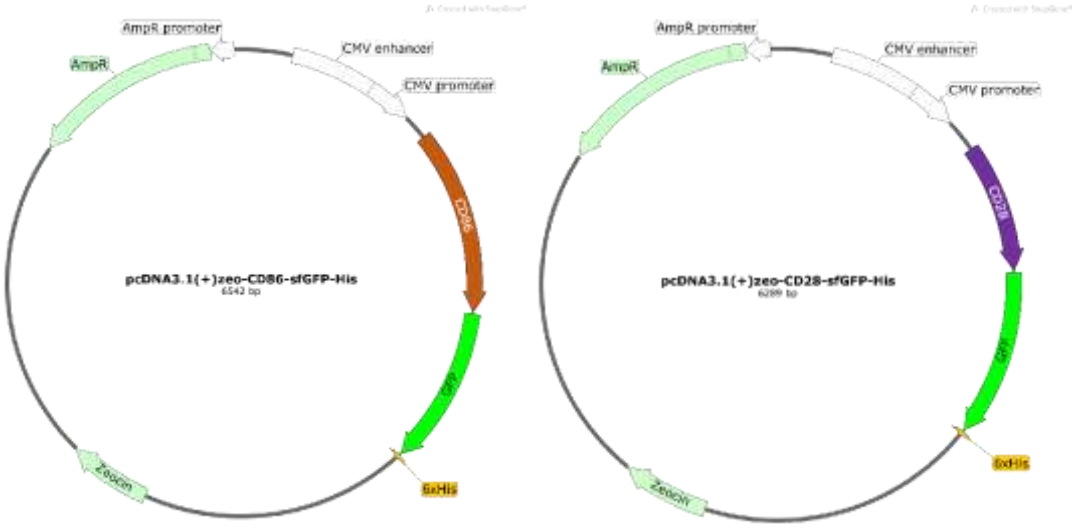


**Figure 3.6 – Schematic outline of the CD86 and CD28 control vectors.** The vectors encode either CD86 or CD28 fused C-terminally with GFP and a polyhistidine tag. The vectors also contains the CMV promoter system for enhanced expression, the bacterial ampicillin resistance gene for genetic engineering in addition to Zeocin resistance for stable selection of mammalian cell lines.

## 3.5 Summary of construct generation and utilisation

This chapter explained the overall design and engineering of DNA constructs encoding the fluorescent fusion proteins suitable for purification to be used throughout this study. These are summarised in Table 3.1. In all cases the insertion and orientation of the polyhistidine tag and the lack of unintended effects on the overall protein constructs were confirmed by DNA sequencing. Subsequent chapters describe the characterisation of these constructs in terms of expression, localisation and function then the use of these constructs in fluorescence studies.

| DNA Vector | Encoded Protein Schematic | Generation Summary |
|---|---|---|
| pcDNA3.1(+)zeo-His-GFP-ABCG2 |  | Starting vectors encoding the protein of interest (ABCG2/CD86/CD28 fused to GFP or SNAP-tag) were polyhistidine tagged by short oligo cloning. |
| pcDNA3.1(+)zeo-His-SNAP-ABCG2 |  | |
| pcDNA3.1(+)zeo-CD86-GFP-His |  | |
| pcDNA3.1(+)zeo-CD28-GFP-His |  | |
| pcDNA4/TO-His-GFP-ABCG2 |  | ABCG2 constructs generated in pcDNA3.1(+)zeo were cloned into pcDNA4/TO. This plasmid facilitates the control of protein expression under the application of tetracycline. |
| pcDNA4/TO-His-SNAP-ABCG2 |  | |

**Table 3.1 - Summary of the main fluorescent protein constructs used in this study.** ABCG2, N-terminally tagged with polyhistidine and either GFP or SNAP-tag and C-terminally tagged CD86 and CD28 were encoded in the pcDNA3.1(+)zeo backbone. The ABCG2 constructs were also cloned into the pcDNA4/TO vector.

# 4 Expression, characterisation and solubilisation of ABCG2

## 4.1 Chapter Overview

In order to facilitate the downstream study of SMALP-encapsulated ABCG2 by fluorescence microscopy, the fluorescent fusion protein constructs designed in Chapter 3 were expressed in a mammalian cell system. They were designed to contain polyhistidine tagged ABCG2, CD86 or CD28 labelled with either GFP or SNAP-tag®. The generated plasmids were stably expressed in HEK293T cells which were grown in large scale adherent as well as suspension cultures. Before use in downstream experiments, the expressed protein constructs were validated by characterisation of cell surface expression by confocal microscopy, and of drug efflux capacity by mitoxantrone accumulation assays. Subsequently, the expression level was optimised and labelling was performed where necessary for the SNAP-tag® constructs. Novel, non-surfactant polymers were then assessed for the ability to solubilise ABCG2 as discussed below to enable analysis of these fusion proteins in solution by fluorescence correlation spectroscopy.

## 4.2 Generation of stable cell lines

The HEK293T cell line was selected to be the expression system for this project. They are a derivative of the HEK-293 (ATCC® CRL-1573™) line which was generated by transformation by type 5 human adenovirus of normal human embryonic kidney cells. This line was later transfected with the SV40 promoter region of Epstein-Barr virus to increase protein production (Graham *et al.*, 1977; DuBridge

*et al.*, 1987; Pear *et al.*, 1993). Due to the requirement to produce protein throughout the duration of this project stable cell lines were generated (as described in Section 2.2.9) for the practicality and reproducibility they afford in comparison to the alternative of a repeated transient expression protocol. This was achieved by the use of PEI mediated transfection of the described pcDNA plasmids and a Zeocin™-mediated selection regime of around 2 weeks in duration that resulted in mixed population stable cell lines expressing the desired constructs (outlined in Figure 4.1). The expression, localisation and function of the tagged ABCG2 were then assessed to validate the constructs.

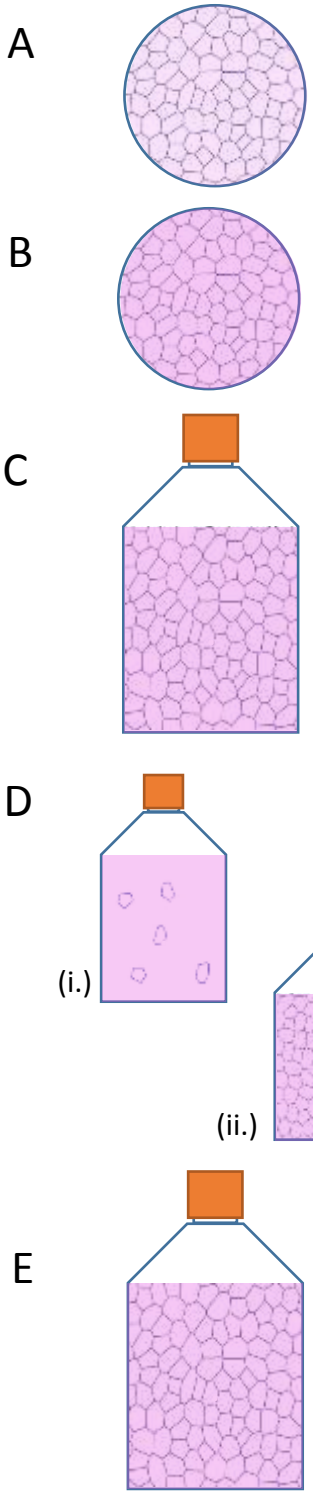


DNA is added to a near confluent HEK293T cultured in a 6-well dish in DMEM supplemented with 5% FBS.

After 24 hours the media is replaced with that containing 10% FBS.

48 hours post-transfection the cells are harvested in ice cold PBS and transferred to a T25 containing DMEM supplemented with 10% FBS and 200µg/mL Zeocin®.

The Zeocin® concentration is maintained at 200µg/mL for 10-14 days during which time the discrete colonies of Zeocin resistant cells (a) expand and subsequently grow to confluency (b). Cells at this stage are harvested for long term storage in liquid nitrogen.

Cells are then transferred to a new flask and maintained at a Zeocin® concentration of 40µg/mL for up to 30 passages.

**Figure 4.1 – Outline of the generation of a stable cell line by Zeocin® mediated selection.** HEK293T cells were transfected (A). Following a media replacement (B) and the addition of Zeocin™ at 200µg/mL (C), near complete cell death is observed (D(i)) followed by a recovery to confluence (D(ii)). The Zeocin™ concentration was reduced and the cell line maintained by regular passage. This process is typically followed the course of at least 2 weeks.

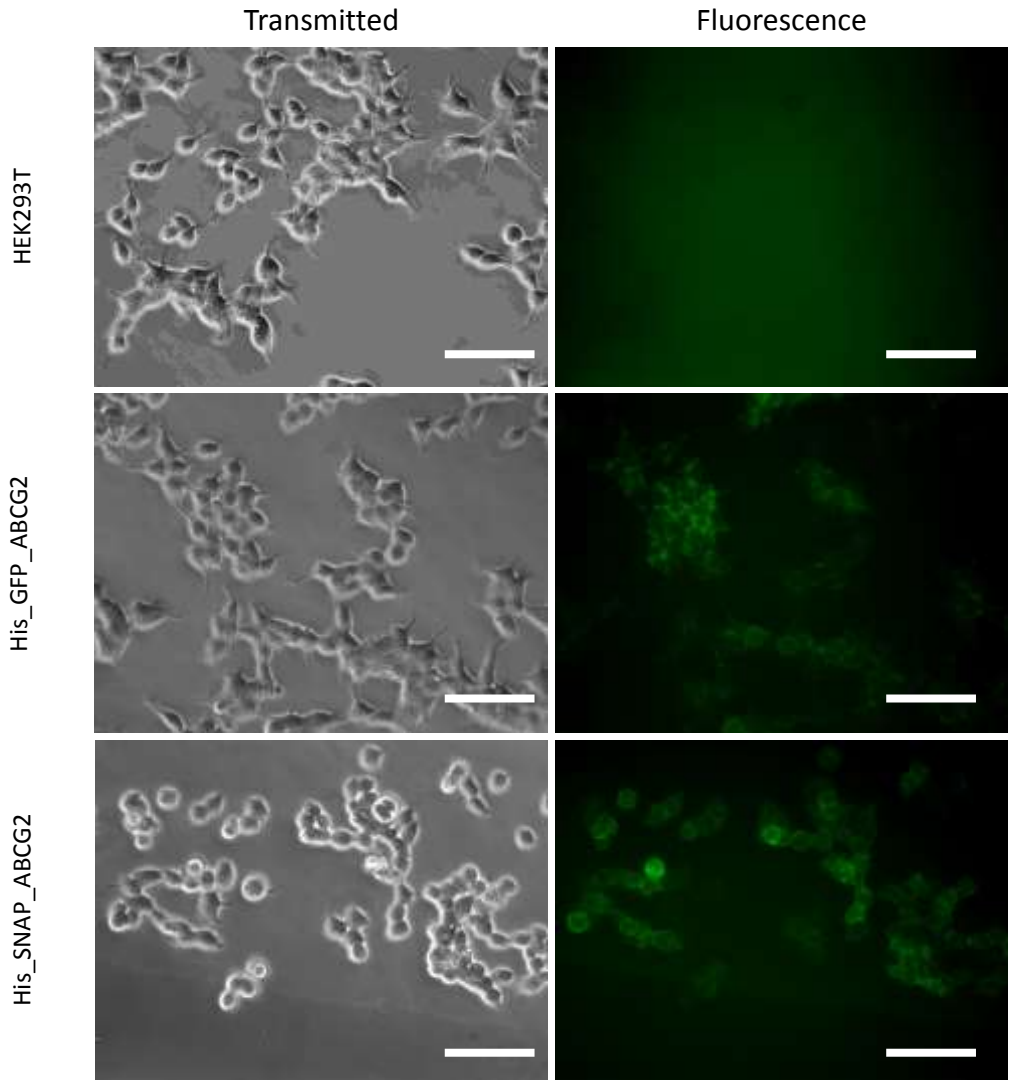


**Figure 4.2 – Demonstration of tagged ABCG2 expression by fluorescence microscopy.** Live parental HEK293T cells and stable lines expressing SNAP-tag or GFP labelled ABCG2 were seeded in a 6 well plate. SNAP-tag expressing cells were labelled for 30 minutes at 37°C 5% $CO_2$ with 1µM SNAP-Cell® Oregon Green®, washed 3 times with media with a final media replacement just prior to imaging on a Zeiss Axiovert 100S inverted microscope equipped with a 10× objective and an Axiocam CCD camera (Carl Zeiss). Scale bar = 100µm.

## 4.3 Demonstration of protein and tag expression by western blot analysis

Protein expression could readily be observed by epifluorescence microscopy for the GFP and the SNAP-tag labelled constructs as shown in Figure 4.2. However, the expression of ABCG2 and the polyhistidine tag was also demonstrated by Western blot analysis for each construct. SDS-PAGE and subsequent western blotting analysis was performed on whole cell lysates of the stable cell lines as described in Methods. A representative result is shown in Figure 4.3. Blots were probed with anti-polyhistidine or BXP-21 primary antibodies. In each case this revealed a construct of approximately 100kDa which corresponds to that which would be expected for ABCG2 (72kDa) expressed alongside the tags (26kDa for GFP or 20kDa for SNAP-tag®). Multiple bands were observed around 100kDa and were presumed to represent the glycosylation of ABCG2 at a single asparagine residue (N596) which has been reported previously and has no impact on the expression, localisation or function of ABCG2 (Diop and Hrycyna, 2005). This was confirmed by PNGase F treatment which results in the endoglycosydic removal of Asn-linked glycans and subsequently shows one band by SDS-PAGE and western blot analysis (Tarentino, Trimble and Plummer, 1989).

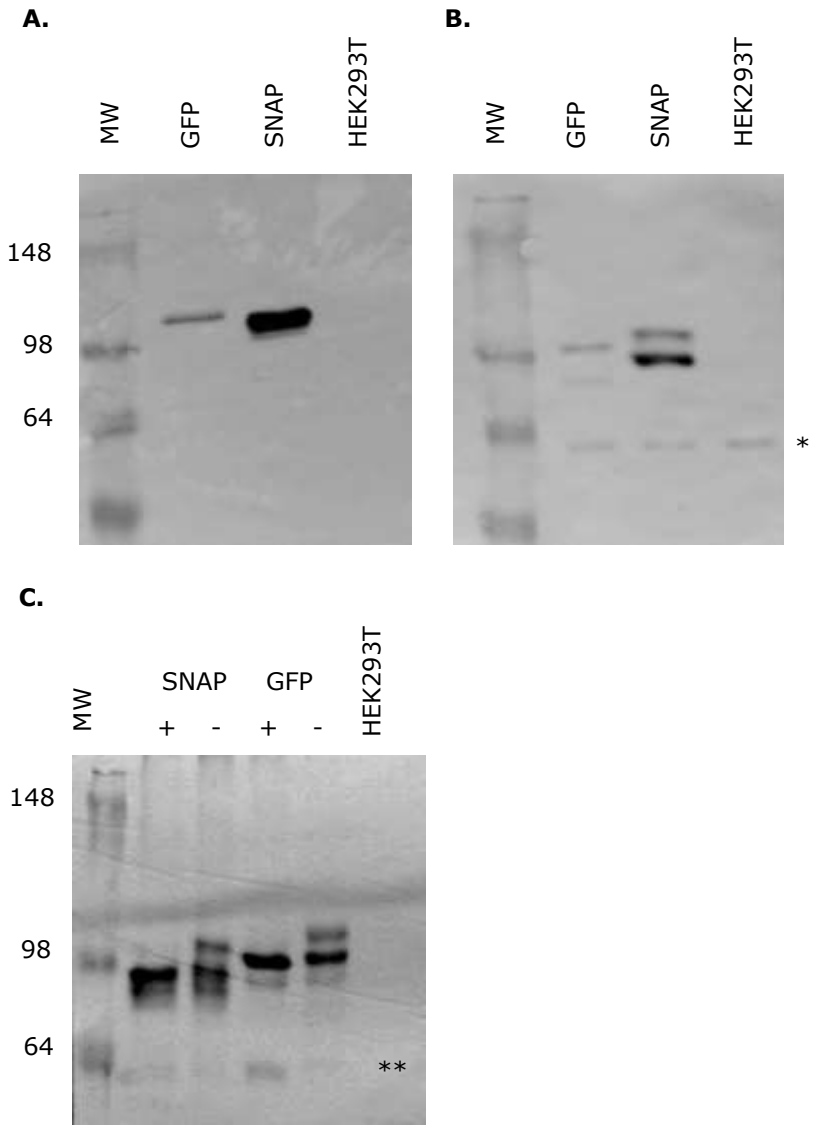


**Figure 4.3 – Demonstration of tagged ABCG2 expression by Western blot analysis.** Lysates were prepared by sonication of parental HEK293T and cell lines expressing tagged ABCG2. When probed with BXP-21 (**A**) (monoclonal murine anti-ABCG2 antibody) or anti-polyhistidine antibody (**B**), Western blot analysis (probing with BXP-21)revealed a signal corresponding to ABCG2 at around 100kDa. The higher molecular weight band observed around 100kDa was removed by treatment with PNGase F (**C**). A protein showing reactivity with the anti-His antibody in HEK293T cells is indicated (*) in panel B and a probable ABCG2 breakdown product is indicated (**) in panel C.

## 4.4 Demonstration of protein localisation by confocal microscopy

The localisation of ABCG2 to the plasma membrane of a cell is fundamental to its functionality. The addition of fluorescence and purification tags might cause some perturbation of the cell surface localisation of ABCG2. Therefore, subcellular localisation of the ABCG2 fusion proteins was examined by confocal microscopy, which demonstrated that each ABCG2 construct was expressed and localised to the plasma membrane of live cells. To make this observation cells were seeded in dishes and grown overnight, then observed in phenol red-free DMEM by confocal microscopy. As previously observed for similar constructs of ABCG2 (Haider *et al.*, 2011; Wong *et al.*, 2016), labelled protein was predominately localised to the cell surface (Figure 4.4). A small amount of ABCG2 related fluorescence was observed in the intracellular compartments (red arrow in Figure 4.4) which may represent protein in the biosynthesis or degradation pathways, but the vast majority of ABCG2 was clearly located at the plasma membrane of living HEK293T cells.

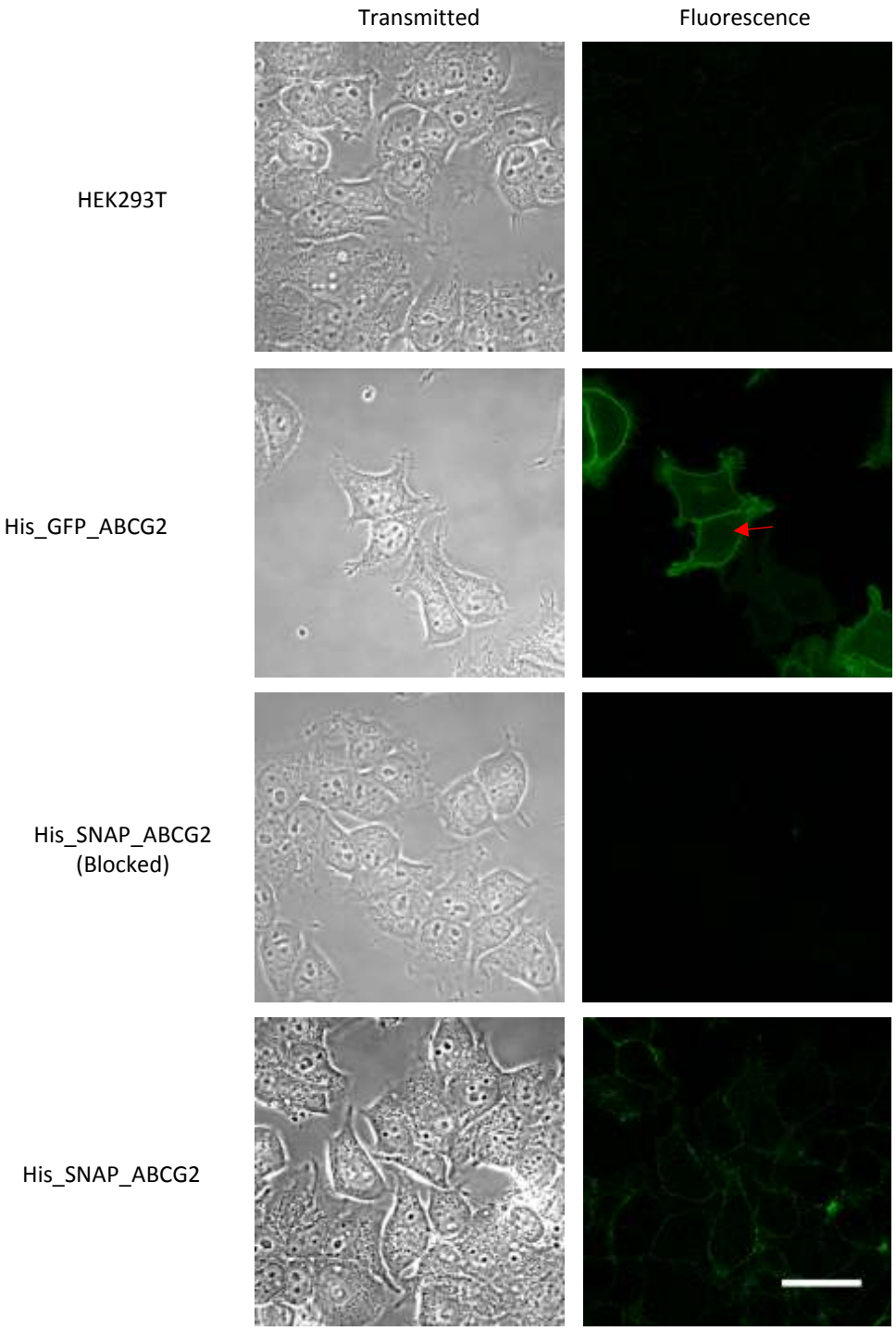


**Figure 4.4 – Expression of ABCG2 at the plasma membrane of stably expressing HEK293T cells.** Representative images showing phase (left) and fluorescence (right) images of live HEK293T cells expressing the ABCG2 constructs used in this study. The images were obtained using an LSM710 confocal microscope (Carl Zeiss) with fluorescence images gathered using 488nm/493-598nm excitation/emission wavelengths. SNAP-tag expressing cells were labelled for 30 minutes at 37°C 5% $CO_2$ with 1µM SNAP-Cell® Oregon Green®, washed 3 times with media with a final media replacement just prior to imaging. 'Blocked' were incubated with 2µM SNAP-Cell®-Block for 20 minutes then washed prior to labelling. Scale bar = 20µm.

## 4.5 Determination of transport activity in tagged ABCG2 constructs

It is also important to demonstrate that the tagged ABCG2 constructs retained drug efflux capability. After the generation of stable clonal cell lines (see 4.6.1 below) the efflux capability of tagged ABCG2 was verified by an established assay (Haider *et al.*, 2015) measuring the intracellular accumulation of a transport substrate of ABCG2 (mitoxantrone) in the presence or absence of a specific inhibitor (Ko143). In the absence of inhibitor, the activity of ABCG2 limits the intracellular mitoxantrone concentration, but this rises as the transport activity is inhibited by Ko143. Thus, Ko143-sensitive accumulation of mitoxantrone (expressed as a percentage of the total) provides an indication of transporter function (Figure 4.5). This was calculated as per Equation 2.2 as described in Section 2.8. Irrespective of the expression level in the clonal cell lines, His_GFP_ABCG2 and His_SNAP_ABCG2 showed significant increases in mitoxantrone accumulation in the presence of Ko143 whereas this was not observed in the parental (HEK293T) cell line. This demonstrated that the N-terminally tagged ABCG2 used in this study was functional in HEK293T cells which is consistent with previous observations using other ABCG2 constructs (Wong *et al.*, 2016).

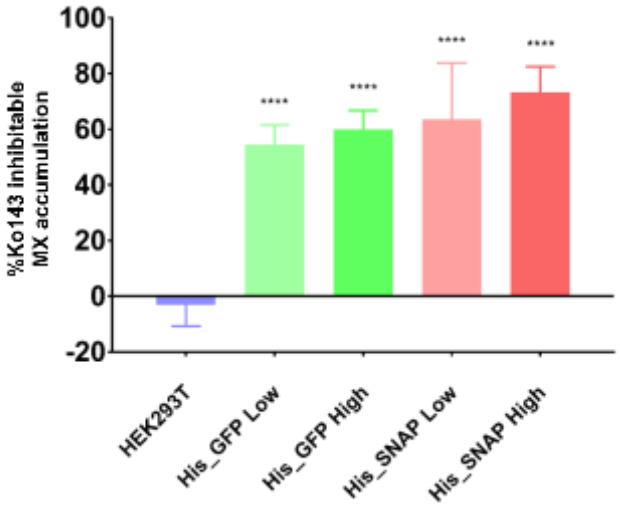


**Figure 4.5 – Function of N-terminally tagged ABCG2 expressed at different levels in HEK293T cells.** Corrected mitoxantrone (MX) fluorescence intensity values were compared in the presence and absence of Ko143 and the function of ABCG2 was determined as % Ko143 inhibitable MX accumulation. Data are plotted as mean ±SD (n=3) with statistical significance (****, $p<0.001$) compared to parental HEK293T assessed by one-way ANOVA followed by Bonferroni's multiple comparisons test.

## 4.6 Optimisation of expression

The overall project aims to use purified ABCG2 protein, combined with initial purification attempts (data not shown), indicated that it would be advantageous to ensure maximum expression in the appropriate mammalian system to facilitate sufficient protein yields being obtained. In comparison to the mammalian systems used, higher protein expression could be achieved with insect based systems but this carries a disadvantage whereby ABCG2 activity is often lost (Sarwat, 2016). A critical advantage of this project was the study of ABCG2 maintained in the native mammalian membrane environment and a vital part of achieving this was

expressing the protein in a mammalian system. Therefore a number of steps were taken to maximise the expression level of ABCG2 in this system and the results of these attempts are discussed below.

### 4.6.1 Clonal dilution

The initial generation of stable cell lines produces a mixed population of cells with varied fluorescently tagged ABCG2 expression levels. By assessing the expression levels of clonal cell lines derived from these mixed populations by fluorescence imaging (as described in Section 2.2.10) it was possible to select high expressing cell lines grown from single cells. Colonies stemming from single cells were imaged and their relative brightness assessed by visual inspection as an indication of the overall expression level of the fluorescently tagged ABCG2. Figure 4.6 shows the identification of cells with the selected relative expression levels. Once colonies had been established with homogeneous expression levels compared to the original mixed population, they were scaled up for ongoing culture and maintained as stable cell lines. The selection of cell lines by dilution cloning resulted in a reduced variability in expression level. Therefore the overall expression on ABCG2 within the population of high expressing clones was higher than the originally generated stable cell lines.

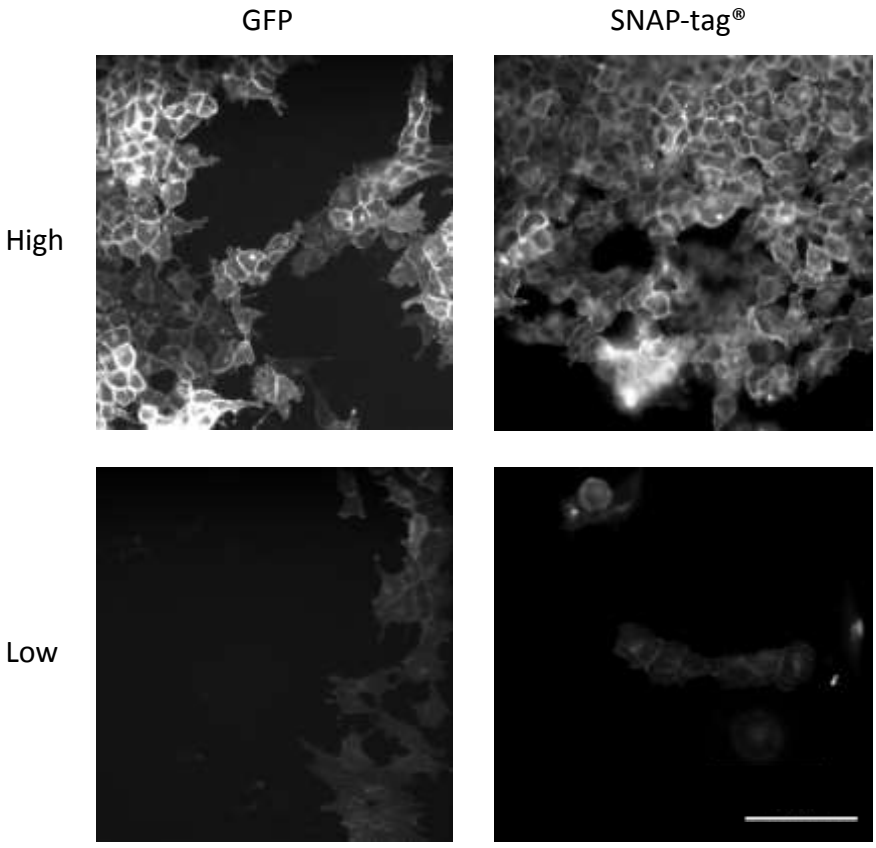


**Figure 4.6 – Selection of high and low ABCG2 expressing clones.** His_GFP_ABCG2 and His_SNAP_ABCG2 expressing HEK293T clonal lines were grown in 96-well plates. SNAP-tag expressing cells were labelled with 0.3µM SNAP-Cell® TMR-Star for 1 hour then washed 3 times with growth media prior to fixation. All cells were then fixed with 4% PFA and washed 3 times with PBS prior to imaging, using the same acquisition settings, on an ImageXpress Micro XLS Widefield High-Content Analysis System. The relative expression levels were determined comparing relative brightness by visual inspection with high and low expressing clones for each construct shown above. Scale bar = 100µm.

### 4.6.2 Enhanced transcription by sodium butyrate addition

Improved heterologous protein expression by use of the general transcriptional activator sodium butyrate has been reported previously (Leder and Leder, 1975). Treatment with 10mM sodium butyrate for 24 hours increased the expression of ABCG2 by approximately 70% as shown by western blot analysis (see Figure 4.7). This addition of 10mM sodium butyrate for 24 hours prior to cell harvesting was subsequently included in all large scale cultures used for protein production unless otherwise stated.

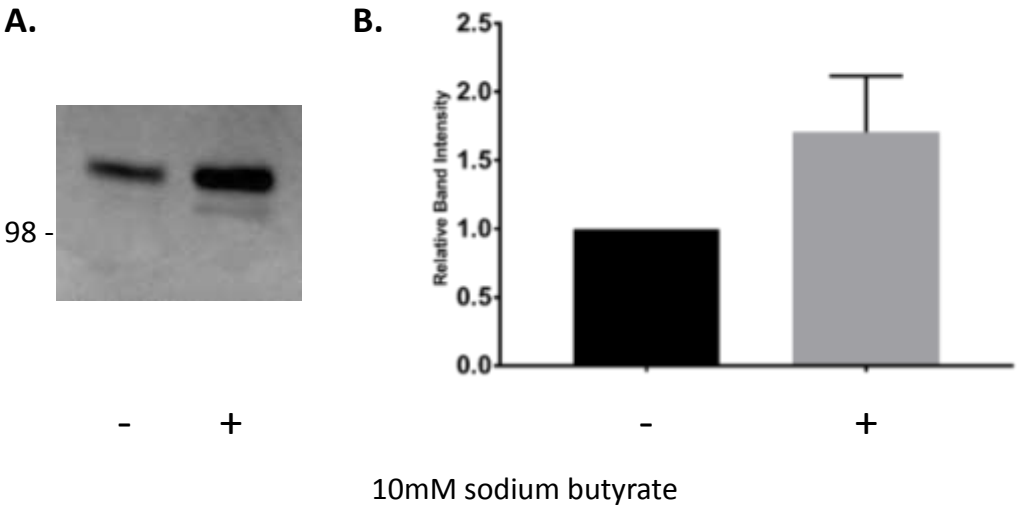


**Figure 4.7– Increased expression of ABCG2 upon the addition of sodium butyrate.** When incubated with 10mM sodium butyrate for 24 hours, expression of ABCG2 was increased by approximately 70%. This was determined by Western blot analysis (**A**) by probing with BXP-21 and subsequent densitometric analysis of the relative band intensity (**B**) (n=3, mean ± SD).

### 4.6.3 Tetracycline induction

The standard cell line used in this study was HEK293T where stable, constitutive expression of the proteins used in this study was achieved. Inducible cell lines offer a degree of control over the expression of proteins and may have offered slightly higher expression levels. Therefore the fluorescent fusion proteins previously described were sub-cloned into a suitable vector for inducible expression (see Chapter 3.3). These were stably expressed in 293TR cells by a selection process identical to that performed for the HEK293T lines. This cell line is also stably transfected with pcDNA6/TR which encodes the tetracycline repressor protein. The TREx-293 line (HEK293T derivative) expresses the protein of interest upon the addition of tetracycline to the growth media by way of inactivating tetracycline repressor protein binding in a system first described by Gossen & Bujard (1992). Figure 4.8 shows a time course demonstrating maximal expression occurs 24 hours post tetracycline addition and that this is achieved with all concentrations used. Increasing the tetracycline concentration by a factor of 10 to 1mg $mL^{-1}$ did not increase the apparent expression level. 100µg $mL^{-1}$ treatment was selected but, even when also treated with sodium butyrate or when the exposure time was increased to 48 hours, the system offered no advantage in terms of increased protein expression level compared to the high expressing clone selected from the initial stable transfection of HEK293T. In addition, the expression level following tetracycline induction varied (see the error bars in Figure 4.8 (B)) in distinct contrast to the consistent level of expression in the stable HEK293T cell lines and there was additional cost associated with operating this system. It is possible that other studies may wish to use this system

for the temporal control granted over expression of ABCG2 but it was not pursued further in this project.

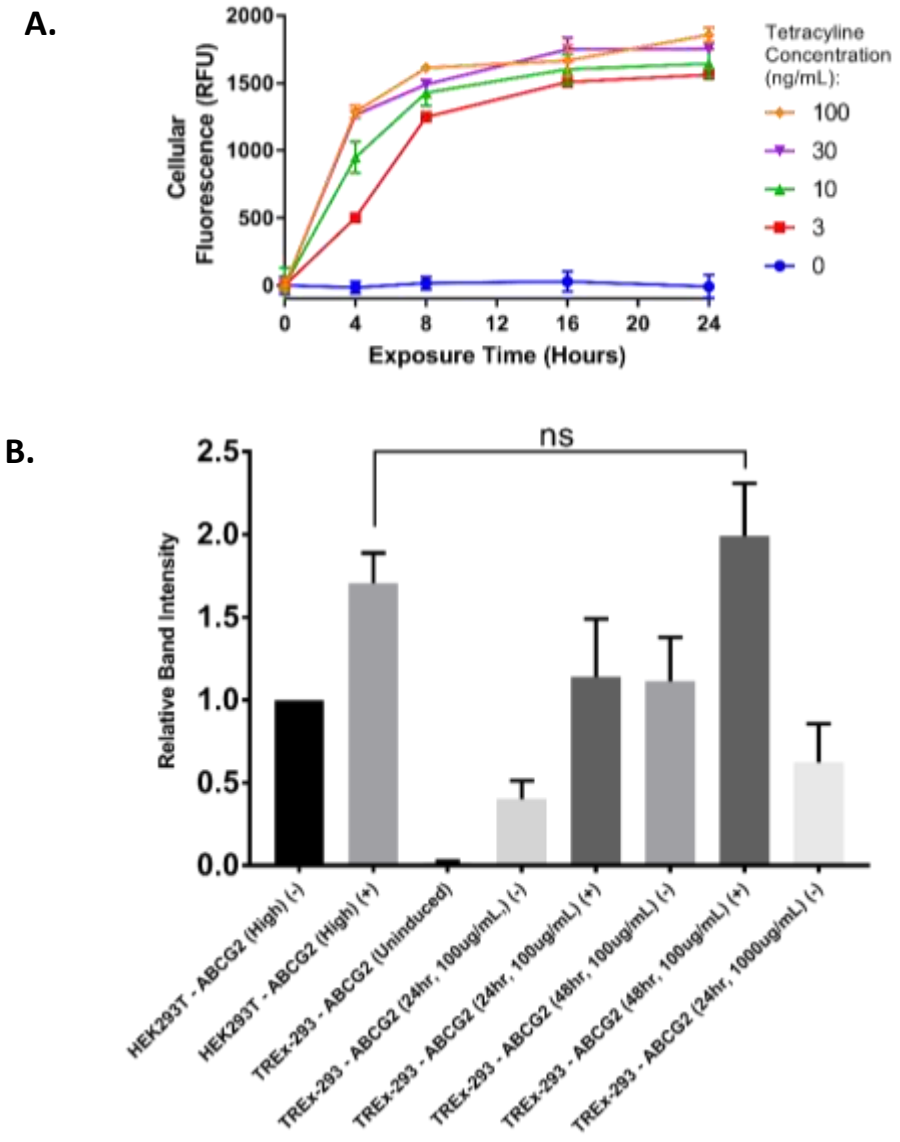


**Figure 4.8– Investigating increased expression by the use of a tetracycline inducible cell line.** An appropriate concentration and incubation time for tetracycline induction was determined by a time course experiment by measuring cellular fluorescence from IX Micro images quantified by a multiwavelength cell scoring algorithm (**A**) (mean ± range, n=2). Relative ABCG2 expression for HEK293T and various tetracycline induced states in the presence (+) and absence (-) of sodium butyrate was investigated by densitometric analysis of western blots (n=5, mean ± SD) where tetracycline induction did not significantly improve expression over the HEK293T system in the presence of 10mM sodium butyrate (**B**).

### 4.6.4 Suspension cell line adaptation

While the expression of ABCG2 in individual mammalian cells was increased by sodium butyrate treatment, the cell number per preparation remained a limiting factor in protein yield. Cell lines grown in suspension typically reach higher densities per unit volume of media than those grown in an adherent culture and this approach was therefore investigated. It was possible to adapt the HEK293T cells to grow in suspension (being constantly agitated at 180 rpm in a flat-bottomed round borosilicate flask) over several weeks of adaptation. As shown in Figure 4.9, several growth curves were performed that demonstrated increased cell density could be achieved and stable growth maintained over three passages, at which point the cell lines were considered adapted to growth in suspension. DMEM +10% FBS, serum-free DMEM and specialised suspension culture media (PeproGrow™ HEK293 Media, Peprotech, AF-CD-HEK293) were all trialled and DMEM +10% FBS gave the most consistent sustained growth. The use of serum-free DMEM was discontinued because of a reduction in cell viability to less than 90% and the specialised suspension culture media was inferior to DMEM +10% FBS in terms of cell densities achieved. Following adaptation, seeding at $2x10^5$ cells $mL^{-1}$ in DMEM +10% FBS achieved final cell densities of $>1.2x10^6$ cells $ml^{-1}$ after 4 days and this growth remained consistent with increasing culture volumes. Stable cell line stocks of GFP and SNAP-tag® labelled ABCG2 as well as untransfected HEK293T were maintained in suspension in this fashion. The cell densities associated with this system were 2-3 fold greater than the equivalent $7x10^5$ cells $mL^{-1}$ achieved in the adherent cultures over the same time frame (See Figure 4.9). Suspension cultures of up to 250mL were used in ABCG2 production yielding up

to approximately 1g of cell pellet per 100mL of culture media. This approach carried the additional advantages of using reusable flasks as opposed to disposable plastic ware therefore reducing waste and also being practically easier to handle.

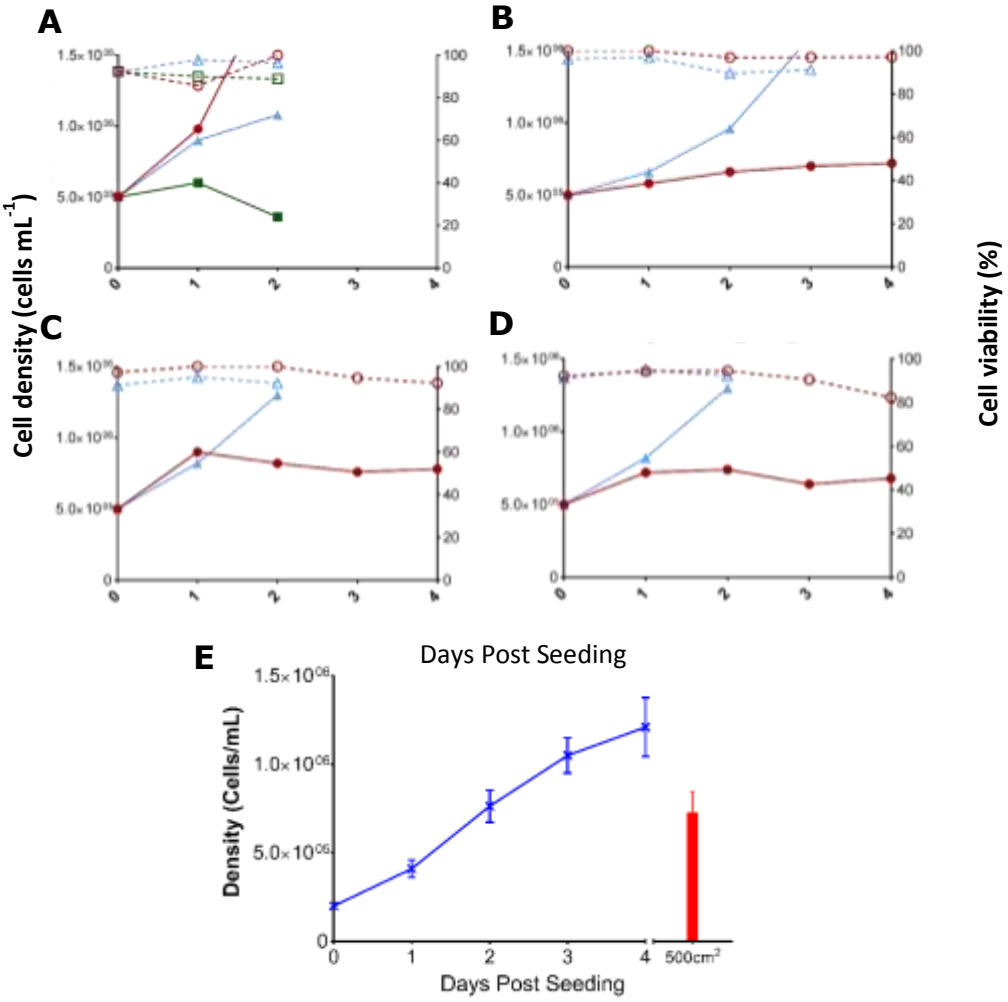


**Figure 4.9 – Adaptation to suspension culture.** HEK293T cells stably expressing ABCG2 were seeded at 500000 cells $mL^{-1}$. Growth and viability were monitored over several passages (A-D) by trypan blue exclusion assays. Media types were PeproGrow™ (Peprotech) (red symbols and lines), DMEM + 10% FBS (blue symbols and lines) and DMEM (green symbols and lines). Cells were passaged once their density reached $1x10^6$ cells $mL^{-1}$ or 5 days after seeding. Below 90% viability cultures were discontinued. Filled symbols represent density and unfilled represent viability. Following adaptation, suspension cultures were seeded at 200000 cells $mL^{-1}$ and their growth monitored over subsequent days until a final density was reached (E). For comparison, the density of cells per unit media was also calculated for a $500cm^2$ plate (n=3, mean ± SD).

## 4.7 Membrane preparation

Once a cell pellet had been generated total membrane fractions were prepared for subsequent solubilisation in the absence of classical detergents. Membrane fraction preparation was performed using established protocols (described in Section 2.3). Briefly, cells were lysed by nitrogen cavitation then centrifuged at 2500g to remove un-lysed cells and large debris. Then the supernatant was subjected to ultracentrifugation at 100000g for 45 minutes which pelleted cellular membrane material. The efficiency of the preparation procedure was qualitatively assessed, in terms of ABCG2 recovery, by western blot analysis of the different membrane fractions. Western blots (such as that shown in Figure 4.10) show that the majority of the ABCG2 was captured in the membrane fraction. This protocol was applied for all the proteins used in this study. The resulting membrane fractions were usually used immediately but, if required, were stored at -80°C prior to use. Membrane fractions for each of the proteins in this study were subjected to solubilisation to enable the study of proteins in solution.

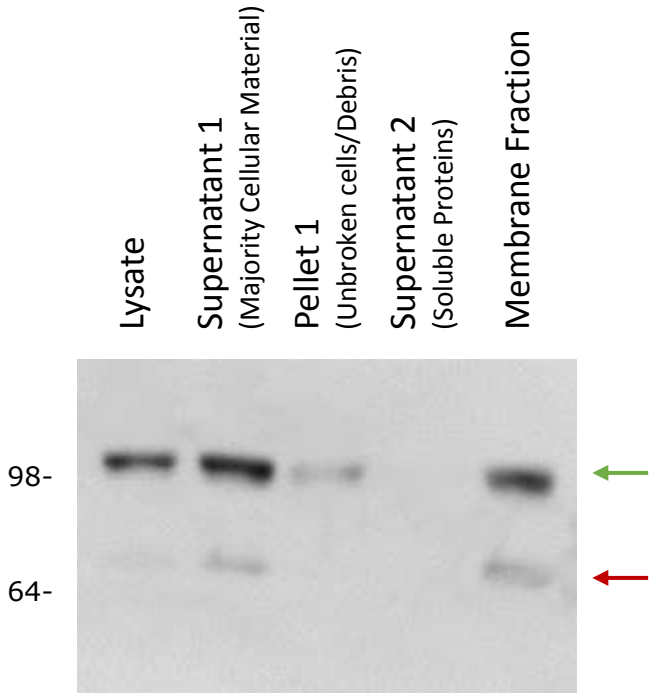


**Figure 4.10 – Isolation of ABCG2 containing membrane fractions.** Volumetrically equivalent samples of fractions generated during a membrane preparation were run on SDS-PAGE and analysed by western blot, probing for ABCG2 with BXP-21. Tagged ABCG2 was visible around 100kDa (green arrow) with small amount of untagged protein sometimes observed around 72kDa (red arrow). The blot shown is representative of many experiments performed regularly to check membrane preparation efficacy.

## 4.8 Labelling strategy

The constructs encoding GFP were intrinsically suitable for study by fluorescence-based methods. For those using a SNAP-tag®, the inclusion of a labelling step was required during the protein preparation process. The advantage of using this system lay within the available fluorophores. It appeared SNAP-tag® labels used fluorophores with superior photophysical properties resulting in enhanced brightness and stability in comparison to fluorescent proteins (Toseland, 2013). In addition to this, the choice of different excitation/emission wavelengths made it possible to ensure spectral separation with fluorescent transport substrates in

downstream analysis. The SNAP-tag itself is a modified DNA repair enzyme $O^6$-alkylguanine-DNA alkyltransferase. It reacts specifically with benzylguanine derivative attached fluorophores in a reaction that results in the covalent labelling of the SNAP-tag with the respective fluorophore.

Labelling was performed on membrane fractions which were prepared as described in Section 2.3. This stage of the protein preparation procedure was chosen for practical reasons. The larger volumes associated to the cell pellet and lysate stages prohibit the addition of a sufficient concentration of SNAP fluorophore ligand at this earlier point. Use of the ligands at or after the solubilisation steps would result in higher levels of residual dye in the product, hindering analysis by fluorescence techniques. Analysis of membrane fraction fluorescence, using two different SNAP fluorophore substrates, through a labelling time course demonstrated that peak labelling was achieved with a 2 hour incubation and that the efficiency could not be increased with the addition of 0.01% v/v Triton X-100 (see Figure 4.11). This labelling procedure was included for downstream analysis involving the His_SNAP_ABCG2 construct for the determination of its diffusion coefficient by FCS, in the development of a substrate binding assay detailed in Chapter 5.1.

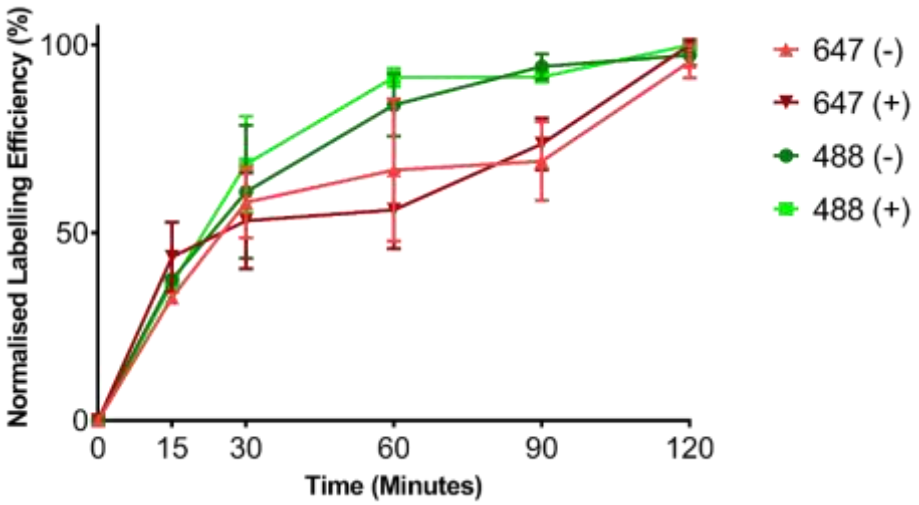


**Figure 4.11 – Labelling of SNAP-tag ABCG2.** Membrane fractions of HEK293T cells expressing His_SNAP_ABCG2 were incubated with either SNAP-Surface Alexa Fluor 647 (red lines) or SNAP-Surface Alexa Fluor 488 (green lines) in the presence (+) or absence (-) of 0.01% Triton X-100. Labelling reactions were incubated with end-over-end mixing at room temperature for the specified times and the fluorescence measured with a fluorimeter. Raw fluorescence values were then normalised to the minimum and maximum fluorescence observed for each dataset (n=3, mean ± SD).

## 4.9 Detergent-free extraction of ABCG2

Traditionally membrane proteins would be solubilised by the use of detergents that displace the native lipids precluding study in a truly 'native' environment. As such, novel polymers were explored for their ability to solubilise ABCG2 in the absence of traditional detergents. As discussed earlier, these polymers extract membrane proteins in nanodiscs embedded within patches of the surrounding lipid bilayer. Styrene Maleic Acid (SMA) was used principally but diisobutylene maleic acid (DIBMA) was also investigated (Rothnie, 2016; Oluwole *et al.*, 2017). Prepared membrane fractions containing overexpressed ABCG2, CD28 or CD86 were resuspended in SMA buffer and solubilised by incubation with 2.5% w/v polymer for 1 hour. Insoluble material was removed by centrifugation at 100000g

for 20 minutes at 4$^{o}$C. In the case of SMA these conditions were described previously and proved consistently effective throughout this work (Gulati *et al.*, 2014). The concentration of membrane material was optimised to minimise the use of polymer and to increase the resulting protein concentration by reduction of overall volume. Solubilisation of ABCG2 (shown by western blot in Figure 4.9) was effective with membranes at 30 and 100mg wet membrane weight per ml SMA buffer, but when increased to 300mg mL$^{-1}$ there was a fraction of ABCG2 that was not effectively solubilised. The increased viscosity of membranes at 300mg mL$^{-1}$ also hindered liquid handling and this concentration was not employed further. 100mg mL$^{-1}$ was the standard membrane concentration used in all solubilisations. The solubilisation efficiency of SMA was consistent for the ABCG2, CD28 and CD86 constructs used in this study (see Figure 4.12). During the course of this project DIBMA was described as an alternative polymer with the possibility of overcoming the sensitivity to magnesium associated to SMA (Oluwole *et al.*, 2017). This was investigated for the ability to solubilise efficiently but it was ineffective for ABCG2, CD28 and CD86. There was no effect in changing the salt (NaCl) concentration, time or temperature used in the solubilisation step (see Figure 4.13). Throughout the project various batches of SMA were used and each appeared to consistently perform at >90% solubilisation efficiency for the proteins tested.

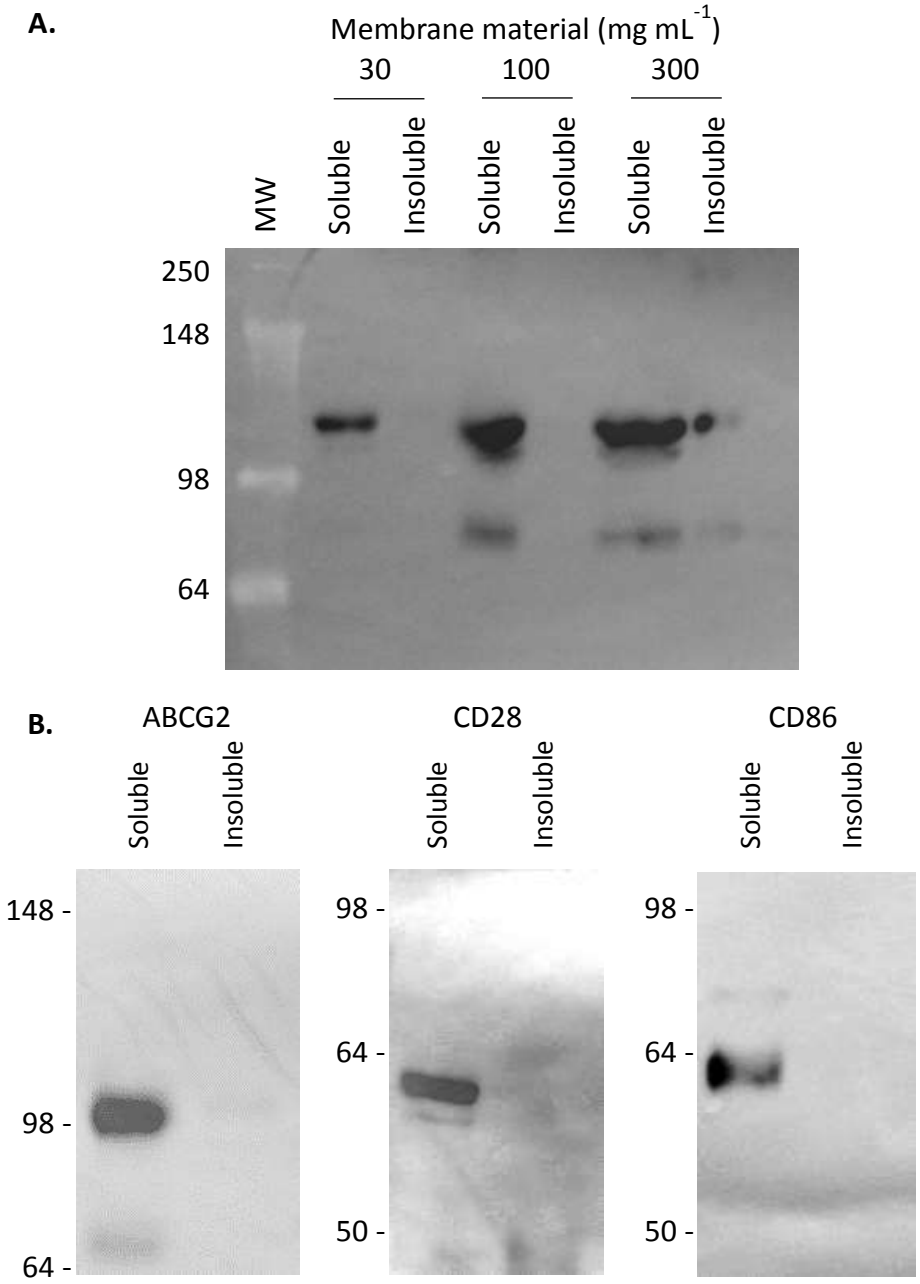


**Figure 4.12 – Solubilisation of membrane proteins by styrene maleic acid.** The effect of increasing starting material concentration on solubilisation efficiency was investigated by increasing the concentration of membrane material obtained from ABCG2 expressing HEK293T and solubilising with 2.5% (w/v) SMA for 1 hour at room temperature (**A**). Each of the proteins used in this project was solubilised at 100mg $mL^{-1}$ in 2.5% SMA for 1 hour at room temperature to investigate the solubilisation efficiency (**B**). Insoluble material was resuspended back into the original volume in SMA buffer supplemented with 2% SDS. Blots shown here are representative of n=3 independent experiments.

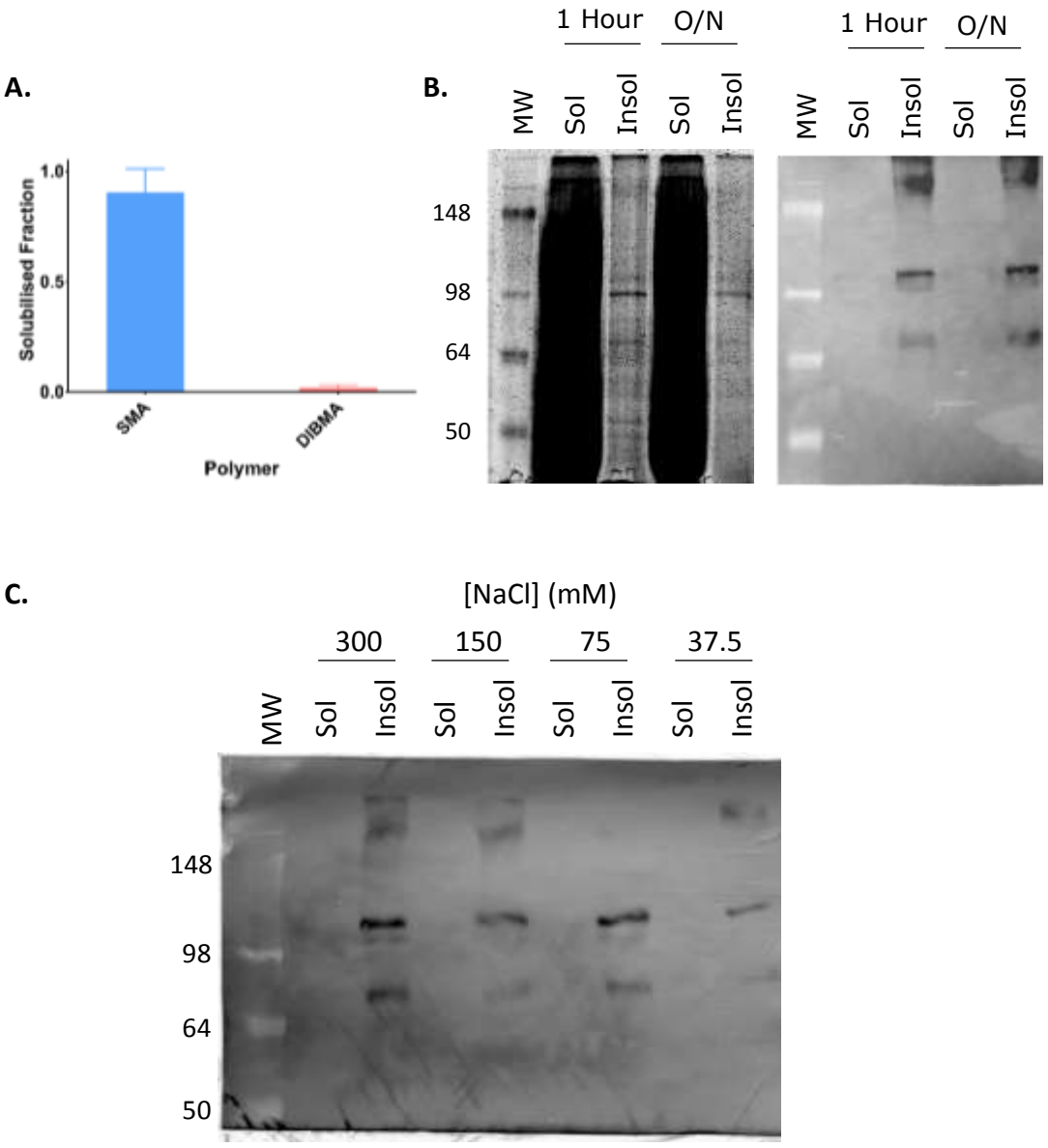


**Figure 4.13 – Western blots showing the solubilisation efficiency of DIBMA.** The solubilisation efficiency of DIBMA was first compared to that of SMA (**A**) (n=3, ± SD). Based on the low efficiency, attempts were made to improve this by changing the solubilisation time and buffer conditions. SDS-PAGE and western blot analysis revealed the overall protein solubilisation and specific ABCG2 solubilisation at 1 hour and overnight solubilisation to be the same (**B**). The impact of NaCl concentration on the solubilisation of ABCG2 was also investigated and shown to be negligible (**C**).

## 4.10 Summary

In this chapter, the expression of ABCG2 and the oligomeric control proteins (CD86 and CD28) used in this project have been validated by western blot and confocal microscopy. In the case of ABCG2, where there is an established functional assay, it was also shown that the addition of the tags did not affect function.

Substantial efforts were made to maximise the protein yield which resulted in the generation of several cell lines. This work culminated in the use of a high expressing clonal cell line grown in suspension and the addition of the transcriptional activator sodium butyrate for regular protein production activities. This process represented a significant advance and facilitated the study of ABCG2 isolated from a mammalian cell line in solution but further improvements could no doubt be made to this process as discussed later.

In addition to yielding large scale protein production capacity, this chapter also explored the used of non-traditional detergent solubilisation factors. Whilst DIBMA showed very little to no solubilisation ability in this study, SMA was particularly successful. As a result SMA was subsequently used in the isolation of ABCG2 and the control proteins for analysis in solution throughout this project.

In summary, this chapter described the development of large scale native system culturing methods for production of the fluorescence-tagged proteins used in this study and the methods to solubilise them. With the eventual aim of studying the interaction of purified ABCG2 with transport substrates, subsequent work first looked to characterise the oligomeric state of ABCG2 in solution.

# 5 Determination of SMALP-encapsulated ABCG2 stoichiometry by FCS and PCH

## 5.1 Chapter overview

The previous chapter described how an effective method for expression and extraction of functional ABCG2 into nanodiscs was achieved by its large scale expression in HEK293T cells followed by SMALP mediated extraction. This was done to support downstream *in vitro* analysis of SMALP encapsulated ABCG2 (SMALP-ABCG2) by fluorescence-based methods to investigate transporter function and ligand interactions; another principal aim of this project. Fluorescence correlation spectroscopy (FCS) and photon counting histogram (PCH) analysis are explored here, selected as appropriate techniques capable of measuring the low concentrations associated with protein extraction from a mammalian system. Despite the progress discussed in the previous chapter, this remained a significant obstacle. Both FCS and PCH are based on monitoring the fluctuations in fluorescence intensity within the defined confocal volume due to the diffusion of fluorescent particles moving through it by Brownian motion. They provide quantitative estimates of fluorescent particle concentration, mobility and molecular brightness. In this chapter it is demonstrated that FCS and PCH in combination can identify and determine the stoichiometry of labelled ABCG2 complexes isolated by SMALP extraction. This is a novel approach to assessing SMALP encapsulated protein and an important questions to answer. The ability for SMA to extract at least dimeric ABCG2 would be key in validating this platform as the available data (including the most recent structures at the time of writing)

indicate a homodimer of ABCG2 is the basic functional unit (M.F. Rosenberg *et al.*, 2015; László, Sarkadi and Hegedüs, 2016; Taylor *et al.*, 2017; Jackson *et al.*, 2018). SMALP-ABCG2 particles were first assessed for suitability for analysis of transporter stoichiometry by investigation of SMALP particle size and homogeneity and basic diffusion properties. This was performed by Dynamic Light Scattering (DLS) to determine particle size distribution followed by FCS experiments to determine a consistent diffusion coefficient for SMALP encapsulated ABCG2. Similarly, SMALPs containing control membrane proteins CD86 (monomeric) and CD28 (dimeric) were prepared and analysed. Following this, the fluorescence intensity data were assessed by PCH analysis to reveal the oligomeric state of SMALP encapsulated ABCG2 by comparison of molecular brightness with the CD86 and CD28 control proteins. The results of these efforts are discussed in the following sections.

## 5.2 Sizing of SMALP solubilised protein samples by DLS

DLS is among the most popular particle sizing techniques and is based on the scattering of light by particles in solution (Xu, 2015). As these particles move under Brownian motion (i.e. randomly, based on collisions with molecules in the solution), the vector of the scattered light is altered.

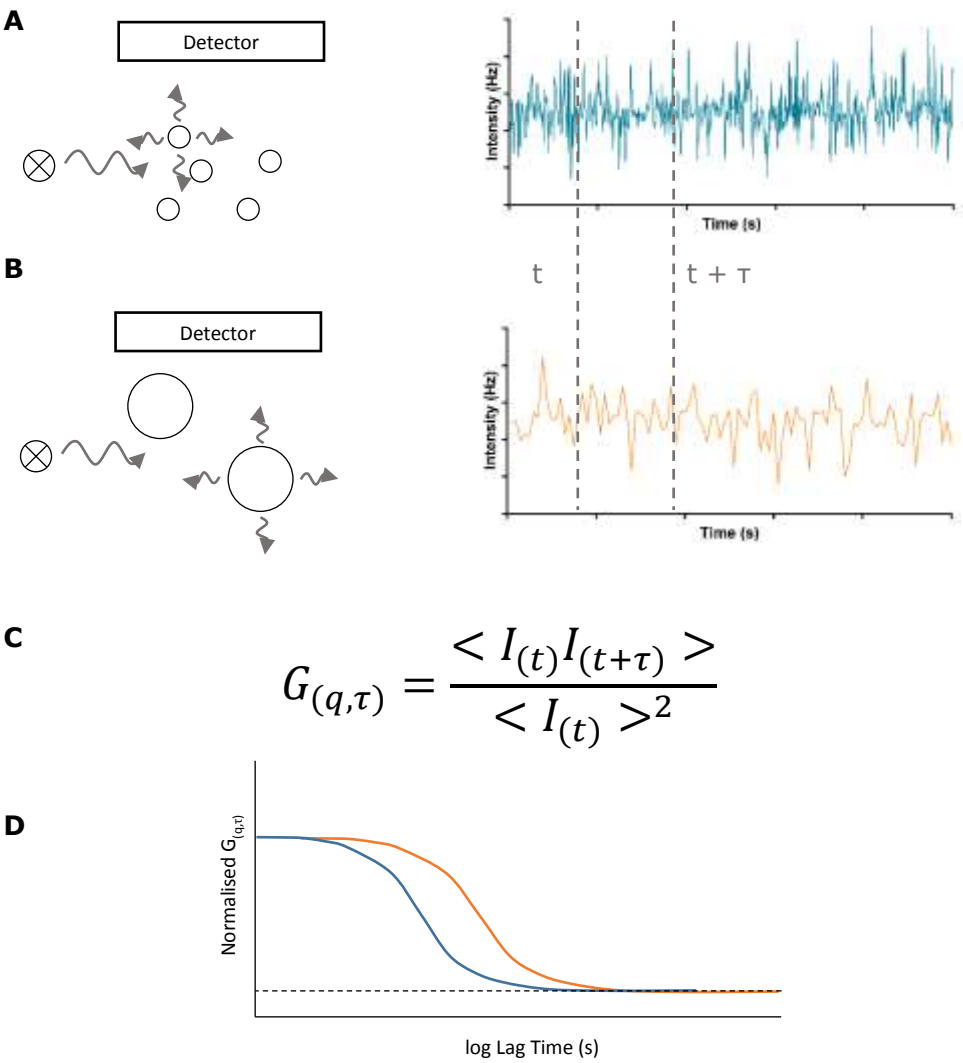


**Figure 5.1 - Principles of DLS in the calculation of particle size.** Even under constant illumination (e.g. monochromatic light source) the intensity of an observed volume fluctuates. This is due to the scattering of incident light by particles in the solution as they move under Brownian motion. The intensity fluctuates at a frequency dependent on the size of the contained particles with smaller particles (**A**) giving rise to a higher frequency than larger particles (**B**). The autocorrelation function at a particular wave vector (q) and delay time (T) is calculated from the intensity (I) at a given time point (t) and a subsequent time point (t + T) by the autocorrelation equation (**C**). When plotted (**D**) the 50% decay point represents the lag time of a particular species with a rightward shift compared to the smaller particles (blue), for example, being representative of larger particles (orange).

By measuring the intensity of scattered monochromatic light from a controlled source at a fixed wave vector it is possible to derive the size and size distribution of the particles responsible for the scattering. This is done by calculation of the autocorrelation function as outlined in Figure 5.1 (C) which can be plotted in a decay curve of the autocorrelation value ($G_{(q,t)}$) (as in Figure 5.1 (D)). The diffusion time of a particle in the solution is derived from this decay curve and used as a measure of size.

The details of interpreting autocorrelation data are discussed later where the same principle applies to FCS. Simply put, in the case of DLS experiments, the size of a particle is determined based on the frequency of the fluctuations in intensity. A larger particle will cause slower fluctuations compared to a smaller particle as it moves more slowly through solution. This data is typically plotted as particle size frequency where the peak value (or values in the case of a polydisperse population) gives the average particle size and the width of the peak provides an indication of monodispersity.

In this project, DLS was used to determine the size of SMALPs containing ABCG2, CD28 or CD86. These proteins were expressed in HEK293T cells and solubilised in SMALPs as discussed in Section 4.9. The solubilised material was passed through a 0.22µm filter to avoid the interference of any large particulate matter. A small amount of sample (40µL) was placed in a dark, small volume cuvette and read on an MD Zetasizer Nano instrument as described in Methods. Example DLS outputs are given in and a summary of the particle sizes automatically calculated by the instrument associated software are given in Figure 5.2.

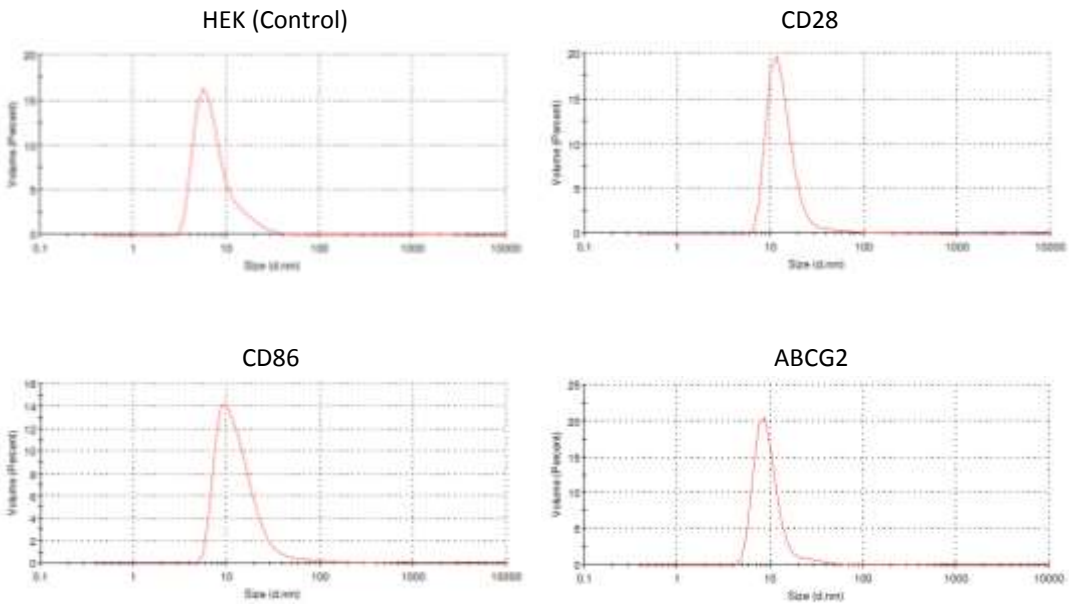


| Protein | Hydrodynamic Radius (nm) | Unit Particle Frequency |
|---|---|---|
| HEK (Control) | 18.91 ± 1.34 | 75.5 ± 23.6% |
| CD86 | 15.09 ± 4.46 | 96.5 ± 3.3% |
| CD28 | 19.08 ± 2.03 | 95.6 ± 3.9% |
| ABCG2 | 19.60 ± 1.54 | 96.9 ± 2.5% |

**Figure 5.2 - Example DLS traces and particle sizing summary.** Samples of solubilised membrane material from cell lines expressing the given proteins were analysed by DLS. Typical DLS plots show the particle size distribution from SMALP- solubilised membrane fractions prepared from HEK293T cells expressing the given proteins. The size distribution showed the predominant particle sizes in each case (n=3, mean ± SD).

The size values for the SMALP encapsulated proteins in this study were in agreement with previous studies, which have described the size of SMALP encapsulated proteins by DLS. Typically, the reported values for protein containing SMALP nanodisc sizes are 10-26nm (Dörr *et al.*, 2016).

SMALP-ABCG2 was the same size as the SMALP encapsulated control proteins CD28 and CD86. This excludes the possibility that variations in overall SMALP size and heterogeneity could contribute to any differences in PCH brightness measurements as discussed in the following section.

DLS was also able to provide evidence that SMALP preparations displayed limited aggregation as there appeared to be only a small number of very large particles. Other than in HEK preparations, the vast majority (>95%) of particles had sizes corresponding to those of single SMALP particles, with a relatively small number of aggregates. However, it is possible that each aggregate consists of many SMALP particles so having >95% of particles corresponding to single SMALPs does not mean that >95% SMALPs are unit particles *(this value could in fact be closer to 70%)*. In the HEK preparations, there was a smaller species present. This possibly represented excess free polymer owing to the reduced number of solubilised protein compared to the preparations from overexpressing cells in the cases of CD86, CD28 and ABCG2 alike. It is worth noting that these results were limited to the size and aggregation state of the samples and no further information on the components of these SMALPs (i.e. the oligomeric state of the contained proteins) could be determined. These DLS data provided confirmation that the particles in solution of the expected size and that the sample was relatively homogeneous which is an important consideration for the solution based FCS experiments that followed.

## 5.3 Diffusion of SMALP-ABCG2 measured in solution by FCS

The SMALP solubilised proteins had been shown by DLS to primarily consist of single particles of 15.1-19.6nm with a small amount of much larger particles associated to aggregates of these SMALP particles. FCS analysis, which is fully described in the Introduction, was then used to compare the diffusion coefficients for each of the SMALP-ABCG2 and the control proteins CD86 and CD28. Based on the consistent SMALP size across these protein species it was expected that the diffusion coefficients would also be consistent as particles of the same hydrodynamic radius should diffuse through solution at the same rate. In order to perform these measurements, the size of the observed volume was defined for each independent experiment by performing a Rhodamine 6G calibration (as described in Section 2.10.2). The volume itself was positioned 200µm above the coverslip, well into solution in order to avoid interference from the surface of the coverglass of the wells in which the samples were placed.

In initial experiments, an appropriate laser power and acquisition time were chosen. The aim of assessing the laser power selection was to maximise signal-to-noise ratio whilst not adversely affecting the measured fluorophore. For example "blinking" would result in an increased proportion of the ACF being associated to photophysics or spot bleaching as the fluorophores pass through the confocal volume which would artificially increase the diffusion coefficient. As such a laser power transmission of 50% with an AOTF of 10% was used (see

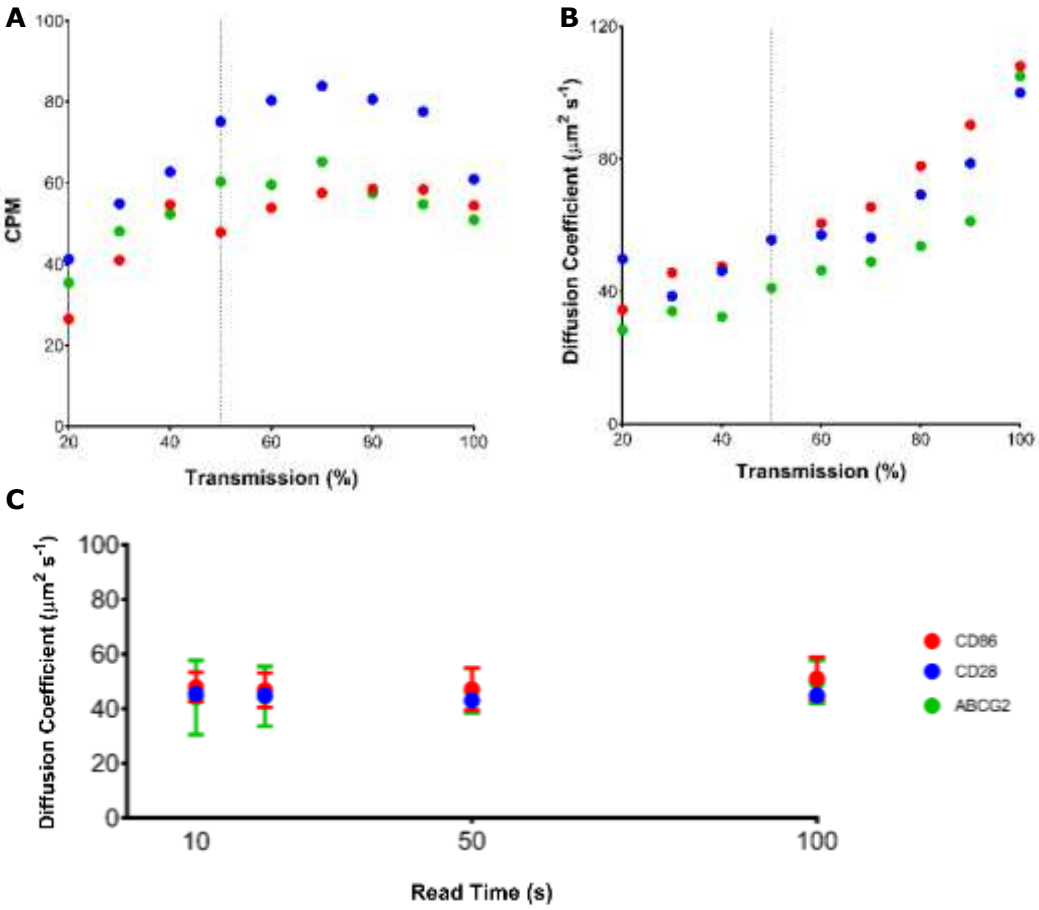


Figure ***5.3***). An optimal acquisition time was defined for these experiments as long enough to ensure traces of stable mean intensity were obtained and not too long as to hinder the overall workflow of any particular experiment. This was typically 30-100s with three technical replicate traces for each measurement. Summary data for these optimisations are shown in

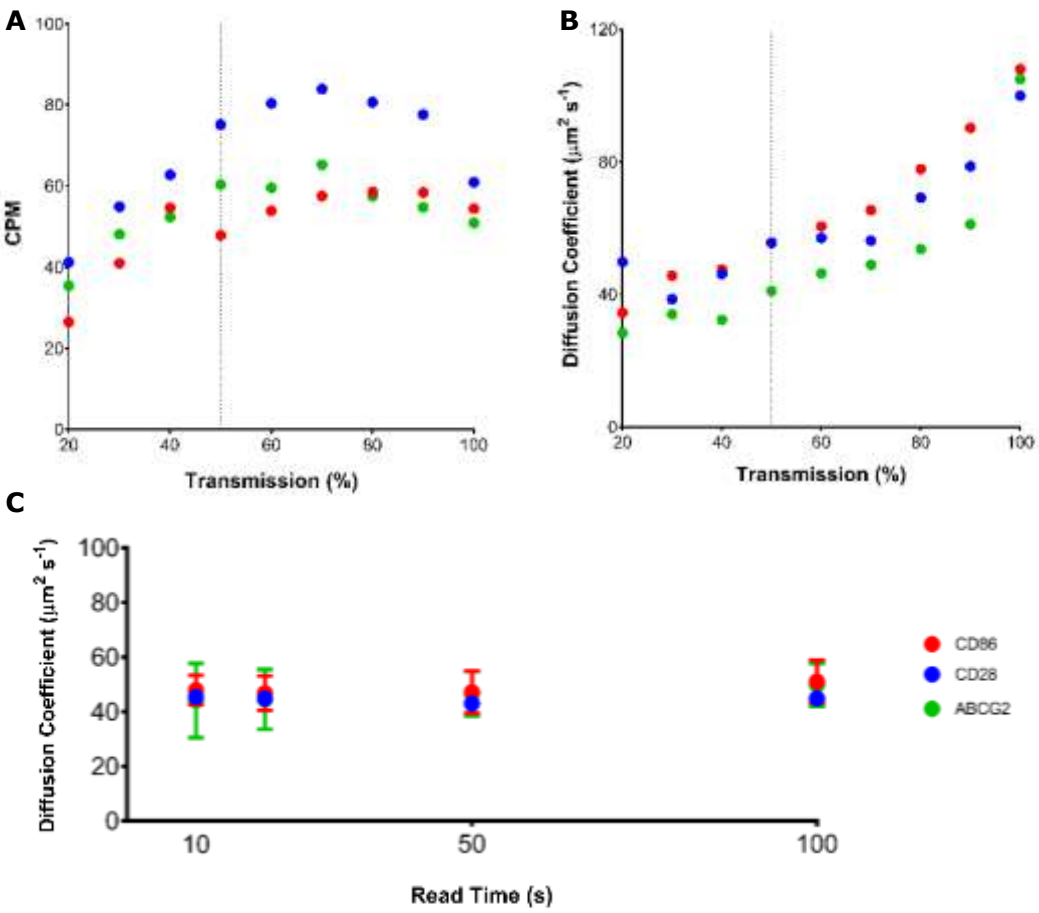


Figure ***5.3***.

Fluorescence fluctuation traces were obtained using the optimised acquisition settings. Undiluted samples of SMALP encapsulated ABCG2, CD86 or CD28 (prepared as previously described) were placed in an 8-well plate and fluorescence fluctuations were recorded. Traces were subjected to a quality check whereby abnormally large peaks (greater than 10-times higher than the average intensity or longer than 1s in duration) were edited from the trace record. Traces would not have been included in further analysis had they not reached asymptote for $G_{(T)}$ approaching 1. However this exclusion criteria was not required, and all traces were subsequently used, with a small number of aberrant peaks removed. Examples of these are given in Supplementary Figure 9.2. The fitted autocorrelation functions (ACF) were then calculated.

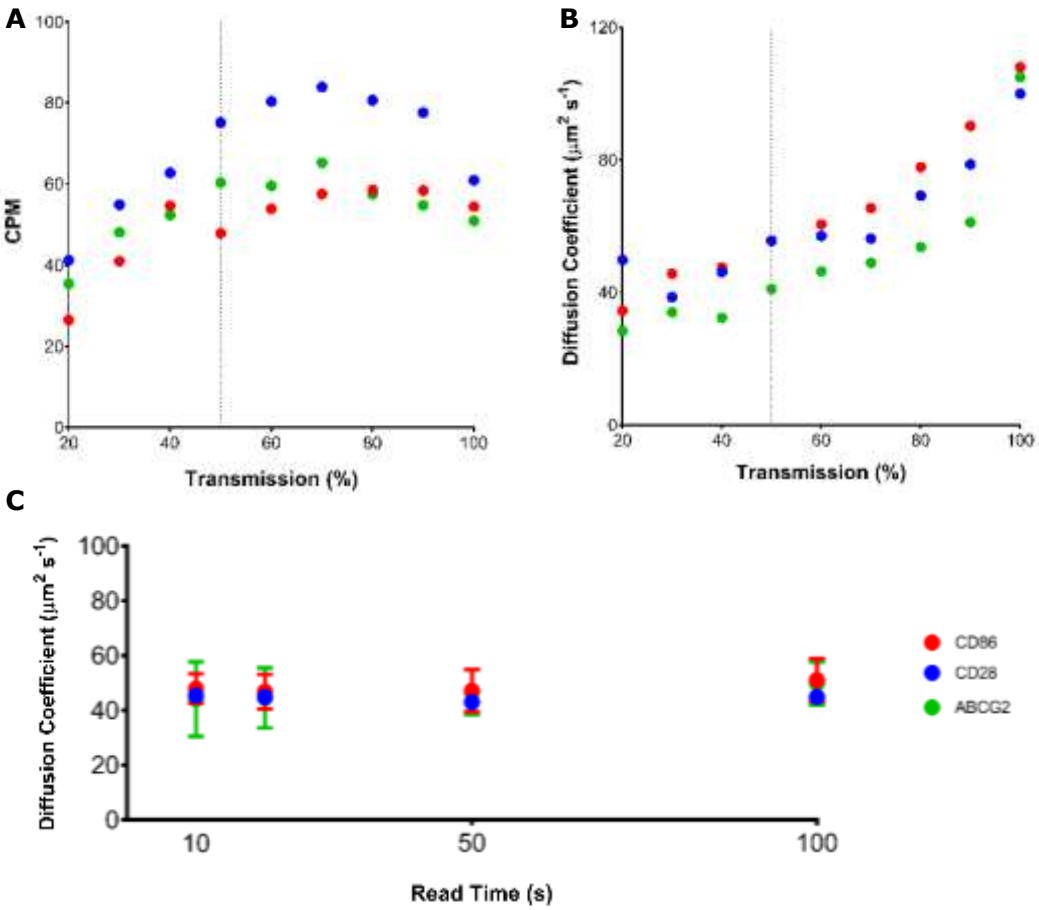


**Figure 5.3 - Effect of laser power and read time in optimisation of FCS data acquisition.** Data from an initial pilot experiment with SMALP solubilised CD86, CD28 and ABCG2 show how some basic output parameters change under different experimental conditions. (**A**) Counts per molecule (CPM, a basic representation of molecular brightness) increased with increasing laser power transmission (%) before starting to reduce. (**B**) The calculated diffusion rate started to increase with higher transmission (%) values. Based on these data 50% transmission was used (dashed line) in subsequent experiments. (**C**) In addition, different read times were also explored and consistent values (average ± SD for n=3 technical replicates) were achieved for each observed read time.

As described earlier, the ACF curves are fitted to mathematical models. These models differ in terms of the components they described by integrating different elements into the ACF calculation. This project sought to capitalise on the advantages of studying ABCG2 in solution. As such, a 3D model was most appropriate as the movement of SMALP particles would be unrestricted in each dimension (where a protein in a membrane would be restricted to two dimensional movement). The nature of the models used for ACF interpretation are described in Section 2.10.2. In the first instance, data were fitted to a single component model to reflect the basic expectation of a single population of SMALP encapsulated fluorescent proteins for each CD86, CD28 and ABCG2. As shown in Figure 5.4, a 1-component fit did not fully explain the data as indicated by the systematic deviation from the ACF seen in the fitted data. As such a 2-component fit was employed for ABCG2 and both control proteins. This resulted in a much improved fit with residual deviation being associated to noise (small deviations equivalent either side of zero). Inclusion of a second component subsequently resolved both a faster, predominant species and a slower, significantly less numerous species.

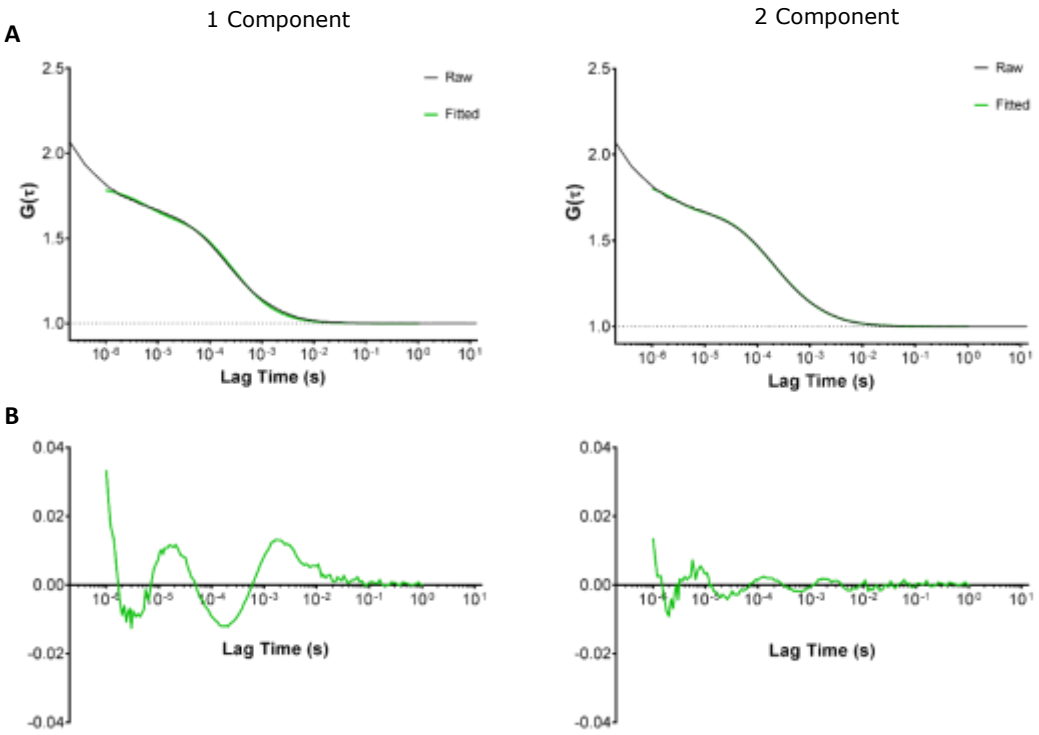


**Figure 5.4- Curve fitting in ACF interpretation.** Data from an example experiment using a preparation of SMALP-ABCG2 show the raw (black) autocorrelation curve (**A**) of a sample fitted (green) with either a 1 or 2 component model. The deviation from the model (**B**) highlights a much better fit is achieved by the use of a 2 component model.

2-component models were subsequently applied to measurements of all the solubilised proteins. Example traces and curve fittings are given in Figure 5.5. Solubilised HEK293T membranes from cells not expressing any of the fluorescent fusion proteins to assess the impact of autofluorescence. The signal observed in these samples was much lower than that seen for the fluorescent protein samples. Although it was still possible to generate an ACF curve Figure 5.5 (A), the principal source of fluorescence fluctuation was background noise and no meaningful data could be extracted.

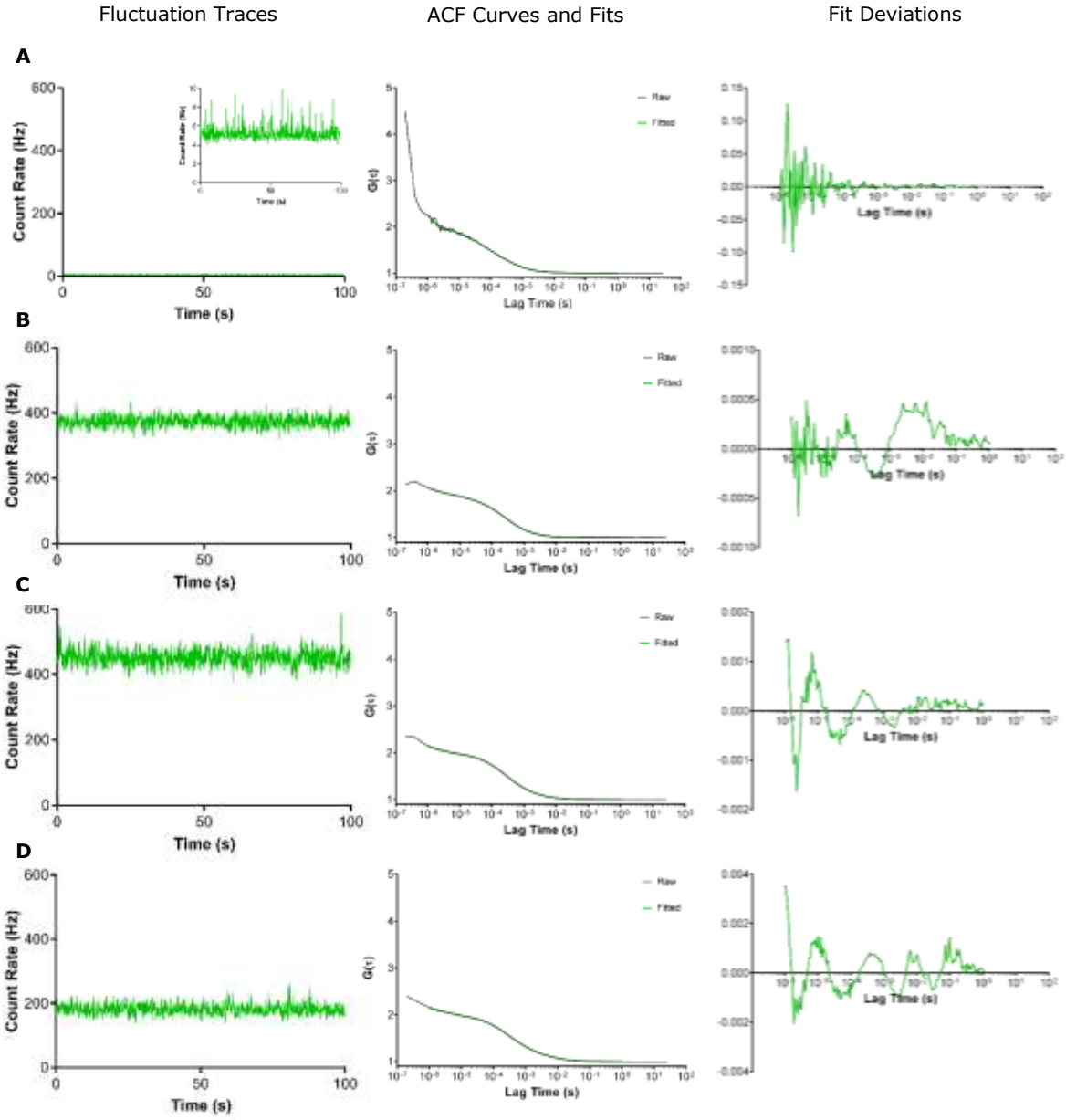


**Figure 5.5 - Example autocorrelation curves and deviations from the curve fitting.** Fluorescence fluctuation traces were obtained by the illumination and observation of a small volume of solubilised protein by a fixed laser power. This was used to generate autocorrelation curves (left) for SMALP preparations from HEK293T (**A**), CD86 (**B**), CD28 (**C**) and ABCG2 (**D**). These were fitted by a two component model and the deviation from the model was also recorded (right).

Using the dimensions of the confocal volume as calculated by the calibration data for each experiment and the diffusion times resolved by ACF analysis, diffusion coefficients were calculated as described in Section 2.10.2 for each protein. The diffusion times for each protein were typically 190-210µs. The component fraction (relative concentration) of each component was also calculated. Together, these data showed the presence of a predominant faster moving particle and a much slower moving, less numerus species (see Figure 5.6 and associated table). These fluorescent species were associated with being single SMALP-protein particles and aggregates respectively. This was in agreement with the DLS observations which showed a predominant SMALP encapsulated protein associated species and a larger, more scarce aggregate. Importantly, the diffusion coefficients for unit SMALP encapsulated CD86, CD28 or ABCG2 were the same as would be expected for particles of the same size as demonstrated by DLS. The diffusion coefficients are not indicative of the nature of the SMALP contained proteins as the overall particles are of the same size. To comment on the oligomeric state of the proteins in SMALPs, PCH analysis was utilised.

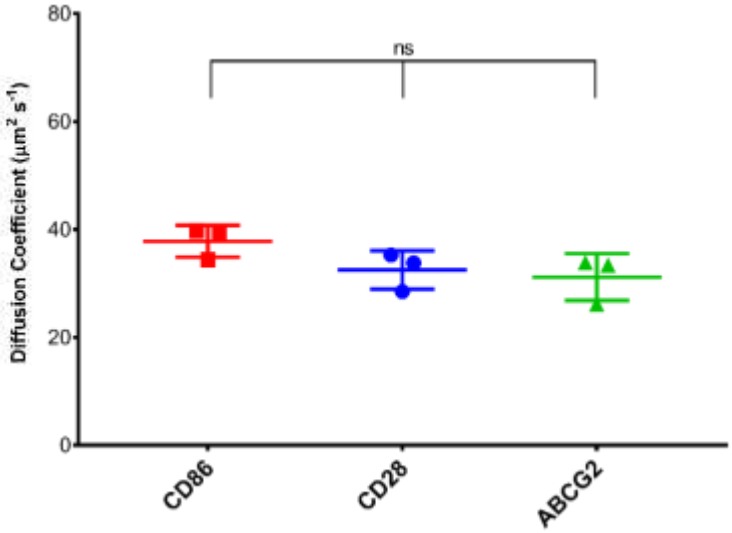


| Protein | Component 1 (C1) | | Component 2 (C2) | |
|---|---|---|---|---|
| | Fraction (%) | D ($\mu m^2 s^{-1}$) | Fraction (%) | D ($\mu m^2 s^{-1}$) |
| CD86 | 98.7±1.4 | 37.8±3.0 | 1.3±1.4 | 2.1±0.9 |
| CD28 | 95.7±2.7 | 32.5±3.6 | 4.3±2.7 | 2.8±0.9 |
| ABCG2 | 88.5±5.2 | 31.2±4.3 | 11.5±5.2 | 1.8±0.5 |

**Figure 5.6 - Summary of diffusion coefficients and component fractions for CD86, CD28 and ABCG2.** The diffusion coefficients, D, for the predominant component (C1) in the case of each protein were compared and revealed to have no statistically significant difference by one-way ANOVA. Fractions and D are also summarised for each component in the analysis of each protein (mean ± SD, n=3).

## 5.4 PCH analysis in the determination of SMALP-ABCG2 oligomeric state

As previously mentioned, the same data used for determining the diffusion coefficients by ACF analysis can also be interpreted by PCH analysis. This analysis uses the frequency distribution of the fluorescence fluctuation amplitudes separated into bins of a discrete sampling time. This allows the determination of both the average number of particles in the confocal volume (N) and their molecular brightness (ε). In this study, comparison of SMALP-ABCG2 molecular brightness to monomeric and dimeric controls was used to determine the oligomeric state of ABCG2 in SMALPs.

The acquisition of data used for PCH analysis was the same as that for FCS. However, the additional impact of bin time (ranging from 0.2µs to 2ms) was investigated. Too short or too long a bin time would have resulted in too few or too many counts per bin for accurate interpretation. In addition, the impact of fast fluctuation frequencies of photophysics effects would be minimised by the use of the longest possible bin time whilst the particles of interest would have to remain within the detection volume for accurate brightness determination. Therefore the diffusion times of the particles (approximately 200µs) were also taken into account. The effect of this on C1 (the predominant, non-aggregate component) for an example data set is shown in Figure 5.7. From 0.2-20µs bin times there appeared to be little effect on the PCH output and at 200µs or 2000µs data fit quality became reduced. As this was equivalent to or above the measured diffusion times for the SMALP-protein particles, a bin time of 20µs was used in PCH experiments aimed at describing the oligomeric state of ABCG2 in SMALPs.

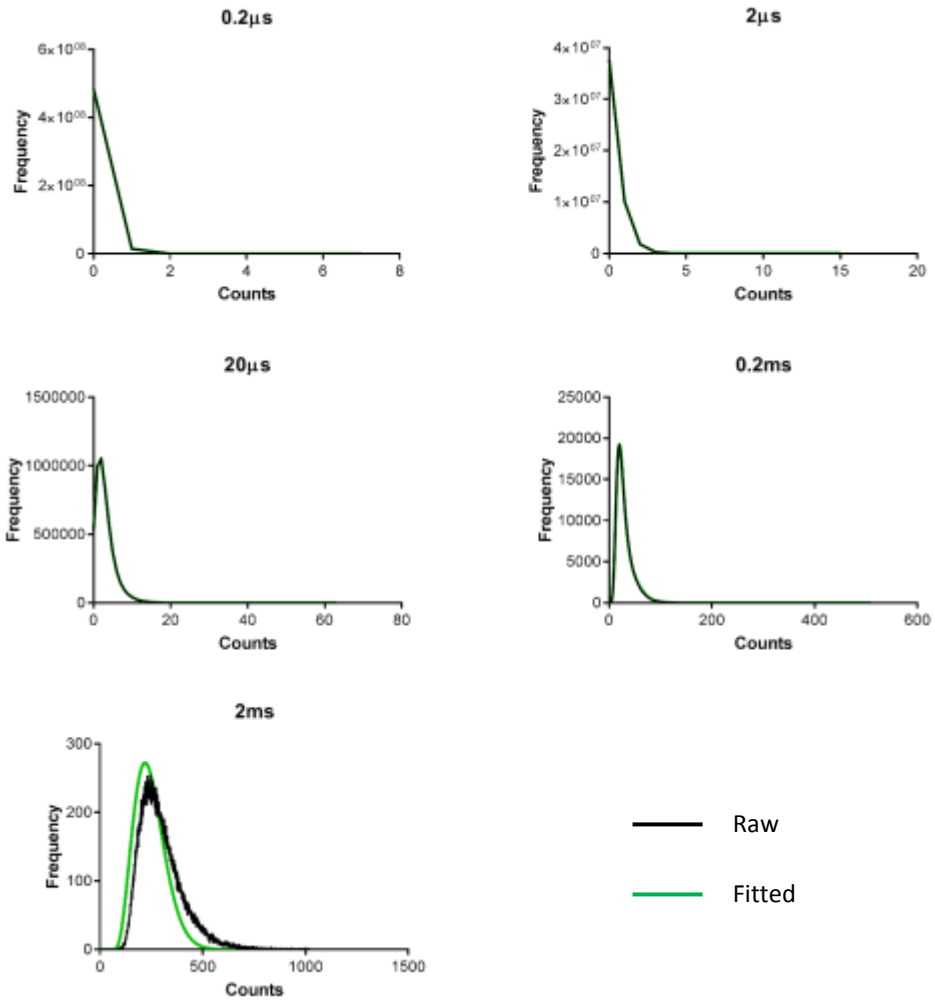


| Bin Time (µs) | CD86 | | CD28 | | ABCG2 | |
|---|---|---|---|---|---|---|
| | ε | CV(%) | ε | CV(%) | ε | CV(%) |
| 0.2 | 28131.4 | 5.1 | 61796.0 | 0.3 | 61481.6 | 0.3 |
| 2 | 29218.6 | 5.9 | 53407.1 | 6.0 | 51481.6 | 1.6 |
| 20 | 28533.9 | 16.7 | 53544.7 | 4.6 | 46981.9 | 1.6 |
| 200 | 19987.6 | 6.4 | 33077.1 | 5.7 | 24528.9 | 0.4 |
| 2000 | 1963.7 | 1.7 | 552.1 | 123.7 | 45.6 | 9345.5 |

**Figure 5.7- Effect of bin time on PCH analysis.** An example dataset derived from a 100 second measurement of fluorescence fluctuations for SMALP-ABCG2 analysed by various PCH bin times. The raw data (black) was fitted with a 2-component PCH model (green) using bin times as shown in the panel titles. Average molecular brightness (and %CV) over 3 technical replicates are shown in the table for each protein at each bin time to demonstrate the relationship between difference analysis bin times and the derived molecular brightness values.

The next step in PCH analysis was to investigate the appropriate mathematical model (in terms of number of fluorescent components). The fits of both 1-component and 2-component models to the 20µs binned data were investigated. Ñ and ε were obtained in the case of each protein using both 1-component and 2-component PCH models. Based on an improved $Chi^2$ value as a measure of the goodness of fit, the 2-component models were shown to better explain the data. In addition, the relative proportions of the two components resolved the PCH analysis matched that of the FCS and DLS measurements. Component 1 (C1) was typically a dimmer, more prevalent species and Component 2 (C2) was far brighter and less numerous. As before this supports the presence of both single unit particles and a low proportion of aggregated particles respectively. Specifically, the brighter C2 fractions contributed <10% for each protein, similar to the proportions observed for aggregated particles for the same samples by the other techniques. To establish the stoichiometry of ABCG2 in comparison to the control proteins, the C1 species were used. These data are summarised in Figure 5.8 where the ε of C1 for ABCG2 was found to be approximately 2-fold that of CD86 (the monomeric control) and equivalent to that of CD28 (the dimeric control).

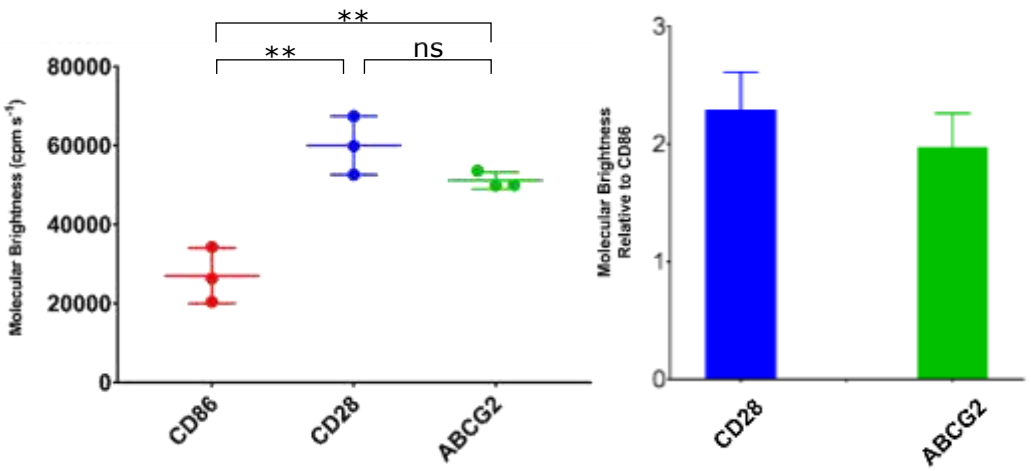


| Protein | Component 1 (C1) | | Component 2 (C2) | |
|---|---|---|---|---|
| | Fraction | ε | Fraction | ε |
| CD86 | 93.0 ± 1.5 | 27074 ± 6975 | 7.0 ± 1.5 | 271957 ± 47354 |
| CD28 | 93.8 ± 1.3 | 60030 ± 7406 | 6.2 ± 1.3 | 465789 ± 71770 |
| ABCG2 | 94.6 ± 1.6 | 51199 ± 2135 | 5.4 ± 1.6 | 408163 ± 12498 |

**Figure 5.8 - Summary of PCH molecular brightness analysis.** PCH analysis revealed the molecular brightness of SMALP encapsulated ACBG2 and allowed comparison with that of CD86 and CD28 (monomeric and dimeric controls respectively) to assess the oligomeric state of ABCG2. The mean of three measurements in each of three independent experiments were assessed for differences in molecular brightness for the predominant component (C1) by one way ANOVA followed by Sidak post-analysis. The relative molecular brightness compared to CD86 for ABCG2 and CD28 were also calculated with the particle number and brightness of each component for each protein summarised in the above table (mean ± SD, n=3, **=p<0.01).

## 5.5 Summary

Previous studies characterising ABCG2 with FCS and PCH analysis have been performed to determine the oligomeric state of ABCG2 (albeit with analysis differing with that in this study) in the membrane of live cells (Wong *et al.*, 2016). These previous studies have been incredibly valuable but one aim of this project was to develop a way to study ABCG2 in solution whilst retaining the advantage of native (mammalian) system expression and maintenance of the surrounding membrane. As discussed in previous chapters, the first step of this was to express ABCG2 in HEK293T cells then extract and solubilise the protein by the use of SMALPs. The next step was to characterise this SMALP contained product and, specifically, assess the oligomeric nature of SMALP extracted ABCG2.

SMALP solubilised proteins were assessed by DLS, FCS and PCH analysis. Each of these techniques identified single SMALP particles with a low incidence of aggregates. Although diffusion based techniques, such as FRAP (fluorescence recovery after photobleaching), can be used to measure protein mobility (possibly as an indicator of protein size or oligomerisation), this was not applicable to the measure of oligomeric state of SMALP extracted proteins in solution. This is because the rate of diffusion, D, is expected to vary with the square root of the molecular mass. It would therefore be impractical to demonstrate monomeric vs dimeric vs tetrameric as an 8-fold change in molecular mass would be required to observe even a 2-fold change in D. This is especially relevant considering that the mass of a SMALP-protein particle would be largely dictated by the mass of the SMALP rather than the contained protein. Instead, the molecular brightness was

determined by PCH analysis and was used to describe the oligomeric state of ABCG2 in SMALPs.

The molecular brightness of ABCG2 was twice that of the monomeric control, CD86, and equivalent to that of the dimeric control, CD28. Other authors have previously reported the extraction of ABCG2 in SMALPs but have not otherwise commented on the oligomeric state therein (Rothnie, 2016). This is vitally important as it is considered fundamental for ABCG2 to form at least dimers to function and all structural data resolved for ABCG2 at the time of writing describe homodimers to the exclusion of any structural evidence for larger oligomers. It is therefore possible to conclude that SMALPs solubilise ABCG2 as a potentially 'active' dimer though the activity in terms of substrate recognition, ATPase activity or translocation capacity is not demonstrated in this set of experiments. It is also important to note differences from previous FCS experiments in living cells which identified a mix of dimer and predominantly tetrameric ABCG2 (Wong *et al.*, 2016). As this previous work was performed in live cells it is possible that the tetramers form transiently but exist for a sufficient period of time to be detected by PCH analysis data in the associated experiments (where the bin time was 1ms). Another possibility is that the SMALP selectively excludes tetramers during solubilisation. However, assuming that the size of an ABCG2 tetramer would be the limiting factor in this scenario this is unlikely to be the case. As in this and other studies, the overall size of a SMALP particle (15-20nm) is enough to accommodate a tetramer of ABCG2 where the diameter of the transmembrane region of a tetramer would be similar to that of a dimer (5.2nm) but in both dimensions in the membrane. The challenges are further discussed later.

This work was performed on solubilised but not affinity purified SMALP preparations, which could increase non-specific signal. However this is largely overcome by the specificity of FCS which only detects the fluorescent proteins and this did not pose any problems during data acquisition. Autocorrelation data could be generated from the fluorescence traces associated to samples not containing fluorescently tagged proteins. This is due to autofluorescence of the other SMALP-encapsulated proteins present in solution. The signal associated to this autofluorescence is significantly (approximately 40-fold) less than that of the fluorescent protein samples. As mentioned above, no useful information could be inferred from the data of these samples and the contribution of this signal to the fluorescent protein samples was negligible. This element of the project was limited to unpurified proteins due to difficulty in purifying the monomeric control, CD86 (data not shown).

Development of an effective purification strategy would prove an incredibly useful tool for performing *in vitro* analysis of ABCG2 interactions with ATP, transport substrates and inhibitors. In this project, an effective purification strategy was employed to yield sufficient purified protein to perform FCS based binding assays with a transport substrate for the first time. These experiments followed the optimisation of the purification workflow, the determination of basic diffusion characteristics and optimal binding assay conditions all of which are discussed in the following chapter.

# 6 Investigation of ABCG2 interaction with a transport substrate and inhibitor by FCS

## 6.1 Overview

In previous chapters, ABCG2 constructs have been designed, expressed in HEK293T cells and solubilised in SMALPs. Data were gathered that showed, for the first time, that SMALPs extract dimeric ABCG2. This finding supported investigations into interactions with transport substrates by providing a novel platform for these studies.

The dimeric state of SMALP-encapsulated ABCG2 tagged with GFP was investigated by comparison of molecular brightness to GFP-tagged monomeric and dimeric control proteins. It would not have been possible to resolve this by comparison of diffusion coefficients because of the relatively small differences in mass. For example, it has been shown that a 1.6-fold change in D may require a 6-fold change in mass (Meseth *et al.*, 1999). However, the differences between a small molecule drug and SMALP-ABCG2 would be sufficient to resolve the diffusion coefficients of 'free' and 'bound' drug (see Figure 6.4).

The molecular brightness measurements used to determine oligomeric state were performed in unpurified samples. This was possible because the contribution to the measurements by non-fluorescent components (e.g. protein-free SMALPs) was insignificant in comparison to that of the proteins of interest. In performing drug binding experiments, the diffusion of a fluorescent drug substrate was measured and a decrease in the diffusion coefficient upon binding to a much larger SMALP could be used to distinguish 'bound' from 'free' drug. However, non-

specific binding of the fluorescent drug to other SMALP-protein or 'empty' SMALP particles would also yield a similar decrease in diffusion co-efficient. As discussed below, this is because the drug substrate may interact non-specifically with other solubilised proteins, the associated lipids or even the SMA polymer itself. The effect may be amplified by the expected hydrophobicity of many drug transport substrates. Therefore SMALP-ABCG2 particles were purified for this element of the project to facilitate a reduction in non-specific interactions and the efforts to optimise this process are discussed. SMALP-ABCG2 was purified to sufficient quantities to perform binding studies and preparations from cells not expressing ABCG2 were used to determine the non-specific binding components.

The purified protein was applied to FCS-based binding assays based on the principles mentioned above. Firstly, an appropriate drug substrate was selected. These were identified by review of the available literature and assessed based on the evidence for ABCG2-specific transport (Ivnitski-Steele *et al.*, 2008; Strouse *et al.*, 2013), recovery and fluorescence properties (e.g. suitable excitation/emission spectra, acceptable triplet state fraction and signal to noise ratio). Pilot experiments were used to first test the feasibility of the assay and whether substrate binding could be detected and the parameters were subsequently optimised. This included determination of the diffusion coefficients for free drug and labelled SMALP-ABCG2 for data fitting and assay timings and conditions. Binding assays were then used in attempts to determine affinities for substrate and were accompanied by inhibition assays that demonstrated specificity and provided some evidence to challenge existing models of substrate binding by ABCG2.

## 6.2 Purification of SMALP-ABCG2

As previously described, membrane fractions were prepared from HEK293T cells expressing the His_SNAP-tag®_ABCG2 construct. The expressed membrane proteins were solubilised into SMALPs. Though cells pellets may have been stored at -80°C, the purification procedure was performed without additional freeze-thaw steps. Solubilised membrane material was incubated with metal ions immobilised to resin beads. Nickel ions are most common but cobalt ions were also investigated as an alternative in this project. Cobalt is often reported as having a higher specificity for polyhistidine-tagged proteins over histidine rich proteins owing to a lower overall affinity (Bornhorst and Falke, 2000).

The respective metal ion is attached at the end of a chain anchored to resin beads by a dative bond between the metal ion and appropriate chelator group. The positive charge of the metal ions facilitates the formation of ionic bonds with the imidazole rings in a polyhistidine peptide sequence. This interaction, which captures the protein, is overcome by competition with excess imidazole to elute the target protein after washing away unbound material. As shown in Figure 6.1, initial purifications were performed to compare the use of nickel and cobalt purification resins.

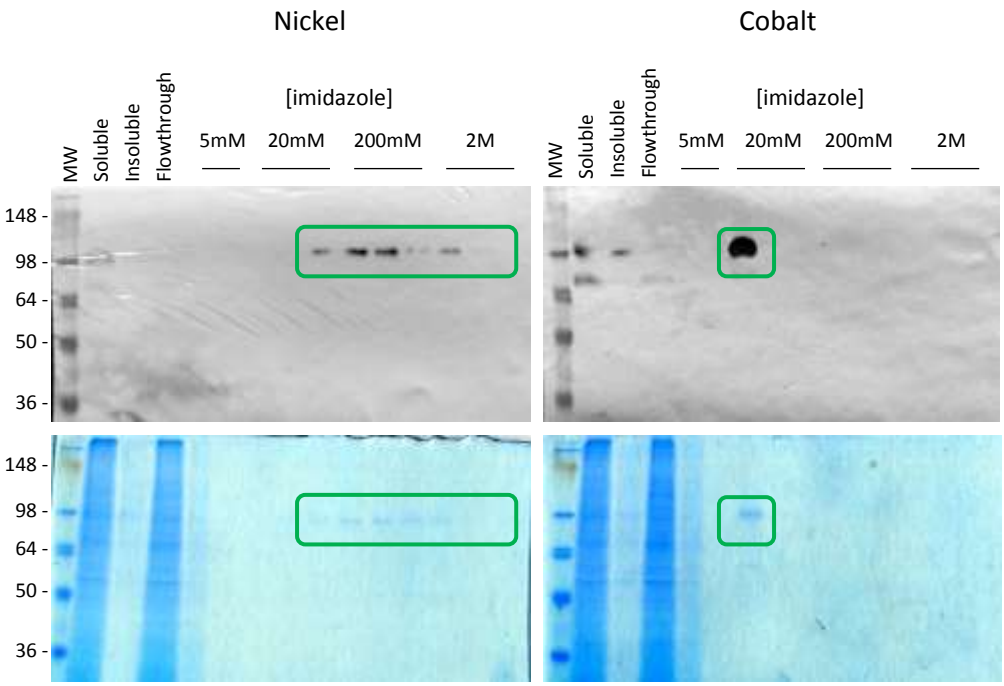


**Figure 6.1 – Comparison of nickel and cobalt ions in IMAC for SMALP-ABCG2.** Membranes from cells expressing ABCG2 were solubilised into SMALPs by incubation for 1 hour with 2.5% (w/v) SMA then separated from the insoluble material by centrifugation at 100000g for 20 minutes. The solubilised material was incubated overnight with 10% (v/v) of the associated ion coated resin ($Ni^{2+}$ or $Co^{2+}$). The solution was applied to a gravity flow column, the flowthrough collected and the protein was then eluted with increasing concentrations of imidazole in 5 times the bed volume of resin of SMA buffer. Samples of each fraction were run on 8% (w/v) polyacrylamide gels and either stained for total protein with InstantBlue (lower panels) or transferred to nitrocellulose and probed for ABCG2 with BXP-21 antibody (upper panels). ABCG2 bands are highlighted (green).

Both metal ions were capable of capturing the SMALP-ABCG2 particles but cobalt had a lower apparent affinity as the protein was eluted in fractions at a lower concentration of imidazole. The ABCG2 captured in the nickel resin was eluted over 2x bed volume fractions ranging from 20mM to 2M imidazole though was found predominantly in the 200mM imidazole fractions. The cobalt resin also captured the SMALP particles but in these samples, the bulk of the ABCG2-SMALP was eluted in the early 20mM imidazole fractions. As a result, ABCG2 was eluted in a lower total volume (less fractions) and lower concentration of imidazole. This offered the possibility of a higher concentration of purified protein with less imidazole contamination, which was important as the presence of excess imidazole in the purified protein could increase fluorescence background in the samples. Cobalt resin was therefore used in subsequent optimisation experiments where 3x washes in SMA buffer (0mM imidazole) were also included prior to addition of imidazole.

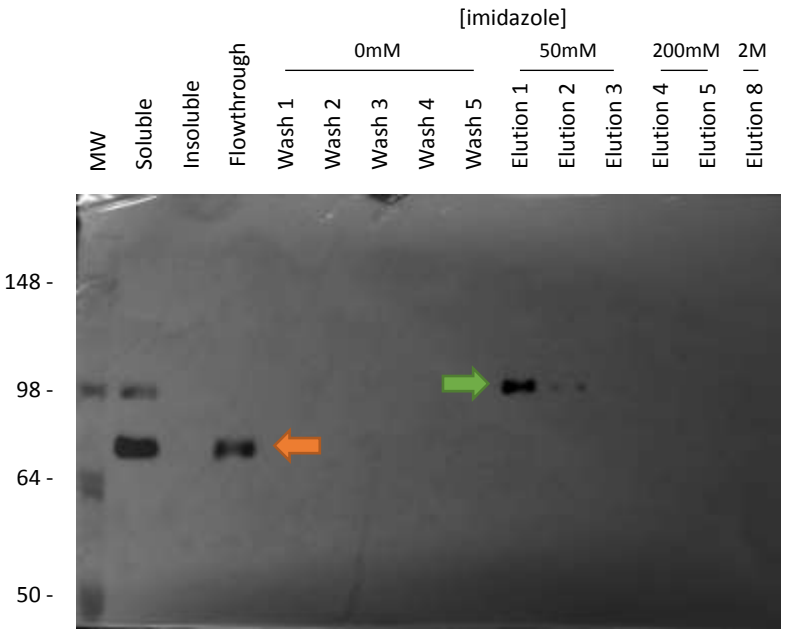


**Figure 6.2 – Optimisation of SMALP-ABCG2 purification by cobalt ion affinity chromatography.** Membranes from cells expressing ABCG2 were solubilised into SMALPs by incubation for 1 hour with 2.5% (w/v) SMA then separated from the insoluble material by centrifugation at 100000g for 20 minutes. The solubilised material was incubated overnight with 10% (v/v) cobalt resin. The solution was applied to a gravity flow column and the flowthrough collected. The resin bed was washed 5 times with 5 times the bed volume of SMA buffer (0mM imidazole). Three elutions using 2 times the bed volume of SMA buffer (50mM imidazole) were performed followed by increasing concentrations of imidazole. Samples of each fraction were analysed by western blot where probing with BXP-21 revealed tagged ABCG2 (100kDa, green arrow) purified in the 50mM imidazole elution fractions. Occasionally untagged ABCG2 was detected in the soluble and flowthrough fractions (72kDa, orange arrow).

On occasion, there was incomplete elution over the 20mM imidazole fractions and elutions were therefore performed using 50mM imidazole. This ensured maximum protein recovery over the earliest elution fractions (see Figure 6.3). There was occasionally a second, lower molecular weight protein revealed when probing with BXP-21 (anti-ABCG2 antibody). This was present in the soluble and flowthrough fractions and corresponded to the predicted molecular weight of

untagged ABCG2 (72kDa) which offers an explanation as to why this fraction of the solubilised ABCG2 is not purified. A purification procedure based on this optimisation (as described in Section 2.6) was subsequently used in all purified protein preparation.

Fractions containing ABCG2 were concentrated by spin-concentration in a 10000mwco spin concentrator (Sartorius, VS0601). This process also facilitated the reduction in imidazole concentration by repeated resuspension followed by concentration resulting in a final theoretical imidazole concentration of <0.5µM. This was performed in every purification and there was no evidence of significant protein loss. This process typically produced 300-500µL at 0.8-2µM depending on requirements. There were a number of contaminating proteins (see Figure 6.3), which are likely proteins with polyhistidine-rich regions and their presence in the concentrated fraction implies they may be SMALP encapsulated with the SMALP polymer ring precluding their passage through the membrane of the spin concentration unit. These proteins were not identified but were quantifiable. Preparations of ABCG2 (-) cells were included in all purifications and, as discussed later, the contaminant proteins were included in binding and displacement experiments as a negative control.

Overall, following the solubilisation of ABCG2 into SMALPs, purification by immobilised metal ion affinity chromatography was able to yield protein at concentrations of up to 2µM. This concentration was sufficient for analysis of drug binding by FCS with the development and application of these experiments discussed in the following section.

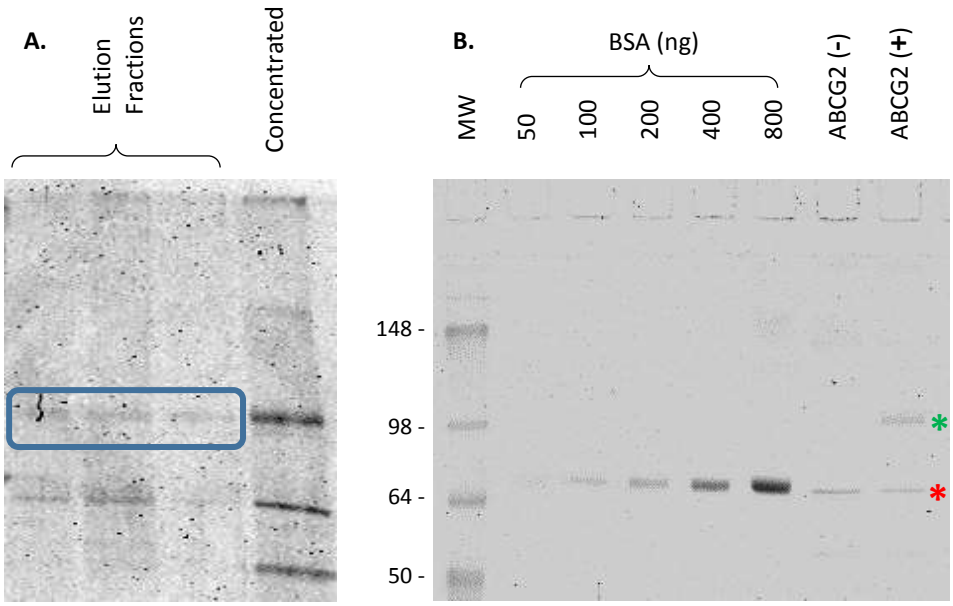


**Figure 6.3 – Concentration and quantification of purified ABCG2.** Purification fractions containing purified SMALP-ABCG2 (orange rectangle) were pooled and applied to a spin-concentration column. The protein was then concentrated by centrifugation at 300-1000g to reduce the final volume to 500µL (**A**). The volume was topped up several times as required with SMA buffer (0mM imidazole) to reduce the concentration of imidazole in the final sample to <0.5mM. A preparation of material from cells not expressing ABCG2 was treated similarly. 10µL of each of these samples was run on an 8% (w/v) polyacrylamide gel alongside known quantities of BSA (**B**). When stained with InstantBlue concentrated ABCG2 (green) and some contaminants (red) were revealed. The concentrations of these components were calculated by densitometric comparison to a standard curve constructed from the band intensities of samples with a known protein (BSA) concentration.

## 6.3 Development of an FCS-based binding assay

ABCG2 was extracted from HEK293T cells by the use of SMALPs and was subsequently purified as discussed above. This purified protein was used to explore drug transport substrate binding by FCS. As reviewed earlier, there are limited data regarding the molecular mode of substrate binding and recognition by ABCG2. While there is consensus on the presence of multiple drug binding sites, mapping of specific binding sites for transport substrates within the ABCG2 protein has not yet been achieved (Clark, Kerr and Callaghan, 2006; Horsey *et al.*,

2016; Cox *et al.*, 2018). One origin of these difficulties is that there has been very limited implementation of equilibrium binding assays to measure substrate or inhibitor affinity (for example as a dissociation constant $K_d$), despite established assays measuring dynamic ABCG2 transport of substrate. There are reports that use measurement of pheophorbide A fluorescence or quenching of internal tryptophan fluorescence as an indicator of binding (Gulati *et al.*, 2014). An ABCG2 radioligand binding study has also been reported using [$^3$H]daunorubicin in membranes, giving its dissociation constant as 564nM (Clark, Kerr and Callaghan, 2006). To date the fluorescence based approaches lack suitability for medium to high throughput assays and have not provided quantitative affinity data. Radioligand binding assays require separation of bound from free ligand, a limitation in both maintaining true binding equilibrium and in developing homogenous assay technologies suitable for screening. They also carry practical and safety issues. Therefore fluorescence based binding techniques that could be more easily used for larger scale screens of the effects of transporter mutations and SAR studies could prove incredibly valuable. The use of FCS in investigating the binding of drug substrates was explored with this potential in mind and this was also supported by a number of previous studies using FCS in similar applications (Briddon and Hill, 2007; Sridharan *et al.*, 2014). For example the binding of tetramethylrhodamine-labelled endothelin-1 to VLiP-integrated endothelin A receptor in virus-like particles or a series of BODIPY 630/650-X labelled agonists to the adenosine A1-receptor (Zemanova *et al.*, 2004; Middleton *et al.*, 2007). In each case, it is the change in fluorophore mobility that is measured.

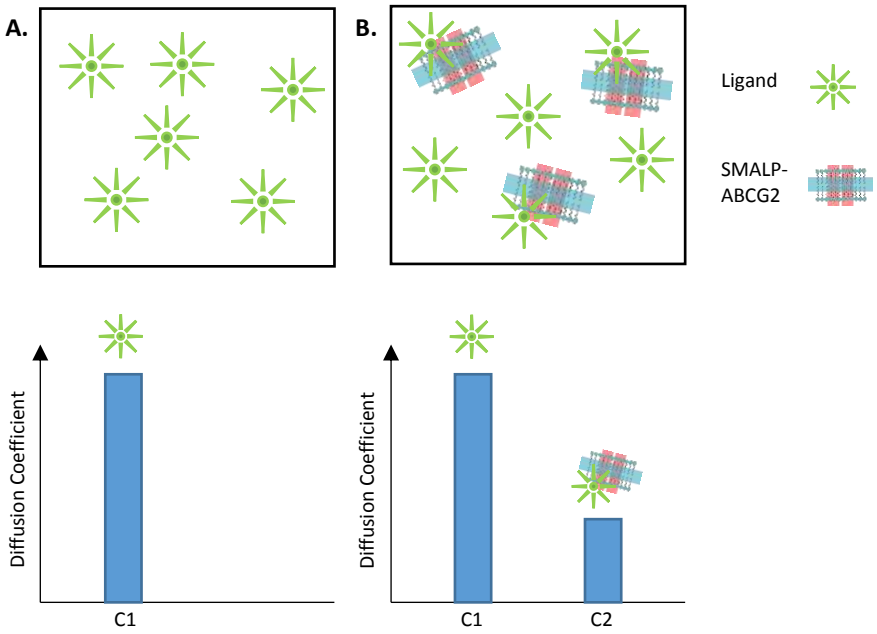


**Figure 6.4 – Principles of an FCS based SMALP-ABCG2 binding assay.** In a sample containing drug in the absence of SMALP-ABCG2 (**A**) it is expected that it will diffuse freely and will therefore have a high diffusion coefficient reflective of a small molecule moving in solution. In the presence of SMALP-ABCG2 (**B**) a proportion of the drug is expected to bind to the ABCG2 and therefore move with a diffusion coefficient reflective of a large molecule moving in solution.

As shown above in Figure 6.4, the principle of this technique would be the ability to measure the change in diffusion of a fluorescent substrate on it binding to the much slower moving SMALP encapsulated ABCG2. In autocorrelation analysis the components associated to free (fast) and bound (slow) are additive, forming a biphasic curve, so do not require further separation. As such, both free and bound substrate can be quantified. This is in contrast to radioligand binding, as described above, which required unbound ligand to be removed before measurements of bound ligand alone can be made. A suitable fluorescent substrate was required to facilitate this investigation and ABCG2 has a wide range of chemically different substrates but most were expected to be non-fluorescent (at least at the

appropriate wavelengths for investigation). A number of fluorescent substrates for ABCG2 were identified by a review of the relevant literature (Ivnitski-Steele *et al.*, 2008; Strouse *et al.*, 2013; Haider *et al.*, 2015). The evidence for specific transport was critically assessed and the fluorescence spectra were checked for compatibility with FCS based analysis. Only a few substrates were reported with good evidence for specific transport in the correct excitation and emission wavelengths and which were readily commercially available. Based on these criteria, mitoxantrone (MX), CellTracker Green CMFDA (5-chloromethylfluorescein diacetate) (CT), Syto™ 9 (S9) and BODIPY™-FL-Prazosin (BD-P) were investigated further in trial FCS experiments using free ligand in solution (Figure 6.5). Optimal laser powers were assessed as in Section 5.3 (data not shown), by collecting 60 second traces of fluorescence fluctuation data from 50nM solutions of the compounds in SMA buffer. To ensure signal from the fluorescent particles was significantly above that of the background noise, the signal to noise ratio was assessed by comparing the average intensity for the drug solution to that of buffer alone under the same acquisition conditions. The signal for MX and S9 was unacceptably low (<10x background); that for CT and BD-P was usable. There appeared to be low recovery in all cases with concentrations calculated from autocorrelation function analysis being much lower than the theoretical concentration. MX and S9 were subsequently disregarded as substrates for this study. The contributions of the triplet state to the autocorrelation curves for both CT and BD-P were also acceptable for analysis (Figure 6.5 (D and E)). However CT was not a well-established transport substrate of ABCG2 with low selectivity reported compared to interaction with other

transporters (Strouse *et al.*, 2013). In contrast, BD-P has been used in a number of previous studies (e.g. Robey et al. 2001; Haider et al. 2015) and also benefits from the availability of the non-conjugated prazosin as a non-fluorescent competitive substrate. As a result, BD-P was selected for further investigation.

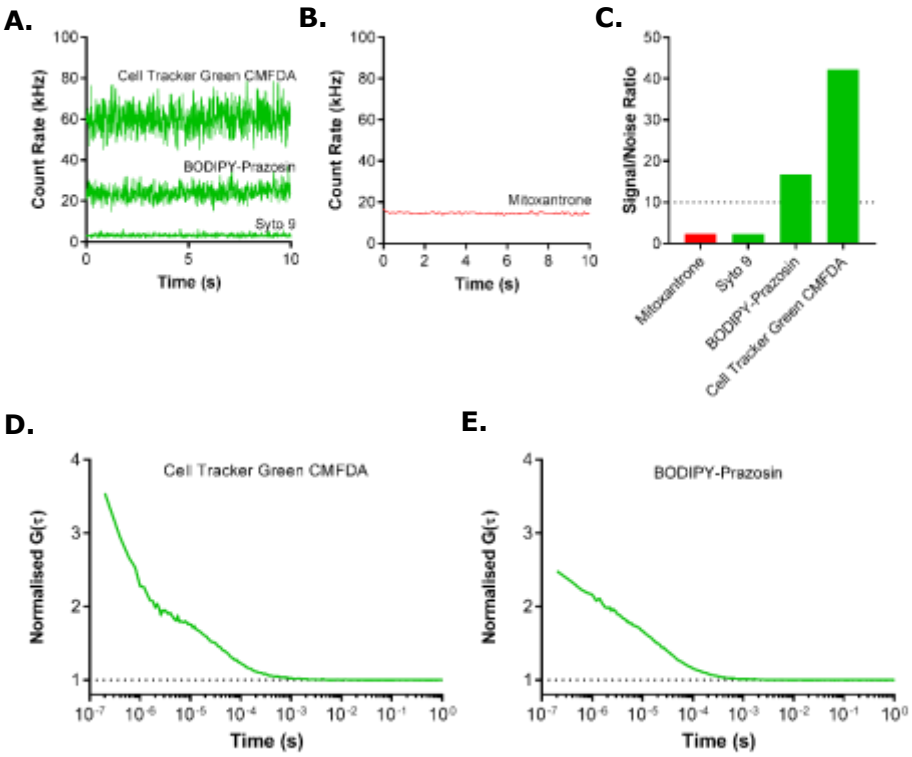


**Figure 6.5– Selection of drug substrates for FCS analysis.** 50nM samples of various fluorescent ABCG2 substrates were applied to 8-well plates and analysed by FCS using either 488nm excitation (CT, BD-P and S9) or 633nm excitation (MX). 6 x 10s traces were collected for each compound (**A** and **B**). Average intensity for each compound were compared to that of the buffer alone to assess the signal/noise ratio (**C**). CT and BD-P had signal/noise ratios >10. Autocorrelation function curves for each CT (**D**) and BD-P (**E**) were inspected for assessment of triplet state interference (apparent at $<10^{-5}$s).

The disparity between the measured BD-P and CT concentrations using FCS analysis and the theoretical concentration was observed at several concentrations of the drugs (Figure 6.6 (A)), in comparison to the expected linear relationship, seen with the calibration fluorophore R6G. This might be attributable to non-specific binding of the drug to the plastic chambers, or the glass coverslip during the experiment. The FCS setup allowed this to be assessed by performing a Z-scan to assess count rate and drug concentration at various distances from the coverslip surface. The confocal volume was positioned at the coverslip surface of a well containing 50nM BD-P and fluctuation traces were then obtained systematically at increasing distances from the coverslip. This revealed that the count rate of the sample was highest at the coverslip and the concentration of fluorescent particles was highest just above the coverslip (Figure 6.6 (B, C)).

The lowest concentration of particles at the coverslip, prior to the peak at +5µm, are explained because particles in contact with the coverslip would be relatively immobile, and do not move at a rate to generate fluctuations detected by FCS. Following the highest concentrations being observed 5µm from the coverslip, the measured concentration rapidly reduced as the confocal volume is moved up into solution but remained relatively constant from 20µm to 250µm above the coverslip. In all other experiments the fluctuation traces were recorded 200µm from the coverslip to avoid interference. As a result BD-P was used as the fluorescent drug for initial binding assays but the concentration was increased to 500nM in an effort to overcome the lower than expected concentration observed in solution.

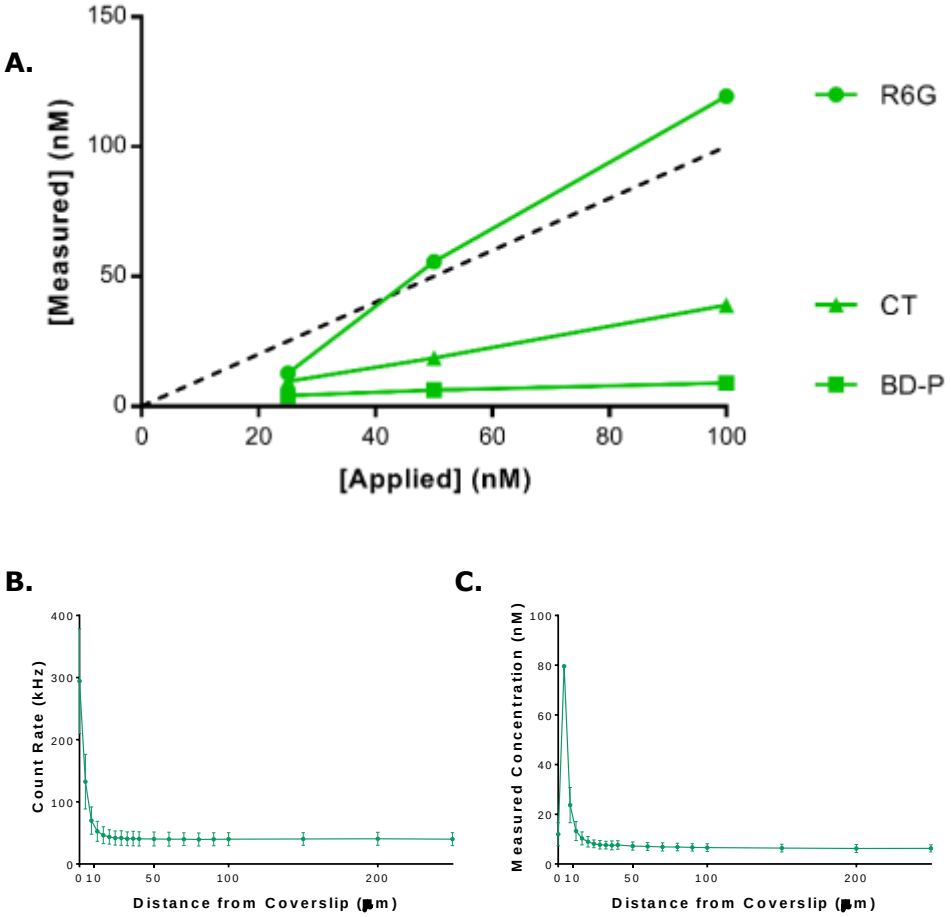


**Figure 6.6 – Assessment of compound recovery by FCS.** 25-100nM samples of CT and BD-P as well as rhodamine 6G (R6G) were applied to wells of an 8-well plate and analysed by FCS. The measured concentrations in solution (**A**) were compared to those expected (dashed line). The reason for the low concentration observed was investigated by measuring the count rate (**B**) and concentration of BD-P (**C**) at different distances from the coverslip.

Following the identification of a suitable substrate for investigation, further experiments sought to explore the feasibility of detecting BD-P binding to ABCG2. As discussed, the principle of the FCS binding assay is that the fast diffusion of a free small molecule drug in solution would be slowed by binding to a much larger protein complex (i.e. SMALP-ABCG2) in solution. First of all D for free BD-P and, separately, SMALP-SNAP_ABCG2 (see also Chapter 5) were determined. For 'free'

BD-P in solution, D was measured to be 453.3 ± 11.9$\mu m^2 s^{-1}$(mean ± SEM, n=3 independent experiments) by interpretation of ACF curves from measurements of 500nM solutions as discussed previously using a 1-component model of free 3D diffusion. His_SNAP-tag_ABCG2 was labelled with SNAP-Surface® Alexa Fluor® 647 as described in Section 4.8 and was then extracted and purified in SMALPs. Purified SMALP-SNAP_ABCG2 labelled with SNAP-Surface® Alexa Fluor® 647 was applied to wells of an 8-well plate and fluorescence fluctuation traces were recorded using a 633nm excitation. Due to the different acquisition settings compared to BD-P measurements, the size of the confocal volume was calibrated with Cy5 dye as described in Section 2.10.2. For SMALP-SNAP_ABCG2 in solution the diffusion coefficient, D, was determined to be 26.7 ± 1.4$\mu m^2 s^{-1}$ (mean ± SEM, n=5 independent experiments) by interpretation of ACF curves using a 1-component 3D model of diffusion as summarised in Figure 6.7 (A). Following this, 500nM BD-P was then incubated with unlabelled SMALP-ABCG2 (20-30nM) for 30 minutes. Fluorescence fluctuation traces were obtained measuring the diffusion of BD-P (488nm excitation) and, as shown in Figure 6.7 (C, D), bound and free species could be resolved from the autocorrelation analysis. In contrast to the measurement of free BD-P alone, a 1-component 3D model now failed to fit the autocorrelation curve from BD-P / SMALP-ABCG2 solutions without substantial deviation. An improved fit (reduced fit deviation) was observed by the use of a 2 x 3D component model and the diffusion coefficients for these separate 'free' and 'bound' components closely matched those calculated for BD-P alone and also labelled SMALP-SNAP_ABCG2. This indicates that a proportion of the BD-P binds

SMALP-ABCG2 and therefore moves at the same rate as the much larger particle.

These data are summarised in Figure 6.7 (E).

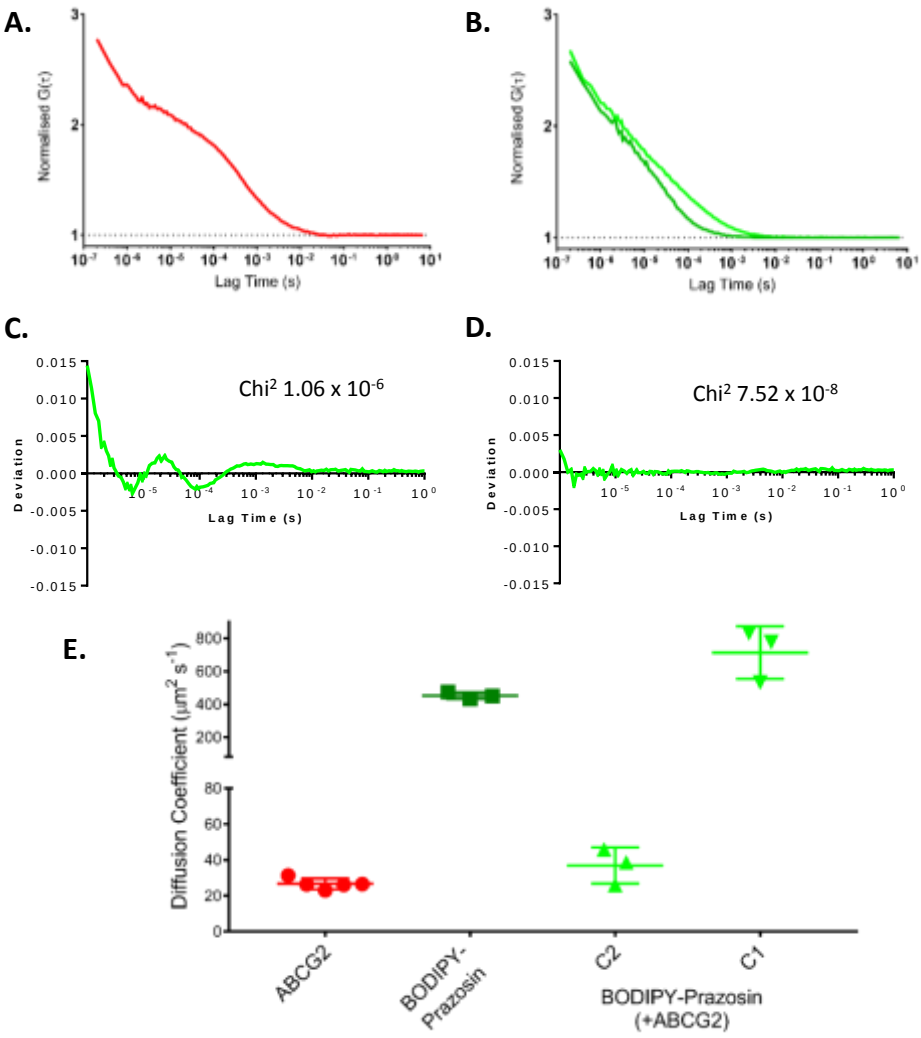


**Figure 6.7 – Summary of initial BD-P binding analysis to SMALP-ABCG2.** Example ACF curves are given for SNAP-Surface® Alexa Fluor® 647 labelled SMALP-ABCG2 (**A**) and BD-P in the presence (light green) and absence (dark green) of unlabelled SMALP-ABCG2 (**B**). Deviation in fit and associated $Chi^2$ values for 1x 3D component (**C**) and 2 x 3D component (**D**) fitting models to the BD-P autocorrelation curve in the presence of SMALP-ABCG2 are shown. The 'free' and 'bound' diffusion coefficients from the 2 x 3D model were then compared to those of SNAP-Surface® Alexa Fluor® 647 labelled SMALP-ABCG2 and BD-P alone (**E**).

To use this technique in a quantitative binding assay, the key factor is the accurate quantification of the ACF curve in terms of the concentration of each component ('bound and 'free' drug) as the concentration of SMALP-ABCG2 or the presence/absence of competing drug is varied. This relies on adequately resolving the component fractions when analysing the ACF with the actual dwell time, $\tau_{D,}$ of each being less significant. Expected values for free and SMALP-ABCG2 bound BD-P were known based on the initial binding analysis. Fitting the relative amplitudes of free and bound BD-P could subsequently be made more robust by placing constraints on the allowed $\tau_D$ for each component when applying the 2x 3D model. Pilot data indicated this was particularly important at high SMALP-ABCG2 concentrations as greater diffusion coefficients were observed when the component $\tau_D$ was allowed to vary freely which was unexpected. It is possible that this was due to small amounts of aggregated sample which had a disproportionate impact on the ACF curve. It is also likely that this would be due to the much lower amplitude of the ACF curve at high protein concentration which much reduced the robustness of the curve fitting. Options for fixing $\tau_D$ for free and bound components in the fitting were explored.

The dwell time for free BD-P could be measured in each experiment but, as the protein was unlabelled, this was not possible for SMALP-ABCG2 samples. The dwell time was measured for BD-P in the absence of SMALP-ABCG2 and this value was fixed for the free BD-P fraction in each sample. $\tau_D$ for the bound fraction was allowed to vary freely or given a range. This range was back-calculated (to account

for the different excitation wavelength) based on the diffusion coefficient calculated for SNAP-Surface® Alexa Fluor® 647 labelled SMALP-ABCG2 (see Figure 6.7). The 'fixed' fit shown slightly increased deviation compared than when $T_D$ for bound drug was allowed to vary freely.

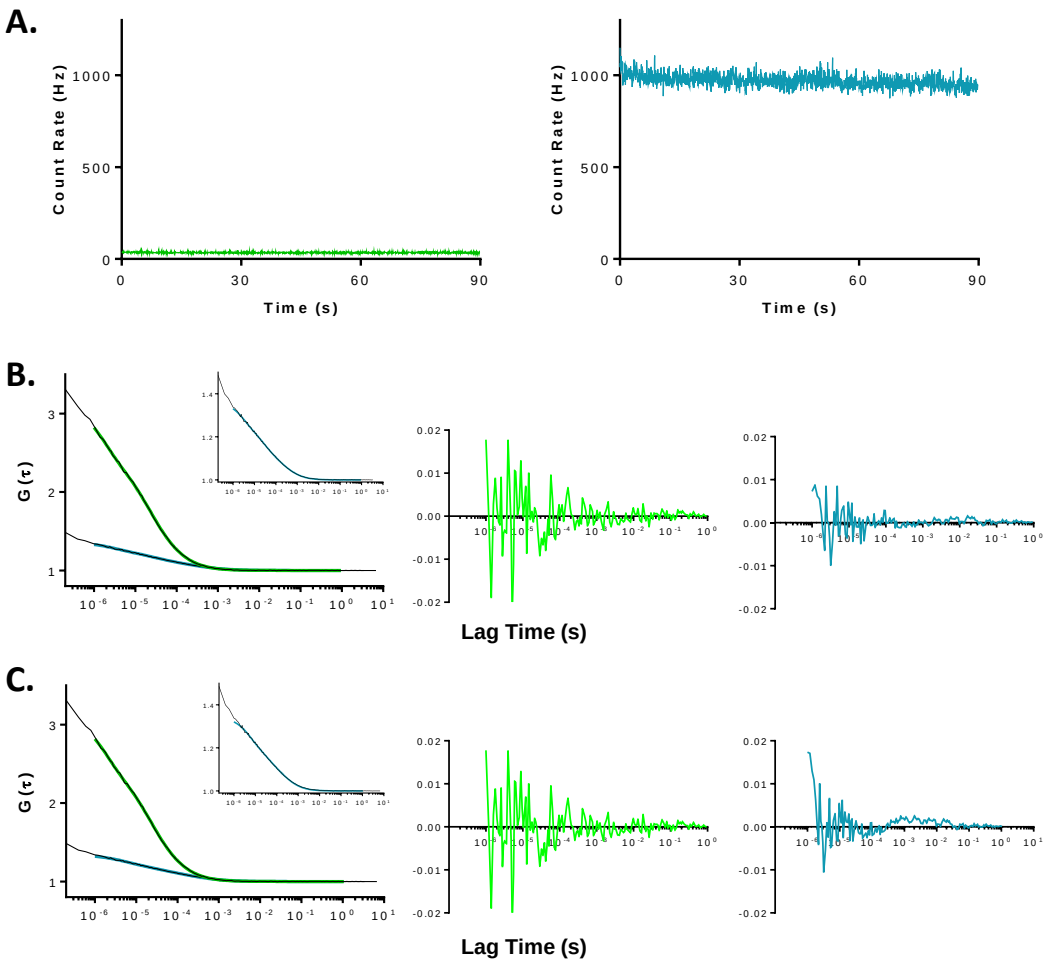


**Figure 6.8 – Analysis of approaches to fit the FCS Binding data.** Fluctuation traces (**A**) were recorded for samples of 500nM BD-P in the absence (green, cpm = 27) or presence of various concentrations (500nM shown) of SMALP-ABCG2 (blue, cpm = 33). These data were fitted with 2-component models of diffusion that either allowed the dwell time for each component to vary freely (**B**), to vary within a given range based on the diffusion coefficient of SMALP-ABCG2 26.7±1.351µm$^2$s$^{-1}$ (**C**). In each case, the left hand panel shows the ACF (with the ACF for the 500nM protein sample also inset), the centre panels show the deviation from the model for the sample in the absence of protein and the right hand panel shows the deviation for the 500nM protein sample.

The increased deviations were nonetheless acceptably small (<1% of curve) and this allowed for better standardisation of the ACF analysis workflow. Conceptually, this interpretation was appropriate for the expected properties of the system in that D for each free BD-P and SMALP-ABCG2 bound BD-P should be independent of the concentration of each particular species. In all subsequent experiments, D for free drug was fixed based on the measurement of drug alone in a particular experiment and D for bound drug was fixed to within a range based on the previously measured diffusion coefficient for SNAP-Surface® Alexa Fluor® 647 labelled SMALP-ABCG2.

When performing the binding analysis by FCS it was expected that increasing concentrations of SMALP-ABCG2 would result in increasing concentrations of bound BD-P and a reduced concentration of free BD-P due to ligand depletion. An important advantage of the FCS assay set up is that both the free and bound proportions of BD-P can be measured directly. At a high enough concentration of SMALP-ABCG2 both free and bound curves should reach an asymptote, as binding of BD-P to ABCG2 causes ligand depletion. This is simulated in Figure 6.9 for several drug binding affinities ($K_d$) (10nM, 100nM and 1μM) where ligand depletion is taken into account by Equation 6.1.

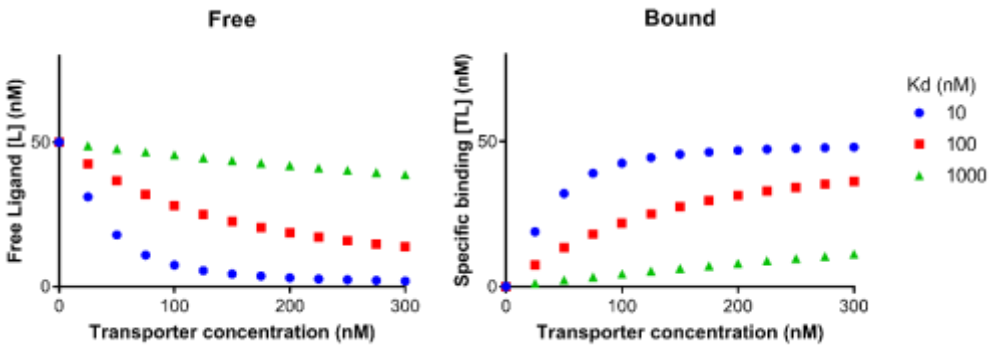


**Figure 6.9 – Simulated transporter binding data.** The expected observations of the transporter binding assay used in this project were predicted using a model accounting for ligand depletion (see Equation 6.1). The predicted concentrations for each free and transporter bound ligand at varying concentrations of transporter are given for several affinity ($K_d$) values.

*Equation 6.1*

$$[RL] = \frac{([R_T] + [L_T] + K_{d)} - \sqrt{([R_T + L_T + K_d)^2 - 4 \cdot [R_T] \cdot [L_T]}}{2}$$

Where $[RL]$ is the concentration of transporter bound ligand, $[R_T]$is the total concentration of transporter, $[L_T]$ is the total concentration of ligand (Hulme and Trevethick, 2010).

In line with this model, data (see Figure 6.10) showed that increasing the concentration of SMALP-ABCG2 increased the fraction of bound BD-P whilst decreasing the fraction of free drug. As a result, the increased concentration of SMALP-ABCG2 resulted in an increased concentration of bound BD-P. However, the concentration of free drug also increased. This reflected the observation that the total concentration of BD-P in solution was much lower than expected in the absence of SMALP-ABCG2 and increased on the addition of greater concentrations of protein. This was possibly due to non-specific binding of BD-P to the coverslip

as was indicated in Figure 6.6. ABCG2 (-) samples were prepared from HEK293T cells not expressing ABCG2 in an otherwise identical fashion to the ABCG2 (+) samples. This resulted in 'purification' of just the contaminant proteins (see Figure 6.3). The concentration of the ABCG2 (-) material added to each sample was normalised based on the concentration of the contaminant proteins that were also present in ABCG2 (+) samples. The binding observed in ABCG2 (-) samples was reduced.

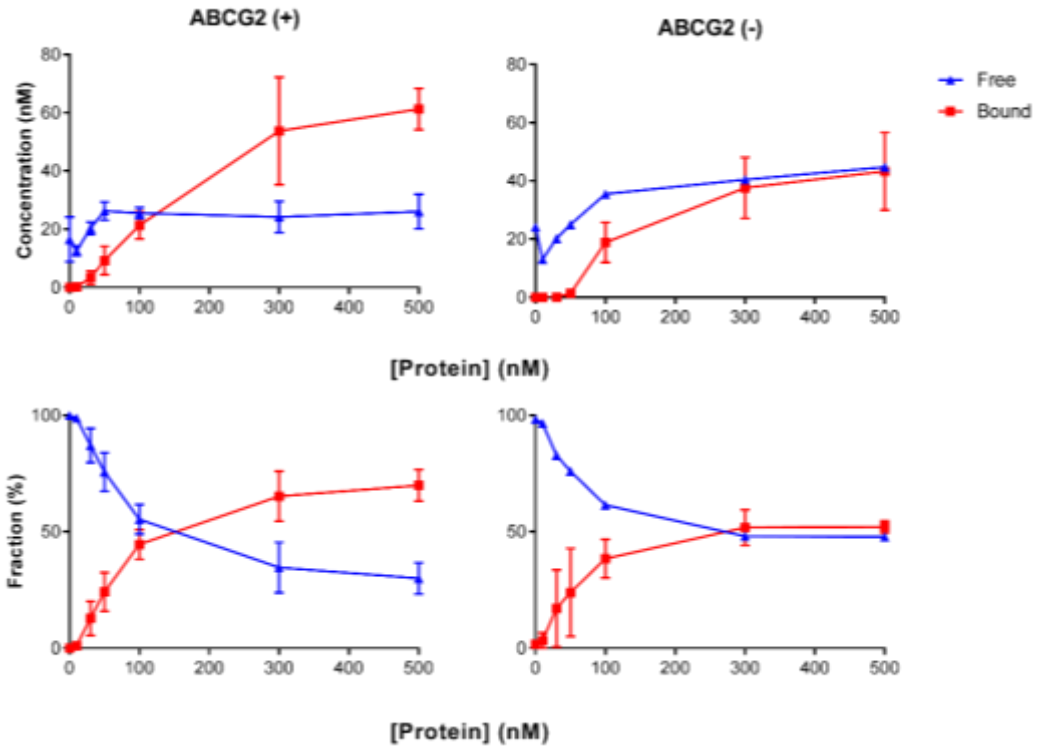


**Figure 6.10 – Binding analysis of BD-P to varying concentrations of SMALP-ABCG2.** Samples of 500nM BD-P were incubated with varying concentrations of SMALP-SNAP_ABCG2 (left hand panels) or the equivalent concentration of contaminating proteins (right hand panels). These samples were analysed by FCS using a 2-component model and data were reported as both component concentration (top panels) and component fraction (lower panels). Bound drug was defined as the slow moving fluorescent component (red). Free drug was defined as the fast moving component (blue) (mean ± SD, n=3 independent experiments).

The unexpected behaviour of free drug measurements, especially at low concentrations, together with background binding to SMALP ABCG2 negative preparations, meant that there was no estimate attempted of $K_d$ concentration using the data in Figure 6.10. As previously noted (Figure 6.6), BD-P is prone to high levels of non-specific binding. The existence of bound reservoirs of BD-P (for example to well surfaces) in the experiments may complicate the analysis of Figure 6.10 significantly. For example the presence of SMALP-ABCG2 at increasing concentrations may lead to recruitment of more drug from the surface of the well as the free drug in solution is depleted, leading to complex equilibria between the free, ABCG2 bound and non-specifically bound BD-P species. Furthermore it was also noted that the concentration-dependent measurements were variable and potentially this could arise through differences in the time of drug incubations with the well surfaces, before addition of SMALP-ABCG2. This might lead to differences in the extent of the non-specific BD-P bound reservoir from experiment to experiment. Therefore a further optimisation was performed to examine the impact of incubation time on free BD-P concentration measurements by FCS.

To investigate the sticking of BD-P to the wells during incubation 100µL of 1µM BD-P was applied to wells of an 8-well plate or an Eppendorf tube for 25 minutes. FCS measurements were taken over this time from the 8 well plate (Figure 6.11A). 100µL of SMA buffer was then added to simulate the addition of SMALP-ABCG2 leaving a final applied concentration of BD-P of 500nM. The samples incubated in the Eppendorf were then applied to wells of an 8-well plate and FCS data were again acquired for both sets of samples over another 25 minute incubation (Figure

6.11B and C). The initial concentration of the solution applied to the 8-well plate was close to expected on average but was most variable. This variability reduced over time but so did the concentration in solution. Initial FCS reads reflected the expect concentration of 1000nM, but there was a rapid decline in free concentration (~90 % over 25 min) regardless of using 8 well plate or Eppendorf tube – there was no well-to-well variation in 8 well plate measurements nor the effect of NSB (data not shown).

After 25 minutes, measurements of (lower) free concentration remained stable throughout the second set of reads. Therefore, to limit the effects NSB variation at early time points post mixing, samples were preincubated in an Eppendorf for 30 minutes prior to transfer to FCS plates as described fully in Methods. Though the change in overall concentration would still limit the interpretation of affinity, these experiments could still be performed in exploring the interaction of transport substrate and inhibitor by displacement of consistent BD-P binding.

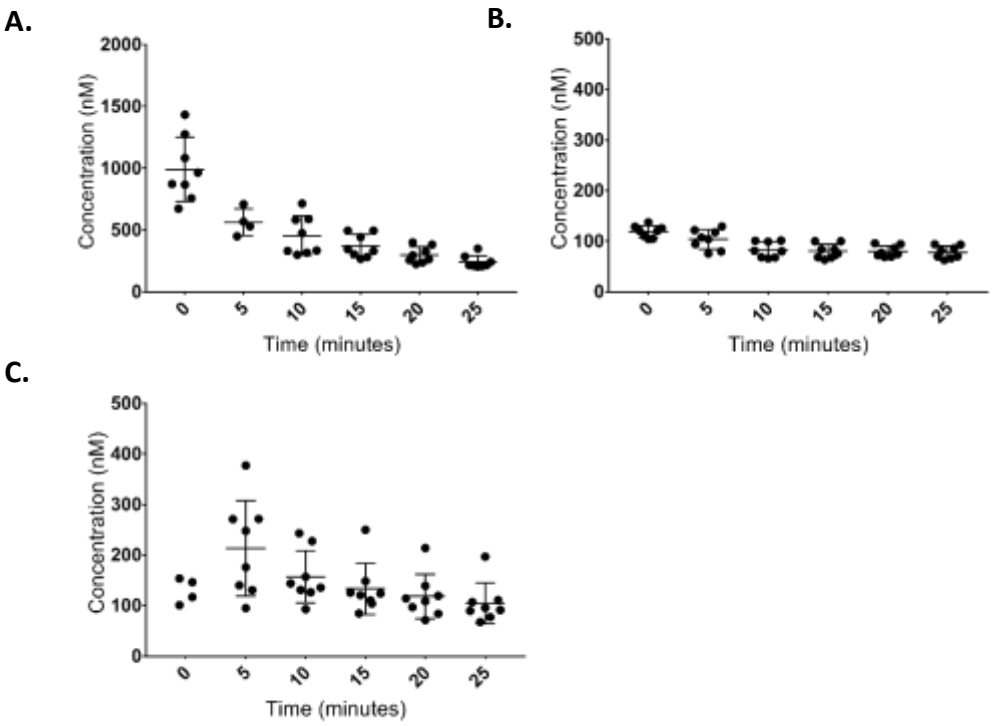


**Figure 6.11 – Effect of incubation time on non-specific binding to plate surfaces and the measured BD-P concentration by FCS.** 1µM BD-P was applied to an 8-well plate and fluorescence traces were recorded at subsequent time points to measure the concentration of BD-P available in solution (**A**). An equal volume of buffer was then added and the measurements repeated (**B**). Measurements were also made of samples first pre-incubated for 25 minutes in a separate Eppendorf tube, prior to transferring to an 8 well plate (**C**). Bars represent the mean ± range over n=2 independent experiments and each data point represents the mean of 4 replicate measurements.

## 6.4 Investigation of transport substrate and inhibitor interaction with ABCG2

In the previous section, the optimisation of an assay using FCS to measure the binding of BD-P, a wild-type transport substrate, to ABCG2 was described. This set up presented a novel tool for the investigation of transport substrate binding and its competition by inhibitor molecules.

As previously described (Figure 6.10) the presence of SMALP protein led to apparent increases in the total concentration of BD-P measured by FCS. As a result

the high concentration (500nM) of BD-P that was previously used to address the lower than expected observed concentration in solution was not employed in the next set of experiments. Instead, 50nM of BD-P was incubated with varying concentrations of SMALP-ABCG2 or control SMALPs and analysed by FCS using the optimised preincubation period described in the previous section. A 2-component 3D model was used to fit the data with the dwell times of each component defined as described before in order to calculate the concentrations of both free and bound BD-P. Similarly to the previous datasets, the total concentration of BD-P in solution increased with increasing concentrations of SMALP-protein. There was also substantial experiment to experiment variation observed in the bound concentration of BD-P, particularly using higher SMALP-ABCG2 concentrations (>100nM). Notably however, these experiments revealed greater differences in binding capacity to ABCG2 (+) and ABCG2 (-) samples (see Figure 6.12).

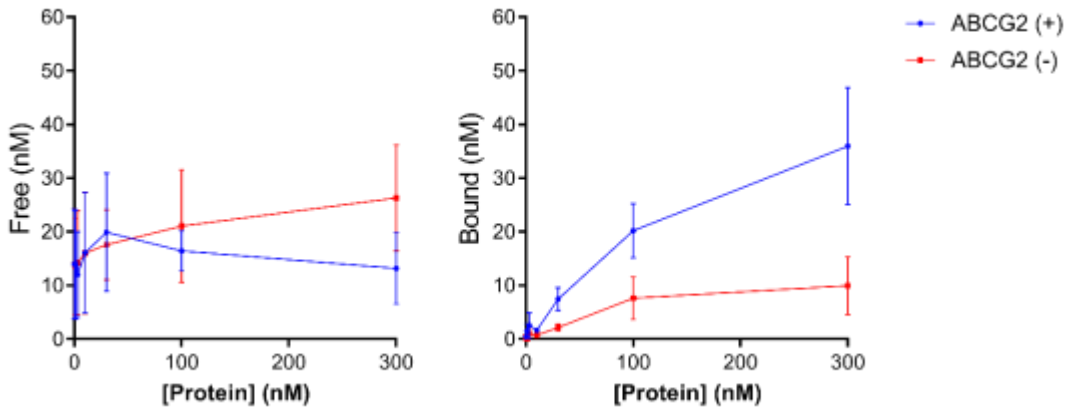


**Figure 6.12 – Analysis of BD-P binding using the FCS assay and optimised conditions.** Varying concentrations of SMALP-ABCG2 (blue) or equivalent negative control (red) were incubated with 50nM BD-P for 30 minutes. The free and bound component concentrations are shown for each, defined as the slower or faster moving components respectively as resolved by FCS analysis. 100nM ABCG2 was used in subsequent experiments (mean ± SEM, n=3 independent experiments).

Using the highest ABCG2 (+) concentration, the measured bound BD-P approached the limit possible for the input concentration (50nM). However, more extensive saturation analysis was limited by the overall low SMALP purified concentration in these experiments, and it was not possible to collect sufficient data points for an accurate estimate of BD-P $K_d$.

Additionally, competition assays were also performed to investigate the specificity of the observed transporter binding and explore the possibility of assessing the affinity of non-fluorescent transport ligands using this platform in future. As mentioned, one advantage of using BD-P in the above experiments is that it is a fluorescent derivative of the readily available ABCG2 substrate prazosin. 100nM ABCG2 was first incubated with varying concentrations of prazosin for 30 minutes at room temperature (Figure 6.13). These samples were then added to solutions of BD-P to a final BD-P concentration of 50nM then incubated as previously. The concentration of bound BD-P was determined by FCS analysis for each sample and this was expressed as a percentage of total binding in the absence of prazosin. As shown in Figure 6.13, there was a significant concentration dependent inhibition of BD-P binding by prazosin in ABCG2 (+) SMALPs, of up to 50 %. No significant effect on BD-P binding in ABCG2 (-) SMALPs was observed.

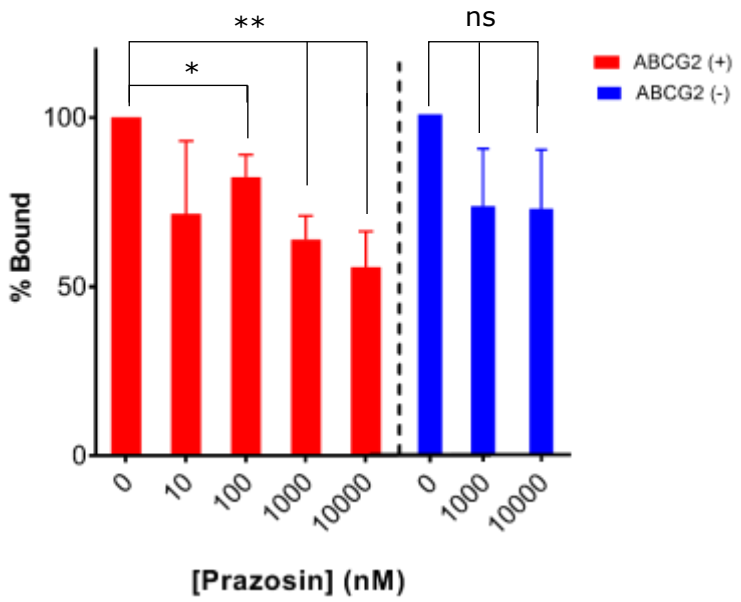


**Figure 6.13 – Inhibition of BD-P binding to SMALP-ABCG2 by addition of prazosin.** 100nM SMALP-ABCG2 (or equivalent control) was incubated with varying concentrations of prazosin for 30 minutes prior to incubation with 50nM BD-P for a further 30 minutes. % Bound was calculated based on comparison to the binding in the absence of prazosin. Data were assessed for significance by one-way ANOVA followed by Dunnett post-analysis (*<0.1, **<0.05) (mean ± SD, n=3 independent experiments).

During the course of this study, cryo-EM structural data of ABCG2 bound to Ko143, a potent inhibitor, became available (Jackson *et al.*, 2018). This proposed the inhibitory mechanism of Ko143 to be the occupation of the central cavity, preventing transport substrates from binding. However work by other authors identified distinct substrate binding sites separate from the central cavity (Cox *et al.*, 2018). Though this work was limited to molecular docking studies it suggested that a binding site for mitoxantrone, another therapeutic transport substrate of ABCG2, was separate from the central cavity. To investigate this, the effect of Ko143 in BD-P competition binding experiments was also investigated in comparison to prazosin, under identical conditions. 100nM samples of SMALP-

ABCG2 were incubated with Ko143 or prazosin. These samples were then added to solutions of BD-P to make up a final BD-P concentration of 50nM. These samples were analysed by FCS and the concentration of bound BD-P, expressed as a percentage of total binding in the absence of competing ligand. These data are shown in Figure 6.14 below and demonstrated that in contrast to the effect of prazosin, the presence of Ko143 up to 10µM had no effect on BD-P binding to SMALP-ABCG2.

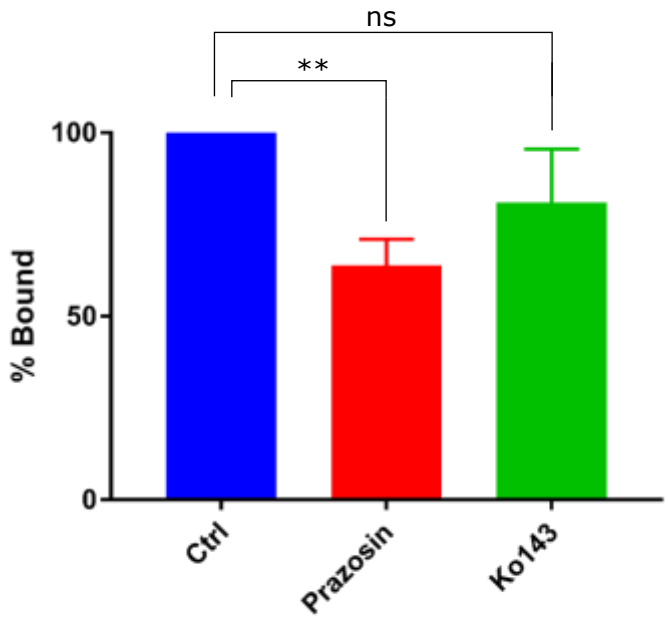


**Figure 6.14 – Analysis of BD-P binding inhibition by prazosin and Ko143.** 100nM SMALP-ABCG2 was incubated with 1µM prazosin or 1µM Ko143 for 30 minutes prior to incubation with 50nM BD-P for a further 30 minutes. % Bound was calculated based on comparison to the binding in the absence of prazosin or Ko143 (Ctrl). Data were assessed for significance by one-way ANOVA followed by Sidak post-analysis (**<0.01) (mean ± SD, n=3 independent experiments).

## 6.5 Summary

Our understanding of substrate binding and recognition by ABCG2 is limited. This is in part due to the lack of suitable binding assays. In the preceding chapters, the extraction of dimeric ABCG2 in SMALPs was described and the purpose of the work in this chapter was to explore the development of a binding assay using purified SMALP-ABCG2. Following development of a purification strategy and the identification of an appropriate fluorescent substrate (BD-P), FCS analysis was employed as a means to establish such an assay. After optimisation, data provided convincing evidence that selective binding of BD-P to SMALP-ABCG2 can be measured by this technique. This platform was then utilised in competition assays indicating the possibility of using unlabelled substrates and inhibitors in this fashion. Further work could improve the quantification and throughput of this technique to provide quantitative estimates of affinity for various known and novel substrates or inhibitors.

The demonstration of dimeric ABCG2 extraction by the use of SMALPs was possible without purification (Chapter 5). However, work looking at specific binding of transport substrate to ABCG2 required purified protein to minimise the impact of non-specific components. The constructs had been engineered to facilitate IMAC purification; a standard strategy for protein purification, and this was able to yield concentrations of protein (2μM) sufficient for analysis of binding by FCS.

The principle of this FCS binding assay is that the diffusion of a fluorescent small molecule is slowed to the rate of the much larger protein to which it is bound. There are a number of established fluorescent substrates of ABCG2 (e.g. MX,

methotrexate, daunorubicin or doxorubicin). Many of these native substrates with intrinsic fluorescence are poor fluorophores though still useful when used in whole cell assays. A review of several studies identified a number of other fluorescent substrates and BD-P was selected for the development of a binding assay.

Consistent diffusion coefficients for both free drug and labelled protein were established. In the presence of unlabelled protein, it was possible to resolve two species with some drug being equivalent to the BD-P alone and a proportion being equivalent to SMALP-ABCG2 which indicates it is bound. Optimisation of the assay conditions (e.g. inclusion of a pre-incubation step) and the data analysis appeared to provide a robust platform for performing binding analysis. However it was not possible to perform fully quantitative affinity estimation because of limits to available protein concentration and additional complications in interpretation. In particular, there was a substantial degree of non-specific binding (NSB) to the well surface due to BD-P hydrophobicity. As a result the measured concentration was much reduced in comparison to the theoretically applied concentration which meant there was a more complex binding system in which an additional NSB reservoir of drug needed to be considered. This led to paradoxical changes in the free concentration of drug as SMALP was added and it would have been inappropriate to measure BD-P Kd from the experiments to date. This limitation might be overcome by synthesis of *de novo* fluorescent substrates.

Regardless of the above limitations, optimised conditions demonstrated clear specific binding in comparison to ABCG2 (-) SMALPs suggesting binding to SMALP lipids, or contaminating proteins was not as a significant factor. This was

reinforced by the competition of BD-P for unlabelled prazosin at concentrations above 1µM suggestive of specific binding. Using this method, competition by Ko143 was also investigated. This is a well-documented inhibitor of ABCG2 transport (see Figure 4.5) but, even at 10µM, no inhibition of BD-P binding was observed. This suggests Ko143 may bind non-competitively to a different part of ABCG2. Recent structural data show Ko143 bound in the central cavity (Jackson *et al.*, 2018). Therefore data from this study support the findings of Cox et al. (2018) who suggested the binding site for ABCG2 substrates may be distinct from the central cavity. In particular, the recognition site may reside on the lipid facing side of the intracellular end of the TMDs.

A more complete picture could be gained by assessing a larger panel of competing ligands. In addition, probe substrates other than BD-P (including those synthesised *de novo*) could provide further information regarding any possibility of multiple translocation pathways as it is possible that some inhibitors may limit the binding of some substrates but not others. The result of this chapter is a platform suitable for performing FCS-based binding analysis which was subsequently used to challenge current theory on the molecular mechanism of a widely used ABCG2 inhibitor. This, and the implications of the preceding work in this thesis are considered further and the future perspectives considered in the following chapter.

# 7 Discussion

## 7.1 Key Findings and Limitations

This project set out to develop techniques to isolate and analyse ABCG2 in solution. This was achieved by the generation and validation of appropriate protein constructs, SMALP-based extraction and purification followed by analysis by quantitative fluorescence microscopy. The achievements made using these methods were not without limitations which are discussed below.

ABCG2 N-terminally tagged with hexahistidine and GFP or SNAP-tag® was shown to be active (ABCG2-specific mitoxantrone efflux) and correctly localised to the plasma membrane (confocal microscopy). These characteristics were important to validate in light of the added tags which may have adversely affected protein function. Maintained activity and correct localisation had been observed in previous studies that also used N-terminally tagged ABCG2 (Haider *et al.*, 2011; Wong *et al.*, 2016). The GFP and histidine tag was also employed for the monomeric and dimeric control proteins (CD28 and CD86). GFP was the most appropriate fluorescence tag for these as they were intended for studies of oligomeric state. Genetically encoded fluorescence tag would support a 1:1 ratio of protein to fluorophore where systems that require labelling (e.g. the SNAP-tag constructs) may not necessarily have the same result. These oligomeric control proteins act as T-cell receptors and, though their activity was not measured in this study, their monomeric and dimeric states are previously documented (Wong *et al.*, 2016).

The tagged protein constructs were then expressed and extracted in SMALPs. This was performed to solubilise ABCG2 and the control proteins for them to be

studied in a purified system. Detergents could be used to achieve the same aim. As discussed earlier, the mechanism of action of detergents inherently results in the displacement of the native lipids surrounding a given protein (Seddon, Curnow and Booth, 2004). SMALPs are described as an alternative that avoids this by extracting proteins in a patch of native lipid (Knowles *et al.*, 2009). Other nanodiscs technologies might bring about similar results (e.g. MSPs) but none are as easy to use as SMALPs and others involve the use of detergents to initially extract proteins before reconstitution in nanodiscs (Bayburt, Grinkova and Sligar, 2002; Grinkova, Denisov and Sligar, 2010). Despite the potential advantage over the use of detergents, no work in this project sought to identify the lipids present in the SMALPs produced. This could form an interesting avenue for investigation; identifying lipid:protein interactions using this system. Although the lipids were not identified, SMALPs were successfully able to isolate ABCG2 and the oligomeric control proteins.

Following the extraction by SMALPs, studies on the oligomeric state were performed. Data already supported the use of SMALP in extracting ABC transporters (Gulati *et al.*, 2014). This included ABCG2 but there was no evidence on the oligomeric state of ABCG2 in SMALPs. Given previous successes using FCS to assess oligomeric state of ABCG2 in live cells, it was an appropriate tool to investigate this especially considering its downstream applications as later discussed (Wong *et al.*, 2016). The technique was able to resolve monomeric and dimeric control proteins based on molecular brightness. The brightness of the dimer was twice that of the monomer. Some studies have estimated that only 55% of GFP molecules are fluorescent at any one time which may have hindered

interpretation of higher order oligomeric state of ABCG2 in live cells. However, the monomeric and dimeric controls were robustly resolved in this study with no difference in brightness observed between ABCG2 and the dimeric control. This dimeric nature is in line with the best resolved structural cryo-EM data (Taylor *et al.*, 2017; Jackson *et al.*, 2018). However, it does stand contrary to other previous data. Some early studies proposed tetramers or even tetramers of dimers (Xu *et al.*, 2004; McDevitt *et al.*, 2009; Dezi *et al.*, 2010; Wong *et al.*, 2016). These organisations may be explained by the packing of molecules during the generation of these data. The presence of these high order oligomers in EM grids may not be indicative of their physiological relevance. One limitation of the approach used in this current study is that the data are unable to preclude the possibility of tetrameric organisation of ABCG2 in the live cell environment. Importantly however, the SMALP should not exclude tetramers based on size and, in light of the most recent structural data showing dimers of ABCG2 in agreeance with this study, the SMALP/FCS platform appeared suitable for further work.

The further work of this study focussed particularly on developing a substrate binding assay. In support of this a purification strategy for ABCG2 was established. This was able to achieve concentrations of up to 2µM of SMALP-purified ABCG2 which represented a significant advance on previous attempts within the lab group. However, there could certainly be improvements in terms of both yield and purity. Using a cleavable tag (e.g. Tobacco Etch Virus (TEV) cleavage site) could help achieve better ABCG2 purity by enabling two step purification – whilst also removing any undesired additional tags enabling study of purified, untagged protein (Kimple, Brill and Pasker, 2013). Yield could also be increased by the use

of other cell lines such as those used in structural studies of ABCG2 (e.g. HEK293 EBNA (Thermo Fisher Scientific)) that were unavailable in this project (Taylor *et al.*, 2017; Jackson *et al.*, 2018). Even the low protein concentration achieved was conducive to the development of a substrate binding assay.

When designing the SMALP-ABCG2 drug binding assay, a number of techniques were considered. FCS, as used in this project, has been used in previous studies to drug binding (Caballero-George *et al.*, 2012; Li, Nath and Atkins, 2017). However, other techniques were also considered. Microscale thermophoresis (MST) and fluorescence thermal shift assays were also investigated (Gulati *et al.*, 2014; Jackson *et al.*, 2018). MST measures the change in response of a molecule of interest to an infrared laser due to changes in the solvation shell of the molecule on binding of another substance (Jerabek-Willemsen *et al.*, 2014). Thermal shift assays measure the binding of a fluorescent dye that attaches to hydrophobic protein regions as they become available as the protein unfolds at increasing temperatures. Each could potentially be adapted to medium/high throughput assay formats. However the signal in initial fluorescence thermal shift assays using coumarin dye was too low probably due to low protein concentration (data not shown). MST was plagued with issues due to the available fluorescent substrates similarly to FCS. The substrates adhered to the sides of the capillaries used in MST and the concentrations remaining in solution were too low to be measured (data not shown). These challenges were overcome by using FCS which was able to detect drug binding. Specifically, these challenges were overcome by the ability of FCS to measure both free and bound fluorescent drug substrate. Interestingly, previous work with ABCB1 isolated in non-SMALP nanodiscs did not distinguish

the free and bound drug by $\tau_D$ but instead used a single apparent $\tau_D$ which was treated as an weighted average of the $\tau_D$ for each component (Li, Nath and Atkins, 2017). In the current study, fully quantitative data were not achieved though due to additional complexities associated with a reservoir of non-specifically bound drug which resulted in a system represented by:

$$Drug_{NSB} \leftrightarrow Drug_{free} \leftrightarrow Drug_{Protein\ Bound}$$

Another limitation of the binding data in this study was that the stoichiometry of drug binding was not assessed due to time constraints. Initial PCH analysis of drug binding experiment data implied only one drug molecule was bound but no appropriate control experiments could be performed to assess the ability of this technique to resolve drug binding stoichiometry. However, strong evidence for specific binding was gathered and this extended to measuring the effect of Ko143 on substrate binding. At concentrations of Ko143 in excess of those that would inhibit ABCG2-mediated transport in whole cell assays, no inhibition of substrate (BD-P) binding was observed. This supports both the recent structural data showing a Ko143 derivative in the central cavity of ABCG2 and a mechanistic study that identified a distinct binding site outside the cavity (Cox *et al.*, 2018; Jackson *et al.*, 2018). It is therefore likely that the binding site for BD-P is outside the cavity though no specific assessment was made to identify the exact location in this study.

This project has made progress in a variety avenues and provided novel evidence for inhibitor mechanism. Additionally, as it originally set out to achieve, a platform for study ABCG2 in solution has been developed. As well as addressing some of the limitations highlighted above, future work should be able to capitalise on this

project to further study ABCG2 and its interactions with transport substrates and inhibitors.

## 7.2 Future Perspectives

### 7.2.1 Exploring the Role of Lipids-

There are a number of questions about the role of the lipids surrounding membrane proteins and their influence over pharmacology and activity. In addition to exploring this with SMALPs, other related polymers might be utilised. This could also carry the advantage of reduced sensitivity to magnesium. No ATPase activity can be measured in SMALPs as they precipitate at the $Mg^{2+}$ concentrations required for ATPase assays. By using polymers with reduced $Mg^{2+}$ sensitivity (e.g. DIBMALPs as discussed earlier) this might be addressed. As the role of lipids may include signal and energy transduction in ABCG2 function, being able to control the composition of lipids in a SMALP-like nanodiscs and measure ABCG2 activity could provide interesting details on the role of lipids.

### 7.2.2 Development of a Fully Quantitative Assay

The main limitation that prevented the development of a fully quantitative binding assay in this project was the behaviour of the available fluorescent substrates. As such, future work would require the use of different transport substrates. Further literature searches might reveal possible candidates but it is likely that *de novo* synthesis of novel fluorescent substrates might be necessary. By adding fluorescent moieties to well established substrates it might be possible to even create a panel of different drugs with different attached fluorophores (see Figure 7.1).

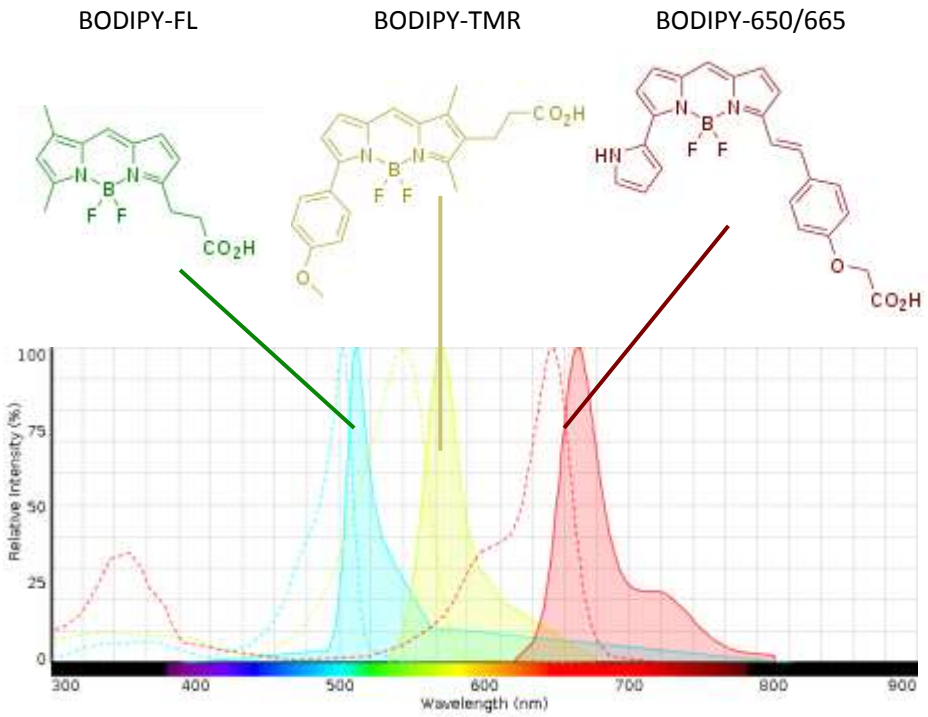


**Figure 7.1 – Example fluorophores for *de novo* drug synthesis.** BODIPY-based fluorophores (such as BODIPY-FL-prazosin used in this study) that have well separated emission spectra (filled curves) could be incorporated into transport substrates to create a panel of fluorescent drugs to explore the pharmacology of different binding sites (generated using Fluorescence SpectraViewer (Thermo Fisher Scientific).

Some current efforts in establishing wider accepted probe substrates have highlighted sulfasalazine as a potential probe substrate for ABCG2 (e.g. Adkison *et al*. 2010). By conforming to these other studies, the transferability of data gathered from this FCS-based platform would be supported.

The novel fluorescent substrates would hopefully have greater availability in solution by reducing hydrophobicity where possible. This would facilitate the analysis of data similar to that generated in this study because there would be a much reduced change in overall concentration of drug. As such, data would likely conform to the model of binding initially proposed in this project. Quantitative affinity analysis could be supplemented with some mechanistic studies where the

effect of ATP binding and hydrolysis to describe the allosteric coupling of changes in drug binding affinity during the translocation cycle. In addition to facilitating quantitative affinity analysis, a panel of different fluorescent drugs would be useful in other related binding and inhibition of binding experiments.

### 7.2.3 Expansion of Assay Scale

Work in this project demonstrated the ability of FCS to resolve free from bound BD-P by differences in diffusion rate and this assay format was able to detect the inhibition of binding by a competitive substrate. This was only employed on small scale using the unlabelled version (prazosin) of the fluorescent drug initially used. However, this assay could be used to explore structure activity relationship or even screen for novel substrates.

A drug (BD-P or newly synthesised fluorescent compound) at a fixed concentration pre-incubated with a fixed concentration of protein across a 96-well plate could offer a higher throughput screening assay. Pre-incubating the protein with varied concentrations of investigational compound or compounds would reveal any inhibitory effects. If this was performed with a panel of validated fluorescent substrates, reflecting the presence of several binding sites as previously discussed, then this format could be both sensitive and also indicative of mechanisms of inhibiting different drug transport in a selective manner. The development of the existing assay into this expanded format would provide two key pathways for investigation.

Firstly, the investigational compounds could be identified as substrates or inhibitors of ABCG2 by an initial FCS screen. As a result they could be explored for their therapeutic potential in further *in vitro* analysis. The identification of ABCG2

substrates currently occurs at a fairly late stage with much work coming from early *in vivo* studies as identified in the introduction. This screening method would therefore be much faster and cost effective (due to reduced staff time and no animal handling costs).

Secondly, as data became available on newly identified substrates it could contribute to a large SAR database. In conjunction with any identifiable differences in the inhibition of binding of different fluorescent probe substrates, this could provide detailed information that could be used to improve drug design efforts. It is possible that such a data set might have to be analysed in a machine learning setting with the gathered data used to train algorithms to distinguish substrates from non-substrates. This setup could then be used to predict therapeutic compounds that would either be non-substrates (and therefore circumvent ABCG2-mediated resistance) or substrates/inhibitors (which could then be used to supplement existing therapies by inducing desirable DDIs). The FCS assay developed in this study would support this workflow as highlighted in Figure 7.2.

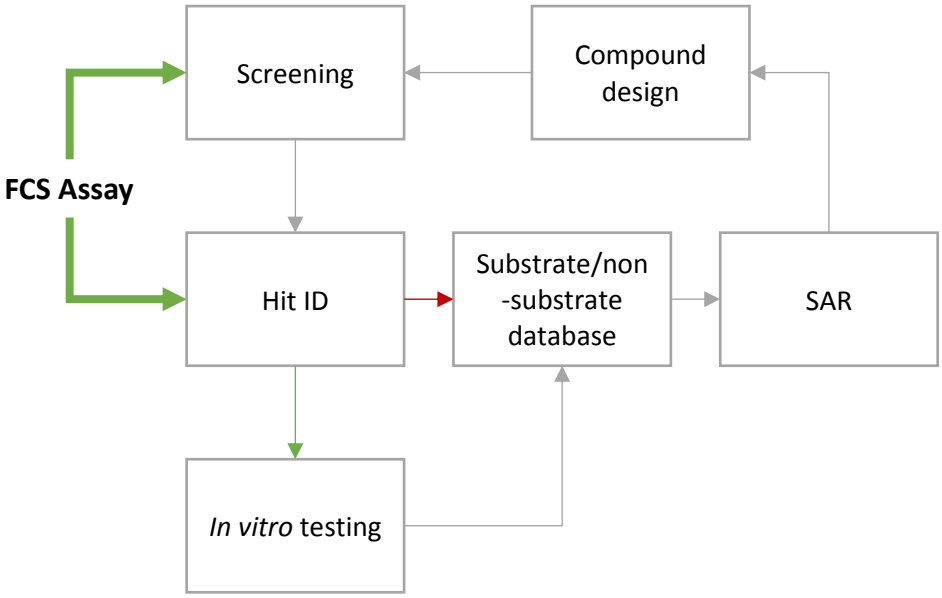


**Figure 7.2 – Workflow for improved drug design supported by an FCS screening assay.** The FCS assay developed in this project could be extended into a higher throughput platform (e.g. 96-well plate). Compounds that inhibit the binding of a fluorescent probe substrate in an FCS screen (identified as hits) could be investigated in transport assays and the outcome from these avenues would be recorded in a database. This database would feed structure activity relationship (SAR) studies that would in turn contribute to the design of new compounds for further screening.

### 7.2.4 Expansion to Mutant Isoforms and Other Proteins

As it stands, the methods developed in the project could be expanded to include mutant isoforms of ABCG2 or even other membrane proteins altogether.

The application to mutant isoforms could be useful in providing additional information regarding functionally relevant mutations. Where current data show that some point mutations reduce transport activity, they are unable to distinguish between changes in transport activity or simply in initial drug binding (Haider *et al.*, 2015; Cox *et al.*, 2018).

Additionally, clinically relevant point mutations could be used (e.g. the gout associated Q141K (Woodward *et al.*, 2013)). During current clinical trials it is often unlikely that there are sufficient carriers of ABCG2 polymorphisms for this group

to be adequately assessed for differences in response to wild type subjects (Lee *et al.*, 2015). By including ABCG2 polymorphisms in the developed screening assay, this could act as an early indicator as to whether particular efforts to recruit non-wild type ABCG2 subject in a given study.

Furthermore, this technique is suited to the analysis of other membrane proteins. The triumvirate of ABCG2, ABCB1 and ABCC1 for example could all be analysed in a similar fashion as could members of other protein families (e.g. GPCRs).

### 7.2.5 Final Comments

Overall, this project has achieved the aims that were set out. Despite the limits outlined above there is a promising new method for the analysis of the ever-challenging ABCG2. Towards the conclusion of this project, funding was obtained from the BBSRC (ref: BB/S001611/1, “Channelling a path for substrates through a multidrug transporter”). Many of the above concepts for future work are included in this grant based on the SMALP/FCS platform developed in this project. Work on this and other similar studies will certainly be interesting to follow.

# 8 References


Adkison, K. K., Vaidya, S. S., Lee, D. Y., Koo, S. H., Li, L., Mehta, A. A., Gross, A. S., Polli, J. W., Humphreys, J. E., Lou, Y. and Lee, E. J. D. (2010) 'Oral sulfasalazine as a clinical BCRP probe substrate: pharmacokinetic effects of genetic variation (C421A) and pantoprazole coadministration.', *Journal of pharmaceutical sciences*. United States, 99(2), pp. 1046–1062. doi: 10.1002/jps.21860.

Albrecht, C. and Viturro, E. (2007) 'The ABCA subfamily--gene and protein structures, functions and associated hereditary diseases.', *Pflugers Archiv : European journal of physiology*. Germany, 453(5), pp. 581–589. doi: 10.1007/s00424-006-0047-8.

Allen, J. D., van Loevezijn, A., Lakhai, J. M., van der Valk, M., van Tellingen, O., Reid, G., Schellens, J. H. M., Koomen, G.-J. and Schinkel, A. H. (2002) 'Potent and specific inhibition of the breast cancer resistance protein multidrug transporter in vitro and in mouse intestine by a novel analogue of fumitremorgin C.', *Molecular cancer therapeutics*, 1(6), pp. 417–425.

Aller, S. G., Yu, J., Ward, A., Weng, Y., Chittaboina, S., Zhuo, R., Harrell, P. M., Trinh, Y. T., Zhang, Q., Urbatsch, I. L. and Chang, G. (2009) 'Structure of P-glycoprotein Reveals a Molecular Basis for Poly-Specific Drug Binding', *Science (New York, N.Y.)*, 323(5922), pp. 1718–1722. doi: 10.1126/science.1168750.

Allikmets, R., Schriml, L. M., Hutchinson, A., Romano-Spica, V. and Dean, M. (1998) 'A human placenta-specific ATP-binding cassette gene (ABCP) on chromosome 4q22 that is involved in multidrug resistance.', *Cancer research*. United States, 58(23), pp. 5337–5339.

Allred, A. J., Bowen, C. J., Park, J. W., Peng, B., Williams, D. D., Wire, M. B. and Lee, E. (2011) 'Eltrombopag increases plasma rosuvastatin exposure in healthy volunteers.', *British journal of clinical pharmacology*. England, 72(2), pp. 321–329. doi: 10.1111/j.1365-2125.2011.03972.x.

Ambudkar, S. V (1998) 'Drug-stimulatable ATPase activity in crude membranes of human MDR1-transfected mammalian cells.', *Methods in enzymology*. United States, 292, pp. 504–514.

Ambudkar, S. V, Kim, I.-W. and Sauna, Z. E. (2006) 'The power of the pump: mechanisms of action of P-glycoprotein (ABCB1).', *European journal of pharmaceutical sciences : official journal of the European Federation for Pharmaceutical Sciences*. Netherlands, 27(5), pp. 392–400. doi: 10.1016/j.ejps.2005.10.010.

Ambudkar, S. V, Kim, I.-W., Xia, D. and Sauna, Z. E. (2006) 'The A-loop, a novel conserved aromatic acid subdomain upstream of the Walker A motif in ABC transporters, is critical for ATP binding.', *FEBS letters*. England, 580(4), pp. 1049–1055. doi: 10.1016/j.febslet.2005.12.051.

An, G., Gallegos, J. and Morris, M. E. (2011) 'The bioflavonoid kaempferol is an Abcg2 substrate and inhibits Abcg2-mediated quercetin efflux.', *Drug metabolism and disposition: the biological fate of chemicals*. United States, 39(3), pp. 426–432. doi: 10.1124/dmd.110.035212.

Anderson, M. P., Berger, H. A., Rich, D. P., Gregory, R. J., Smith, A. E. and Welsh, M. J. (1991) 'Nucleoside triphosphates are required to open the CFTR chloride channel.', *Cell*. United States, 67(4), pp. 775–784.

Ando, T., Kusuhara, H., Merino, G., Alvarez, A. I., Schinkel, A. H. and Sugiyama, Y. (2007) 'Involvement of breast cancer resistance protein (ABCG2) in the biliary excretion mechanism of fluoroquinolones.', *Drug metabolism and disposition: the biological fate of chemicals*. United States, 35(10), pp. 1873–1879. doi: 10.1124/dmd.107.014969.

Arnau, J., Lauritzen, C., Petersen, G. E. and Pedersen, J. (2006) 'Current strategies for the use of affinity tags and tag removal for the purification of recombinant proteins', *Protein Expression and Purification*, 48(1), pp. 1–13. doi: 10.1016/j.pep.2005.12.002.

Azzaria, M., Schurr, E. and Gros, P. (1989) 'Discrete mutations introduced in the predicted nucleotide-binding sites of the mdr1 gene abolish its ability to confer multidrug resistance.', *Molecular and cellular biology*. United States, 9(12), pp. 5289–5297.

Bai, X. chen, McMullan, G. and Scheres, S. H. W. (2014) 'How cryo-EM is revolutionizing structural biology', *Trends in Biochemical Sciences*. Elsevier Ltd, 40(1), pp. 49–57. doi: 10.1016/j.tibs.2014.10.005.

Bailey-Dell, K. J., Hassel, B., Doyle, L. A. and Ross, D. D. (2001) 'Promoter characterization and genomic organization of the human breast cancer resistance protein (ATP-binding cassette transporter G2) gene.', *Biochimica et biophysica acta*. Netherlands, 1520(3), pp. 234–241.

Bakos, E., Klein, I., Welker, E., Szabó, K., Müller, M., Sarkadi, B. and Váradi, A. (1997) 'Characterization of the human multidrug resistance protein containing mutations in the ATP-binding cassette signature region.', *Biochemical Journal*, 323(Pt 3), pp. 777–783.

Bayburt, T. H., Grinkova, Y. V and Sligar, S. G. (2002) 'Self-Assembly of Discoidal Phospholipid Bilayer Nanoparticles with Membrane Scaffold Proteins', *Nano Letters*. American Chemical Society, 2(8), pp. 853–856. doi: 10.1021/nl025623k.

Bear, C. E., Li, C. H., Kartner, N., Bridges, R. J., Jensen, T. J., Ramjeesingh, M. and Riordan, J. R. (1992) 'Purification and functional reconstitution of the cystic fibrosis transmembrane conductance regulator (CFTR).', *Cell*. United States, 68(4), pp. 809–818.

ter Beek, J., Guskov, A. and Slotboom, D. J. (2014) 'Structural diversity of ABC transporters', *The Journal of General Physiology*. The Rockefeller University Press, 143(4), pp. 419–435. doi: 10.1085/jgp.201411164.

Benderra, Z., Faussat, A. M., Sayada, L., Perrot, J.-Y., Tang, R., Chaoui, D., Morjani, H., Marzac, C., Marie, J.-P. and Legrand, O. (2005) 'MRP3, BCRP, and P-glycoprotein activities are prognostic factors in adult acute myeloid leukemia.', *Clinical cancer research : an official journal of the American Association for Cancer Research*. United States, 11(21), pp. 7764–7772. doi: 10.1158/1078-0432.CCR-04-1895.

Birmingham, B. K., Bujac, S. R., Elsby, R., Azumaya, C. T., Wei, C., Chen, Y., Mosqueda-Garcia, R. and Ambrose, H. J. (2015) 'Impact of ABCG2 and SLCO1B1 polymorphisms on pharmacokinetics of rosuvastatin, atorvastatin and simvastatin acid in Caucasian and

Asian subjects: a class effect?', *European journal of clinical pharmacology*. Germany, 71(3), pp. 341–355. doi: 10.1007/s00228-014-1801-z.

Vander Borght, S., Libbrecht, L., Katoonizadeh, A., van Pelt, J., Cassiman, D., Nevens, F., Van Lommel, A., Petersen, B. E., Fevery, J., Jansen, P. L. and Roskams, T. A. (2006) 'Breast cancer resistance protein (BCRP/ABCG2) is expressed by progenitor cells/reactive ductules and hepatocytes and its expression pattern is influenced by disease etiology and species type: possible functional consequences.', *The journal of histochemistry and cytochemistry : official journal of the Histochemistry Society*. United States, 54(9), pp. 1051–1059. doi: 10.1369/jhc.5A6912.2006.

Bornhorst, J. A. and Falke, J. J. (2000) 'Purification of proteins using polyhistidine affinity tags', in, pp. 245–254. doi: 10.1016/S0076-6879(00)26058-8.

Breedveld, P., Zelcer, N., Pluim, D., Sonmezer, O., Tibben, M. M., Beijnen, J. H., Schinkel, A. H., van Tellingen, O., Borst, P. and Schellens, J. H. M. (2004) 'Mechanism of the pharmacokinetic interaction between methotrexate and benzimidazoles: potential role for breast cancer resistance protein in clinical drug-drug interactions.', *Cancer research*. United States, 64(16), pp. 5804–5811. doi: 10.1158/0008-5472.CAN-03-4062.

Brendel, C., Scharenberg, C., Dohse, M., Robey, R. W., Bates, S. E., Shukla, S., Ambudkar, S. V, Wang, Y., Wennemuth, G., Burchert, A., Boudriot, U. and Neubauer, A. (2007) 'Imatinib mesylate and nilotinib (AMN107) exhibit high-affinity interaction with ABCG2 on primitive hematopoietic stem cells.', *Leukemia*. England, 21(6), pp. 1267–1275. doi: 10.1038/sj.leu.2404638.

Briddon, S. J. and Hill, S. J. (2007) 'Pharmacology under the microscope: the use of fluorescence correlation spectroscopy to determine the properties of ligand-receptor complexes', *Trends in Pharmacological Sciences*. Elsevier Ltd, 28(12), pp. 637–645. doi: 10.1016/j.tips.2007.09.008.

Brooker, R., Widmaier, E., Graham, L. and Stiling, P. (2010) 'Membrane Structure, Synthesis and Transport', in *Biology*. 2nd edn. New York, NY: McGraw-Hill, pp. 97–118.

Burger, H., Foekens, J. A., Look, M. P., Meijer-van Gelder, M. E., Klijn, J. G. M., Wiemer, E. A. C., Stoter, G. and Nooter, K. (2003) 'RNA expression of breast cancer resistance protein, lung resistance-related protein, multidrug resistance-associated proteins 1 and 2, and multidrug resistance gene 1 in breast cancer: correlation with chemotherapeutic response.', *Clinical cancer research : an official journal of the American Association for Cancer Research*. United States, 9(2), pp. 827–836.

Burger, H., van Tol, H., Boersma, A. W. M., Brok, M., Wiemer, E. A. C., Stoter, G. and Nooter, K. (2004) 'Imatinib mesylate (STI571) is a substrate for the breast cancer resistance protein (BCRP)/ABCG2 drug pump.', *Blood*. United States, 104(9), pp. 2940–2942. doi: 10.1182/blood-2004-04-1398.

Busti, A. J., Bain, A. M., Hall, R. G. 2nd, Bedimo, R. G., Leff, R. D., Meek, C. and Mehvar, R. (2008) 'Effects of atazanavir/ritonavir or fosamprenavir/ritonavir on the pharmacokinetics of rosuvastatin.', *Journal of cardiovascular pharmacology*. United States, 51(6), pp. 605–610. doi: 10.1097/FJC.0b013e31817b5b5a.

Caballero-George, C., Sorkalla, T., Jakobs, D., Bolaños, J., Raja, H., Shearer, C.,

Bermingham, E. and Häberlein, H. (2012) 'Fluorescence Correlation Spectroscopy in Drug Discovery: Study of Alexa532-Endothelin 1 Binding to the Endothelin ET(A) Receptor to Describe the Pharmacological Profile of Natural Products', *The Scientific World Journal*. The Scientific World Journal, 2012, p. 524169. doi: 10.1100/2012/524169.

Carrier, I., Urbatsch, I. L., Senior, A. E. and Gros, P. (2007) 'Mutational analysis of conserved aromatic residues in the A-loop of the ABC transporter ABCB1A (mouse Mdr3).', *FEBS letters*. England, 581(2), pp. 301–308. doi: 10.1016/j.febslet.2006.12.030.

Cascorbi, I. (2011) 'P-glycoprotein: tissue distribution, substrates, and functional consequences of genetic variations.', *Handbook of experimental pharmacology*. Germany, (201), pp. 261–283. doi: 10.1007/978-3-642-14541-4_6.

Castilho, L. and Reid, M. E. (2013) 'A review of the JR blood group system.', *Immunohematology*. United States, 29(2), pp. 63–68.

Catterall, W. A., Goldin, A. L. and Waxman, S. G. (2005) 'International Union of Pharmacology. XLVII. Nomenclature and structure-function relationships of voltage-gated sodium channels.', *Pharmacological reviews*. United States, 57(4), pp. 397–409. doi: 10.1124/pr.57.4.4.

Chen, J., Lu, G., Lin, J., Davidson, A. L. and Quiocho, F. A. (2003) 'A tweezers-like motion of the ATP-binding cassette dimer in an ABC transport cycle.', *Molecular cell*. United States, 12(3), pp. 651–661.

Chen, Y., Johnson, J., Macdonald, P., Wu, B. and Mueller, J. D. (2010) 'Observing protein interactions and their stoichiometry in living cells by brightness analysis of fluorescence fluctuation experiments.', *Methods in enzymology*. United States, 472, pp. 345–363. doi: 10.1016/S0076-6879(10)72026-7.

Cisternino, S., Mercier, C., Bourasset, F., Roux, F. and Scherrmann, J.-M. (2004) 'Expression, up-regulation, and transport activity of the multidrug-resistance protein Abcg2 at the mouse blood-brain barrier.', *Cancer research*. United States, 64(9), pp. 3296–3301.

Clark, R., Kerr, I. D. and Callaghan, R. (2006) 'Multiple drugbinding sites on the R482G isoform of the ABCG2 transporter.', *British journal of pharmacology*. England, 149(5), pp. 506–515. doi: 10.1038/sj.bjp.0706904.

Clausen, M. V, Hilbers, F. and Poulsen, H. (2017) 'The Structure and Function of the Na,K-ATPase Isoforms in Health and Disease.', *Frontiers in physiology*. Switzerland, 8, p. 371. doi: 10.3389/fphys.2017.00371.

Cole, S. P., Bhardwaj, G., Gerlach, J. H., Mackie, J. E., Grant, C. E., Almquist, K. C., Stewart, A. J., Kurz, E. U., Duncan, A. M. and Deeley, R. G. (1992) 'Overexpression of a transporter gene in a multidrug-resistant human lung cancer cell line.', *Science (New York, N.Y.)*. UNITED STATES, 258(5088), pp. 1650–1654.

Cole, S. P. C. (2014) 'Targeting multidrug resistance protein 1 (MRP1, ABCC1): past, present, and future.', *Annual review of pharmacology and toxicology*. United States, 54, pp. 95–117. doi: 10.1146/annurev-pharmtox-011613-135959.

Cortez, M. A. A., Scrideli, C. A., Yunes, J. A., Valera, E. T., Toledo, S. R. C., Pavoni-Ferreira, P. C. B., Lee, M. L. M., Petrilli, A. S., Brandalise, S. R. and Tone, L. G. (2009) 'mRNA expression profile of multidrug resistance genes in childhood acute lymphoblastic leukemia. Low expression levels associated with a higher risk of toxic death.', *Pediatric blood & cancer*. United States, 53(6), pp. 996–1004. doi: 10.1002/pbc.22220.

Cox, M. H., Kapoor, P., Briggs, D. A. and Kerr, I. D. (2018) 'Residues contributing to drug transport by ABCG2 are localised to multiple drug-binding pockets.', *The Biochemical journal*, p. BCJ20170923. doi: 10.1042/BCJ20170923.

Crivat, G. and Taraska, J. W. (2012) 'Imaging proteins inside cells with fluorescent tags', *Trends in Biotechnology*, 30(1), pp. 8–16. doi: 10.1016/j.tibtech.2011.08.002.

Cusatis, G., Gregorc, V., Li, J., Spreafico, A., Ingersoll, R. G., Verweij, J., Ludovini, V., Villa, E., Hidalgo, M., Sparreboom, A. and Baker, S. D. (2006) 'Pharmacogenetics of ABCG2 and adverse reactions to gefitinib.', *Journal of the National Cancer Institute*. United States, 98(23), pp. 1739–1742. doi: 10.1093/jnci/djj469.

Dafforn, T. R., Overduin, M. and Knowles, T. J. (2010) 'Solubilisation of membrane proteins'.

Dassa, E. (2011) 'Natural history of ABC systems: not only transporters.', *Essays in biochemistry*. England, 50(1), pp. 19–42. doi: 10.1042/bse0500019.

Dawson, R. J. P. and Locher, K. P. (2006) 'Structure of a bacterial multidrug ABC transporter.', *Nature*. England, 443(7108), pp. 180–185. doi: 10.1038/nature05155.

Day, R. N. and Davidson, M. W. (2009) 'The fluorescent protein palette: tools for cellular imaging', *Chemical Society Reviews*, 38(10), p. 2887. doi: 10.1039/b901966a.

Dean, M., Hamon, Y. and Chimini, G. (2001) 'The Human ATP-Binding Cassette transporter superfamily', *Journal of Lipid Research*, 42, pp. 1007–1017. doi: 10.1101/gr.184901.The.

Deeley, R. G., Westlake, C. and Cole, S. P. C. (2006) 'Transmembrane transport of endo- and xenobiotics by mammalian ATP-binding cassette multidrug resistance proteins', *Physiological Reviews*, 86(3), pp. 849–899. doi: 10.1152/physrev.00035.2005.

DeGroot, J. (2009) 'Drug-drug interactions: tools for drug transporter protein studies', *European Pharmaceutical Review*, (4).

Dezi, M., Fribourg, P.-F., Di Cicco, A., Arnaud, O., Marco, S., Falson, P., Di Pietro, A. and Lévy, D. (2010) 'The multidrug resistance half-transporter ABCG2 is purified as a tetramer upon selective extraction from membranes.', *Biochimica et biophysica acta*, 1798(11), pp. 2094–101. doi: 10.1016/j.bbamem.2010.07.034.

Diop, N. K. and Hrycyna, C. A. (2005) 'N-linked glycosylation of the human ABC transporter ABCG2 on asparagine 596 is not essential for expression, transport activity, or trafficking to the plasma membrane', *Biochemistry*, 44(14), pp. 5420–5429. doi: 10.1021/bi0479858.

Do, T. M., Noel-Hudson, M.-S., Ribes, S., Besengez, C., Smirnova, M., Cisternino, S., Buyse, M., Calon, F., Chimini, G., Chacun, H., Scherrmann, J.-M., Farinotti, R. and

Bourasset, F. (2012) ‘ABCG2- and ABCG4-mediated efflux of amyloid-beta peptide 1-40 at the mouse blood-brain barrier.’, *Journal of Alzheimer’s disease : JAD*. Netherlands, 30(1), pp. 155–166. doi: 10.3233/JAD-2012-112189.

Dobson, P. D. and Kell, D. B. (2008) ‘Carrier-mediated cellular uptake of pharmaceutical drugs: an exception or the rule?’, *Nature Reviews Drug Discovery*. Nature Publishing Group, 7, p. 205.

Dohse, M., Scharenberg, C., Shukla, S., Robey, R. W., Volkmann, T., Deeken, J. F., Brendel, C., Ambudkar, S. V, Neubauer, A. and Bates, S. E. (2010) ‘Comparison of ATP-binding cassette transporter interactions with the tyrosine kinase inhibitors imatinib, nilotinib, and dasatinib.’, *Drug metabolism and disposition: the biological fate of chemicals*. United States, 38(8), pp. 1371–1380. doi: 10.1124/dmd.109.031302.

Dörr, J. M., Scheidelaar, S., Koorengevel, M. C., Dominguez, J. J., Schäfer, M., van Walree, C. A. and Killian, J. A. (2016) ‘The styrene–maleic acid copolymer: a versatile tool in membrane research’, *European Biophysics Journal*, 45(1), pp. 3–21. doi: 10.1007/s00249-015-1093-y.

Doyle, L. A., Yang, W., Abruzzo, L. V, Krogmann, T., Gao, Y., Rishi, A. K. and Ross, D. D. (1998) ‘A multidrug resistance transporter from human MCF-7 breast cancer cells’, *Proceedings of the National Academy of Sciences of the United States of America*. The National Academy of Sciences, 95(26), pp. 15665–15670.

Drach, J., Gsur, A., Hamilton, G., Zhao, S., Angerler, J., Fiegl, M., Zojer, N., Raderer, M., Haberl, I., Andreeff, M. and Huber, H. (1996) ‘Involvement of P-glycoprotein in the transmembrane transport of interleukin-2 (IL-2), IL-4, and interferon-gamma in normal human T lymphocytes.’, *Blood*. United States, 88(5), pp. 1747–1754.

Dubin, A. E. and Patapoutian, A. (2010) ‘Nociceptors: the sensors of the pain pathway’, *The Journal of Clinical Investigation*. American Society for Clinical Investigation, 120(11), pp. 3760–3772. doi: 10.1172/JCI42843.

DuBridge, R. B., Tang, P., Hsia, H. C., Leong, P. M., Miller, J. H. and Calos, M. P. (1987) ‘Analysis of mutation in human cells by using an Epstein-Barr virus shuttle system.’, *Molecular and Cellular Biology*, 7(1), pp. 379–387.

Ee, P. L. R., Kamalakaran, S., Tonetti, D., He, X., Ross, D. D. and Beck, W. T. (2004) ‘Identification of a novel estrogen response element in the breast cancer resistance protein (ABCG2) gene.’, *Cancer research*. United States, 64(4), pp. 1247–1251.

Eisenblätter, T., Hüwel, S. and Galla, H. J. (2003) ‘Characterisation of the brain multidrug resistance protein (BMDP/ABCG2/BCRP) expressed at the blood-brain barrier’, *Brain Research*, 971(2), pp. 221–231. doi: 10.1016/S0006-8993(03)02401-6.

Ejendal, K. F. K., Diop, N. K., Schweiger, L. C. and Hrycyna, C. A. (2006) ‘The nature of amino acid 482 of human ABCG2 affects substrate transport and ATP hydrolysis but not substrate binding.’, *Protein science : a publication of the Protein Society*. United States, 15(7), pp. 1597–1607. doi: 10.1110/ps.051998406.

Elson, E. L. (2011) ‘Fluorescence correlation spectroscopy: Past, present, future’, *Biophysical Journal*. Biophysical Society, 101(12), pp. 2855–2870. doi:

10.1016/j.bpj.2011.11.012.

EMA (2012) 'Guideline on the investigation of drug interactions', *Guidance Document*, 44(June), p. 59. doi: 10.1093/deafed/ens058.

Fang, D. D., Kim, Y. J., Lee, C. N., Aggarwal, S., McKinnon, K., Mesmer, D., Norton, J., Birse, C. E., He, T., Ruben, S. M. and Moore, P. A. (2010) 'Expansion of CD133(+) colon cancer cultures retaining stem cell properties to enable cancer stem cell target discovery.', *British journal of cancer*. England, 102(8), pp. 1265–1275. doi: 10.1038/sj.bjc.6605610.

Fetsch, P. A., Abati, A., Litman, T., Morisaki, K., Honjo, Y., Mittal, K. and Bates, S. E. (2006) 'Localization of the ABCG2 mitoxantrone resistance-associated protein in normal tissues.', *Cancer letters*. Ireland, 235(1), pp. 84–92. doi: 10.1016/j.canlet.2005.04.024.

Fletcher, J. I., Williams, R. T., Henderson, M. J., Norris, M. D. and Haber, M. (2016) 'ABC transporters as mediators of drug resistance and contributors to cancer cell biology', *Drug Resistance Updates*, 26, pp. 1–9. doi: 10.1016/j.drup.2016.03.001.

Fung, K. L. and Gottesman, M. M. (2009) 'A synonymous polymorphism in a common MDR1 (ABCB1) haplotype shapes protein function', *Biochimica et biophysica acta*, 1794(5), pp. 860–871. doi: 10.1016/j.bbapap.2009.02.014.

Furman, W. L., Navid, F., Daw, N. C., McCarville, M. B., McGregor, L. M., Spunt, S. L., Rodriguez-Galindo, C., Panetta, J. C., Crews, K. R., Wu, J., Gajjar, A. J., Houghton, P. J., Santana, V. M. and Stewart, C. F. (2009) 'Tyrosine kinase inhibitor enhances the bioavailability of oral irinotecan in pediatric patients with refractory solid tumors.', *Journal of clinical oncology : official journal of the American Society of Clinical Oncology*. United States, 27(27), pp. 4599–4604. doi: 10.1200/JCO.2008.19.6642.

Gall, J. G. (1954) 'Observations on the nuclear membrane with the electron microscope.', *Experimental cell research*. United States, 7(1), pp. 197–200.

Gedeon, C., Anger, G., Piquette-Miller, M. and Koren, G. (2008) 'Breast cancer resistance protein: mediating the trans-placental transfer of glyburide across the human placenta.', *Placenta*. Netherlands, 29(1), pp. 39–43. doi: 10.1016/j.placenta.2007.08.004.

Giacomini, K. M., Balimane, P. V, Cho, S. K., Eadon, M., Edeki, T., Hillgren, K. M., Huang, S.-M., Sugiyama, Y., Weitz, D., Wen, Y., Xia, C. Q., Yee, S. W., Zimdahl, H. and Niemi, M. (2013) 'International Transporter Consortium commentary on clinically important transporter polymorphisms.', *Clinical pharmacology and therapeutics*. United States, 94(1), pp. 23–26. doi: 10.1038/clpt.2013.12.

Giacomini, K. M., Huang, S.-M., Tweedie, D. J., Benet, L. Z., Brouwer, K. L. R., Chu, X., Dahlin, A., Evers, R., Fischer, V., Hillgren, K. M., Hoffmaster, K. A., Ishikawa, T., Keppler, D., Kim, R. B., Lee, C. A., Niemi, M., Polli, J. W., Sugiyama, Y., Swaan, P. W., Ware, J. A., Wright, S. H., Yee, S. W., Zamek-Gliszczynski, M. J. and Zhang, L. (2010) 'Membrane transporters in drug development.', *Nature reviews. Drug discovery*. England, 9(3), pp. 215–236. doi: 10.1038/nrd3028.

Giri, N., Agarwal, S., Shaik, N., Pan, G., Chen, Y. and Elmquist, W. F. (2009) 'Substrate-dependent breast cancer resistance protein (Bcrp1/Abcg2)-mediated interactions:

consideration of multiple binding sites in in vitro assay design.', *Drug metabolism and disposition: the biological fate of chemicals*. United States, 37(3), pp. 560–570. doi: 10.1124/dmd.108.022046.

Goñi, F. M. (2014) 'The basic structure and dynamics of cell membranes: An update of the Singer–Nicolson model', *Biochimica et Biophysica Acta (BBA) - Biomembranes*, 1838(6), pp. 1467–1476. doi: 10.1016/j.bbamem.2014.01.006.

Goodell, M. A., Brose, K., Paradis, G., Conner, A. S. and Mulligan, R. C. (1996) 'Isolation and functional properties of murine hematopoietic stem cells that are replicating in vivo.', *The Journal of experimental medicine*. United States, 183(4), pp. 1797–1806.

de Gooijer, M. C., de Vries, N. A., Buckle, T., Buil, L. C. M., Beijnen, J. H., Boogerd, W. and van Tellingen, O. (2018) 'Improved Brain Penetration and Antitumor Efficacy of Temozolomide by Inhibition of ABCB1 and ABCG2', *Neoplasia (New York, N.Y.)*. Neoplasia Press, 20(7), pp. 710–720. doi: 10.1016/j.neo.2018.05.001.

Gossen, M. and Bujard, H. (1992) 'Tight control of gene expression in mammalian cells by tetracycline-responsive promoters.', *Proceedings of the National Academy of Sciences of the United States of America*, 89(12), pp. 5547–51. doi: 10.1073/pnas.89.12.5547.

Graham, F. L., Smiley, J., Russell, W. C. and Nairn, R. (1977) 'Characteristics of a human cell line transformed by DNA from human adenovirus type 5.', *The Journal of general virology*. England, 36(1), pp. 59–74. doi: 10.1099/0022-1317-36-1-59.

Grinkova, Y. V, Denisov, I. G. and Sligar, S. G. (2010) 'Engineering extended membrane scaffold proteins for self-assembly of soluble nanoscale lipid bilayers', *Protein Engineering, Design and Selection*. Oxford University Press, 23(11), pp. 843–848. doi: 10.1093/protein/gzq060.

di Guan, C., Li, P., Riggs, P. D. and Inouye, H. (1988) 'Vectors that facilitate the expression and purification of foreign peptides in Escherichia coli by fusion to maltose-binding protein.', *Gene*. Netherlands, 67(1), pp. 21–30.

Gulati, S., Jamshad, M., Knowles, T. J., Morrison, K. a, Downing, R., Cant, N., Collins, R., Koenderink, J. B., Ford, R. C., Overduin, M., Kerr, I. D., Dafforn, T. R. and Rothnie, A. J. (2014) 'Detergent free purification of ABC transporters.', *Biochem J*, 44(0), pp. 1–24. doi: 10.1042/BJ20131477.

Gutmann, H., Hruz, P., Zimmermann, C., Beglinger, C. and Drewe, J. (2005) 'Distribution of breast cancer resistance protein (BCRP/ABCG2) mRNA expression along the human GI tract', *Biochemical Pharmacology*, 70(5), pp. 695–699. doi: 10.1016/j.bcp.2005.05.031.

Haenisch, S., Werk, A. N. and Cascorbi, I. (2014) 'MicroRNAs and their relevance to ABC transporters', *British Journal of Clinical Pharmacology*. Oxford, UK: Blackwell Publishing Ltd, 77(4), pp. 587–596. doi: 10.1111/bcp.12251.

Hafkemeyer, P., Dey, S., Ambudkar, S. V, Hrycyna, C. A., Pastan, I. and Gottesman, M. M. (1998) 'Contribution to substrate specificity and transport of nonconserved residues in transmembrane domain 12 of human P-glycoprotein.', *Biochemistry*. United States, 37(46), pp. 16400–16409. doi: 10.1021/bi980871+.

Haider, A. J., Briggs, D., Self, T. J., Chilvers, H. L., Holliday, N. D. and Kerr, I. D. (2011) 'Dimerization of ABCG2 analysed by bimolecular fluorescence complementation', *PLoS ONE*, 6(10). doi: 10.1371/journal.pone.0025818.

Haider, A. J., Cox, M. H., Jones, N., Goode, A. J., Bridge, K. S., Wong, K., Briggs, D. and Kerr, I. D. (2015) 'Identification of residues in ABCG2 affecting protein trafficking and drug transport, using co-evolutionary analysis of ABCG sequences', *Bioscience Reports*, 35(4), pp. e00241–e00241. doi: 10.1042/BSR20150150.

Hanson, P. I. and Whiteheart, S. W. (2005) 'Aaa+ proteins: have engine, will work', 6(July), pp. 519–529. doi: 10.1038/nrm1684.

Hediger, M. a., Romero, M. F., Peng, J. B., Rolfs, A., Takanaga, H. and Bruford, E. a. (2004) 'The ABCs of solute carriers: Physiological, pathological and therapeutic implications of human membrane transport proteins', *Pflugers Archiv European Journal of Physiology*, 447(5), pp. 465–468. doi: 10.1007/s00424-003-1192-y.

van der Heijden, J., de Jong, M. C., Dijkmans, B. A. C., Lems, W. F., Oerlemans, R., Kathmann, I., Scheffer, G. L., Scheper, R. J., Assaraf, Y. G. and Jansen, G. (2004) 'Acquired resistance of human T cells to sulfasalazine: stability of the resistant phenotype and sensitivity to non-related DMARDs.', *Annals of the rheumatic diseases*. England, 63(2), pp. 131–137.

Henriksen, U., Fog, J. U., Litman, T. and Gether, U. (2005) 'Identification of intra- and intermolecular disulfide bridges in the multidrug resistance transporter ABCG2', *Journal of Biological Chemistry*, 280(44), pp. 36926–36934. doi: 10.1074/jbc.M502937200.

Henriksen, U., Gether, U. and Litman, T. (2005) 'Effect of Walker A mutation (K86M) on oligomerization and surface targeting of the multidrug resistance transporter ABCG2.', *Journal of cell science*. England, 118(Pt 7), pp. 1417–1426. doi: 10.1242/jcs.01729.

van Herwaarden, A. E., Jonker, J. W., Wagenaar, E., Brinkhuis, R. F., Schellens, J. H. M., Beijnen, J. H. and Schinkel, A. H. (2003) 'The breast cancer resistance protein (Bcrp1/Abcg2) restricts exposure to the dietary carcinogen 2-amino-1-methyl-6-phenylimidazo[4,5-b]pyridine.', *Cancer research*. United States, 63(19), pp. 6447–6452.

van Herwaarden, A. E., Wagenaar, E., Karnekamp, B., Merino, G., Jonker, J. W. and Schinkel, A. H. (2006) 'Breast cancer resistance protein (Bcrp1/Abcg2) reduces systemic exposure of the dietary carcinogens aflatoxin B1, IQ and Trp-P-1 but also mediates their secretion into breast milk.', *Carcinogenesis*. England, 27(1), pp. 123–130. doi: 10.1093/carcin/bgi176.

van Herwaarden, A. E., Wagenaar, E., Merino, G., Jonker, J. W., Rosing, H., Beijnen, J. H. and Schinkel, A. H. (2007) 'Multidrug transporter ABCG2/breast cancer resistance protein secretes riboflavin (vitamin B2) into milk.', *Molecular and cellular biology*. United States, 27(4), pp. 1247–1253. doi: 10.1128/MCB.01621-06.

Higgins, C. F. (1992) 'ABC transporters: from microorganisms to man.', *Annual review of cell biology*. United States, 8, pp. 67–113. doi: 10.1146/annurev.cb.08.110192.000435.

Higgins, C. F., Hiles, I. D., Salmond, G. P., Gill, D. R., Downie, J. A., Evans, I. J., Holland, I. B., Gray, L., Buckel, S. D. and Bell, A. W. (1986) 'A family of related ATP-binding subunits

coupled to many distinct biological processes in bacteria.', *Nature*. England, 323(6087), pp. 448–450. doi: 10.1038/323448a0.

Higgins, C. F. and Linton, K. J. (2004) 'The ATP switch model for ABC transporters', (March). doi: 10.1038/nsmb836.

Hiwase, D. K., Saunders, V., Hewett, D., Frede, A., Zrim, S., Dang, P., Eadie, L., To, L. B., Melo, J., Kumar, S., Hughes, T. P. and White, D. L. (2008) 'Dasatinib cellular uptake and efflux in chronic myeloid leukemia cells: therapeutic implications.', *Clinical cancer research : an official journal of the American Association for Cancer Research*. United States, 14(12), pp. 3881–3888. doi: 10.1158/1078-0432.CCR-07-5095.

Hlaváč, V. and Souček, P. (2015) 'Role of family D ATP-binding cassette transporters (ABCD) in cancer', *Biochemical Society Transactions*, 43(5), p. 937 LP-942.

Hodges, L. M., Markova, S. M., Chinn, L. W., Gow, J. M., Kroetz, D. L., Klein, T. E. and Altman, R. B. (2011) 'Very important pharmacogene summary: ABCB1 (MDR1, P-glycoprotein)', *Pharmacogenetics and Genomics*, 21(3), pp. 152–161. doi: 10.1097/FPC.0b013e3283385a1c.

Hopfner, K.-P. (2016) 'Invited review: Architectures and mechanisms of ATP binding cassette proteins', *Biopolymers*, 105(8), pp. 492–504. doi: 10.1002/bip.22843.

Hori, S., Ohtsuki, S., Tachikawa, M., Kimura, N., Kondo, T., Watanabe, M., Nakashima, E. and Terasaki, T. (2004) 'Functional expression of rat ABCG2 on the luminal side of brain capillaries and its enhancement by astrocyte-derived soluble factor(s).', *Journal of neurochemistry*. England, 90(3), pp. 526–536. doi: 10.1111/j.1471-4159.2004.02537.x.

Horsey, A. J., Cox, M. H., Sarwat, S. and Kerr, I. D. (2016) 'The multidrug transporter ABCG2: still more questions than answers.', *Biochemical Society transactions*, 44(3), pp. 824–30. doi: 10.1042/BST20160014.

Hou, Y., Li, C.-Z., Palaniyandi, K., Magtibay, P. M., Homolya, L., Sarkadi, B. and Chang, X. (2009) 'Effects of Putative Catalytic Base Mutation E211Q on ABCG2-Mediated Methotrexate Transport', *Biochemistry*, 48(38), pp. 9122–9131. doi: 10.1021/bi900675v.

Houghton, P. J., Germain, G. S., Harwood, F. C., Schuetz, J. D., Stewart, C. F., Buchdunger, E. and Traxler, P. (2004) 'Imatinib Mesylate Is a Potent Inhibitor of the ABCG2 (BCRP) Transporter and Reverses Resistance to Topotecan and SN-38 in Vitro', *Cancer Research*, 64(7), pp. 2333–2337. doi: 10.1158/0008-5472.CAN-03-3344.

Hu, W. and Liu, W. (2010) 'Side populations of glioblastoma cells are less sensitive to HSV-TK/GCV suicide gene therapy system than the non-side population.', *In vitro cellular & developmental biology. Animal*. Germany, 46(6), pp. 497–501. doi: 10.1007/s11626-010-9274-6.

Huang, B., Perroud, T. D. and Zare, R. N. (2004) 'Photon counting histogram: One-photon excitation', *ChemPhysChem*, 5(10), pp. 1523–1531. doi: 10.1002/cphc.200400176.

Huang, L., Wang, Y. and Grimm, S. (2006) 'ATP-dependent transport of rosuvastatin in membrane vesicles expressing breast cancer resistance protein.', *Drug metabolism and*

*disposition: the biological fate of chemicals*. United States, 34(5), pp. 738–742. doi: 10.1124/dmd.105.007534.

Hulme, E. C. and Trevethick, M. A. (2010) 'Ligand binding assays at equilibrium: validation and interpretation', *British Journal of Pharmacology*. Blackwell Science Inc, 161(6), pp. 1219–1237. doi: 10.1111/j.1476-5381.2009.00604.x.

Huls, M., Brown, C. D. A., Windass, A. S., Sayer, R., van den Heuvel, J. J. M. W., Heemskerk, S., Russel, F. G. M. and Masereeuw, R. (2008) 'The breast cancer resistance protein transporter ABCG2 is expressed in the human kidney proximal tubule apical membrane.', *Kidney international*. United States, 73(2), pp. 220–225. doi: 10.1038/sj.ki.5002645.

Hvorup, R. N., Goetz, B. A., Niederer, M., Hollenstein, K., Perozo, E. and Locher, K. P. (2007) 'Asymmetry in the structure of the ABC transporter-binding protein complex BtuCD-BtuF.', *Science (New York, N.Y.)*. United States, 317(5843), pp. 1387–1390. doi: 10.1126/science.1145950.

Hyde, S. C., Emsley, P., Hartshorn, M. J., Mimmack, M. M., Gileadi, U., Pearce, S. R., Gallagher, M. P., Gill, D. R., Hubbard, R. E. and Higgins, C. F. (1990) 'Structural model of ATP-binding proteins associated with cystic fibrosis, multidrug resistance and bacterial transport.', *Nature*. England, 346(6282), pp. 362–365. doi: 10.1038/346362a0.

Imai, Y., Ishikawa, E., Asada, S. and Sugimoto, Y. (2005) 'Estrogen-mediated post transcriptional down-regulation of breast cancer resistance protein/ABCG2.', *Cancer research*. United States, 65(2), pp. 596–604.

Inoué, S. (2006) 'Foundations of confocal scanned imaging in light microscopy', in *Handbook of Biological Confocal Microscopy: Third Edition*. Marine Biological Laboratory, Woods Hole, MA 02543, United States: Springer US, pp. 1–19. doi: 10.1007/978-0-387-45524-2_1.

Ivnitski-Steele, I., Larson, R. S., Lovato, D. M., Khawaja, H. M., Winter, S. S., Oprea, T. I., Sklar, L. A. and Edwards, B. S. (2008) 'High-Throughput Flow Cytometry to Detect Selective Inhibitors of ABCB1, ABCC1, and ABCG2 Transporters', *ASSAY and Drug Development Technologies*, 6(2), pp. 263–276. doi: 10.1089/adt.2007.107.

Jackson, S. M., Manolaridis, I., Kowal, J., Zechner, M., Taylor, N. M. I., Bause, M., Bauer, S., Bartholomaeus, R., Bernhardt, G., Koenig, B., Buschauer, A., Stahlberg, H., Altmann, K.-H. and Locher, K. P. (2018) 'Structural basis of small-molecule inhibition of human multidrug transporter ABCG2', *Nature Structural & Molecular Biology*. Springer US, 25(4), pp. 333–340. doi: 10.1038/s41594-018-0049-1.

Jameson, D. M. (2014) 'Introduction', in *Introduction to Fluorescence*. Boca Raton: Taylor & Francis, pp. 1–12.

Jamshad, M., Lin, Y.-P., Knowles, T. J., Parslow, R. A., Harris, C., Wheatley, M., Poyner, D. R., Bill, R. M., Thomas, O. R. T., Overduin, M. and Dafforn, T. R. (2011) 'Surfactant-free purification of membrane proteins with intact native membrane environment', *Biochemical Society Transactions*, 39(3), pp. 813–818. doi: 10.1042/BST0390813.

Janson, J.-C. (2011) *Protein Purification : Principles, High Resolution Methods, and*

*Applications*. Hoboken, UNITED STATES: Wiley.

Janvilisri, T., Shahi, S., Venter, H., Balakrishnan, L. and van Veen, H. W. (2005) 'Arginine-482 is not essential for transport of antibiotics, primary bile acids and unconjugated sterols by the human breast cancer resistance protein (ABCG2).', *The Biochemical journal*. England, 385(Pt 2), pp. 419–426. doi: 10.1042/BJ20040791.

Jardetzky, O. (1966) 'Simple Allosteric Model for Membrane Pumps', *Nature*. Nature Publishing Group, 211, p. 969.

Jerabek-Willemsen, M., André, T., Wanner, R., Roth, H. M., Duhr, S., Baaske, P. and Breitsprecher, D. (2014) 'MicroScale Thermophoresis: Interaction analysis and beyond', *Journal of Molecular Structure*, 1077, pp. 101–113. doi: https://doi.org/10.1016/j.molstruc.2014.03.009.

Jiye, Y. I. N. and Jianting, Z. (2011) 'Multidrug resistance-associated protein 1 (MRP1/ABCC1) polymorphism: from discovery to clinical application', *Zhong nan da xue xue bao. Yi xue ban = Journal of Central South University. Medical sciences*, 36(10), pp. 927–938. doi: 10.3969/j.issn.1672-7347.2011.10.002.

Johnson, Z. L. and Chen, J. (2017) 'Structural Basis of Substrate Recognition by the Multidrug Resistance Protein MRP1', *Cell*. Elsevier, 168(6), p. 1075–1085.e9. doi: 10.1016/j.cell.2017.01.041.

Johnson, Z. L. and Chen, J. (2018) 'ATP Binding Enables Substrate Release from Multidrug Resistance Protein 1.', *Cell*. United States, 172(1–2), p. 81–89.e10. doi: 10.1016/j.cell.2017.12.005.

Jones, P. M. and George, A. M. (2002) 'Mechanism of ABC transporters: a molecular dynamics simulation of a well characterized nucleotide-binding subunit.', *Proceedings of the National Academy of Sciences of the United States of America*. United States, 99(20), pp. 12639–12644. doi: 10.1073/pnas.152439599.

Jones, P. M. and George, A. M. (2004) 'The ABC transporter structure and mechanism: Perspectives on recent research', *Cellular and Molecular Life Sciences*, 61(6), pp. 682–699. doi: 10.1007/s00018-003-3336-9.

Jones, P. M. and George, A. M. (2012) 'Role of the D-loops in allosteric control of ATP hydrolysis in an ABC transporter.', *The journal of physical chemistry. A*. United States, 116(11), pp. 3004–3013. doi: 10.1021/jp211139s.

Jonker, J. W., Buitelaar, M., Wagenaar, E., Van Der Valk, M. A., Scheffer, G. L., Scheper, R. J., Plosch, T., Kuipers, F., Elferink, R. P. J. O., Rosing, H., Beijnen, J. H. and Schinkel, A. H. (2002) 'The breast cancer resistance protein protects against a major chlorophyll-derived dietary phototoxin and protoporphyria.', *Proceedings of the National Academy of Sciences of the United States of America*. United States, 99(24), pp. 15649–15654. doi: 10.1073/pnas.202607599.

Jonker, J. W., Smit, J. W., Brinkhuis, R. F., Maliepaard, M., Beijnen, J. H., Schellens, J. H. and Schinkel, a H. (2000) 'Role of breast cancer resistance protein in the bioavailability and fetal penetration of topotecan.', *Journal of the National Cancer Institute*, 92(20), pp. 1651–1656. doi: 10.1093/jnci/92.20.1651.

Juliano, R. L. and Ling, V. (1976) 'A surface glycoprotein modulating drug permeability in Chinese hamster ovary cell mutants', *Biochimica et Biophysica Acta (BBA) - Biomembranes*, 455(1), pp. 152–162. doi: http://dx.doi.org/10.1016/0005-2736(76)90160-7.

Kage, K., Fujita, T. and Sugimoto, Y. (2005) 'Role of Cys-603 in dimer/oligomer formation of the breast cancer resistance protein BCRP/ABCG2', *Cancer Science*, 96(12), pp. 866–872. doi: 10.1111/j.1349-7006.2005.00126.x.

Kapoor, P., Horsey, A. J., Cox, M. H. and Kerr, I. D. (no date) 'ABCG2: Does resolving its structure elucidate the mechanism?', *Biochemical Society Transactions*.

Kell, D. B. (2015) 'What would be the observable consequences if phospholipid bilayer diffusion of drugs into cells is negligible?', *Trends in Pharmacological Sciences*, 36(1), pp. 15–21. doi: https://doi.org/10.1016/j.tips.2014.10.005.

Kell, D. B., Dobson, P. D. and Oliver, S. G. (2011) 'Pharmaceutical drug transport: the issues and the implications that it is essentially carrier-mediated only', *Drug Discovery Today*, 16(15), pp. 704–714. doi: https://doi.org/10.1016/j.drudis.2011.05.010.

Kerr, I. D., Haider, A. J. and Gelissen, I. C. (2011) 'The ABCG family of membrane-associated transporters: you don't have to be big to be mighty.', *British journal of pharmacology*, 164(7), pp. 1767–79. doi: 10.1111/j.1476-5381.2010.01177.x.

Keskitalo, J. E., Pasanen, M. K., Neuvonen, P. J. and Niemi, M. (2009) 'Different effects of the ABCG2 c.421C>A SNP on the pharmacokinetics of fluvastatin, pravastatin and simvastatin.', *Pharmacogenomics*. England, 10(10), pp. 1617–1624. doi: 10.2217/pgs.09.85.

Keskitalo, J. E., Zolk, O., Fromm, M. F., Kurkinen, K. J., Neuvonen, P. J. and Niemi, M. (2009) 'ABCG2 polymorphism markedly affects the pharmacokinetics of atorvastatin and rosuvastatin.', *Clinical pharmacology and therapeutics*. United States, 86(2), pp. 197–203. doi: 10.1038/clpt.2009.79.

Khan, K. N., Kasilian, M., Mahroo, O. A. R., Tanna, P., Kalitzeos, A., Robson, A. G., Tsunoda, K., Iwata, T., Moore, A. T., Fujinami, K. and Michaelides, M. (2018) 'Early Patterns of Macular Degeneration in ABCA4-Associated Retinopathy', *Ophthalmology*. Elsevier, 125(5), pp. 735–746. doi: 10.1016/j.ophtha.2017.11.020.

Khunweeraphong, N., Stockner, T. and Kuchler, K. (2017) 'The structure of the human ABC transporter ABCG2 reveals a novel mechanism for drug extrusion', *Scientific Reports*. Springer US, (July), pp. 1–15. doi: 10.1038/s41598-017-11794-w.

Kilpatrick, L. E. and Hill, S. J. (2016) 'The use of fluorescence correlation spectroscopy to characterize the molecular mobility of fluorescently labelled G protein-coupled receptors', *Biochemical Society Transactions*, 44(2), pp. 624–629. doi: 10.1042/BST20150285.

Kim, H.-S., Sunwoo, Y. E., Ryu, J. Y., Kang, H.-J., Jung, H.-E., Song, I.-S., Kim, E.-Y., Shim, J.-C., Shon, J.-H. and Shin, J.-G. (2007) 'The effect of ABCG2 V12M, Q141K and Q126X, known functional variants in vitro, on the disposition of lamivudine.', *British journal of clinical pharmacology*. England, 64(5), pp. 645–654. doi: 10.1111/j.1365-

2125.2007.02944.x.

Kim, Y. and Chen, J. (2018) 'Molecular structure of human P-glycoprotein in the ATP-bound, outward-facing conformation', *Science*.

Kimple, M. E., Brill, A. L. and Pasker, R. L. (2013) 'Overview of affinity tags for protein purification', *Current Protocols in Protein Science*, (SUPPL.73), pp. 608–616. doi: 10.1002/0471140864.ps0909s73.

Kis, E., Nagy, T., Jani, M., Molnar, E., Janossy, J., Ujhellyi, O., Nemet, K., Heredi-Szabo, K. and Krajcsi, P. (2009) 'Leflunomide and its metabolite A771726 are high affinity substrates of BCRP: implications for drug resistance.', *Annals of the rheumatic diseases*. England, 68(7), pp. 1201–1207. doi: 10.1136/ard.2007.086264.

Kiser, J. J., Gerber, J. G., Predhomme, J. A., Wolfe, P., Flynn, D. M. and Hoody, D. W. (2008) 'Drug/Drug interaction between lopinavir/ritonavir and rosuvastatin in healthy volunteers.', *Journal of acquired immune deficiency syndromes (1999)*. United States, 47(5), pp. 570–578. doi: 10.1097/QAI.0b013e318160a542.

Knowles, T. J., Finka, R., Smith, C., Lin, Y.-P., Dafforn, T. and Overduin, M. (2009) 'Membrane proteins solubilized intact in lipid containing nanoparticles bounded by styrene maleic acid copolymer.', *Journal of the American Chemical Society*. United States, 131(22), pp. 7484–7485. doi: 10.1021/ja810046q.

Kondo, C., Onuki, R., Kusuhara, H., Suzuki, H., Suzuki, M., Okudaira, N., Kojima, M., Ishiwata, K., Jonker, J. W. and Sugiyama, Y. (2005) 'Lack of improvement of oral absorption of ME3277 by prodrug formation is ascribed to the intestinal efflux mediated by breast cancer resistant protein (BCRP/ABCG2).', *Pharmaceutical research*. United States, 22(4), pp. 613–618. doi: 10.1007/s11095-005-2487-9.

Konig, J., Muller, F. and Fromm, M. F. (2013) 'Transporters and Drug-Drug Interactions: Important Determinants of Drug Disposition and Effects', *Pharmacological Reviews*, 65(3), pp. 944–966. doi: 10.1124/pr.113.007518.

Koressaar, T. and Remm, M. (2007) 'Enhancements and modifications of primer design program Primer3', *Bioinformatics*, 23(10), pp. 1289–1291. doi: 10.1093/bioinformatics/btm091.

Kourti, M., Vavatsi, N., Gombakis, N., Sidi, V., Tzimagiorgis, G., Papageorgiou, T., Koliouskas, D. and Athanassiadou, F. (2007) 'Expression of multidrug resistance 1 (MDR1), multidrug resistance-related protein 1 (MRP1), lung resistance protein (LRP), and breast cancer resistance protein (BCRP) genes and clinical outcome in childhood acute lymphoblastic leukemia.', *International journal of hematology*. Japan, 86(2), pp. 166–173. doi: 10.1532/IJH97.E0624.

Krishna, R. and Mayer, L. D. (2000) 'Multidrug resistance (MDR) in cancer. Mechanisms, reversal using modulators of MDR and the role of MDR modulators in influencing the pharmacokinetics of anticancer drugs.', *European journal of pharmaceutical sciences : official journal of the European Federation for Pharmaceutical Sciences*. Netherlands, 11(4), pp. 265–283.

Krishnamurthy, P., Ross, D. D., Nakanishi, T., Bailey-Dell, K., Zhou, S., Mercer, K. E.,

Sarkadi, B., Sorrentino, B. P. and Schuetz, J. D. (2004) 'The stem cell marker Bcrp/ABCG2 enhances hypoxic cell survival through interactions with heme.', *The Journal of biological chemistry*. United States, 279(23), pp. 24218–24225. doi: 10.1074/jbc.M313599200.

Kruijtzer, C. M. F., Beijnen, J. H., Rosing, H., ten Bokkel Huinink, W. W., Schot, M., Jewell, R. C., Paul, E. M. and Schellens, J. H. M. (2002) 'Increased oral bioavailability of topotecan in combination with the breast cancer resistance protein and P-glycoprotein inhibitor GF120918.', *Journal of clinical oncology : official journal of the American Society of Clinical Oncology*. United States, 20(13), pp. 2943–2950. doi: 10.1200/JCO.2002.12.116.

Kuppens, I. E. L. M., Witteveen, E. O., Jewell, R. C., Radema, S. A., Paul, E. M., Mangum, S. G., Beijnen, J. H., Voest, E. E. and Schellens, J. H. M. (2007) 'A phase I, randomized, open-label, parallel-cohort, dose-finding study of elacridar (GF120918) and oral topotecan in cancer patients.', *Clinical cancer research : an official journal of the American Association for Cancer Research*. United States, 13(11), pp. 3276–3285. doi: 10.1158/1078-0432.CCR-06-2414.

Kuroda, T. and Tsuchiya, T. (2009) 'Multidrug efflux transporters in the MATE family', *Biochimica et Biophysica Acta (BBA) - Proteins and Proteomics*, 1794(5), pp. 763–768. doi: https://doi.org/10.1016/j.bbapap.2008.11.012.

Laemmli, U. K. (1970) 'Cleavage of Structural Proteins during the Assembly of the Head of Bacteriophage T4', *Nature*. Nature Publishing Group, 227, p. 680.

Lagas, J. S., van der Kruijssen, C. M. M., van de Wetering, K., Beijnen, J. H. and Schinkel, A. H. (2009) 'Transport of diclofenac by breast cancer resistance protein (ABCG2) and stimulation of multidrug resistance protein 2 (ABCC2)-mediated drug transport by diclofenac and benzbromarone.', *Drug metabolism and disposition: the biological fate of chemicals*. United States, 37(1), pp. 129–136. doi: 10.1124/dmd.108.023200.

László, L., Sarkadi, B. and Hegedüs, T. (2016) 'Jump into a new fold-A homology based model for the ABCG2/BCRP multidrug transporter', *PLoS ONE*, 11(10), pp. 1–22. doi: 10.1371/journal.pone.0164426.

Lawson, J., O'Mara, M. L. and Kerr, I. D. (2008) 'Structure-based interpretation of the mutagenesis database for the nucleotide binding domains of P-glycoprotein.', *Biochimica et biophysica acta*. Netherlands, 1778(2), pp. 376–391. doi: 10.1016/j.bbamem.2007.10.021.

Leder, A. and Leder, P. (1975) 'Butyric acid, a potent inducer of erythroid differentiation in cultured erythroleukemic cells.', *Cell*, 5(3), pp. 319–322. doi: 10.1016/0092-8674(75)90107-5.

Lee, A. G. (2004) 'How lipids affect the activities of integral membrane proteins.', *Biochimica et biophysica acta*. Netherlands, 1666(1–2), pp. 62–87. doi: 10.1016/j.bbamem.2004.05.012.

Lee, C. A., O'Connor, M. A., Ritchie, T. K., Galetin, A., Cook, J. A., Ragueneau-Majlessi, I., Ellens, H., Feng, B., Taub, M. E., Paine, M. F., Polli, J. W., Ware, J. A. and Zamek-Gliszczynski, M. J. (2015) 'Breast cancer resistance protein (ABCG2) in clinical

pharmacokinetics and drug interactions: practical recommendations for clinical victim and perpetrator drug-drug interaction study design.', *Drug metabolism and disposition: the biological fate of chemicals*, 43(4), pp. 490–509. doi: 10.1124/dmd.114.062174.

Lee, J.-Y., Kinch, L. N., Borek, D. M., Wang, J., Wang, J., Urbatsch, I. L., Xie, X.-S., Grishin, N. V, Cohen, J. C., Otwinowski, Z., Hobbs, H. H. and Rosenbaum, D. M. (2016) 'Crystal structure of the human sterol transporter ABCG5/ABCG8.', *Nature*. England, 533(7604), pp. 561–564. doi: 10.1038/nature17666.

Lee, S. C., Knowles, T. J., Postis, V. L. G., Jamshad, M., Parslow, R. A., Lin, Y.-P., Goldman, A., Sridhar, P., Overduin, M., Muench, S. P. and Dafforn, T. R. (2016) 'A method for detergent-free isolation of membrane proteins in their local lipid environment.', *Nature protocols*. England, 11(7), pp. 1149–1162. doi: 10.1038/nprot.2016.070.

Leier, I., Jedlitschky, G., Buchholz, U., Cole, S. P., Deeley, R. G. and Keppler, D. (1994) 'The MRP gene encodes an ATP-dependent export pump for leukotriene C4 and structurally related conjugates.', *The Journal of biological chemistry*. United States, 269(45), pp. 27807–27810.

Lepper, E. R., Nooter, K., Verweij, J., Acharya, M. R., Figg, W. D. and Sparreboom, A. (2005) 'Mechanisms of resistance to anticancer drugs: the role of the polymorphic ABC transporters ABCB1 and ABCG2.', *Pharmacogenomics*. England, 6(2), pp. 115–138. doi: 10.1517/14622416.6.2.115.

Li, F., Zeng, H. and Ying, K. (2011) 'The combination of stem cell markers CD133 and ABCG2 predicts relapse in stage I non-small cell lung carcinomas.', *Medical oncology (Northwood, London, England)*. United States, 28(4), pp. 1458–1462. doi: 10.1007/s12032-010-9646-5.

Li, M. J., Nath, A. and Atkins, W. M. (2017) 'Differential Coupling of Binding, ATP Hydrolysis, and Transport of Fluorescent Probes with P-Glycoprotein in Lipid Nanodiscs', *Biochemistry*, 56(19), pp. 2506–2517. doi: 10.1021/acs.biochem.6b01245.

Li, N., Wu, J. X., Ding, D., Cheng, J., Gao, N. and Chen, L. (2017) 'Structure of a Pancreatic ATP-Sensitive Potassium Channel', *Cell*. Elsevier, 168(1–2), p. 101–110.e10. doi: 10.1016/j.cell.2016.12.028.

Li, X., Pan, Y.-Z., Seigel, G. M., Hu, Z.-H., Huang, M. and Yu, A.-M. (2011) 'Breast cancer resistance protein BCRP/ABCG2 regulatory microRNAs (hsa-miR-328, -519c and -520h) and their differential expression in stem-like ABCG2+ cancer cells.', *Biochemical pharmacology*. England, 81(6), pp. 783–792. doi: 10.1016/j.bcp.2010.12.018.

Ling, V. and Thompson, L. H. (1974) 'Reduced permeability in CHO cells as a mechanism of resistance to colchicine.', *Journal of cellular physiology*. United States, 83(1), pp. 103–116. doi: 10.1002/jcp.1040830114.

Linton, K. J. and Higgins, C. F. (2007) 'Structure and function of ABC transporters: The ATP switch provides flexible control', *Pflugers Archiv European Journal of Physiology*, 453(5), pp. 555–567. doi: 10.1007/s00424-006-0126-x.

Litman, T., Brangi, M., Hudson, E., Fetsch, P., Abati, A., Ross, D. D., Miyake, K., Resau, J. H. and Bates, S. E. (2000) 'The multidrug-resistant phenotype associated with

overexpression of the new ABC half-transporter, MXR (ABCG2).', *Journal of cell science*. England, 113 ( Pt 1, pp. 2011–2021.

Magde, D., Elson, E. and Webb, W. W. (1972) 'Thermodynamic fluctuations in a reacting system measurement by fluorescence correlation spectroscopy', *Physical Review Letters*, 29(11), pp. 705–708. doi: 10.1103/PhysRevLett.29.705.

Mahringer, A. and Fricker, G. (2016) 'ABC transporters at the blood-brain barrier', *Expert Opinion on Drug Metabolism and Toxicology*, 12(5), pp. 499–508. doi: 10.1517/17425255.2016.1168804.

Maliepaard, M., Scheffer, G. L., Faneyte, I. F., van Gastelen, M. a, Pijnenborg, a C., Schinkel, a H., van De Vijver, M. J., Scheper, R. J. and Schellens, J. H. (2001) 'Subcellular localization and distribution of the breast cancer resistance protein transporter in normal human tissues.', *Cancer research*, 61(8), pp. 3458–3464.

Mao, Q. and Unadkat, J. D. (2015) 'Role of the Breast Cancer Resistance Protein (BCRP/ABCG2) in Drug Transport—an Update', *The AAPS Journal*. Boston: Springer US, 17(1), pp. 65–82. doi: 10.1208/s12248-014-9668-6.

Marie, J. P., Zittoun, R. and Sikic, B. I. (1991) 'Multidrug resistance (mdr1) gene expression in adult acute leukemias: correlations with treatment outcome and in vitro drug sensitivity.', *Blood*. United States, 78(3), pp. 586–592.

Martin, C., Berridge, G., Mistry, P., Higgins, C., Charlton, P. and Callaghan, R. (1999) 'The molecular interaction of the high affinity reversal agent XR9576 with P-glycoprotein', *British Journal of Pharmacology*, 128(2), pp. 403–411. doi: 10.1038/sj.bjp.0702807.

McDevitt, C. a., Collins, R. F., Conway, M., Modok, S., Storm, J., Kerr, I. D., Ford, R. C. and Callaghan, R. (2006) 'Purification and 3D Structural Analysis of Oligomeric Human Multidrug Transporter ABCG2', *Structure*, 14(November), pp. 1623–1632. doi: 10.1016/j.str.2006.08.014.

McDevitt, C. a., Collins, R., Kerr, I. D. and Callaghan, R. (2009) 'Purification and structural analyses of ABCG2', *Advanced Drug Delivery Reviews*, 61, pp. 57–65. doi: 10.1016/j.addr.2008.07.004.

McDevitt, C. A., Crowley, E., Hobbs, G., Starr, K. J., Kerr, I. D. and Callaghan, R. (2008) 'Is ATP binding responsible for initiating drug translocation by the multidrug transporter ABCG2?', *The FEBS journal*. England, 275(17), pp. 4354–4362. doi: 10.1111/j.1742-4658.2008.06578.x.

Merino, G., Alvarez, A. I., Pulido, M. M., Molina, A. J., Schinkel, A. H. and Prieto, J. G. (2006) 'Breast cancer resistance protein (BCRP/ABCG2) transports fluoroquinolone antibiotics and affects their oral availability, pharmacokinetics, and milk secretion.', *Drug metabolism and disposition: the biological fate of chemicals*. United States, 34(4), pp. 690–695. doi: 10.1124/dmd.105.008219.

Merino, G., Jonker, J. W., Wagenaar, E., van Herwaarden, A. E. and Schinkel, A. H. (2005) 'The breast cancer resistance protein (BCRP/ABCG2) affects pharmacokinetics, hepatobiliary excretion, and milk secretion of the antibiotic nitrofurantoin.', *Molecular pharmacology*. United States, 67(5), pp. 1758–1764. doi: 10.1124/mol.104.010439.

Merino, G., Jonker, J. W., Wagenaar, E., Pulido, M. M., Molina, A. J., Alvarez, A. I. and Schinkel, A. H. (2005) 'Transport of anthelmintic benzimidazole drugs by breast cancer resistance protein (BCRP/ABCG2).', *Drug metabolism and disposition: the biological fate of chemicals*. United States, 33(5), pp. 614–618. doi: 10.1124/dmd.104.003319.

Meseth, U., Wohland, T., Rigler, R. and Vogel, H. (1999) 'Resolution of fluorescence correlation measurements.', *Biophysical journal*. United States, 76(3), pp. 1619–1631. doi: 10.1016/S0006-3495(99)77321-2.

Middleton, R. J., Briddon, S. J., Cordeaux, Y., Yates, A. S., Dale, C. L., George, M. W., Baker, J. G., Hill, S. J. and Kellam, B. (2007) 'New fluorescent adenosine A1-receptor agonists that allow quantification of ligand-receptor interactions in microdomains of single living cells.', *Journal of medicinal chemistry*. United States, 50(4), pp. 782–793. doi: 10.1021/jm061279i.

Mikkaichi, T., Suzuki, T., Tanemoto, M., Ito, S. and Abe, T. (2004) 'The organic anion transporter (OATP) family.', *Drug metabolism and pharmacokinetics*. England, 19(3), pp. 171–179.

Milane, A., Vautier, S., Chacun, H., Meininger, V., Bensimon, G., Farinotti, R. and Fernandez, C. (2009) 'Interactions between riluzole and ABCG2/BCRP transporter.', *Neuroscience letters*. Ireland, 452(1), pp. 12–16. doi: 10.1016/j.neulet.2008.12.061.

Minsky, M. (1957) 'Microscopy apparatus'. US.

Minsky, M. (1988) 'Memoir on inventing the confocal scanning microscope', *Scanning*, 10(4), pp. 128–138. doi: 10.1002/sca.4950100403.

Miyata, H., Takada, T., Toyoda, Y., Matsuo, H., Ichida, K. and Suzuki, H. (2016) 'Identification of Febuxostat as a New Strong ABCG2 Inhibitor: Potential Applications and Risks in Clinical Situations', *Frontiers in Pharmacology*. Frontiers Media S.A., 7, p. 518. doi: 10.3389/fphar.2016.00518.

Mo, W., Qi, J. and Zhang, J.-T. (2012) 'Different roles of TM5, TM6, and ECL3 in the oligomerization and function of human ABCG2.', *Biochemistry*, 51(17), pp. 3634–41. doi: 10.1021/bi300301a.

Muller, M., Bakos, E., Welker, E., Varadi, A., Germann, U. A., Gottesman, M. M., Morse, B. S., Roninson, I. B. and Sarkadi, B. (1996) 'Altered drug-stimulated ATPase activity in mutants of the human multidrug resistance protein.', *The Journal of biological chemistry*. United States, 271(4), pp. 1877–1883.

Myllynen, P., Kummu, M., Kangas, T., Ilves, M., Immonen, E., Rysä, J., Pirilä, R., Lastumäki, A. and Vähäkangas, K. H. (2008) 'ABCG2/BCRP decreases the transfer of a food-born chemical carcinogen, 2-amino-1-methyl-6-phenylimidazo[4,5-b]pyridine (PhIP) in perfused term human placenta', *Toxicology and Applied Pharmacology*, 232(2), pp. 210–217. doi: 10.1016/j.taap.2008.07.006.

Nagel, G., Hwang, T. C., Nastiuk, K. L., Nairn, A. C. and Gadsby, D. C. (1992) 'The protein kinase A-regulated cardiac Cl- channel resembles the cystic fibrosis transmembrane conductance regulator.', *Nature*. England, 360(6399), pp. 81–84. doi: 10.1038/360081a0.

Nakagawa, H., Wakabayashi-Nakao, K., Tamura, A., Toyoda, Y., Koshiba, S. and Ishikawa, T. (2009) 'Disruption of N-linked glycosylation enhances ubiquitin-mediated proteasomal degradation of the human ATP-binding cassette transporter ABCG2', *FEBS Journal*, 276(24), pp. 7237–7252. doi: 10.1111/j.1742-4658.2009.07423.x.

Natarajan, K., Xie, Y., Baer, M. R. and Ross, D. D. (2012) 'Role of breast cancer resistance protein (BCRP/ABCG2) in cancer drug resistance', *Biochemical Pharmacology*, 83, pp. 1084–1103. doi: 10.1016/j.bcp.2012.01.002.

Nicolson, G. L. (2014) 'The Fluid Mosaic Model of Membrane Structure: Still relevant to undd erstanding the structure, function and dynamics of biological membranes after more than 40 years', *Biochimica et Biophysica Acta (BBA) - Biomembranes*, 1838(6), pp. 1451–1466. doi: http://dx.doi.org/10.1016/j.bbamem.2013.10.019.

Nies, A. T., Koepsell, H., Damme, K. and Schwab, M. (2011) 'Organic cation transporters (OCTs, MATEs), in vitro and in vivo evidence for the importance in drug therapy.', *Handbook of experimental pharmacology*. Germany, (201), pp. 105–167. doi: 10.1007/978-3-642-14541-4_3.

Nigam, S. K., Bush, K. T., Martovetsky, G., Ahn, S.-Y., Liu, H. C., Richard, E., Bhatnagar, V. and Wu, W. (2015) 'The Organic Anion Transporter (OAT) Family: A Systems Biology Perspective', *Physiological Reviews*. Bethesda, MD: American Physiological Society, 95(1), pp. 83–123. doi: 10.1152/physrev.00025.2013.

Nöll, A., Thomas, C., Herbring, V., Zollmann, T., Barth, K., Mehdipour, A. R., Tomasiak, T. M., Brüchert, S., Joseph, B., Abele, R., Oliéric, V., Wang, M., Diederichs, K., Hummer, G., Stroud, R. M., Pos, K. M. and Tampé, R. (2017) 'Crystal structure and mechanistic basis of a functional homolog of the antigen transporter TAP', *Proceedings of the National Academy of Sciences of the United States of America*. National Academy of Sciences, 114(4), pp. E438–E447. doi: 10.1073/pnas.1620009114.

Oesterhelt, D. and Tittor, J. (1989) 'Two pumps, one principle: light-driven ion transport in halobacteria', *Trends in Biochemical Sciences*, 14(2), pp. 57–61. doi: https://doi.org/10.1016/0968-0004(89)90044-3.

Oldham, M. L., Khare, D., Quiocho, F. A., Davidson, A. L. and Chen, J. (2007) 'Crystal structure of a catalytic intermediate of the maltose transporter.', *Nature*. England, 450(7169), pp. 515–521. doi: 10.1038/nature06264.

Oluwole, A. O., Danielczak, B., Meister, A., Babalola, J. O., Vargas, C. and Keller, S. (2017) 'Solubilization of Membrane Proteins into Functional Lipid-Bilayer Nanodiscs Using a Diisobutylene/Maleic Acid Copolymer', *Angewandte Chemie - International Edition*, 56(7), pp. 1919–1924. doi: 10.1002/anie.201610778.

Oostendorp, R., Buckle, T., Beijnen, J., van Tellingen, O. and Schellens, J. M. (2009) 'The effect of P-gp (Mdr1a/1b), BCRP (Bcrp1) and P-gp/BCRP inhibitors on the in vivo absorption, distribution, metabolism and excretion of imatinib', *Investigational New Drugs*. Springer US, 27(1), pp. 31–40. doi: 10.1007/s10637-008-9138-z.

Ota, S., Ishii, G., Goto, K., Kubota, K., Kim, Y. H., Kojika, M., Murata, Y., Yamazaki, M., Nishiwaki, Y., Eguchi, K. and Ochiai, A. (2009) 'Immunohistochemical expression of BCRP and ERCC1 in biopsy specimen predicts survival in advanced non-small-cell lung cancer

treated with cisplatin-based chemotherapy.', *Lung cancer (Amsterdam, Netherlands)*. Ireland, 64(1), pp. 98–104. doi: 10.1016/j.lungcan.2008.07.014.

Otsuka, M., Matsumoto, T., Morimoto, R., Arioka, S., Omote, H. and Moriyama, Y. (2005) 'A human transporter protein that mediates the final excretion step for toxic organic cations', *Proceedings of the National Academy of Sciences of the United States of America*, 102(50), pp. 17923–17928. doi: 10.1073/pnas.0506483102.

Ozvegy, C., Varadi, A. and Sarkadi, B. (2002) 'Characterization of drug transport, ATP hydrolysis, and nucleotide trapping by the human ABCG2 multidrug transporter. Modulation of substrate specificity by a point mutation.', *The Journal of biological chemistry*. United States, 277(50), pp. 47980–47990. doi: 10.1074/jbc.M207857200.

Palmgren, M. G. and Nissen, P. (2011) 'P-type ATPases.', *Annual review of biophysics*. United States, 40, pp. 243–266. doi: 10.1146/annurev.biophys.093008.131331.

Pan, G., Giri, N. and Elmquist, W. F. (2007) 'Abcg2/Bcrp1 mediates the polarized transport of antiretroviral nucleosides abacavir and zidovudine.', *Drug metabolism and disposition: the biological fate of chemicals*. United States, 35(7), pp. 1165–1173. doi: 10.1124/dmd.106.014274.

Pauklin, M., Thomasen, H., Pester, A., Steuhl, K.-P. and Meller, D. (2011) 'Expression of pluripotency and multipotency factors in human ocular surface tissues.', *Current eye research*. England, 36(12), pp. 1086–1097. doi: 10.3109/02713683.2011.608238.

Pavek, P., Merino, G., Wagenaar, E., Bolscher, E., Novotna, M., Jonker, J. W. and Schinkel, A. H. (2005) 'Human breast cancer resistance protein: interactions with steroid drugs, hormones, the dietary carcinogen 2-amino-1-methyl-6-phenylimidazo(4,5-b)pyridine, and transport of cimetidine.', *The Journal of pharmacology and experimental therapeutics*. United States, 312(1), pp. 144–152. doi: 10.1124/jpet.104.073916.

Pear, W. S., Nolan, G. P., Scott, M. L. and Baltimore, D. (1993) 'Production of high-titer helper-free retroviruses by transient transfection.', *Proceedings of the National Academy of Sciences of the United States of America*, 90(18), pp. 8392–8396.

Perez, M., Blazquez, A. G., Real, R., Mendoza, G., Prieto, J. G., Merino, G. and Alvarez, A. I. (2009) 'In vitro and in vivo interaction of moxidectin with BCRP/ABCG2.', *Chemico-biological interactions*. Ireland, 180(1), pp. 106–112. doi: 10.1016/j.cbi.2009.02.009.

Pham, P. A., la Porte, C. J. L., Lee, L. S., van Heeswijk, R., Sabo, J. P., Elgadi, M. M., Piliero, P. J., Barditch-Crovo, P., Fuchs, E., Flexner, C. and Cameron, D. W. (2009) 'Differential effects of tipranavir plus ritonavir on atorvastatin or rosuvastatin pharmacokinetics in healthy volunteers.', *Antimicrobial agents and chemotherapy*. United States, 53(10), pp. 4385–4392. doi: 10.1128/AAC.00449-09.

Polli, J. W., Hussey, E., Bush, M., Generaux, G., Smith, G., Collins, D., McMullen, S., Turner, N. and Nunez, D. J. (2013) 'Evaluation of drug interactions of GSK1292263 (a GPR119 agonist) with statins: from in vitro data to clinical study design.', *Xenobiotica; the fate of foreign compounds in biological systems*. England, 43(6), pp. 498–508. doi: 10.3109/00498254.2012.739719.

Procko, E., Ferrin-O'Connell, I., Ng, S.-L. and Gaudet, R. (2006) 'Distinct structural and

functional properties of the ATPase sites in an asymmetric ABC transporter.', *Molecular cell*. United States, 24(1), pp. 51–62. doi: 10.1016/j.molcel.2006.07.034.

Prueksaritanont, T., Chu, X., Gibson, C., Cui, D., Yee, K. L., Ballard, J., Cabalu, T. and Hochman, J. (2013) 'Drug–Drug Interaction Studies: Regulatory Guidance and An Industry Perspective', *The AAPS Journal*. Boston: Springer US, 15(3), pp. 629–645. doi: 10.1208/s12248-013-9470-x.

Pulido, M. M., Molina, A. J., Merino, G., Mendoza, G., Prieto, J. G. and Alvarez, A. I. (2006) 'Interaction of enrofloxacin with breast cancer resistance protein (BCRP/ABCG2): influence of flavonoids and role in milk secretion in sheep.', *Journal of veterinary pharmacology and therapeutics*. England, 29(4), pp. 279–287. doi: 10.1111/j.1365-2885.2006.00744.x.

Qian, H. and Elson, E. L. (1991) 'Analysis of confocal laser-microscope optics for 3-D fluorescence correlation spectroscopy', *Applied Optics*, 30(10), p. 1185. doi: 10.1364/AO.30.001185.

Raaijmakers, M. H. G. P., de Grouw, E. P. L. M., Heuver, L. H. H., van der Reijden, B. A., Jansen, J. H., Scheffer, G., Scheper, R. J., de Witte, T. J. M. and Raymakers, R. A. P. (2005) 'Impaired breast cancer resistance protein mediated drug transport in plasma cells in multiple myeloma.', *Leukemia research*. England, 29(12), pp. 1455–1458. doi: 10.1016/j.leukres.2005.04.013.

Rao, U. S., Fine, R. L. and Scarborough, G. A. (1994) 'Antiestrogens and steroid hormones: substrates of the human P-glycoprotein.', *Biochemical pharmacology*. England, 48(2), pp. 287–292.

Rigler, R., Mets, Ü., Widengren, J. and Kask, P. (1993) 'Fluorescence correlation spectroscopy with high count rate and low background: analysis of translational diffusion', *European Biophysics Journal*, 22(3), pp. 169–175. doi: 10.1016/S0006-3495(76)85776-1.

Rigler, R. and Widengren, J. (1990) 'Ultrasensitive detection of single molecules by fluorescence correlation spectroscopy'.

Robey, R. W., Honjo, Y., Van de Laar, A., Miyake, K., Regis, J. T., Litman, T. and Bates, S. E. (2001) 'A functional assay for detection of the mitoxantrone resistance protein, MXR (ABCG2)', *Biochimica et Biophysica Acta - Biomembranes*, 1512(2), pp. 171–182. doi: 10.1016/S0005-2736(01)00308-X.

Robey, R. W., Honjo, Y., Morisaki, K., Nadjem, T. a, Runge, S., Risbood, M., Poruchynsky, M. S. and Bates, S. E. (2003) 'Mutations at amino-acid 482 in the ABCG2 gene affect substrate and antagonist specificity.', *British journal of cancer*, 89(10), pp. 1971–1978. doi: 10.1038/sj.bjc.6601370.

Robey, R. W., Ierano, C., Zhan, Z. and Bates, S. E. (2011) 'The Challenge of Exploiting ABCG2 in the Clinic', *Current pharmaceutical biotechnology*, 12(4), pp. 595–608.

Robey, R. W., To, K. K. K., Polgar, O., Dohse, M., Fetsch, P., Dean, M. and Bates, S. E. (2009) 'ABCG2: A perspective', *Advanced Drug Delivery Reviews*, 61(1), pp. 3–13. doi: 10.1016/j.addr.2008.11.003.

Rosenberg, M. F., Bikadi, Z., Hazai, E., Starborg, T., Kelley, L., Chayen, N. E., Ford, R. C. and Mao, Q. (2015) 'Three-dimensional structure of the human breast cancer resistance protein (BCRP/ABCG2) in an inward-facing conformation', *Acta Crystallographica Section D Biological Crystallography*. International Union of Crystallography, 71(8), pp. 1725–1735. doi: 10.1107/S1399004715010676.

Rosenberg, M. F., Bikadi, Z., Hazai, E., Starborg, T., Kelley, L., Chayen, N. E., Ford, R. C. and Mao, Q. (2015) 'Three-dimensional structure of the human breast cancer resistance protein (BCRP/ABCG2) in an inward-facing conformation', *Acta Crystallographica Section D: Biological Crystallography*, 71, pp. 1725–1735. doi: 10.1107/S1399004715010676.

Ross, D. D. and Nakanishi, T. (2010) 'Impact of Breast Cancer Resistance Protein on Cancer Treatment Outcomes', in Zhou, J. (ed.) *Multi-Drug Resistance in Cancer*. Totowa, NJ: Humana Press, pp. 251–290. doi: 10.1007/978-1-60761-416-6_12.

Roth, M., Obaidat, A. and Hagenbuch, B. (2012) 'OATPs, OATs and OCTs: the organic anion and cation transporters of the SLCO and SLC22A gene superfamilies', *British Journal of Pharmacology*. Oxford, UK: Blackwell Publishing Ltd, 165(5), pp. 1260–1287. doi: 10.1111/j.1476-5381.2011.01724.x.

Rothnie, A. J. (2016) 'Detergent-Free Membrane Protein Purification', in Mus-Veteau, I. (ed.) *Heterologous Expression of Membrane Proteins: Methods and Protocols*. New York, NY: Springer New York, pp. 261–267. doi: 10.1007/978-1-4939-3637-3_16.

Sane, R., Agarwal, S. and Elmquist, W. F. (2012) 'Brain distribution and bioavailability of elacridar after different routes of administration in the mouse.', *Drug metabolism and disposition: the biological fate of chemicals*. United States, 40(8), pp. 1612–1619. doi: 10.1124/dmd.112.045930.

Sarwat, S. (2016) *Trials and tribulations in the expression and purification of ABCG2*.

Sauerbrey, A., Sell, W., Steinbach, D., Voigt, A. and Zintl, F. (2002) 'Expression of the BCRP gene (ABCG2/MXR/ABCP) in childhood acute lymphoblastic leukaemia.', *British journal of haematology*. England, 118(1), pp. 147–150.

Sauna, Z. E., Nandigama, K. and Ambudkar, S. V (2004) 'Multidrug resistance protein 4 (ABCC4)-mediated ATP hydrolysis: effect of transport substrates and characterization of the post-hydrolysis transition state.', *The Journal of biological chemistry*. United States, 279(47), pp. 48855–48864. doi: 10.1074/jbc.M408849200.

Scheidelaar, S., Koorengevel, M. C., Pardo, J. D., Meeldijk, J. D., Breukink, E. and Killian, J. A. (2015) 'Molecular Model for the Solubilization of Membranes into Nanodisks by Styrene Maleic Acid Copolymers', *Biophysical Journal*. The Biophysical Society, 108(2), pp. 279–290. doi: 10.1016/j.bpj.2014.11.3464.

Schinkel, A. H., Mayer, U., Wagenaar, E., Mol, C. A., van Deemter, L., Smit, J. J., van der Valk, M. A., Voordouw, A. C., Spits, H., van Tellingen, O., Zijlmans, J. M., Fibbe, W. E. and Borst, P. (1997) 'Normal viability and altered pharmacokinetics in mice lacking mdr1-type (drug-transporting) P-glycoproteins.', *Proceedings of the National Academy of Sciences of the United States of America*. United States, 94(8), pp. 4028–4033.

Schinkel, A. H., Smit, J. J., van Tellingen, O., Beijnen, J. H., Wagenaar, E., van Deemter, L.,

Mol, C. A., van der Valk, M. A., Robanus-Maandag, E. C. and te Riele, H. P. (1994) 'Disruption of the mouse mdr1a P-glycoprotein gene leads to a deficiency in the blood-brain barrier and to increased sensitivity to drugs.', *Cell*. United States, 77(4), pp. 491–502.

Schmidt, T. G. and Skerra, A. (1993) 'The random peptide library-assisted engineering of a C-terminal affinity peptide, useful for the detection and purification of a functional Ig Fv fragment.', *Protein engineering*. England, 6(1), pp. 109–122.

Scott, D. O., Ghosh, A., Di, L. and Maurer, T. S. (2017) 'Passive drug permeation through membranes and cellular distribution', *Pharmacological Research*, 117, pp. 94–102. doi: https://doi.org/10.1016/j.phrs.2016.11.028.

Seddon, A. M., Curnow, P. and Booth, P. J. (2004) 'Membrane proteins, lipids and detergents: not just a soap opera.', *Biochimica et biophysica acta*. Netherlands, 1666(1–2), pp. 105–117. doi: 10.1016/j.bbamem.2004.04.011.

Sharom, F. J. (2011) 'The P-glycoprotein multidrug transporter.', *Essays in biochemistry*. England, 50(1), pp. 161–178. doi: 10.1042/bse0500161.

Shukla, S., Robey, R. W., Bates, S. E. and Ambudkar, S. V (2006) 'The calcium channel blockers, 1,4-dihydropyridines, are substrates of the multidrug resistance-linked ABC drug transporter, ABCG2.', *Biochemistry*. United States, 45(29), pp. 8940–8951. doi: 10.1021/bi060552f.

Simonson, S. G., Raza, A., Martin, P. D., Mitchell, P. D., Jarcho, J. A., Brown, C. D. A., Windass, A. S. and Schneck, D. W. (2004) 'Rosuvastatin pharmacokinetics in heart transplant recipients administered an antirejection regimen including cyclosporine.', *Clinical pharmacology and therapeutics*. United States, 76(2), pp. 167–177. doi: 10.1016/j.clpt.2004.03.010.

Singer, S. J. and Nicolson, G. L. (1972) 'The fluid mosaic model of the structure of cell membranes.', *Science (New York, N.Y.)*. United States, 175(4023), pp. 720–731.

Slot, A. J., Molinski, S. V and Cole, S. P. C. (2011) 'Mammalian multidrug-resistance proteins (MRPs).', *Essays in biochemistry*. England, 50(1), pp. 179–207. doi: 10.1042/bse0500179.

Smith, D. B. and Johnson, K. S. (1988) 'Single-step purification of polypeptides expressed in Escherichia coli as fusions with glutathione S-transferase.', *Gene*. Netherlands, 67(1), pp. 31–40.

Smith, P. C., Karpowich, N., Millen, L., Moody, J. E., Rosen, J., Thomas, P. J. and Hunt, J. F. (2002) 'ATP binding to the motor domain from an ABC transporter drives formation of a nucleotide sandwich dimer.', *Molecular cell*. United States, 10(1), pp. 139–149.

Sparreboom, A., Gelderblom, H., Marsh, S., Ahluwalia, R., Obach, R., Principe, P., Twelves, C., Verweij, J. and McLeod, H. L. (2004) 'Diflomotecan pharmacokinetics in relation to ABCG2 421C>A genotype.', *Clinical pharmacology and therapeutics*. United States, 76(1), pp. 38–44. doi: 10.1016/j.clpt.2004.03.003.

Sridharan, R., Zuber, J., Connelly, S. M., Mathew, E. and Dumont, M. E. (2014)

'Fluorescent Approaches for Understanding Interactions of Ligands with G Protein Coupled Receptors', *Biochimica et biophysica acta*, 1838(1 0 0), pp. 15–33. doi: 10.1016/j.bbamem.2013.09.005.

Steinbach, D., Sell, W., Voigt, A., Hermann, J., Zintl, F. and Sauerbrey, A. (2002) 'BCRP gene expression is associated with a poor response to remission induction therapy in childhood acute myeloid leukemia.', *Leukemia*. England, 16(8), pp. 1443–1447. doi: 10.1038/sj.leu.2402541.

Strouse, J. J., Ivnitski-Steele, I., Waller, A., Young, S. M., Perez, D., Evangelisti, A. M., Ursu, O., Bologa, C. G., Carter, M. B., Salas, V. M., Tegos, G., Larson, R. S., Oprea, T. I., Edwards, B. S. and Sklar, L. A. (2013) 'Fluorescent substrates for flow cytometric evaluation of efflux inhibition in ABCB1, ABCC1, and ABCG2 transporters', *Analytical Biochemistry*, 437(1), pp. 77–87. doi: 10.1016/j.ab.2013.02.018.

Suvannasankha, A., Minderman, H., O'Loughlin, K. L., Nakanishi, T., Ford, L. A., Greco, W. R., Wetzler, M., Ross, D. D. and Baer, M. R. (2004) 'Breast cancer resistance protein (BCRP/MXR/ABCG2) in adult acute lymphoblastic leukaemia: frequent expression and possible correlation with shorter disease-free survival.', *British journal of haematology*. England, 127(4), pp. 392–398. doi: 10.1111/j.1365-2141.2004.05211.x.

Szakács, G., Paterson, J. K., Ludwig, J. A., Booth-Genthe, C. and Gottesman, M. M. (2006) 'Targeting multidrug resistance in cancer', *Nature Reviews Drug Discovery*, 5(3), pp. 219–234. doi: 10.1038/nrd1984.

Szymanski, W. G., Zauber, H., Erban, A., Gorka, M., Wu, X. N. and Schulze, W. X. (2015) 'Cytoskeletal Components Define Protein Location to Membrane Microdomains', *Molecular & Cellular Proteomics : MCP*. The American Society for Biochemistry and Molecular Biology, 14(9), pp. 2493–2509. doi: 10.1074/mcp.M114.046904.

Tarentino, A. L., Trimble, R. B. and Plummer, T. H. J. (1989) 'Enzymatic approaches for studying the structure, synthesis, and processing of glycoproteins.', *Methods in cell biology*. United States, 32, pp. 111–139.

Taylor, N. M. I., Manolaridis, I., Jackson, S. M., Kowal, J., Stahlberg, H. and Locher, K. P. (2017) 'Structure of the human multidrug transporter ABCG2', *Nature*. Nature Publishing Group, 546(7659), pp. 504–509. doi: 10.1038/nature22345.

Theile, D., Grebhardt, S., Haefeli, W. E. and Weiss, J. (2009) 'Involvement of drug transporters in the synergistic action of FOLFOX combination chemotherapy.', *Biochemical pharmacology*. England, 78(11), pp. 1366–1373. doi: 10.1016/j.bcp.2009.07.006.

Thompson, A. N., Kim, I., Panosian, T. D., Iverson, T. M., Allen, T. W. and Nimigean, C. M. (2009) 'Mechanism of potassium channel selectivity revealed by Na(+) and Li(+) binding sites within the KcsA pore', *Nature structural & molecular biology*, 16(12), pp. 1317–1324. doi: 10.1038/nsmb.1703.

Tiwari, A. K., Sodani, K., Wang, S.-R., Kuang, Y.-H., Ashby, C. R. J., Chen, X. and Chen, Z.-S. (2009) 'Nilotinib (AMN107, Tasigna) reverses multidrug resistance by inhibiting the activity of the ABCB1/Pgp and ABCG2/BCRP/MXR transporters.', *Biochemical pharmacology*. England, 78(2), pp. 153–161. doi: 10.1016/j.bcp.2009.04.002.

To, K. K. W., Robey, R., Zhan, Z., Bangiolo, L. and Bates, S. E. (2011) 'Upregulation of ABCG2 by romidepsin via the aryl hydrocarbon receptor pathway.', *Molecular cancer research : MCR*. United States, 9(4), pp. 516–527. doi: 10.1158/1541-7786.MCR-10-0270.

To, K. K. W., Zhan, Z. and Bates, S. E. (2006) 'Aberrant promoter methylation of the ABCG2 gene in renal carcinoma.', *Molecular and cellular biology*. United States, 26(22), pp. 8572–8585. doi: 10.1128/MCB.00650-06.

Tombline, G., Bartholomew, L., Gimi, K., Tyndall, G. A. and Senior, A. E. (2004) 'Synergy between conserved ABC signature Ser residues in P-glycoprotein catalysis.', *The Journal of biological chemistry*. United States, 279(7), pp. 5363–5373. doi: 10.1074/jbc.M311964200.

Tombline, G., Muharemagic, A., White, L. B. and Senior, A. E. (2005) 'Involvement of the "occluded nucleotide conformation" of P-glycoprotein in the catalytic pathway.', *Biochemistry*. United States, 44(38), pp. 12879–12886. doi: 10.1021/bi0509797.

Toseland, C. P. (2013) 'Fluorescent labeling and modification of proteins', *Journal of Chemical Biology*, 6(3), pp. 85–95. doi: 10.1007/s12154-013-0094-5.

Tournier, N., Goutal, S., Auvity, S., Traxl, A., Mairinger, S., Wanek, T., Helal, O.-B., Buvat, I., Soussan, M., Caille, F. and Langer, O. (2017) 'Strategies to Inhibit ABCB1- and ABCG2-Mediated Efflux Transport of Erlotinib at the Blood-Brain Barrier: A PET Study on Nonhuman Primates.', *Journal of nuclear medicine : official publication, Society of Nuclear Medicine*. United States, 58(1), pp. 117–122. doi: 10.2967/jnumed.116.178665.

Tournier, N., Valette, H., Peyronneau, M.-A., Saba, W., Goutal, S., Kuhnast, B., Dolle, F., Scherrmann, J.-M., Cisternino, S. and Bottlaender, M. (2011) 'Transport of selected PET radiotracers by human P-glycoprotein (ABCB1) and breast cancer resistance protein (ABCG2): an in vitro screening.', *Journal of nuclear medicine : official publication, Society of Nuclear Medicine*. United States, 52(3), pp. 415–423. doi: 10.2967/jnumed.110.079608.

Trock, B. J., Leonessa, F. and Clarke, R. (1997) 'Multidrug resistance in breast cancer: a meta-analysis of MDR1/gp170 expression and its possible functional significance.', *Journal of the National Cancer Institute*. United States, 89(13), pp. 917–931.

Turner, J. G., Gump, J. L., Zhang, C., Cook, J. M., Marchion, D., Hazlehurst, L., Munster, P., Schell, M. J., Dalton, W. S. and Sullivan, D. M. (2006) 'ABCG2 expression, function, and promoter methylation in human multiple myeloma.', *Blood*. United States, 108(12), pp. 3881–3889. doi: 10.1182/blood-2005-10-009084.

Turrini, E., Haenisch, S., Laechelt, S., Diewock, T., Bruhn, O. and Cascorbi, I. (2012) 'MicroRNA profiling in K-562 cells under imatinib treatment: influence of miR-212 and miR-328 on ABCG2 expression.', *Pharmacogenetics and genomics*. United States, 22(3), pp. 198–205. doi: 10.1097/FPC.0b013e328350012b.

Uggla, B., Stahl, E., Wagsater, D., Paul, C., Karlsson, M. G., Sirsjo, A. and Tidefelt, U. (2005) 'BCRP mRNA expression v. clinical outcome in 40 adult AML patients.', *Leukemia research*. England, 29(2), pp. 141–146. doi: 10.1016/j.leukres.2004.06.004.

Untergasser, A., Cutcutache, I., Koressaar, T., Ye, J., Faircloth, B. C., Remm, M. and Rozen, S. G. (2012) 'Primer3-new capabilities and interfaces', *Nucleic Acids Research*, 40(15), pp. 1–12. doi: 10.1093/nar/gks596.

Urbatsch, I. L., Gimi, K., Wilke-Mounts, S. and Senior, A. E. (2000) 'Investigation of the role of glutamine-471 and glutamine-1114 in the two catalytic sites of P-glycoprotein.', *Biochemistry*. United States, 39(39), pp. 11921–11927.

Vasiliou, V., Vasiliou, K. and Nebert, D. W. (2009) 'Human ATP-binding cassette (ABC) transporter family', *Human Genomics*. BioMed Central, 3(3), pp. 281–290. doi: 10.1186/1479-7364-3-3-281.

Wakabayashi, K., Nakagawa, H., Tamura, A., Koshiba, S., Hoshijima, K., Komada, M. and Ishikawa, T. (2007) 'Intramolecular disulfide bond is a critical check point determining degradative fates of ATP-binding cassette (ABC) transporter ABCG2 protein', *Journal of Biological Chemistry*, 282(38), pp. 27841–27846. doi: 10.1074/jbc.C700133200.

Walker, J. E., Saraste, M., Runswick, M. J. and Gay, N. J. (1982) 'Distantly related sequences in the alpha- and beta-subunits of ATP synthase, myosin, kinases and other ATP-requiring enzymes and a common nucleotide binding fold.', *The EMBO journal*. England, 1(8), pp. 945–951.

Wang, H., Lee, E.-W., Cai, X., Ni, Z., Zhou, L. and Mao, Q. (2008) 'Membrane topology of the human breast cancer resistance protein (BCRP/ABCG2) determined by epitope insertion and immunofluorescence.', *Biochemistry*. United States, 47(52), pp. 13778–13787. doi: 10.1021/bi801644v.

Wang, X., Furukawa, T., Nitanda, T., Okamoto, M., Sugimoto, Y., Akiyama, S.-I. and Baba, M. (2003) 'Breast cancer resistance protein (BCRP/ABCG2) induces cellular resistance to HIV-1 nucleoside reverse transcriptase inhibitors.', *Molecular pharmacology*. United States, 63(1), pp. 65–72.

Ware, J. A., Zhang, L. and Huang, S.-M. (2012) 'Mechanisms and Genetics of Drug Transport', in Atkinson, A. J., Huang, S.-M., Lertora, J. J. L., and Markey, S. P. B. T.-P. of C. P. (Third E. (eds) *PRINCIPLES OF CLINICAL PHARMACOLOGY*. 3rd edn. Academic Press, pp. 217–237. doi: : http://dx.doi.org/10.1016/B978-0-12-385471-1.00014-3.

Watson, H. (2015) 'Biological membranes', *Essays In Biochemistry*, 59(0), pp. 43–69. doi: 10.1042/bse0590043.

Waugh, D. S. (2005) 'Making the most of affinity tags', *Trends in Biotechnology*, 23(6), pp. 316–320. doi: 10.1016/j.tibtech.2005.03.012.

de Wet, H., Proks, P., Lafond, M., Aittoniemi, J., Sansom, M. S. P., Flanagan, S. E., Pearson, E. R., Hattersley, A. T. and Ashcroft, F. M. (2008) 'A mutation (R826W) in nucleotide-binding domain 1 of ABCC8 reduces ATPase activity and causes transient neonatal diabetes', *EMBO Reports*. Nature Publishing Group, 9(7), pp. 648–654. doi: 10.1038/embor.2008.71.

Wilkens, S. (2015) 'Structure and mechanism of ABC transporters', *F1000Prime Reports*, 7. doi: 10.12703/P7-14.

Wong, K., Briddon, S. J., Holliday, N. D. and Kerr, I. D. (2016) 'Plasma membrane dynamics and tetrameric organisation of ABCG2 transporters in mammalian cells revealed by single particle imaging techniques', *Biochimica et Biophysica Acta (BBA) - Molecular Cell Research*. Elsevier B.V., 1863(1), pp. 19–29. doi: 10.1016/j.bbamcr.2015.10.002.

Woodward, O. M. (2015) 'ABCG2: The molecular mechanisms of urate secretion and gout', *American Journal of Physiology - Renal Physiology*, 309(6), pp. F485–F488. doi: 10.1152/ajprenal.00242.2015.

Woodward, O. M., Köttgen, A., Coresh, J., Boerwinkle, E., Guggino, W. B. and Köttgen, M. (2009) 'Identification of a urate transporter, ABCG2, with a common functional polymorphism causing gout.', *Proceedings of the National Academy of Sciences of the United States of America*, 106(25), pp. 10338–10342. doi: 10.1073/pnas.0901249106.

Woodward, O. M., Tukaye, D. N., Cui, J., Greenwell, P., Constantoulakis, L. M., Parker, B. S., Rao, A., Kottgen, M., Maloney, P. C. and Guggino, W. B. (2013) 'Gout-causing Q141K mutation in ABCG2 leads to instability of the nucleotide-binding domain and can be corrected with small molecules.', *Proceedings of the National Academy of Sciences of the United States of America*. United States, 110(13), pp. 5223–5228. doi: 10.1073/pnas.1214530110.

Xiang, L., Su, P., Xia, S., Liu, Z., Wang, Y., Gao, P. and Zhou, G. (2011) 'ABCG2 is associated with HER-2 Expression, lymph node metastasis and clinical stage in breast invasive ductal carcinoma', *Diagnostic Pathology*. BioMed Central, 6, p. 90. doi: 10.1186/1746-1596-6-90.

Xiong, H., Callaghan, D., Jones, A., Bai, J., Rasquinha, I., Smith, C., Pei, K., Walker, D., Lue, L.-F., Stanimirovic, D. and Zhang, W. (2009) 'ABCG2 Is Upregulated in Alzheimer's Brain with Cerebral Amyloid Angiopathy and May Act as a Gatekeeper at the Blood-Brain Barrier for A 1-40 Peptides', *Journal of Neuroscience*, 29(17), pp. 5463–5475. doi: 10.1523/JNEUROSCI.5103-08.2009.

Xu, J., Liu, Y., Yang, Y., Bates, S. and Zhang, J.-T. (2004) 'Characterization of Oligomeric Human Half-ABC Transporter ATP-binding Cassette G2', *Journal of Biological Chemistry*, 279(19), pp. 19781–19789. doi: 10.1074/jbc.M310785200.

Xu, R. (2015) 'Light scattering: A review of particle characterization applications', *Particuology*. Chinese Society of Particuology, 18, pp. 11–21. doi: 10.1016/j.partic.2014.05.002.

Xue, M., Cheng, L., Faustino, I., Guo, W. and Marrink, S. J. (2018) 'Molecular Mechanism of Lipid Nanodisk Formation by Styrene-Maleic Acid Copolymers.', *Biophysical journal*. United States, 115(3), pp. 494–502. doi: 10.1016/j.bpj.2018.06.018.

Yamada, A., Maeda, K., Kamiyama, E., Sugiyama, D., Kondo, T., Shiroyanagi, Y., Nakazawa, H., Okano, T., Adachi, M., Schuetz, J. D., Adachi, Y., Hu, Z., Kusuhara, H. and Sugiyama, Y. (2007) 'Multiple human isoforms of drug transporters contribute to the hepatic and renal transport of olmesartan, a selective antagonist of the angiotensin II AT1-receptor.', *Drug metabolism and disposition: the biological fate of chemicals*. United States, 35(12), pp. 2166–2176. doi: 10.1124/dmd.107.017459.

Yang, B., Ma, Y.-F. and Liu, Y. (2015) 'Elevated Expression of Nrf-2 and ABCG2 Involved in Multi-drug Resistance of Lung Cancer SP Cells.', *Drug research*. Germany, 65(10), pp. 526–531. doi: 10.1055/s-0034-1390458.

Yang, N. J. and Hinner, M. J. (2015) 'Getting Across the Cell Membrane: An Overview for Small Molecules, Peptides, and Proteins', *Methods in molecular biology (Clifton, N.J.)*, 1266, pp. 29–53. doi: 10.1007/978-1-4939-2272-7_3.

Yang, Y., Liu, Y., Dong, Z., Xu, J., Peng, H., Liu, Z. and Zhang, J.-T. (2007) 'Regulation of function by dimerization through the amino-terminal membrane-spanning domain of human ABCC1/MRP1.', *The Journal of biological chemistry*. United States, 282(12), pp. 8821–8830. doi: 10.1074/jbc.M700152200.

Yasuda, S., Itagaki, S., Hirano, T. and Iseki, K. (2006) 'Effects of sex hormones on regulation of ABCG2 expression in the placental cell line BeWo.', *Journal of pharmacy & pharmaceutical sciences : a publication of the Canadian Society for Pharmaceutical Sciences, Societe canadienne des sciences pharmaceutiques*. Canada, 9(1), pp. 133–139.

Yoh, K., Ishii, G., Yokose, T., Minegishi, Y., Tsuta, K., Goto, K., Nishiwaki, Y., Kodama, T., Suga, M. and Ochiai, A. (2004) 'Breast cancer resistance protein impacts clinical outcome in platinum-based chemotherapy for advanced non-small cell lung cancer.', *Clinical cancer research : an official journal of the American Association for Cancer Research*. United States, 10(5), pp. 1691–1697.

Young, C. L., Britton, Z. T. and Robinson, A. S. (2012) 'Recombinant protein expression and purification: A comprehensive review of affinity tags and microbial applications', *Biotechnology Journal*, 7(5), pp. 620–634. doi: 10.1002/biot.201100155.

Yu, S. P. and Choi, D. W. (1997) 'Na(+)-Ca2+ exchange currents in cortical neurons: concomitant forward and reverse operation and effect of glutamate.', *The European journal of neuroscience*. France, 9(6), pp. 1273–1281.

Zemanova, L., Schenk, A., Hunt, N., Nienhaus, G. U. and Heilker, R. (2004) 'Endothelin receptor in virus-like particles: ligand binding observed by fluorescence fluctuation spectroscopy.', *Biochemistry*. United States, 43(28), pp. 9021–9028. doi: 10.1021/bi035901+.

Zhang, W., Ding, W., Chen, Y., Feng, M., Ouyang, Y., Yu, Y. and He, Z. (2018) 'Up-regulation of breast cancer resistance protein plays a role in HER2-mediated chemoresistance through PI3K / Akt and nuclear factor-kappa B signaling pathways in MCF7 breast cancer cells', 43(8), pp. 647–653. doi: 10.1093/abbs/gmr050.Advance.

Zhang, W., Mojsilovic-Petrovic, J., Andrade, M. F., Zhang, H., Ball, M. and Stanimirovic, D. B. (2003) 'The expression and functional characterization of ABCG2 in brain endothelial cells and vessels.', *FASEB journal : official publication of the Federation of American Societies for Experimental Biology*. United States, 17(14), pp. 2085–2087. doi: 10.1096/fj.02-1131fje.

Zhang, Y., Gupta, A., Wang, H., Zhou, L., Vethanayagam, R. R., Unadkat, J. D. and Mao, Q. (2005) 'BCRP transports dipyridamole and is inhibited by calcium channel blockers.', *Pharmaceutical research*. United States, 22(12), pp. 2023–2034. doi: 10.1007/s11095-005-8384-4.

Zhou, S., Morris, J. J., Barnes, Y., Lan, L., Schuetz, J. D. and Sorrentino, B. P. (2002) 'Bcrp1 gene expression is required for normal numbers of side population stem cells in mice, and confers relative protection to mitoxantrone in hematopoietic cells in vivo.', *Proceedings of the National Academy of Sciences of the United States of America*. United States, 99(19), pp. 12339–12344. doi: 10.1073/pnas.192276999.

Zhou, Y., Ojeda-May, P. and Pu, J. (2013) 'H-loop histidine catalyzes ATP hydrolysis in the E. coli ABC-transporter HlyB.', *Physical chemistry chemical physics : PCCP*. England, 15(38), pp. 15811–15815. doi: 10.1039/c3cp50965f.

# 9 Appendix

## 9.1 Sequencing Data




**Supplementary Figure 9.1– Example sequence alignment for His_SNAP_ABCG2.** DNA sequencing data (Sbjct) was obtained using p31zeo_up sequencing primer and aligned against the predicted sequence (Query). The novel start codon (green) and hexahistidine encoding sequence (yellow) and altered internal start codon (orange) are shown.

## 9.2 FCS Data Processing

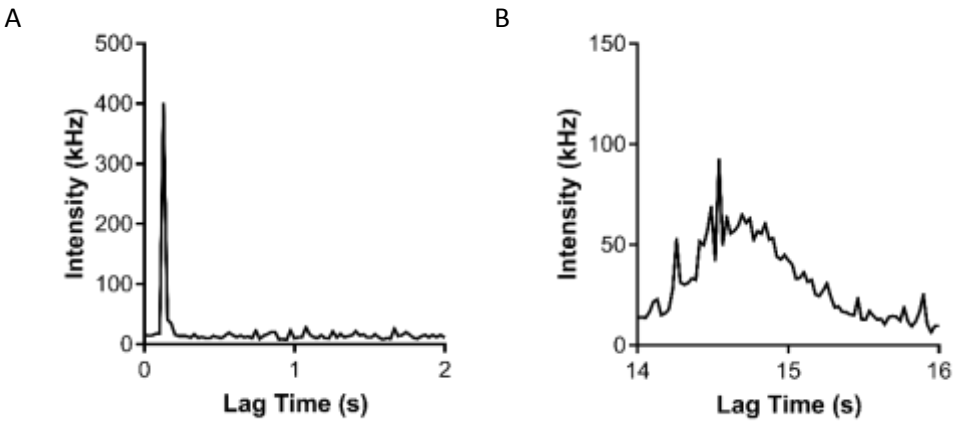


**Supplementary Figure 9.2 – Examples of FCS data excluded from analysis.** When the count rate trace of a particular sample had peaks >10 times the average intensity (**A**) or longer than 1 second in duration (**B**) these peaks were masked using the 'cut region' tool in Zen2010 and the remaining trace was analysed.

## 9.3 List of Publications

**Horsey, A. J.**, Cox, M. H., Sarwat, S. and Kerr, I. D. (2016) 'The multidrug transporter ABCG2: still more questions than answers.', Biochemical Society transactions, 44(3), pp. 824–30. doi: 10.1042/BST20160014.

Kapoor, P., **Horsey, A. J.**, Cox, M. H. and Kerr, I. D. (in press) 'ABCG2: Does resolving its structure elucidate the mechanism?', Biochemical Society Transactions

**Conferences Attended:**

April 2018 – "7th Focused Meeting on Cell Signalling", Nottingham, UK – Poster Presentation

March 2018 – "ATP-Binding Cassette (ABC) Proteins:From Multidrug Resistance to Genetic Disease", Innsbruck, Austria – Oral Presentation

September 2017 – "Transmembrane Transporters in Health and Disease", Vienna, Austria – Poster Presentation

August 2017 – "Transporters and channels in drug discovery and preclinical development", Lausanne, Switzerland – Poster Presentation

July 2017 – "Life Sciences Research Symposium", Nottingham, UK – Oral Presentation

June 2017 – "Nanoparticle technologies for membrane protein research", Leeds, UK – Poster Presentation

October 2016 – "Advanced Imaging with. Light Microscopy: Capturing Tissues to Single Molecules", Imperial College London, UK – Attendee

January 2016 – "Detergent Free Extraction of Membrane Proteins", Birmingham, UK – Attendee

December 2015 – Biochemical Society Meeting: "Membrane Proteins from Amino Acids to Zinc", Leeds, UK – Poster Presentation

**Funding Awards:**

COMPARE - 'Team Science' Conference Attendance Funding (£664)

Biochemical Society - Travel Grant (£400)

FEBS Youth Travel Fund - (£691)

Royal Microscopical Society - Travel Grant (£200)

## 9.4 DTP Notice to Examiners

The University of Nottingham
UNITED KINGDOM • CHINA • MALAYSIA

ROTHAMSTED RESEARCH

BBSRC Doctoral Training Partnerships

The University of Nottingham BBSRC Doctoral Training Partnership (DTP) is undertaken in partnership with Rothamsted Research. Its aim is to develop an innovative, integrated, student-led programme of individualised research training in the Biosciences through an effective cohort-based programme. Students are not recruited to an individual project but, through a series of lab rotations, identify a PhD programme that they wish to pursue in one of three BBSRC priority research areas (Food Security; Industrial Biotechnology and Bioenergy; World Class Biosciences)

**Research Training Structure**

The research training structure is framed by individual development needs analysis and has the following core components:

- Generic and research skills development
- High-level modular training
- Laboratory rotations
- Experiential learning through public engagement and outreach activity

Generic and research skills development comprises the following: induction, introductory training programme, annual 'Spring School' conference-style training event, participation in Sysmic (online systems and mathematical biology course), specialist training days at partner organisations, twilight (after-lab) training which is arranged on an *ad hoc* basis to meet identified needs, and seminar series.

In Year One there is an initial period of intensive training which takes place over the course of the first six months. This comprises a two-week introductory training programme, 24 weeks of laboratory rotations, followed by a week-long 'Spring School' (conference-style training event for all DTP cohorts) and ending in a science outreach event. Each lab rotation is assessed focussing on a different form of scientific communication (Report, Poster, Presentation) and students receive feedback from supervisors. The PhD project begins in Month 7. Students are also encouraged to choose from a portfolio of relevant Master Courses which they can attend alongside their lab rotation projects.

In Years Two to Four training is mainly concentrated in the week long annual Spring School, although additional training and seminars are delivered where required throughout the year. A three month Professional Internship for PhD Students (PIPS) placement is usually taken in Year Three and, as BBSRC specifies, this is not in an area related to the students' PhD research programme.

The integrated programme of training is mapped to BBSRC priority areas, BBSRC Skills Statement: Scientific and Core Skills for UK Bioscience and the Researcher Development Framework (RDF) to ensure breadth and depth of provision, and to encompass vulnerable skills and strategic competencies. It builds on the best practice principles outlined in the Statement of Expectations for Doctoral Training, RCUK (2013) and the 'Good Practice Elements in Doctoral Training', LERU (2014).

It offers a wide range of skills development opportunities to prepare students for a successful bioscience-related career and supports the exchange of ideas and experiences within and across cohorts. It also generates a strong community of postgraduates and supervisors to stimulate the formation of cross-disciplinary links through cohort development, which prepares students for a career in an increasingly multidisciplinary environment.

## 9.5 Placement Report and Reflection

As detailed in the Notice to Examiners (Section 9.3), during this project a 3 month professional internship for PhD students (PIPS) was undertaken at the Royal Microscopical Society. On the conclusion of this placement, a report was written regarding the results of the project and, as required for the BBSRC DTP, a version that included some personal reflection on the experience is given on the proceeding pages.